Insights into microbial metal reduction through implementation of proteomic-based techniques: A focus on the Gram-positive bacterium *Desulfotomaculum reducens* MI-1

A Dissertation

Presented to the Faculty of the Graduate School of Cornell University

In partial fulfillment of the Requirements of the Degree of Doctor of Philosophy

Anne Elyse Otwell

May 2016

Insights into microbial metal reduction through implementation of proteomic-based techniques: A focus on the Gram-positive bacterium *Desulfotomaculum reducens* MI-1

Anne Elyse Otwell, Ph.D.
Cornell University 2016

Certain microorganisms are capable of extracellular metal reduction. Fe(III) is an abundant element in the Earth's crust and serves as a common terminal electron acceptor in anaerobic environments. Decades of research have focused on pathways of extracellular electron transfer to metals since the discovery of enzymatic microbial metal reduction in the late 1980's. Most of these studies have analyzed two model genera of Gram-negative proteobacteria, specifically *Geobacter* and *Shewanella*. It is now understood that a variety of phylogenetically diverse microorganisms are capable of metal reduction, including species of Gram-positive bacteria, but studies on microbial metal reduction are scarce outside of the Gram-negative model organisms. In this dissertation, parallel proteomic approaches were employed in order to study microbial metal reduction. Several studies focused on *Desulfotomaculum reducens* MI-1, a Gram-positive sulfate-reducing bacterium capable of Fe(III), Mn(IV), Cr(VI), and U(VI) reduction. This included a 'top-down' proteomic approach (activity screens of fractionated proteins) to identify proteins capable of Fe(III) reduction. Fe(III) reductases identified from *D. reducens*, which were also shown to have *in vitro* Cr(VI) and U(VI) reductase activity, were Dred_2421 and Dred_1685-6 (a protein complex). A 'bottom-up' proteomic approach was also utilized in order to perform comparative proteomic analysis. The proteomes of *D. reducens* were compared during sulfate reduction, soluble Fe(III) reduction, insoluble Fe(III) reduction, and pyruvate fermentation. This was the first global comparative proteomic analysis of a Gram-positive organism cultivated on either sulfate or Fe(III)-reducing conditions. Based on

differential abundance patterns, certain proteins were predicted to be involved in either Fe(III) or sulfate reduction in *D. reducens*. These included proteins within several heterodisulfide reductase-containing loci with previously unknown function. Evidence for flavin-based electron bifurcation was also revealed in this comparative proteomic study. Another proteomic technique employed was targeted biomarker peptide quantification. Various peptide biomarkers of metal reductases from diverse metal-reducing bacteria were created. Using multiple reaction monitoring (MRM) mass spectrometry, these peptides were quantified in laboratory cultures including Fe(III)-reducing co-cultures established between *D. reducens* and *Geobacter sulfurreducens* PCA. These co-cultures exhibited enhanced rates of both soluble and insoluble Fe(III) reduction as well as increased rates of pyruvate oxidation. Furthermore, *D. reducens* and *G. sulfurreducens* cells grew faster in co-culture than in pure cultures. Altogether, these observations suggest formation of a mutually beneficial association. Along with the targeted MRM technique, global comparative proteomic analysis was performed on *D. reducens*-*G. sulfurreducens* co-cultures in order to provide further biological insight. Interestingly, multiple proteins previously associated with Fe(III) reduction in *G. sulfurreducens* (including multiheme c-type cytochromes and type IV pili-related proteins) were significantly increased in abundance during growth with *D. reducens*. In summary, through employment of varied proteomic techniques, this work strives to progress the study of microbial metal reduction, with a particular focus on the Gram-positive bacterium *D. reducens*.

BIOGRAPHICAL SKETCH

I grew up in Traverse City, MI—a small town in northern Michigan. The middle child of three daughters, my family has always been a central part of my life. I attended the University of Wisconsin for my freshman year of undergraduate as a member of the cross-country and track teams. After deciding to end the competitive running chapter of my life, I transferred to Michigan State University for my sophomore year. Rooted in values instilled from my parents, environmental sustainability has always been important to me, and I started in an environmental studies program. During an introductory microbiology class, the lecturer mentioned a professor researching bacteria of interest for bioremediation as well as electricity production. I started working in the lab of Professor Gemma Reguera the following week and switched my major to microbiology shortly after. My decision to become a microbiologist was inspired by my time in the Reguera lab, and I am grateful for the supportive group of researchers I worked with.

In exploring potential schools to pursue PhD work, Cornell University was my top choice based on the wide range of environmental microbiology research in progress. The town of Ithaca also seemed like a place in which I would really enjoy living. I am very happy with my decision to attend Cornell, and I am grateful for the experiences and opportunities I have over the last 5.5 years. During my time in Ithaca, I grew both academically and personally in ways I could not have predicted, and I will look back with very fond memories. In December I moved to San Diego in order to live with my partner and finish writing this dissertation. I am currently working with the Synthetic Biology and Bioenergy Group at J. Craig Venter Institute in San Diego. We plan to move from San Diego in May, at which time I will likely pursue postdoctoral research.

ACKNOWLEDGEMENTS

I would like to thank my advisor Ruth Richardson. I am grateful for the opportunities I have had while working with you, including the ability to pursue research that I am truly interested in. I am also grateful that you helped me pursue valuable teaching experiences during my time at Cornell. I would also like to thank my minor advisors Stephen Zinder and Jeffrey Werner for helpful discussions throughout the course of this dissertation work. Thank you to every member of the Richardson Lab that I crossed paths with during my time at Cornell, especially Cristina, Cresten, and Alex.

I would like to thank collaborators involved in the work described here, including Robert Sherwood and Sheng Zhang of the Cornell Proteomics & Mass Spectrometry Facility, Stephen Callister and Lee Ann McCue of Pacific Northwest National Laboratory, and Ornella Nelson, Zhi Li, and Hening Lin from the Department of Chemistry and Chemical Biology. We were collectively involved in a grant funded by the Department of Energy's Office of Biological and Environmental Research, and I am grateful for the opportunities that this provided.

I met wonderful people at Cornell. Thank you to Cristina for being a wonderful lab mate and friend. Thank you to Parvin, Yael, and all of the mice of Stewart Little for making my experience at Cornell so much happier and richer. Thank you to Maxim. I have learned so much from you and with you and I am very excited for our life together! Thank you to my amazing sisters Claire and Julia who are also my best friends. I couldn't imagine life without you. Thank you to my parents for your love, your support, and so much more. You are two of the best people I know and I feel so lucky to be your daughter.

Table of Contents

Chapter 1

Introduction

Background on microbial metal reduction

In 1988, two foundational studies were published in the field of anaerobic respiration. Both of them demonstrated for the first time that certain microorganisms are capable of metal respiration. In the first, a *Shewanella* species was isolated that could oxidize lactate to acetate with Mn(IV) oxide as terminal electron acceptor (Myers and Nealson, 1988). The second study showed complete oxidation of a carbon compound (acetate) with Fe(III) or Mn(IV) oxide as terminal electron acceptor by a *Geobacter* species (Lovley and Phillips, 1988). Before this time, it was assumed that most Fe(III) reduction in sedimentary environments occurred through nonenzymatic reactions (Lovley, 1993). It is now understood that Fe(III) is a dominant terminal electron acceptor in anaerobic environments, including soils and aquatic sediments. As such, dissimilatory metal-reducing microorganisms (DMRM) not only affect the state of the essential trace metal, but also influence the carbon cycle through decomposition of organic matter (Bird et al., 2011; Hori et al., 2015; Lovley, 1993).

Shortly after the discovery Fe(III) and Mn(IV) respiration, utilization of U(VI) as a terminal electron acceptor by a species of *Geobacter* was demonstrated (Lovley et al., 1991). Uranium is a widespread subsurface contaminant due to anthropogenic practices such as mining and nuclear weapons development (Wall and Krumholz, 2006). It is primarily present in the environment as soluble salts of the uranyl ion. Reduction from this +6 oxidation state to +4 greatly decreases the solubility, resulting in immobilization and potential precipitation of uranium out of groundwater (Mohapatra et al., 2010; Wall and Krumholz, 2006). Since the discovery of microbial-based enzymatic uranium reduction, the application of DMRM for bioremediation has also been a focus of research in the field. Other contaminant metals and

radionuclides including Cr(VI), Se(VI), Tc(VII), Pu (VI) and Np(V) can potentially be remediated through reduction by DMRM (Lloyd and Lovley, 2001; Mohapatra et al., 2010).

For nearly three decades, research on species of *Shewanella* and *Geobacter* has driven understanding of microbial metal reduction. At or above circumneutral pH, Fe(III) exists primarily as insoluble minerals (Bird et al., 2011). Therefore, utilization of Fe(III) as an electron acceptor requires extracellular electron transfer—electrons are shuttled out of the cell in order to reduce the metal in the environment. This unique method of respiration has been the focus of many studies, which aim to elucidate proteins involved in pathways of electron transfer. Similar mechanisms of extracellular electron transfer have been characterized in *Shewanella* and *Geobacter*, both species of Gram-negative proteobacteria. These organisms, along with other Gram-negative DMRM, encode a multitude of putative multiheme c-type cytochromes (MHCs) in their genome (Shi et al., 2007). For example, across all sequenced *Geobacter* species, c-type cytochromes have an average of 7.7 hemes, and some species *of Geobacter* contain over 100 putative c-type cytochromes in their genomes (Butler et al., 2010). In both model genera, the predicted pathways of electron transfer to metals involve multiple MHCs. In model species *Geobacter sulfurreducens*, a number of MHCs including periplasmic protein PpcA, outer membrane proteins OmcB and OmcS, and extracellular protein OmcZ have been characterized and are predicted to be involved in extracellular electron transfer (Inoue et al., 2010; Leang et al., 2003, 2010; Lloyd et al., 2003; Qian et al., 2011). Electron transfer research in *Shewanella* has led to the description of the Mtr (Metal reduction) pathway. Characterized components include an inner-membrane MHC (CymA), three outer membrane MHCs (MtrA, MtrC, and OmcA), and an outer membrane porin-like protein (MtrB) (Shi et al., 2012).

Along with the critical role of MHCs, studies have demonstrated that 'nanowires' and flavins play a role in extracellular electron transfer in both *Geobacter* and *Shewanella* species. 'Nanowires' was originally a term describing the electrically conductive type IV pili of *Geobacter* (Reguera et al., 2005). Evidence suggests that these conductive pili play a role in Fe(III) reduction, U(VI) reduction, and electron transfer to the surface of an electrode during growth in microbial fuel cells (Cologgi et al., 2011; Reguera et al., 2005; Richter et al., 2009). Pili-nanowires were suggested for *Shewanella* species in 2006, as electrically conductive pilus-like appendages were reported (Gorby et al., 2006). Recently, it was shown that in *Shewanella* the nanowires are actually extensions of the periplasm and outer membrane and that MHCs including MtrC and OmcA localize to these extensions (Pirbadian et al., 2014). While structural components of the nanowires appear to be different across organisms, conductive nanowires are thought to play a key role in extracellular electron transfer in both model organisms. Studies also recently demonstrated that flavins likely play a role in metal reduction in both organisms. It has been established for some time that *Shewanella* spp. secrete flavins (including riboflavin and flavin mononucleotide) that mediate extracellular electron transfer by serving as a soluble electron shuttle (Brutinel and Gralnick, 2012; von Canstein et al., 2008; Marsili et al., 2008). In *Geobacter*, flavins were believed to not play a role, however, as direct contact was shown to be required for reduction of Fe(III)-oxides (Nevin and Lovley, 2000). A new model was recently proposed for the role of flavins in both *Shewanella* and *Geobacter* species, though (Okamoto et al., 2014a). It describes a role for flavins as bound redox cofactors, secreted by the cells and bound to MHCs involved in extracellular electron transfer (Okamoto et al., 2013, 2014a, 2014b). Defined as the 'bound flavin model,' this finding brings even closer together the mechanisms for extracellular electron transfer described for the two model DMRM.

While research has focused heavily on *Shewanella* and *Geobacter* species, the capability for metal reduction is a trait that has been identified in a wide range of phylogenetically diverse organisms (Barton et al., 2015; Weber et al., 2006). This includes Gram-positive organisms (for instance species of Firmicutes and Actinobacteria) as well as multiple Archaeal species (Itoh et al., 2011; Kashefi and Lovley, 2000; Kim et al., 2012; Tebo and Obraztsova, 1998; Weber et al., 2006). However, very little is known about proteins involved in electron transfer to metals in these organisms. For one Gram-positive DMRM, *Thermincola potens*, there is evidence that MHCs are involved in extracellular electron transfer (Carlson et al., 2012; Wrighton et al., 2011). It is rare for Gram-positive organisms to encode multiple MHCs, however (Sharma et al., 2010). For instance, species within the closely-related Gram-positive genera *Desulfotomaculum, Desulfitobacterium*, and *Desulfosporosinus* have been described as DMRM but encode few MHCs (Amin et al., 2013; Kim et al., 2012; Suzuki et al., 2004; Tebo and Obraztsova, 1998). Over the past few years, *Desulfotomaculum reducens* MI-1 has become the most studied of these Peptococcaceae for its metal reduction capability.

D. reducens MI-1 is a sulfate-reducing bacteria (SRB) that was isolated from sediments contaminated with high concentrations of Cr(VI) and other heavy metals in the San Francisco Bay estuary in 1998 (Tebo and Obraztsova, 1998). It has been shown to utilize Fe(III), Mn(IV), Cr(VI), and U(VI) as electron acceptor while partially oxidizing lactate and butyrate. It is also capable of pyruvate fermentation (Tebo and Obraztsova, 1998). The genome of *D. reducens* was sequenced in 2010, and since this time there have been multiple studies on metal reduction (Junier et al., 2010). This includes studies performed by Bernier-Latmani's group from École Polytechnique Fédérale de Lausanne (EPFL) as well as research performed in our group and included in this dissertation. Dr. Bernier-Latmani's group studied U(VI) reduction by endospores

of *D. reducens*, analyzed the effect of competing electron acceptors on U(VI) reduction, and performed a transcriptomic analysis of *D. reducens* searching for genes differentially expressed during U(VI) reduction (Junier et al., 2009, 2010, 2011). Researchers also analyzed Fe(III) reduction during pyruvate fermentation, where they proposed that Fe(III)-oxide reduction during growth with pyruvate occurs through a soluble electron shuttle, as direct contact was found to not be required for Fe(III) reduction while fermenting pyruvate (Dalla Vecchia et al., 2014b). The most recent study published about Fe(III) reduction in *D. reducens* by Dr. Bernier-Latmani's group found that direct contact was required for Fe(III)-oxide reduction while lactate was electron donor and is therefore not mediated by a soluble shuttle (Dalla Vecchia et al., 2014a). This study also analyzed the surface proteins (or surfaceome) of *D. reducens* while fermenting pyruvate or reducing soluble Fe(III) with lactate as electron donor. The studies reported in this dissertation add to the expanding literature focusing on metal reduction in *D. reducens*.

In our analyses of microbial metal reduction, we mainly employed proteomic techniques. This included function-based analyses of extracted proteins ('top-down' analyses) as well as comparative proteomic analyses ('bottom-up' analyses). Previous studies in model DMRM have utilized similar approaches. For instance, the first MHC shown to play an *in vivo* role in Fe(III) reduction (both soluble and insoluble) in *G. sulfurreducens*, OmcB, was initially identified using protein purification-based functional assays similar to our 'top-down' approach (Leang et al., 2003; Magnuson et al., 2000, 2001). Our specific workflow was developed based on modifications to an approach used in *Shewanella oneidensis*. In this study, multiple proteins were identified as Fe(III) reductase candidates, including all known proteins in the Mtr pathway (Elias et al., 2007). A characterized MHC Fe(III) and U(VI) reductase from the Gram-negative SRB *Desulfovibrio vulgaris* was also identified from a function-based activity screen (Lovley et

al., 1993). Comparative proteomic analysis has also proven to be a useful tool for generating hypotheses about protein function, especially as mass spectrometry-based techniques continues to improve (Lipton et al., 2002; Pasa-Tolić et al., 2004). In *G. sulfurreducens*, a study compared protein abundance during growth with fumarate versus Fe(III)-citrate as electron acceptor and identified 14 MHCs that were significantly upregulated on iron conditions, 12 of which had not previously been characterized (Ding et al., 2006). Another proteomic study, comparing Fe(III)-citrate and Fe(III)-oxide conditions, supported the vital role of OmcB for both soluble and insoluble iron reduction and the requirement of OmcS only for the reduction of insoluble substrates (Ding et al., 2008). Also in this study, the structural pilin protein (PilA) was more abundant on Fe(III)-oxide, supporting the role of nanowires in electron transfer to insoluble substrates.

A final proteomic tool that we implemented in this project was targeted biomarker peptide quantification through multiple reaction monitoring (MRM). In this technique, proteotypic peptides (unique signatures of a particular protein) are designed and synthesized with isotopic labels. These synthetic peptides serve as standards in order to quantify biomarker peptides in experimental samples. MRM is currently utilized mainly in clinical fields (Arsène-Ploetze et al., 2015). The major example of application of MRM to environmental microbiology research currently is in the field of chlorinated compound bioremediation (Rowe et al., 2012, 2015; Werner et al., 2009). In our work, we developed peptide biomarkers designed to target known metal reductases from a variety of microorganisms. Monitoring of the biomarkers at sites of interest for metal reduction processes, including U(VI)-contaminated sites, is an eventual goal.

Overview of research chapters

A broad goal of this dissertation research was to improve understanding of microbial metal reduction. As *D. reducens* is a poorly characterized organism, and related to other poorly characterized DMRM (*Desulfitobacterium*, *Desulfosporosinus*), this Gram-positive bacterium became a major focus of my work. Towards the goal of better elucidating metal reduction, we employed parallel proteomic-based techniques. We developed a 'top-down' proteomic workflow for identifying Fe(III) reductases. A major advantage of this 'top-down' approach is that it allows for selection and identification of a protein with a particular function (in this case Fe(III) reduction activity) from a complex pool of proteins. The workflow involves extracting functional proteins, fractionating the protein pool with a series of non-denaturing separations, screening the fractionated proteome for Fe(III) reduction activity, and then identifying the active protein with tandem mass spectrometry. Once specific proteins are identified, heterologous expression and purification can then be used to confirm function and perform further characterization. This dissertation is organized into five research chapters, and the first three (Chapters 2-4) focus on research that utilizes the 'top-down' approach, along with experiments that were motivated based on findings from these studies. This includes a function-based screen for Fe(III) reductases from the proteomes of *D. reducens* as well as *G. sulfurreducens*. Interestingly, orthologous proteins were identified from these organisms. This was studied further by creating a gene knockout in *G. sulfurreducens,* as a genetic system is available in this model organism. While creating the knockout construct, a new cloning technique was developed, which is the content of Chapter 4.

'Bottom-up' proteomic analyses are complementary to the top-down approach in that they allow for global comparisons of protein abundance across various proteomes of interest (in our case, different growth conditions including Fe(III) reduction). In work presented in this

dissertation, we utilized the accurate mass and time (AMT) tag approach to perform global comparative proteomic analyses. In research chapter 4 (Chapter 5), abundance comparisons of various *D. reducens* proteomes are analyzed. Cells were cultivated on different conditions (sulfate reduction, soluble Fe(III) reduction, insoluble Fe(III) reduction, and pyruvate fermentation), proteins were extracted and digested, the ion intensity of detected peptides was measured, and patterns of differential protein abundance were analyzed. This study is the first full-proteome analysis of a Gram-positive organism on either sulfate or Fe(III)-reducing conditions. The final research chapter (Chapter 6) reports findings from Fe(III)-reducing co-cultures established between *D. reducens* and *G. sulfurreducens*, where clear phenotypic differences were observed between co-culture and pure culture growth. Comparative proteomic analysis was performed, comparing co-culture and pure culture proteomes. We also performed targeted quantification of peptide biomarkers from *D. reducens* and *G. sulfurreducens* proteins. MRM assays were designed to target proteotypic peptides representing metal reduction-related proteins from both of these metal-reducing bacteria. We were able to validate several of these peptide biomarkers for *G. sulfurreducens* and *D. reducens* during pure culture and co-culture growth. This work is the first example of proteomic analyses being applied to an Fe(III)-reducing co-culture.

References

Amin, O., Fardeau, M.-L., Valette, O., Hirschler-Réa, A., Barbe, V., Médigue, C., et al. (2013). Genome Sequence of the Sulfate-Reducing Bacterium Desulfotomaculum hydrothermale Lam5T. *Genome Announc.* 1. doi:10.1128/genomeA.00114-12.

Arsène-Ploetze, F., Bertin, P. N., and Carapito, C. (2015). Proteomic tools to decipher microbial community structure and functioning. *Environ. Sci. Pollut. Res. Int.* 22, 13599–612. doi:10.1007/s11356-014-3898-0.

Barton, L., Tomei-Torres, F., Xu, H., and Zocco, T. (2015). *Bacteria-Metal Interactions*. , ed. D. Saffarini Cham: Springer International Publishing doi:10.1007/978-3-319-18570-5.

Bird, L. J., Bonnefoy, V., and Newman, D. K. (2011). Bioenergetic challenges of microbial iron metabolisms. *Trends Microbiol.* 19, 330–340. doi:10.1016/j.tim.2011.05.001.

Brutinel, E. D., and Gralnick, J. A. (2012). Shuttling happens: soluble flavin mediators of extracellular electron transfer in Shewanella. *Appl. Microbiol. Biotechnol.* 93, 41–48. doi:10.1007/s00253-011-3653-0.

Butler, J. E., Young, N. D., and Lovley, D. R. (2010). Evolution of electron transfer out of the cell: comparative genomics of six Geobacter genomes. *BMC Genomics* 11, 40. doi:10.1186/1471-2164-11-40.

von Canstein, H., Ogawa, J., Shimizu, S., and Lloyd, J. R. (2008). Secretion of flavins by Shewanella species and their role in extracellular electron transfer. *Appl. Environ. Microbiol.* 74, 615–623. doi:10.1128/AEM.01387-07.

Carlson, H. K., Iavarone, A. T., Gorur, A., Yeo, B. S., Tran, R., Melnyk, R. A., et al. (2012). Surface multiheme c-type cytochromes from Thermincola potens and implications for respiratory metal reduction by Gram-positive bacteria. *Proc. Natl. Acad. Sci.* doi:10.1073/pnas.1112905109.

Cologgi, D. L., Lampa-Pastirk, S., Speers, A. M., Kelly, S. D., and Reguera, G. (2011). Extracellular reduction of uranium via Geobacter conductive pili as a protective cellular mechanism. *Proc. Natl. Acad. Sci.* doi:10.1073/pnas.1108616108.

Dalla Vecchia, E., Shao, P. P., Suvorova, E., Chiappe, D., Hamelin, R., and Bernier-Latmani, R. (2014a). Characterization of the surfaceome of the metal-reducing bacterium Desulfotomaculum reducens. *Front. Microbiol.* 5, 432. doi:10.3389/fmicb.2014.00432.

Dalla Vecchia, E., Suvorova, E. I., Maillard, J., and Bernier-Latmani, R. (2014b). Fe(III) reduction during pyruvate fermentation by Desulfotomaculum reducens strain MI-1. *Geobiology* 12, 48–61. doi:10.1111/gbi.12067.

Ding, Y.-H. R., Hixson, K. K., Aklujkar, M. A., Lipton, M. S., Smith, R. D., Lovley, D. R., et al. (2008). Proteome of Geobacter sulfurreducens grown with Fe(III) oxide or Fe(III) citrate as the electron acceptor. *Biochim. Biophys. Acta - Proteins Proteomics* 1784, 1935–1941. doi:10.1016/j.bbapap.2008.06.011.

Ding, Y.-H. R., Hixson, K. K., Giometti, C. S., Stanley, A., Esteve-Núñez, A., Khare, T., et al. (2006). The proteome of dissimilatory metal-reducing microorganism Geobacter sulfurreducens under various growth conditions. *Biochim. Biophys. Acta - Proteins Proteomics* 1764, 1198–1206. doi:10.1016/j.bbapap.2006.04.017.

Elias, D. A., Yang, F., Mottaz, H. M., Beliaev, A. S., and Lipton, M. S. (2007). Enrichment of functional redox reactive proteins and identification by mass spectrometry results in several terminal Fe(III)-reducing candidate proteins in Shewanella oneidensis MR-1. *J. Microbiol. Methods* 68, 367–375. doi:10.1016/j.mimet.2006.09.023.

Gorby, Y. A., Yanina, S., McLean, J. S., Rosso, K. M., Moyles, D., Dohnalkova, A., et al. (2006). Electrically conductive bacterial nanowires produced by Shewanella oneidensis strain MR-1 and other microorganisms. *Proc. Natl. Acad. Sci.* 103, 11358–11363. doi:10.1073/pnas.0604517103.

Hori, T., Aoyagi, T., Itoh, H., Narihiro, T., Oikawa, A., Suzuki, K., et al. (2015). Isolation of microorganisms involved in reduction of crystalline iron(III) oxides in natural environments. *Front. Microbiol.* 6, 386. doi:10.3389/fmicb.2015.00386.

Inoue, K., Qian, X., Morgado, L., Kim, B.-C., Mester, T., Izallalen, M., et al. (2010). Purification

and Characterization of OmcZ, an Outer-Surface, Octaheme c-Type Cytochrome Essential for Optimal Current Production by Geobacter sulfurreducens. *Appl. Environ. Microbiol.* 76, 3999–4007. doi:10.1128/AEM.00027-10.

Itoh, T., Yamanoi, K., Kudo, T., Ohkuma, M., and Takashina, T. (2011). Aciditerrimonas ferrireducens gen. nov., sp. nov., an iron-reducing thermoacidophilic actinobacterium isolated from a solfataric field. *Int. J. Syst. Evol. Microbiol.* 61, 1281–5. doi:10.1099/ijs.0.023044-0.

Junier, P., Frutschi, M., Wigginton, N. S., Schofield, E. J., Bargar, J. R., and Bernier-Latmani, R. (2009). Metal reduction by spores of Desulfotomaculum reducens. *Environ. Microbiol.* 11, 3007–3017. doi:10.1111/j.1462-2920.2009.02003.x.

Junier, P., Junier, T., Podell, S., Sims, D. R., Detter, J. C., Lykidis, A., et al. (2010). The genome of the Gram-positive metal- and sulfate-reducing bacterium Desulfotomaculum reducens strain MI-1. *Environ. Microbiol.* 12, 2738–2754. doi:10.1111/j.1462-2920.2010.02242.x.

Junier, P., Suvorova, E.I., Bernier-Latmani, R. (2010). Effect of Competing Electron Acceptors on the Reduction of U(VI) by Desulfotomaculum reducens. *Geomicrobiol. J*. 27, 435-443. doi: 10.1080/01490450903480293.

Junier, P., Vecchia, E. D., and Bernier-Latmani, R. (2011). The Response of Desulfotomaculum reducens MI-1 to U(VI) Exposure: A Transcriptomic Study. *Geomicrobiol. J.* 28, 483–496. doi:10.1080/01490451.2010.512031.

Kashefi, K., and Lovley, D. R. (2000). Reduction of Fe(III), Mn(IV), and Toxic Metals at 100 C by Pyrobaculum islandicum. *Appl. Environ. Microbiol.* 66, 1050–1056. doi:10.1128/AEM.66.3.1050-1056.2000.

Kim, S.-H., Harzman, C., Davis, J. K., Hutcheson, R., Broderick, J. B., Marsh, T. L., et al. (2012). Genome sequence of Desulfitobacterium hafniense DCB-2, a Gram-positive anaerobe capable of dehalogenation and metal reduction. *BMC Microbiol.* 12, 21. doi:10.1186/1471-2180-12-21.

Leang, C., Coppi, M. V., and Lovley, D. R. (2003). OmcB, a c-Type Polyheme Cytochrome, Involved in Fe(III) Reduction in Geobacter sulfurreducens. *J. Bacteriol.* 185, 2096–2103. doi:10.1128/JB.185.7.2096-2103.2003.

Leang, C., Qian, X., Mester, T., and Lovley, D. R. (2010). Alignment of the c-Type Cytochrome OmcS along Pili of Geobacter sulfurreducens. *Appl. Environ. Microbiol.* 76, 4080–4084. doi:10.1128/AEM.00023-10.

Lipton, M. S., Paša-Tolić, L., Anderson, G. A., Anderson, D. J., Auberry, D. L., Battista, J. R., et al. (2002). Global analysis of the Deinococcus radiodurans proteome by using accurate mass tags. *Proc. Natl. Acad. Sci.* 99, 11049–11054. doi:10.1073/pnas.172170199.

Lloyd, J. R., Leang, C., Hodges Myerson, A. L., Coppi, M. V, Cuifo, S., Methe, B., et al. (2003). Biochemical and genetic characterization of PpcA, a periplasmic c-type cytochrome in Geobacter sulfurreducens. *Biochem. J.* 369, 153–161. doi:10.1042/BJ20020597.

Lloyd, J. R., and Lovley, D. R. (2001). Microbial detoxification of metals and radionuclides. *Curr. Opin. Biotechnol.* 12, 248–253. Available at: http://www.ncbi.nlm.nih.gov/pubmed/11404102.

Lovley, D. R. (1993). Dissimilatory metal reduction. *Annu. Rev. Microbiol.* 47, 263–290.

doi:10.1146/annurev.mi.47.100193.001403.

Lovley, D. R., and Phillips, E. J. P. (1988). Novel Mode of Microbial Energy Metabolism: Organic Carbon Oxidation Coupled to Dissimilatory Reduction of Iron or Manganese. *Appl. Environ. Microbiol.* 54, 1472–1480. Available at: http://www.ncbi.nlm.nih.gov/pmc/articles/PMC202682/.

Lovley, D. R., Phillips, E. J. P., Gorby, Y. A., and Landa, E. R. (1991). Microbial reduction of uranium. *Nature* 350, 413–416. doi:10.1038/350413a0.

Lovley, D. R., Widman, P. K., Woodward, J. C., and Phillips, E. J. (1993). Reduction of uranium by cytochrome c3 of Desulfovibrio vulgaris. *Appl. Environ. Microbiol.* 59, 3572–3576. Available at: http://aem.asm.org/content/59/11/3572.

Magnuson, T. S., Hodges-Myerson, A. L., and Lovley, D. R. (2000). Characterization of a membrane-bound NADH-dependent Fe3+ reductase from the dissimilatory Fe3+-reducing bacterium Geobacter sulfurreducens. *FEMS Microbiol. Lett.* 185, 205–211. doi:10.1111/j.1574-6968.2000.tb09063.x.

Magnuson, T. S., Isoyama, N., Hodges-Myerson, A. L., Davidson, G., Maroney, M. J., Geesey, G. G., et al. (2001). Isolation, characterization and gene sequence analysis of a membrane-associated 89 kDa Fe(III) reducing cytochrome c from Geobacter sulfurreducens. *Biochem. J.* 359, 147–152. Available at: http://www.ncbi.nlm.nih.gov/pmc/articles/PMC1222130/.

Marsili, E., Baron, D. B., Shikhare, I. D., Coursolle, D., Gralnick, J. A., and Bond, D. R. (2008). Shewanella secretes flavins that mediate extracellular electron transfer. *Proc. Natl. Acad. Sci.* 105, 3968–3973. doi:10.1073/pnas.0710525105.

Mohapatra, B. R., Dinardo, O., Gould, W. D., and Koren, D. W. (2010). Biochemical and genomic facets on the dissimilatory reduction of radionuclides by microorganisms – A review. *Miner. Eng.* 23, 591–599. doi:10.1016/j.mineng.2010.03.004.

Myers, C. R., and Nealson, K. H. (1988). Bacterial Manganese Reduction and Growth with Manganese Oxide as the Sole Electron Acceptor. *Science (80-.).* 240, 1319–1321. doi:10.1126/science.240.4857.1319.

Nevin, K. P., and Lovley, D. R. (2000). Lack of production of electron-shuttling compounds or solubilization of Fe(III) during reduction of insoluble Fe(III) oxide by Geobacter metallireducens. *Appl. Environ. Microbiol.* 66, 2248–2251. Available at: http://www.ncbi.nlm.nih.gov/pubmed/10788411.

Okamoto, A., Hashimoto, K., Nealson, K. H., and Nakamura, R. (2013). Rate enhancement of bacterial extracellular electron transport involves bound flavin semiquinones. *Proc. Natl. Acad. Sci.* 110, 7856–7861. doi:10.1073/pnas.1220823110.

Okamoto, A., Nakamura, R., Nealson, K. H., and Hashimoto, K. (2014a). Bound Flavin Model Suggests Similar Electron-Transfer Mechanisms in Shewanella and Geobacter. *ChemElectroChem* 1, 1808–1812. doi:10.1002/celc.201402151.

Okamoto, A., Saito, K., Inoue, K., Nealson, K. H., Hashimoto, K., and Nakamura, R. (2014b). Uptake of self-secreted flavins as bound cofactors for extracellular electron transfer in Geobacter species. *Energy Environ. Sci.* 7, 1357. doi:10.1039/c3ee43674h.

Pasa-Tolić, L., Masselon, C., Barry, R. C., Shen, Y., and Smith, R. D. (2004). Proteomic analyses using an accurate mass and time tag strategy. *Biotechniques* 37, 621–4, 626–33,

636 passim. Available at: http://europepmc.org/abstract/med/15517975 [Accessed September 8, 2015].

Pirbadian, S., Barchinger, S. E., Leung, K. M., Byun, H. S., Jangir, Y., Bouhenni, R. A., et al. (2014). Shewanella oneidensis MR-1 nanowires are outer membrane and periplasmic extensions of the extracellular electron transport components. *Proc. Natl. Acad. Sci. U. S. A.* 111, 12883–8. doi:10.1073/pnas.1410551111.

Qian, X., Mester, T., Morgado, L., Arakawa, T., Sharma, M. L., Inoue, K., et al. (2011). Biochemical characterization of purified OmcS, a c-type cytochrome required for insoluble Fe(III) reduction in Geobacter sulfurreducens. *Biochim. Biophys. Acta - Bioenerg.* 1807, 404–412. doi:10.1016/j.bbabio.2011.01.003.

Reguera, G., McCarthy, K. D., Mehta, T., Nicoll, J. S., Tuominen, M. T., and Lovley, D. R. (2005). Extracellular electron transfer via microbial nanowires. *Nature* 435, 1098–1101. doi:10.1038/nature03661.

Richter, H., Nevin, K. P., Jia, H., Lowy, D. A., Lovley, D. R., and Tender, L. M. (2009). Cyclic voltammetry of biofilms of wild type and mutant Geobacter sulfurreducens on fuel cell anodes indicates possible roles of OmcB, OmcZ, type IV pili, and protons in extracellular electron transfer. *Energy Environ. Sci.* 2, 506. doi:10.1039/b816647a.

Rowe, A. R., Heavner, G. L., Mansfeldt, C. B., Werner, J. J., and Richardson, R. E. (2012). Relating chloroethene respiration rates in Dehalococcoides to protein and mRNA biomarkers. *Environ. Sci. Technol.* 46, 9388–97. doi:10.1021/es300996c.

Rowe, A. R., Mansfeldt, C. B., Heavner, G. L., and Richardson, R. E. (2015). Relating mRNA and protein biomarker levels in a Dehalococcoides and Methanospirillum-containing community. *Appl. Microbiol. Biotechnol.* 99, 2313–27. doi:10.1007/s00253-014-6220-7.

Sharma, S., Cavallaro, G., and Rosato, A. (2010). A systematic investigation of multiheme c-type cytochromes in prokaryotes. *JBIC J. Biol. Inorg. Chem.* 15, 559–571. doi:10.1007/s00775-010-0623-4.

Shi, L., Rosso, K. M., Clarke, T. A., Richardson, D. J., Zachara, J. M., and Fredrickson, J. K. (2012). Molecular Underpinnings of Fe(III) Oxide Reduction by Shewanella Oneidensis MR-1. *Front. Microbiol.* 3. doi:10.3389/fmicb.2012.00050.

Shi, L., Squier, T. C., Zachara, J. M., and Fredrickson, J. K. (2007). Respiration of metal (hydr)oxides by Shewanella and Geobacter: a key role for multihaem c-type cytochromes. *Mol. Microbiol.* 65, 12–20. doi:10.1111/j.1365-2958.2007.05783.x.

Suzuki, Y., Kelly, S. D., Kemner, K. M., and Banfield, J. F. (2004). Enzymatic U(VI) reduction by Desulfosporosinus species. *Radiochim. Acta* 92, 11–16. doi:10.1524/ract.92.1.11.25404.

Tebo, B. M., and Obraztsova, A. Y. (1998). Sulfate-reducing bacterium grows with Cr(VI), U(VI), Mn(IV), and Fe(III) as electron acceptors. *FEMS Microbiol. Lett.* 162, 193–198. doi:10.1111/j.1574-6968.1998.tb12998.x.

Wall, J. D., and Krumholz, L. R. (2006). Uranium reduction. *Annu. Rev. Microbiol.* 60, 149–166. doi:10.1146/annurev.micro.59.030804.121357.

Weber, K. A., Achenbach, L. A., and Coates, J. D. (2006). Microorganisms pumping iron: anaerobic microbial iron oxidation and reduction. *Nat. Rev. Microbiol.* 4, 752–64. doi:10.1038/nrmicro1490.

Werner, J. J., Ptak, A. C., Rahm, B. G., Zhang, S., and Richardson, R. E. (2009). Absolute quantification of Dehalococcoides proteins: enzyme bioindicators of chlorinated ethene dehalorespiration. *Environ. Microbiol.* 11, 2687–2697. doi:10.1111/j.1462-2920.2009.01996.x.

Wrighton, K. C., Thrash, J. C., Melnyk, R. A., Bigi, J. P., Byrne-Bailey, K. G., Remis, J. P., et al. (2011). Evidence for direct electron transfer by a gram-positive bacterium isolated from a microbial fuel cell. *Appl. Environ. Microbiol.* 77, 7633–9. doi:10.1128/AEM.05365-11.

Chapter 2

Identification of proteins capable of metal reduction from the proteome of the Gram-positive bacterium *Desulfotomaculum reducens* MI-1 using an NADH-based activity assay

Summary

Understanding of microbial metal reduction is based almost solely on studies of Gram-negative organisms. In this study, we focus on *Desulfotomaculum reducens* MI-1, a Gram-positive metal reducer whose genome lacks genes with similarity to any characterized metal reductase. Using non-denaturing separations and mass spectrometry identification, in combination with a colorimetric screen for chelated Fe(III)-NTA reduction with NADH as electron donor, we have identified proteins from the *D. reducens* proteome not previously characterized as iron reductases. Their function was confirmed by heterologous expression in *E. coli*. Furthermore, we show that these proteins have the capability to reduce soluble Cr(VI) and U(VI) with NADH as electron donor. The proteins identified are NADH:flavin oxidoreductase (Dred_2421) and a protein complex composed of oxidoreductase FAD/NAD(P)-binding subunit (Dred_1685) and dihydroorotate dehydrogenase 1B (Dred_1686). Dred_2421 was identified in the soluble proteome and is predicted to be a cytoplasmic protein. Dred_1685 and Dred_1686 were identified in both the soluble as well as the insoluble protein fraction, suggesting a type of membrane-association, although PSORTb predicts both proteins are cytoplasmic. This study is the first functional proteomic analysis of *D. reducens* and one of the first analyses of metal and radionuclide reduction in an environmentally relevant Gram-positive bacterium.

Introduction

Microorganisms capable of dissimilatory iron reduction are of interest due to their integral ecological roles and applications for heavy metal and radionuclide bioremediation (Weber et al., 2006; Mohapatra et al., 2010; Bird et al., 2011). Over two decades of research in model Gram-negative bacteria (i.e. species of *Geobacter* and *Shewanella*) focusing on electron transfer to Fe(III) and U(VI) has shaped understanding of microbial metal reduction. Common to

model Gram-negative metal respirers is the abundance of annotated multiheme c-type cytochromes (MHCs), many of which are membrane-bound and predicted to be involved in iron and/or uranium reduction (Wall and Krumholz, 2006; Shi et al., 2009; Sharma et al., 2010).

Becoming increasingly apparent, however, is the diversity and environmental prevalence of Gram-positive organisms capable of dissimilatory metal reduction. Specifically, numerous Clostridia species have been detected commonly in subsurface environments with heavy metal contamination, and several of these species have been demonstrated to use various metals (including Fe(III) and U(VI)) as electron acceptors (Petrie et al., 2003; Suzuki et al., 2003; Cardenas et al., 2010; Williamson et al., 2013; Newsome et al., 2014). Mechanisms of electron transfer to metals in these phylogenetically distinct organisms are far less elucidated. Recent studies in two thermophilic Firmicutes, *Carboxydothermus ferrireducens* and *Thermincola potens*, support the involvement of MHCs localized on the cell surface (Carlson et al., 2012; Gavrilov et al., 2012). These MHC-rich thermophiles may be exceptions, however, as MHCs are scarce across the genomes of sequenced mesophilic Firmicutes (Sharma et al., 2010).

The sulfate reducing bacterium (SRB) *Desulfotomaculum reducens* MI-1, isolated from heavy-metal contaminated sediment, serves as a useful and novel system for the study of Gram-positive dissimilatory metal reduction. *D. reducens* has been shown to use a variety of metals including U(VI), Fe(III), Cr(VI), Mn(IV) as electron acceptors while oxidizing lactate or butyrate (Tebo and Obraztsova, 1998). *D. reducens* also reduces metals when grown fermentatively with pyruvate, and some studies have focused on metal reduction during this growth condition (Junier et al., 2009; Dalla Vecchia et al., 2014). A recent study concluded that although *D. reducens* does not appear to gain energy directly from the reduction of Fe(III) during fermentative growth on pyruvate, the Fe(III) serves as an electron sink, relieving thermodynamic

limitations of fermentation resulting from H_2-buildup. Furthermore, the study suggested that direct contact was not required for the reduction of insoluble Fe(III), and riboflavin and small amounts of FMN (flavin mononucleotide) in spent media were identified as potential electron shuttles (Dalla Vecchia et al., 2014). However, no insights regarding enzymes involved in Fe(III) reduction were provided in that study. Another unique capability of *D. reducens* following growth with pyruvate is U(VI) and Fe(III)-citrate reduction in the sporulated state, relevant to particular environments where conditions may vary dramatically over time (Junier et al., 2009).

The genome of *D. reducens* has been sequenced and contains only one operon annotated as a c-type cytochrome, encoded by the two genes Dred_0700 and Dred_0701 (Junier et al., 2010). However, all evidence to date suggests that this cytochrome is not involved in metal reduction. A transcriptomic study comparing gene expression in *D. reducens* when grown fermentatively with pyruvate versus pyruvate and U(VI) did not find differential expression of this c-type cytochrome (Junier et al., 2011). Furthermore, qRT-PCR analysis targeting Dred_0700 and Dred_0701 found expression levels to be around two orders of magnitude lower during Fe(III) reduction as compared with pyruvate fermentation. This study also failed to detect any peptides corresponding to the c-type cytochrome under Fe(III) reduction or fermentative conditions (Dalla Vecchia et al., 2014). Studies in our lab support these findings. Isobaric tag for relative and absolute quantitation (iTRAQ) based proteomic analysis of duplicate cultures of *D. reducens* grown with Fe(III)-citrate, pyruvate, and sulfate identified over 22,000 unique peptides. None of the detected peptides correspond to either gene encoding the c-type cytochrome (unpublished data).

A member of the Peptococcaceae family, *D. reducens* is a close relative of other environmentally relevant metal and radionuclide reducing Firmicutes, namely *Desulfosporosinus*

and *Desulfitobacterium* species (Suzuki et al., 2004; Kim et al., 2012). No metal-reducing proteins have yet been described in any of these three genera. Our major objective of this study was to identify proteins capable of iron reduction from the proteome of *D. reducens*. Not only were iron reductases identified and confirmed through heterologous expression, but these reductases were also shown to reduce soluble Cr(VI) (in the form of sodium dichromate) and U(VI) (in the form of uranyl acetate). To the best of our knowledge, this is the first report identifying and validating metal reductases from a Gram-positive organism through heterologous expression.

Results

To accomplish our objective, we optimized and applied an efficient and high-resolution, non-denaturing protein separation workflow that allows for the purification of functional proteins and protein complexes. Resulting protein fractions were screened for iron reduction activity using a colorimetric assay for Fe(II), based on the reagent ferrozine, where the reduction of Fe(III)-NTA with NADH as electron donor was monitored. Subsequent LC-MS/MS analysis was performed, leading to the identification of proteins/protein complexes capable of iron reduction from the proteome of *D. reducens*. An overview of our implemented workflow is summarized in **Figure 2.1**. Proteins/protein complexes identified by this technique were then selected for functional validation by heterologous expression and biochemical characterization.

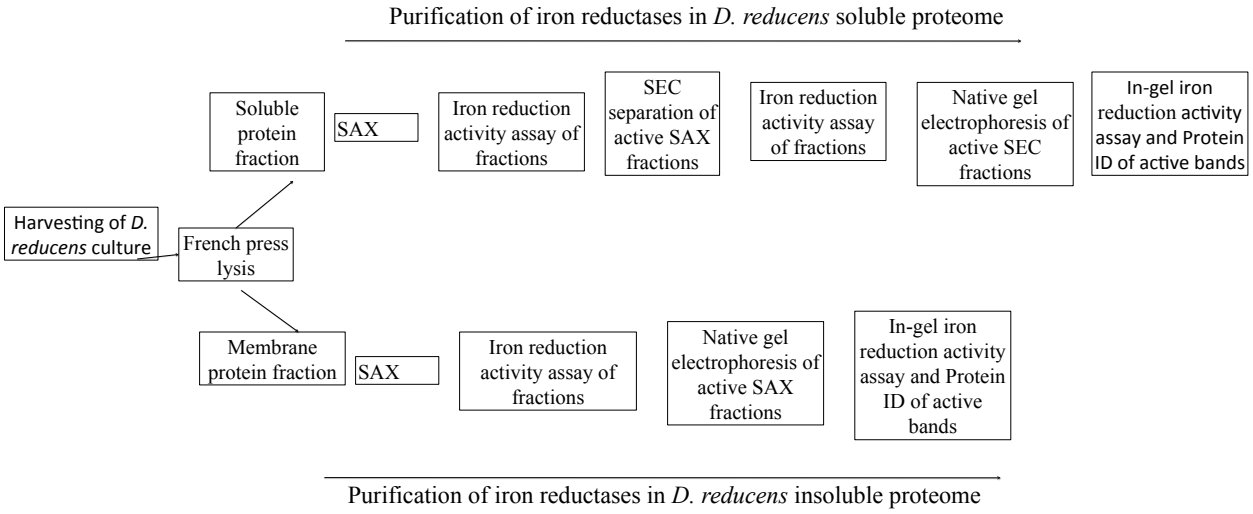

Figure 2.1: Workflow implemented to identify iron reduction candidate proteins in *D. reducens:* A series of non-denaturing protein separation steps, with a screen for iron reduction activity following each step, was implemented in order to identify iron reductases from the proteome of *D. reducens*. SAX= strong anion exchange chromatography. SEC= size exclusion chromatography.

The D. reducens proteome under sulfate-reducing conditions confers an Fe(III) reducing phenotype

Initial proteomic separations were attempted with *D. reducens* cells grown with Fe(III)-citrate as electron acceptor and lactate as electron donor. However, attempts to extract active proteins from these cells were unsuccessful due to interference with Fe-precipitates. Therefore, cell culture conditions were modified to growth with sulfate as electron acceptor. Before protein separations were performed, cell suspension experiments were carried out to confirm Fe(III) reduction capability under these experimental culture conditions. Washed *D. reducens* cells grown with 28 mM sulfate and 20 mM lactate were shown to reduce Fe(III)-NTA immediately

(Figure 2.2), suggesting that the sulfate-grown *D. reducens* proteome is capable of Fe(III) reduction. Reduction was dependent on lactate, although controls without lactate displayed a small amount of reduction. A likely explanation for Fe(III)-NTA reduction by live *D. reducens* cells lacking added electron donor is utilization of stored electrons. *D. reducens* was recently predicted to contain a type of capacitor that stores reducing equivalents for later reduction of Fe(III) (Dalla Vecchia et al., 2014).

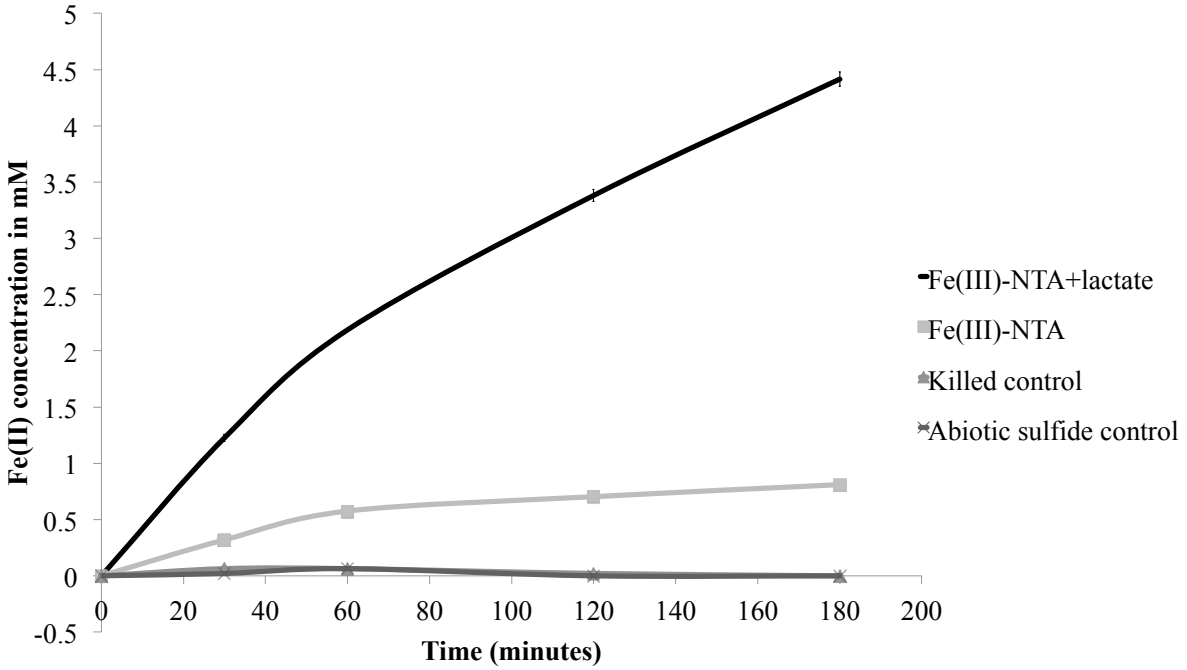

Figure 2.2: Fe(III) reduction by *D. reducens* cell suspensions grown on sulfate reduction: Washed cell suspensions of *D. reducens* grown with 28 mM sulfate and 20 mM lactate were tested for iron reduction capability and shown to express the proteome necessary for immediate dissimilatory reduction of Fe(III)-NTA. Cells killed by boiling and an abiotic sulfide control determined by the concentration of sulfide measured following cell washing (0.25 mM) demonstrated lack of iron reduction capability. Cell concentration was $3x10^9$ cells/mL, equal to a protein concentration of ~0.9 mg/mL of protein assuming 60% protein per cell dry mass. Error bars display standard error duplicate reactions.

Recovery of iron reduction activity in extracted proteins

Following protein extraction, the soluble and insoluble proteomes of *D. reducens* were analyzed through implementation of the workflow outlined in **Figure 2.1.** Iron reduction activity

obtained from the total soluble and insoluble fractions was quantified and is reported as nmol Fe(II) formed/minute and specific activity (nmol Fe(II) formed/mg protein/minute) (**Table 2.1**). The specific activity in the insoluble fraction is nearly two times that of the soluble fraction (22.42 versus 12.64 nmol Fe(II) formed/mg protein/minute).

Sample	Protein Concentration (mg/mL)	Iron Reduction Activity (nmol Fe(II) formed/ minute)	Specific Activity (nmol Fe(II) formed/mg protein/minute)
Soluble (S) fraction	**5.45**	2.07	12.64
Insoluble (IS) fraction	**1.21**	0.81	22.42
S Peak 1: SAX 16'	<0.125	0.79	>210.82
S Peak 1: SAX 16' SEC 9.5’	<0.125	0.50	>132.14
S Peak 2: SAX 31-32'	<0.125	0.19	>50.09
S Peak 2: SAX 31-32' SEC 10.5’	<0.125	0.16	>43.94
IS Peak 1: SAX 31'	<0.125	0.08	>22.16

Table 2.1: Recovery of iron reduction activity in protein fractions: Specific iron reduction activity is calculated for protein fractions using the iron reduction activity assay. Nearly twice the specific iron reduction activity was recovered in the total insoluble fraction versus the soluble fraction. Specific activities described as “>” values were limited in precision due to below detect protein concentrations as determined by Bradford assay. SAX= anion exchange chromatography. SEC= size exclusion chromatography.

i. Soluble protein fraction: The soluble proteome of *D. reducens* was separated using a series of three non-denaturing separation steps: strong anion exchange chromatography (SAX), size exclusion chromatography (SEC), and native gel electrophoresis. Iron reduction activity was screened for following each subsequent separation. Following SAX separation of the soluble protein fraction, peaks of iron reduction activity were recovered at 13’, 16’, 31-32’, and 47-48’,

depicted by the gray line plotted in **Figure 2.3a**. These fractions were selected for high-resolution SEC separation, and iron reduction activity was retained following separation of both SAX 16' and 31-32' fractions, identified as Peak 1 and 2 respectively in **Figure 2.3a**, but not from the other fractions. The SEC-separated 16' SAX fraction produced a peak of iron reduction activity in the 9.5' SEC fraction, and the third dimension of separation (native gel electrophoresis followed by the in-gel activity assay) led to the identification of an iron reductase band (~280 kDa) visualized as a pink band due to the formation of the ferrozine-Fe(II) complex (**Figure 2.3b).** After analysis of in-gel digests of the active gel-band by LC-MS/MS and based on detection of at least two unique peptides, four proteins were identified including NADH:flavin oxidoreductase (Dred_2421), oligoendopeptidase F (Dred_2457), acetyl-CoA acetyltransferase (Dred_1784), and sulfate adenylyltransferase (Dred_0635) **(Supplementary Table 2.1a).**

The SAX 31-32' fraction (Peak 2 in **Figure 2.3a**) was further separated with SEC and produced a peak of activity in the 10.5' SEC fraction. Native gel electrophoresis followed by the in-gel activity assay indicated an iron reductase band at ~244 kDa **(Figure 2.3c),** again visualized as a pink band**.** LC-MS/MS identified four proteins in the excised band by at least two unique peptides including oxidoreductase FAD/NAD(P)-binding subunit (Dred_1685), dihydroorotate dehydrogenase 1B (Dred_1686), 4Fe-4S ferredoxin (Dred_0137), and pyruvate flavodoxin/ferredoxin oxidoreductase domain-containing protein (Dred_0047) **(Supplementary Table 2.1b).** Specific iron reduction activity of active fractions identified following separation of the soluble proteome is reported in **Table 2.1**. Due to protein concentrations below the detection limit of the Bradford assay, specific activities could only be approximated in separated fractions.

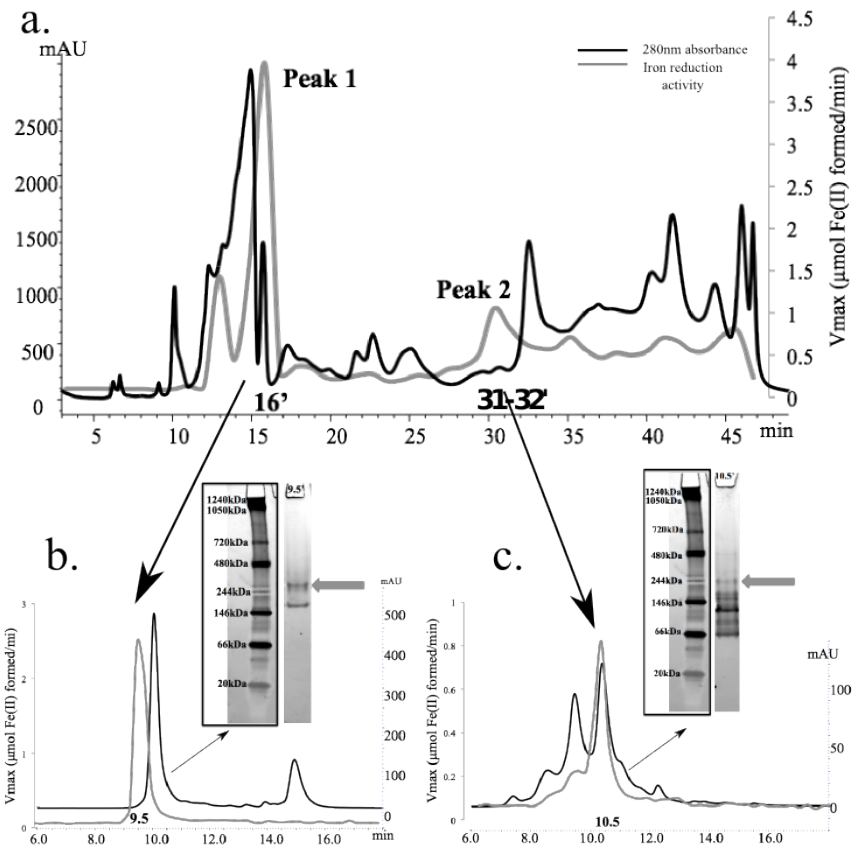

Figure 2.3: Identification of iron reduction activity in the soluble proteome of *D. reducens*: Protein concentration (determined by absorbance at 280nm and presented as mAU) is represented by the black chromatogram, while the gray line presents an overlay of iron reduction activity (µmol Fe(II) formed/minute). **a.** SAX separation of the soluble protein fraction led to the recovery of two dominant iron reduction peaks that are maintained through two subsequent dimensions of separation. **b.** SEC separation of Peak 1 (SAX 16' fraction) led to the recovery of iron reduction activity in fraction 9.5'. Further separation with native gel electrophoresis recovered an active iron reductase band (visualized as a pink band at ~280 kDa, designated by gray arrow). SEC separation of Peak 2 (SAX 31-32' fraction) led to the recovery of iron reduction activity in fraction 10.5'. Further separation with native gel electrophoresis recovered an active iron reductase band (visualized as a pink band at ~244 kDa, designated by gray arrow). SAX= strong anion exchange chromatography. SEC= size exclusion chromatography.

ii. Insoluble protein fraction: The insoluble proteome of *D. reducens,* which was extracted in the presence of the detergent n-Dodecyl β-D-maltoside (DDM), was separated using two non-denaturing separation steps, including SAX and native gel electrophoresis. Previous experiments with all three phases of separation led to a loss of Fe(III) reduction activity in the insoluble fraction, and for this reason the SEC step was excluded from this workflow. Following SAX, a dominant activity peak was recovered at 31' **(Figure 2.4).** Further separation of the 31' fraction with native gel electrophoresis led to the identification of an iron reductase band at ~244 kDa **(Figure 2.4).** The subsequent LC-MS/MS analysis of the gel band identified five proteins based on at least two unique peptides, including again the proteins Dred_1685 and Dred_1686. The

other proteins identified were ATP synthase F1 subunit alpha (Dred_3152), GntR family transcriptional regulator (Dred_0095), and adenylylsulfate reductase subunit alpha (Dred_0637) **(Supplementary Table 2.1c)**. Specific iron reduction activity of the active fraction identified following separation of the insoluble proteome is reported in **Table 2.1**. Because protein concentration was below the detection limit of the Bradford assay, specific activity could only be approximated in this fraction.

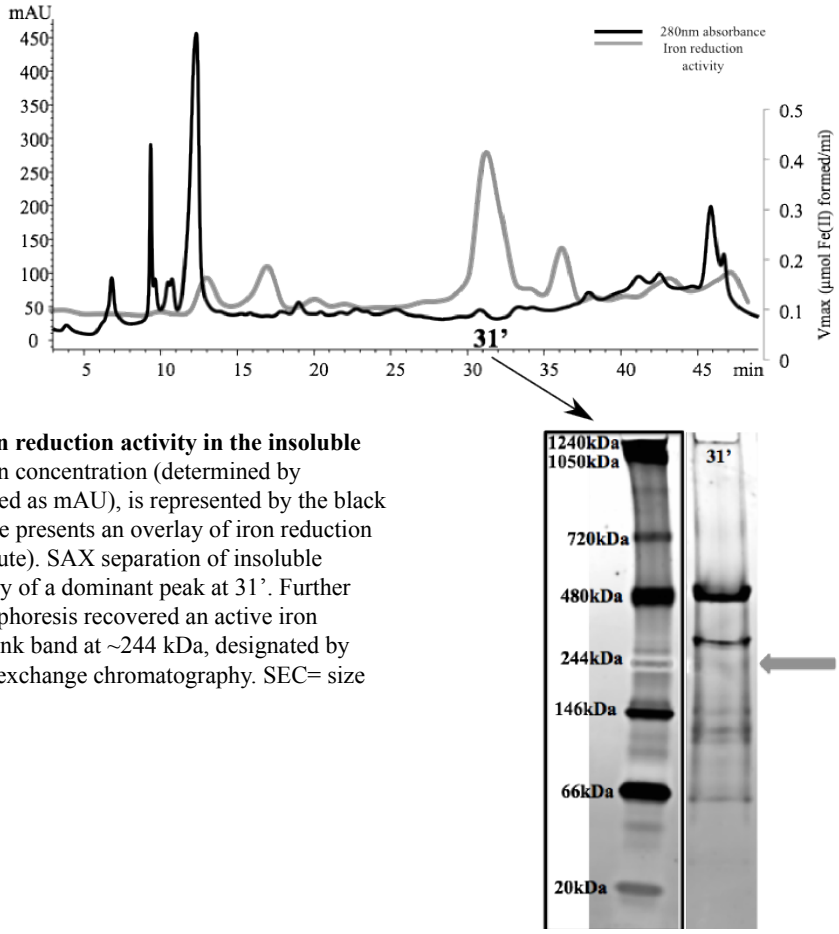

Figure 2.4: Identification of iron reduction activity in the insoluble proteome of *D. reducens*: Protein concentration (determined by absorbance at 280nm and presented as mAU), is represented by the black chromatogram, while the gray line presents an overlay of iron reduction activity (µmol Fe(II) formed/minute). SAX separation of insoluble protein fraction led to the recovery of a dominant peak at 31'. Further separation with native gel electrophoresis recovered an active iron reductase band (visualized as a pink band at ~244 kDa, designated by gray arrow). SAX= strong anion exchange chromatography. SEC= size exclusion chromatography.

Heterologous expression and characterization of metal reductase capability

The workflow outlined in **Figure 2.1** led to short lists of potential iron reductases from the proteome of *D. reducens* (**Supplementary Table 2.1)**. In order to confirm iron reductase

activity, targets were selected for heterologous expression and affinity purification. Following tests for iron reduction activity, further characterization was performed.

i. Confirmation of iron reduction activity: From peak 1 of the soluble fraction, Dred_2421 (NADH: flavin oxidoreductase) was selected as the primary target for heterologous expression based on the highest protein score and its annotation as the sole oxidoreductase from the list **(Supplementary Table 2.1a)**. An SDS gel of heterologously expressed and purified Dred_2421 confirmed its predicted molecular weight of ~72 kDa (**Supplementary Figure 2.1)**. The purified protein was yellow in color due to bound flavin, and both FMN and FAD (flavin adenine dinucleotide) were detected with reversed-phase high performance liquid chromatography **(Supplementary Figure 2.2).**

Tests for iron reduction activity were performed, and Dred_2421 was confirmed as an iron reductase (**Figure 2.5**). Activity was found to be NADH-dependent, as Dred_2421 does not use NADPH as an electron donor. The specific activity was calculated (based on the first 6 minutes of the iron reduction activity assay following Fe(III)-NTA injection), and is displayed in **Table 2.2.** Based on recovery of the active band at ~280 kDa in the native gel **(Figure 2.3b)**, we predict that Dred_2421 (~72 kDa) functions as a homotetramer.

Locus Tag	Peak identified from (corresponding to Table 1)	Specific Activity (nmol Fe(II) formed/mg protein/minute)
Dred_2421	S Peak 1	361.95
Dred_1685-1686	S Peak 2, IS Peak 1	627.68

Table 2.2: Iron reduction activity in heterologously expressed proteins: Specific iron reduction activity is calculated for heterologously expressed and purified proteins identified in fractions described in Table 1. Micromoles of Fe(II) formed per minute were calculated based on the first 6 minutes (following Fe(III) injection) of the reactions displayed in Figures 5 and 6.

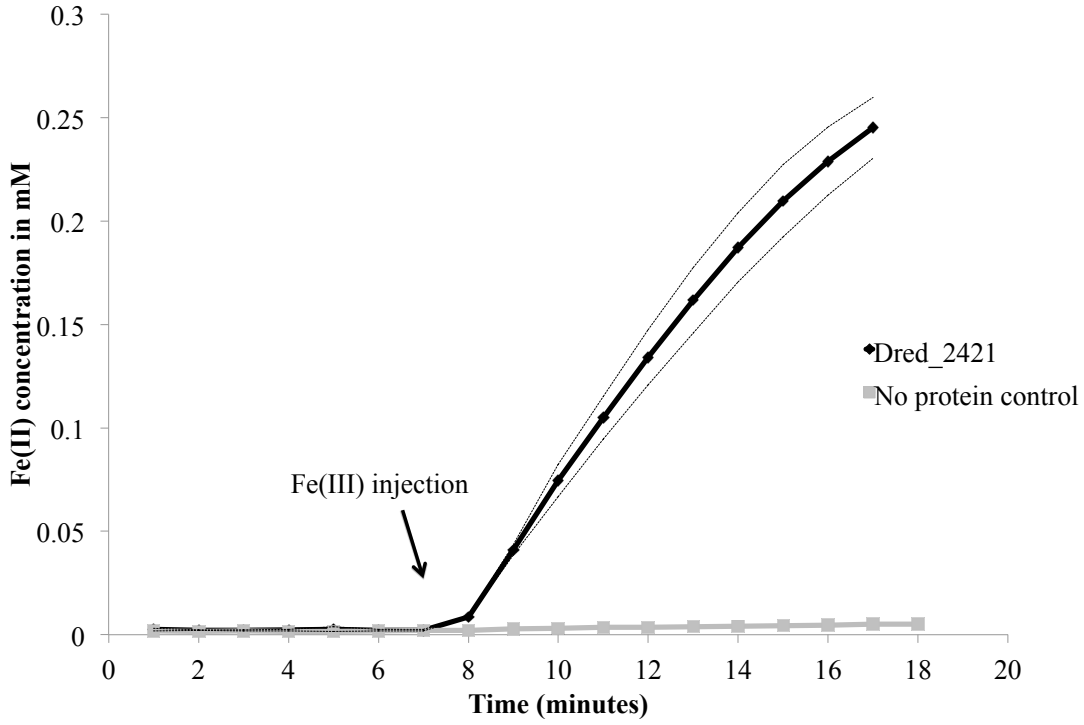

Figure 2.5: Iron reduction by Dred_2421: Following heterologous expression and purification of Dred_2421, iron reduction capability was confirmed using the iron reduction activity assay. 0.5 mM Fe(III) was added at 7 minutes. The dotted lines display standard deviation across triplicate reactions. Reactions contained 1 µM Dred_2421 and 0.2 mM NADH as electron donor.

Dred_1685 and Dred_1686 were two other primary targets for heterologous expression based on their predicted annotations involving oxidoreductase activity as well as their identification in protein lists from Peak 2 of the soluble fraction as well as in the insoluble fraction peak **(Supplementary Table 2.1b and 2.1c).** Matching charge and size evidence leading to these protein lists (31-32' or 31' SAX fraction from the soluble and insoluble fractions respectively and ~244 kDa in both in-gel activity assays) supports that the same iron reductase was active in peak 2 of the soluble fraction and the insoluble fraction peak **(Figures 2.3 and 2.4).** Both individual proteins were expressed successfully. Dred_1685 was brownish in color, consistent with its annotated 2 iron, 2 sulfur cluster binding activity (https://img.jgi.doe.gov/).

Dred_1686 was yellow in color, suggesting the presence of bound flavin. The iron reduction activity assay was initially performed with purified Dred_1685 and Dred_1686 expressed separately, and no iron reduction activity for each individual protein was observed (**Figure 2.6)**. However, upon mixing of the two purified proteins, iron reduction was observed, providing evidence that the two proteins form a complex. In order to confirm this prediction, Dred_1685 and Dred_1686 were co-expressed on a single plasmid with a His_6-tag only on Dred_1685. Nickel affinity column purification followed by SDS-PAGE electrophoresis resulted in the identification of two distinct protein bands of appropriate size (29 kDa for Dred_1685 and 32 kDa for Dred_1686), confirming the formation of a complex and suggesting a 1:1 stoichiometry **(Supplementary Figure 2.3)**. The iron reduction activity assay demonstrated iron reduction capability in this complex **(Figure 2.6).** The specific activity was calculated (based on the first 6 minutes of the iron reduction activity assay following Fe(III)-NTA injection), and is displayed in **Table 2.2.** NADPH was also used as an electron donor for Fe(III)-NTA reduction by the Dred_1685-1686 complex, but at a rate nearly 5 times slower over the first 6 minutes than that calculated with NADH as electron donor. Based on the predicted size of the active complex in native gels (~244 kDa), we predict the complex is a heterooctamer consisting of four molecules from each of the two proteins.

In order to thoroughly investigate proteins identified in the fractions with iron reduction activity, other proteins whose annotations suggested potential involvement were heterologously expressed. This included pyruvate flavodoxin/ferredoxin oxidoreductase domain-containing protein (Dred_0047), which was identified in peak 2 of the soluble fraction. Following heterologous expression and purification, Dred_0047 was found to not be able to reduce iron. Dred_0137, a 4Fe-4S ferredoxin, was also selected for heterologous expression, but multiple

mutations throughout the cloning process have prevented expression, meaning Fe(III) reduction capability could not be tested. Although Dred_0637 was identified in the insoluble fraction peak and has an annotation as an oxidoreductase (adenylylsulfate reductase subunit alpha), it was not selected as it had a low protein score and its predicted involvement in the sulfate reduction pathway suggests that its presence in the active gel band was incidental.

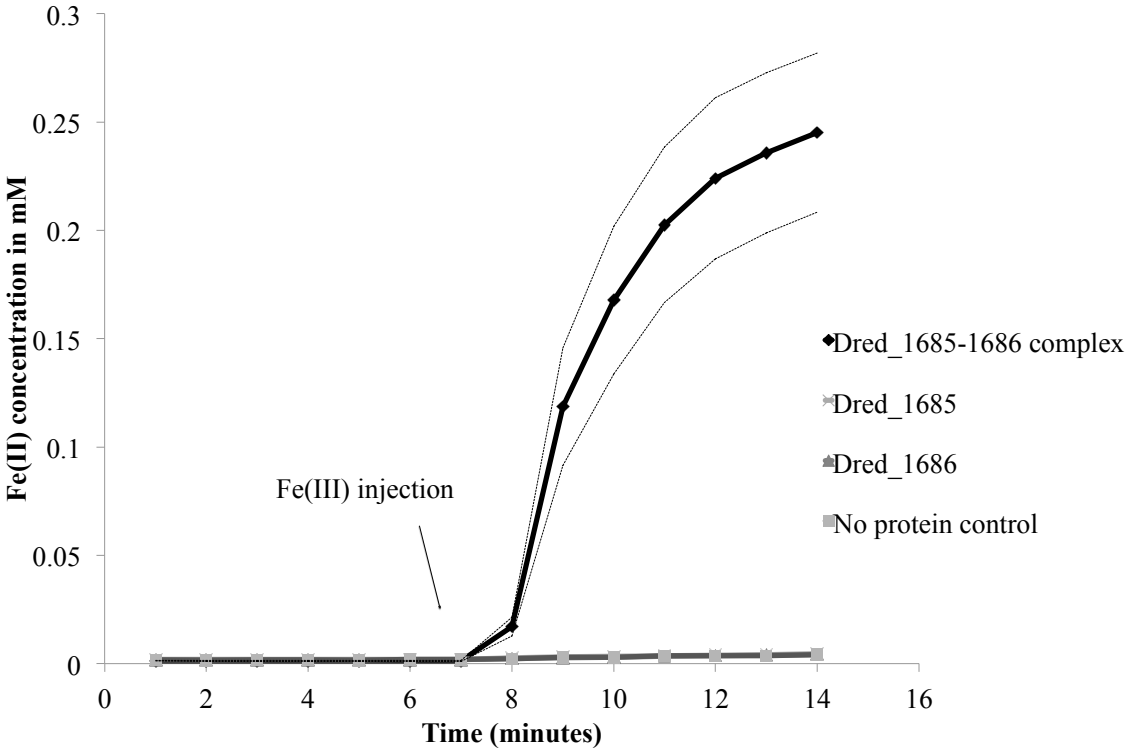

Figure 2.6: Iron reduction by Dred_1685-1686 complex: Following heterologous expression and copurification of Dred_1685 and Dred_1686, iron reduction capability was confirmed using the iron reduction activity assay. 0.5mM Fe(III)-NTA was added at 7 minutes. The copurified complex is necessary for iron reduction, as Dred_1685 and Dred_1686 individually do not demonstrate iron reduction capability. The dotted black lines display the standard deviation across triplicate reactions. Reactions contained 1 μM of purified proteins and 0.2 mM NADH as electron donor.

ii. Discovery of Cr(VI) and U(VI) reductase capability: As *D. reducens* is capable of reducing contaminant heavy metals and radionuclides, specifically Cr(VI) and U(VI), the discovered Fe(III) reductases were tested for soluble Cr(VI) (in the form of sodium dichromate) and U(VI) (in the form of uranyl acetate) reduction capability. For both metals, colorimetric assays were

employed and the disappearance of the +6 oxidation state was monitored. Both Dred_2421 and the Dred_1685-1686 complex were capable of Cr(VI) reduction with NADH as electron donor **(Figure 2.7)**. As we found that NADH was capable of some abiotic Cr(VI) reduction, we added 1 mM NADH in two steps, first at time zero and then at 80 minutes, in order to best visualize enzymatic reduction. The individual proteins Dred_1685 and Dred_1686 resembled the no protein control, again providing evidence that Dred_1685 and Dred_1686 form a functional complex that is capable of metal reduction.

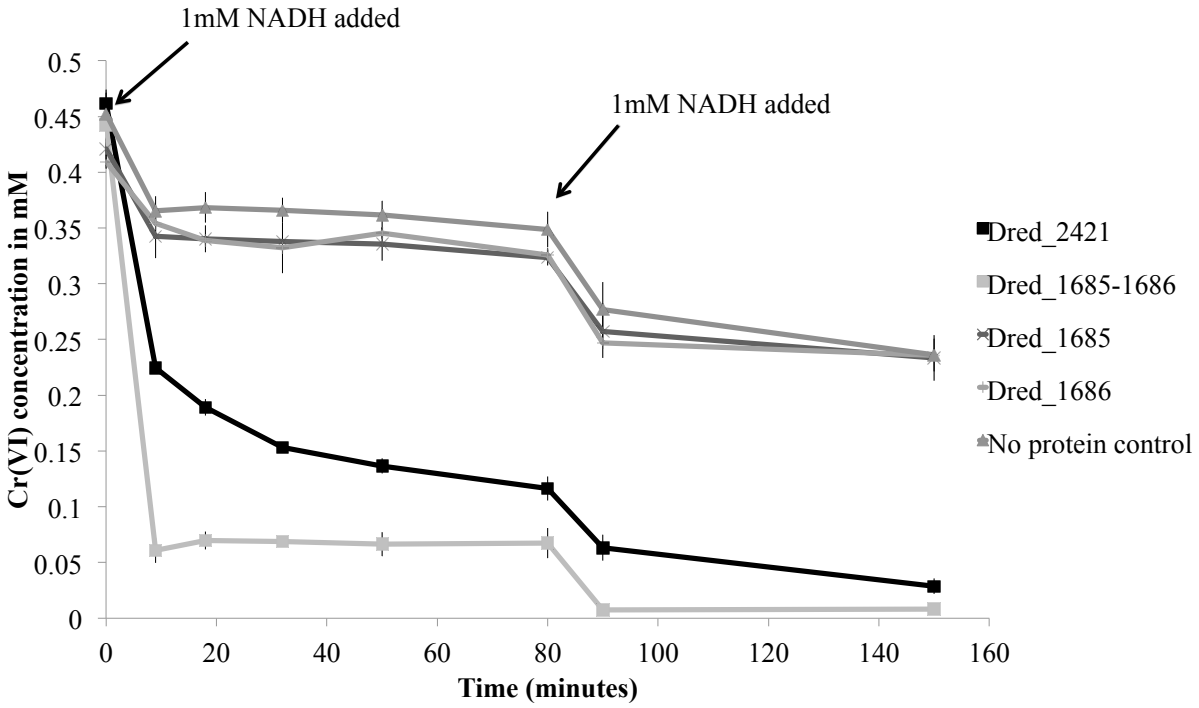

Figure 2.7: Cr(VI) reduction by Dred_2421 and Dred_1685-1686 complex: The disappearance of Cr(VI) over time is monitored based on the diphenylcarbazide method. In order to reduce the effects of abiotic reduction by NADH, only 1mM NADH was added at time zero. After an additional 1mM NADH was added at 80 minutes, complete Cr(VI) reduction is observed for both Dred_2421 and the Dred_1685-1686 complex. Individual Dred_1685 and Dred_1686 proteins resembled the no protein control. Reactions contained 2 μM purified proteins.

Discovered Fe(III) reductases were also tested for the capability to reduce U(VI) with NADH as electron donor. Both Dred_2421 and the Dred_1685-1686 complex displayed U(VI)

reductase activity **(Figure 2.8)**. As expected, the single proteins Dred_1685 and Dred_1686 were not capable of U(VI) reduction. As U(IV) can be oxidized back to U(VI) by oxygen, we exposed our reactions to air following the experiment. Re-oxidation of the reactions following U(VI) reduction provides further support that U(VI) was indeed being reduced, rather than simply disappearing from solution due to sorption **(Supplementary Figure 2.4).**

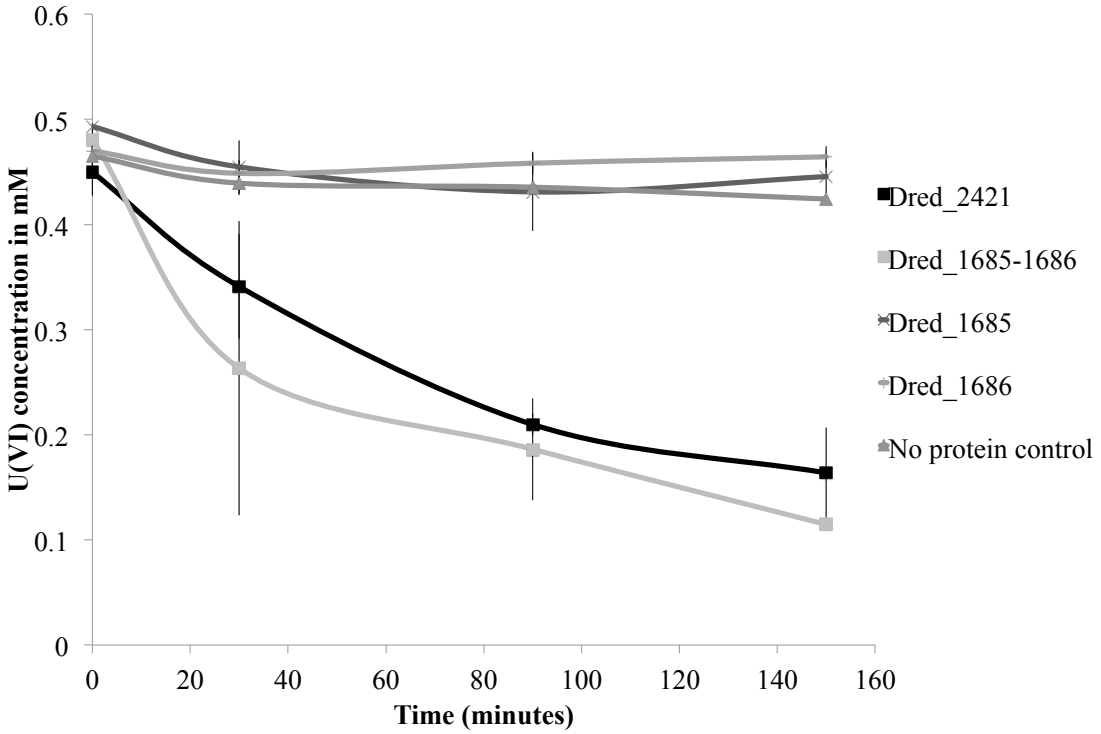

Figure 2.8: U(VI) by Dred_2421 and Dred_1685-1686 complex: The disappearance of U(VI) over time is monitored using a method dependent on the reagent Arsenazo-III. Individual Dred_1685 and Dred_1686 proteins resembled the no protein control. Reactions contained 10 μM purified proteins.

Discussion

The field of microbial metal reduction is dominated by studies in Gram-negative bacteria whose genomes encode an abundance of multiheme c-type cytochromes. Our aim was to discover enzymes capable of iron reduction in *D. reducens*, an organism that encodes only a

single c-type cytochrome in its genome and is phylogenetically distinct from the model metal reducers. This led to the identification of a protein and a protein complex that are not only capable of reducing Fe(III)-NTA but also Cr(VI) and U(VI) with NADH as electron donor. Proteomic studies combined with protein biochemistry, as seen here, are essential in order to validate existing genome annotations and/or discover new functional annotations in uncharacterized organisms such as *D. reducens*, rather than relying on automated curation. Our separation methods were designed with the goal of maintaining the *D. reducens* proteome at a functional level. While it is possible that complexes or interacting complexes necessary for activity were broken up, the identification of two proteins that require the formation of a complex for iron reductase activity (Dred_1685 and Dred_1686) points towards the success of our methods. The non-denaturing separation workflow described allows rapid and high-resolution protein fractionation and can be employed for a diverse range of functional screens in a variety of organisms in the future.

Based on the lack of understanding of energy-producing processes in *D. reducens,* or the physiologically relevant electron donor for Fe(III) reduction, NADH was selected as an electron donor based on previous studies in model organisms (Magnuson et al., 2001; Elias et al., 2007). As such, the use of NADH as electron donor to screen for iron reduction activity leads to inherent selectivity towards NADH-dependent oxidoreductases, and thus it is uncertain whether the identified proteins have a physiologically relevant role in metal reduction. It is possible that these proteins are involved in the recently described thermodynamic relief mechanism when *D. reducens* is grown fermentatively with pyruvate, where Fe(III) reduction serves as an electron dump rather than an energy-deriving process (Dalla Vecchia et al., 2014). It is unclear at this time whether this is also the case for Fe(III) reduction by *D. reducens* with lactate as electron

donor, although the original isolation paper reports use of Fe(III) by *D. reducens* as a true electron acceptor under these conditions (Tebo and Obraztsova, 1998). However, preliminary evidence suggests that *D. reducens* is not using its annotated Type 1 NADH dehydrogenase (Dred_2036-2046) in a classic respiration sense when grown on Fe(III)-citrate and lactate. Under this growth condition, global proteomic analysis detected only one of the 11 subunits of the NADH dehydrogenase operon (unpublished data). Additional studies are required in order to elucidate catabolic processes in *D. reducens*, and genetic inactivation studies are necessary in order to provide a link between the proteins identified in this study and an *in vivo* role in metal reduction. However, without a genetic system currently available, our study serves as an initial functional survey of a poorly characterized proteome and has identified Fe(III)-NTA, Cr(VI), and U(VI) reductase activity in a protein and protein complex distinct from described metal reductases.

One of the proteins identified in this study, Dred_2421, is a soluble protein classified as an Old Yellow Enzyme (OYE). The first class of flavin-dependent enzymes identified, this group has been studied for many years, but physiological roles remain elusive (Williams and Bruce, 2002). Previous reports have identified iron reduction capability in proteins annotated as flavin oxidoreductases, but these are described as assimilatory iron reductases and require the addition of exogenous flavin (Fontecave et al., 1994; Vadas et al., 1999; Mazoch et al., 2004). Dred_2421, however, contains tightly bound flavins (FMN and FAD, as shown in **Supplementary Figure 2.2**) and reduces Fe(III)-NTA without the addition of exogenous flavin. In fact, tests adding exogenous riboflavin did not increase rates of Fe(III)-NTA reduction by Dred_2421. Based on the annotation of Dred_2421 as an NADH:flavin oxidoreductase, as well as the predicted involvement of riboflavin and FMN in Fe(III) reduction in *D. reducens* when grown on pyruvate,

Dred_2421 was tested for the ability to reduce riboflavin and FMN with NADH as electron donor (Dalla Vecchia et al., 2014). Neither flavin was reduced by Dred_2421, further supporting the role of Dred_2421 as a metal reductase.

Dred_2421 is predicted to be in its own operon, and in fact on the genome falls in the middle of a region encoding genes predicted to be involved in flagella-related processes. This presumable genetic rearrangement is not conserved in any other sequenced *Desulfotomaculum* species (https://img.jgi.doe.gov/). Interestingly, the twelve proteins with highest sequence similarity to Dred_2421 (60-80% identity across 99% query coverage) are all from species of *Desulfosporosinus* and *Desulfitobacterium,* both genera of Gram-positive metal reducers (http://blast.ncbi.nlm.nih.gov/). No studies have investigated pathways of Fe(III) reduction in either of these two genera. Close relatives of *D. reducens*, we predict that similar metal reductase activity would be found in these *Desulfosporosinus* and *Desulfitobacterium* NADH:flavin oxidoreductases. *E. coli* species encode an orthologous protein to Dred_2421 (36% identity across 98% query coverage), and the crystal structure has been solved (Hubbard et al., 2003, http://blast.ncbi.nlm.nih.gov/). This protein was heterologously expressed and purified by our group and found to lack Fe(III)-NTA reduction with both NADH and NADPH as electron donor (unpublished data). This finding supports the possibility that Dred_2421 has a specifically evolved physiological role as a metal reductase. Furthermore, a published transcriptomic study, with microarray data deposited at NCBI's Gene Expression Omnibus, compares conditions of *D. reducens* grown with pyruvate versus pyruvate and U(VI) (Junier et al., 2011). Dred_2421 is increased in expression on U(VI) conditions by ~1.3 times during both mid and late exponential phase (http://www.ncbi.nlm.nih.gov/geo/).

Our studies also identified a complex capable of Fe(III), Cr(VI), and U(VI) reduction, composed of Dred_1685 and Dred_1686. This complex was recovered from both the soluble as well as the insoluble (presumably membrane) protein fraction. These genes are predicted to be involved in the fourth step of pyrimidine biosynthesis, oxidizing dihydroorotate to orotate with NAD^+, and are in a predicted operon composed of Dred_1685-9. This operon is conserved across five sequenced species of *Desulfotomaculum*. One of these is the only other known Fe(III) reducing species in the genus, *Desulfotomaculum hydrothermale*, while tests of Fe(III) reduction aren't reported in the literature for the other four species. This operon includes a lipoprotein signal peptidase, which is predicted to be localized to the cytoplasmic membrane according to PSORTb (Yu et al., 2010). This peptidase is missing in other sequenced *Desulfotomaculum* species including *Desulfotomaculum acetoxidans*, a species tested and unable to reduce Fe(III) based on a 1993 paper and confirmed in studies in our lab (Lovley et al., 1993).

Other studies have found dihydroorotate dehydrogenase 1B (the annotation for Dred_1686) and homologs of Dred_1685 (annotations vary) to form a complex that is required for functionality. For instance, in the Gram-positive bacterial model for these proteins (*Lactococcus lactis*), a homolog of Dred_1686 (51 % identity across 95% query coverage) and a homolog of Dred_1685 (34& identity across 93% query coverage) form a complex that is required for a functional enzyme (http://blast.ncbi.nlm.nih.gov/). However, in *L. lactis* this complex is predicted to be a heterotetramer, while our findings support the formation of a heterooctamer based on the molecular weight of the active complex in native gels (Nielsen et al., 1996). Furthermore, dihydroorotate dehydrogenase 1B in Gram-positive organisms like *L. lactis* and *D. reducens* are grouped into Type 1 dihydroorotate dehydrogenases, which are predicted to be localized to the cytosol. Type 2 dihydroorotate dehydrogenases, on the other hand, are

associated with the inner membrane (Nørager et al., 2002). We recovered Dred_1685 and Dred_1686 in both the soluble and insoluble fractions. The insoluble protein fraction was thoroughly washed following separation from the soluble fraction, demonstrated by the lack of carryover of the most active soluble peak following SAX separation (peak 1 in **Figure 2.3a**) into the insoluble fraction. Therefore, we believe the localization of Dred_1685 and Dred_1686 to both the soluble and insoluble fraction is a true result and supports the claim that this complex is in some way associated with the membrane, in contrast to other Type 1 dihydroorotate dehydrogenases.

As with Dred_2421, the Dred_1685-1686 complex was found to not have riboflavin or FMN reduction capability with NADH as electron donor, nor was Fe(III)-NTA reduction enhanced with addition of exogenous riboflavin. A small increase was seen in the expression of Dred_1685 and Dred_1686 on pyruvate versus pyruvate and U(VI), based on the available transcriptomic data (http://www.ncbi.nlm.nih.gov/geo/). Furthermore, the Dred_1685-1686 complex is capable of using NADPH as an electron donor for Fe(III)-NTA reduction, although at a slower rate. These findings, along with the predicted role for Dred_1685 and Dred_1686 in pyrimidine biosynthesis, calls into question whether this complex is physiologically relevant to metal reduction. However, because it was identified as the most active fraction from the insoluble (presumably membrane) protein pool, it should not be discounted. In fact, in the study where a fraction containing OmcB, a characterized *in vivo* soluble and insoluble iron reductase, was originally purified from the membrane of *G. sulfurreducens*, specific activity was reported as 17.1 nmol Fe(II) formed/mg protein/minute (Magnuson et al., 2000). The specific activity of the insoluble/membrane fraction where Dred_1685-1686 was identified is >22.16 nmol Fe(II) formed/mg protein/minute (See **Table 2.1**). This specific activity is grossly underestimated, as

protein concentration was below detection but is clearly much lower than other fractions where concentration was also below detection (see **Figures 2.3 and 2.4**). The calculated specific activity of the Dred_1685-1686 complex following heterologous expression and purification is much higher, 627.68 nmol Fe(II) formed/mg protein/minute **(Table 2.2)**.

In conclusion, our studies employing functional screens of fractions of the *D. reducens* proteome have uncovered metal and radionuclide reductases that are quite distinct from the multiheme c-type cytochromes described in Gram-negative iron reducers. Further studies combining proteomic and biochemical techniques are essential for better elucidation of key functional enzymes in the proteome of *D. reducens* and other poorly characterized organisms.

Experimental procedures

Culturing

Desulfotomaculum reducens MI-1 was obtained from ATCC and cultured anaerobically with an 80/20 N_2/CO_2 headspace at 30° C on Widdel Low Phosphate (WLP) media minus pyruvic acid (Junier et al., 2009). Twenty mM sodium lactate (Fisher Scientific, Pittsburgh, PA USA) was added as electron donor with 25 mM Fe(III)-citrate (Santa Cruz Biotechnology, Inc., Dallas, TX USA) or 28 mM sodium sulfate (Fisher Scientific) as electron acceptor.

Iron reduction activity assay

Iron reduction activity of crude extracts and protein fractions was determined and screened for using a 96-well plate ferrozine-based assay described previously (Elias et al., 2007), where the reduction of Fe(III)-NTA with NADH as electron donor was monitored at 562nm. The reaction mixture contained 160 µL of assay buffer (40 mM $MgCl_2$ (Sigma-Aldrich, St. Louis, MO USA) 0.2 mM NADH (Thermo Fisher Scientific Acros Organics, Pittsburgh, PA USA) and

0.5 mM Ferrozine® Iron Reagent (J.T.Baker/Avantor Performance Materials, Inc., Center Valley, PA USA) in 100 mM HEPES (EMD Chemicals, Inc., San Diego, CA USA) (pH 7.0) with 10% (v/v) glycerol (Sigma-Aldrich) and 30 µL of sample. Ten µL of 10mM Fe(III)-NTA ($FeCl_3$ X $6H_2O$ (Fisher Scientific), Nitrilotriacetic acid (Sigma-Aldrich), $NaHCO_3$ (Fisher Scientific)) was added to commence the reaction. Absorbance of the ferrozine-Fe(II) complex was measured every 60 seconds over a 20 minute reaction time in a Spectra MAX plus spectrophotometer (Molecular Devices LLC, Sunnyvale, CA USA). The assay was also implemented for confirmation of iron reduction activity in purified proteins following heterologous expression (Tecan Infinite 200 series microplate reader, Tecan Group Ltd, Männedorf, Switzerland), and an N_2 headspace was used. Reactions were incubated in this N_2 atmosphere for 7 minutes prior to Fe(III)-NTA injection.

Whole cell experiments

The capability for sulfate-grown *D. reducens* cells to reduce Fe(III) was tested. Late exponential phase *D. reducens* cells grown with sulfate and lactate were harvested anaerobically, washed 3 times with HEPES buffer (100 mM HEPES (EMD Chemicals), 40 mM $MgCl_2$ (Sigma-Aldrich), 10% (v/v) glycerol (Sigma-Aldrich), pH 7.0) and resuspended in 3 mL of the buffer to a concentration of $3x10^9$ cells/mL. Residual sulfide was quantified using the Cline Assay in order to take into account any potential abiotic Fe(III) reduction (Strocchi et al., 1992). Ten mM Fe(III)-NTA and 10 mM lactate was added to the cell suspension, and the accumulation of Fe(II) over time was monitored using the ferrozine assay (Lovley and Phillips, 1987).

Soluble and insoluble protein fraction preparation

The soluble and insoluble proteome was prepared with modifications to a previously described protocol (Magnuson et al., 2000). Late exponential phase cells were harvested

anaerobically at 4°C, washed, and resuspended in 5 mL of Tris-HCl extraction buffer (50 mM Tris-HCl (J.T.Baker/Avantor), 2 mM $MgCl_2$ (Sigma-Aldrich) in 10% (v/v) glycerol (Sigma-Aldrich), pH 7) with protease inhibitor (cOmplete, Mini Protease Inhibitor Cocktail Tablets, Roche Applied Science, Indianapolis, IN USA). Following disruption with a French pressure cell at 8000 psi, unlysed cells were removed through centrifugation for 20 minutes at 7000g. Total protein extract in the supernatant was ultracentrifuged in a tabletop ultracentrifuge (Beckman Coulter, Brea, CA USA) at 100,000g for 60 minutes, the soluble fraction was removed to a separate tube, and the insoluble pellet was washed three times with Tris-HCl buffer and resuspended in 2 mL of Tris-HCl buffer with 0.5% wt/wt n-Dodecyl-β-D-maltoside (DDM) (Thermo Fisher Scientific Acros Organics). The insoluble protein fraction was extracted (solubilized) by stirring anaerobically at 4°C overnight and separated from unextracted protein by ultracentrifugation at 100,000g. Protein concentrations were quantified using the Bradford Assay (Bradford, 1976) (Thermo Scientific ™ Pierce ™ Coomassie (Bradford) Protein Assay, Fisher Scientific).

Strong anion exchange chromatography (SAX) separation

The soluble and extracted insoluble proteins were fractionated separately using strong anion exchange (SAX). SAX was performed on an Agilent 1100 Binary Solvent HPLC (Agilent Technologies, Inc., Wilmington, DE USA) using a Mono Q HR 5/5 column (GE Healthcare Bio-sciences, Pittsburgh, PA USA). All buffers were vacuum filtered through a 0.22 μm Durapore GV membrane (EMD Millipore Corporation, Billerica, MA USA) and stored at 4°C until use. A linear gradient (0-2-2.5-42-42.5-47.5-48-58 minutes, 0-0-5-50-75-75-0-0 % B) was employed using Buffer A (20 mM bis-tris (Sigma-Aldrich)/10% (w/v) glycerol (Fisher Scientific) pH = 6.9) and Buffer B (20 mM bis-Tris/1M sodium chloride (Fisher Scientific)/10% (w/v) glycerol

pH = 6.9). The flow rate was set to 0.5 mL/min and 100 µL injections were performed. All samples were filtered through a Costar Spin-X 0.22 µm cellulose acetate centrifuge tube filter (Corning Incorporated, Corning, NY USA) prior to injection. Column effluent was monitored by UV absorbance at 280nm. Manual fraction collection was performed at 1-minute intervals beginning at 2 minutes and ending at 49 minutes post-injection for a total of 48 fractions. Fractions were stored on ice until the assay for iron reduction activity, and active fractions were selected for subsequent separation.

Size exclusion chromatography (SEC) separation

Fractions from the soluble protein fraction that retained activity after SAX were filtered through a Costar Spin-X 0.22 µm cellulose acetate centrifuge tube filter and concentrated using an Amicon Ultra 0.5 mL 10K MWCO Ultracel regenerated cellulose centrifugal filter (EMD Millipore) to a final volume of <100 µL. Concentrates were diluted to ~200 µL with SEC running buffer prior to injection. SEC fractionations were carried out using a Dionex UltiMate 3000 HPLC (Dionex Corporation, Sunnyvale, CA USA) outfitted with the fraction collection option and operated in isocratic mode. A high-resolution aqueous SEC Yarra SEC-2000 column (3 µm, 4.6 X 250mm) with column-appropriate guard cartridges (Phenomenex, Inc., Torrance, CA USA) was used for sample fractionation. Column performance was checked periodically by injecting Aqueous SEC 1 Standard (Phenomenex). SEC running buffer contained 20 mM Tris-base (PlusOne, GE Healthcare Bio-sciences, Pittsburgh, PA USA), 2 mM $MgCl_2$ (Fisher Scientific), 150 mM NaCl (Fisher Scientific), and 10% (w/v) glycerol (Fisher Scientific) at pH = 6.8. Buffer was filtered as above and refrigerated prior to use. The maximum sample injection volume of 230 µL was used, the flow rate was set to 0.75 mL/min, and column effluent was monitored by dual wavelength UV absorbance at 230nm and 280nm. Fractions were collected in

0.5 mL 96-well microplates (Thermo Fisher Scientific Nunc A/S, Roskiide Denmark) at 15-second intervals beginning at 6 minutes and ending at 18 minutes and fractions were maintained at 4°C until the iron reduction activity assay. Active SEC fractions were selected for subsequent separation.

Native gel electrophoresis and in-gel activity assay

Active protein fractions selected following SAX or SEC separation were separated further with native gel electrophoresis using a discontinuous buffer system. For the native gel, the upper (cathode) buffer was 43 mM Tris-base (Fisher Scientific), 52 mM glycine (Fisher Scientific) adjusted to pH = 8.9 with hydrochloric acid (VWR International, West Chester, PA USA) in Milli-Q water (Millipore Corporation, Bedford, MA USA). The lower (anode) buffer was 120 mM Tris-base, 60 mM hydrochloric acid in Milli-Q water, pH = 8.1. The indicator running dye was bromophenol blue (Bio-Rad, Hercules, CA USA) saturated in water. The electrophoresis apparatus consisted of a Novex Mini-cell XCell Sure Lock PAGE unit (Life Technologies, Carlsbad, CA USA) connected to a PowerPac 300 power supply (Bio-Rad). Precast Tris-glycine gradient mini-gels, Novex 4-12% 1.5mm x 10 well or Novex 8-16% 1.0mm x 10 well were purchased from Life Technologies. Novex NativeMark Unstained Protein Standard (Life Technologies, Carlsbad, CA USA) was used as the molecular weight standard. Active fractions from SAX or SEC preparative runs (38 µL sample + 2 mL bromophenol blue solution) were loaded directly into the wells and 5 µL of molecular weight standard was used. Electrophoresis was performed at ambient temperature under constant voltage of 50V for 10 minutes, to allow the proteins to enter the gel and salts to dissipate, followed by separation at 125V for ~2 hours or until the dye front reached the bottom of the gel cassette. The developed gels were removed from the cassette, rinsed briefly in deionized water, and then an in-gel iron

reduction activity assay was subsequently performed, designed by modifying an existing protocol (Gaspard et al., 1998). Gels were submerged in the iron reduction activity assay buffer (described above) with 0.5 mM Fe(III)-NTA for 40 minutes. Protein bands with enzymes/enzyme complexes capable of Fe(III)-NTA reduction stained pink and were excised and transferred to a 0.6 mL microcentrifuge tube (low retention polypropylene, Fisher Scientific). Gel-fixing solution (200mL) consisting of 50% methanol/7% glacial acetic acid (Fisher Scientific) in Milli-Q water was added to each gel slice followed by incubation at room temperature for a minimum of 45 minutes with occasional vortexing. The fixing solution was removed and gel storage solution (10% methanol/7% glacial acetic acid in Milli-Q water) was added to submerge the gel bands and then stored at 4°C until in-gel reduction/alkylation/digestion. To visualize banding patterns, gels were fixed as above, rinsed with deionized water and stained overnight in Invitrogen SYPRO Ruby protein gel stain (Life Technologies). Stained gels were destained following manufacturer's recommended protocol and gel images were captured by a Typhoon 9400 Variable Mode Imager (GE Healthcare).

Protein identification by GeLC-MS/MS analysis

In-gel digestion (using modified trypsin from Promega (Madison, WI)) and tryptic peptide extraction were performed following a protocol from Shevchenko *et al.* 1996 and modified as described by Zhang *et al.* 2003 (Shevchenko et al., 1996; Zhang et al., 2003). All gel-extracted supernatants were combined and evaporated to dryness in a Speedvac SC110 (Thermo Savant, Milford, MA). Protein identification was carried out using nanoLC-MS/MS analysis with a Dionex UltiMate3000 system (Dionex, Sunnyvale, CA) and a hybrid triple quadrupole linear ion trap mass spectrometer, 4000 Q Trap from ABSciex (Framingham, MA). The gel-extracted peptides (5-10 μL) were injected onto a PepMap100 C18 trap column (5 μm,

100 Å, Dionex) at a flow rate of 20 μL/min for on-line desalting. They were then separated on a PepMap C18 RP nano column (3 μm, 75 μm x 15 cm, Dionex) and eluted in a 90-minute gradient of 5% to 40% acetonitrile in 0.1% formic acid at 300 nL/min. The 4000 Q Trap was equipped with Micro Ion Spray ion source II. MS data acquisition was performed using Analyst 1.4.2 software (Applied Biosystems) in the positive ion mode for information dependant acquisition (IDA) analysis. The nanospray voltage was 1.6 kV for all experiments in positive ion mode. Nitrogen was used as the curtain (value of 10) and collision gas (set to high) with heated interface on. The declustering potential was set at 50 eV and Gas1 was 20 (arbitrary unit). In IDA analysis, after each survey scan for *m/z* 400 to *m/z* 1550 and an enhanced resolution scan, the three highest intensity ions with multiple charge states were selected for tandem MS (MS/MS) with rolling collision energy applied for detected ions based on different charge states and *m/z* values. The exclusion time was set to 45 seconds.

MS/MS data generated from LC/ESI-based IDA analysis were submitted to Mascot 2.3 for database searching using an in-house licensed Mascot local server and the search was performed using the *D. reducens* MI-1 protein database (downloaded from NCBI on September 20th, 2012 with 3276 entries) with one missed cleavage site by trypsin allowed. The peptide tolerance was set to 1.5 Da and MS/MS tolerance was set to 0.6 Da. Carbobamidomethyl modification of cysteine and a methionine oxidation were set as variable modifications. Peptides with significant scores, defined with >95% identity based on Mascot probability analysis, were considered (Mascot server, Matrix Science).

Heterologous expression of predicted iron reductases

i. Single protein heterologous expression: Locus tag Dred_2421, Dred_1685 and Dred_1686 from *D. reducens* MI-1 were amplified from genomic DNA by PCR and cloned into NdeI/XhoI,

BamHI/SalI and BamHI/XhoI restriction sites of pET28a, respectively. The plasmids were transformed into 10G *Escherichia coli* cells selecting for kanamycin resistance. Based on colony PCR results, colonies containing the desired genes were selected, and plasmid DNA was isolated and sequenced using T7 primers. Sequence-confirmed plasmids were then transformed and expressed in BL-21 Rosetta cells. Cells were cultured at 37°C in 2 liters of Luria Broth (LB) media (VWR) with 50 μg/mL kanamycin and 20μg/mL chloramphenicol. At an OD_{600} of 0.7, 200 μM IPTG was used to induce expression and cells were further incubated at 16°C for 24 hours. Cells were harvested at 8000 rpm for 5 minutes and the cell pellet was stored in 30 mL of lysis buffer (20 mM Tris pH 8.0, 5 mM imidozale, 500 mM NaCl, 2% (v/v) glycerol) at -80°C until use. Cells were lysed using a cell disruptor and lysate was centrifuged at 20,000 rpm for 30 minutes. The soluble fraction was loaded onto a column containing 2.4 ml of Ni-NTA agarose resin (Qiagen), as each target protein contained an N-terminus His_6 tag. The column was first washed with wash buffer (20 mM Tris pH 8.0, 30 mM imidozale, 500 mM NaCl) and then a linear gradient of 50-250 mM imidozale in wash buffer was used to elute the proteins. Fractions containing pure target protein were collected and the buffer was changed to 20 mM Tris pH 8.0, 150 mM NaCl using either dialysis or a desalting column (Econo-Pac, Bio-Rad).

ii. Duet plasmid copurification: To co-express the predicted complex, Dred_1685 and Dred_1686 were cloned into BamHI/SalI and BglII/XhoI restriction sites in pETDuet vector, respectively. The co-expressed plasmid was transformed into 10G *Escherichia coli* cells selecting for ampicilin resistance. Based on colony PCR results, colonies containing the desired genes were selected and the plasmids were obtained and sequenced. The obtained plasmids were then transformed into BL-21 Rosetta cells for protein expression. Cells harboring the expression plasmid were cultured at 37°C in LB media with 100 μg/mL ampicillin and 20 μg/mL

chloramphenicol. Induction, expression, and protein purification were performed as described above. In this expression construct, only Dred_1685 contained an N-terminus His_6 tag. Following affinity purification, the Dred_1685-1686 complex was separated from excess Dred_1685 using size exclusion chromatography.

Cr(VI) reduction assay

Cr(VI) reduction was tested in anaerobic serum vials (N_2 headspace) with 2 mL reaction volumes containing 1 mM NADH (Thermo Fisher Scientific Acros Organics), 0.5 mM sodium dichromate (Alfa Aesar, Ward Hill, MA USA) and 1 μM in HEPES buffer. Following the 80 minutes timepoint, an additional 1 mM NADH was added in order to allow for complete reduction of the 0.5 mM Cr(VI) to presumably Cr(III). The disappearance of Cr(VI) was monitored at 540nm using the diphenylcarbazide method (Urone, 1955). At each timepoint, the concentration of Cr(VI) in a reaction subsample was measured using an anaerobic plate reader (Tecan) at 540 nm. The reaction included 20 μL sample, 13 μL diphenylcarbazide solution (6mM 1,5-diphenylcarbazide (Sigma-Aldrich) in acetone (Fisher-Scientific)), and 167 μL 0.12M H_2SO_4 (Fisher-Scientific).

U(VI) reduction assay

U(VI) reduction was tested in anaerobic serum vials (N_2 headspace) with 2 mL reaction volumes containing 1 mM NADH (Thermo Fisher Scientific Acros Organics), 0.5 mM uranyl acetate, (J.T.Baker/Avantor Performance Materials) and 10 μM protein in HEPES buffer. The disappearance of U(VI) was monitored over time with the reagent Arsenazo (III) based on an updated Arsenazo protocol (Golmohammadi et al., 2012). At each timepoint, the concentration of U(VI) in a reaction subsample was measured using an anaerobic plate reader (Tecan) at 651nm. The reaction included 8 μL of sample, 8 μL DTPA solution (2.5%

diethylenetriaminepenta-acetic acid (Sigma-Aldrich)), 4 µL 10% L-tartaric acid (Sigma-Aldrich), 4 µL Arsenazo Solution (3.2 mM Arsenazo-III (Sigma-Aldrich), 0.5 N NaOH (Sigma-Aldrich)), and 176 µL of dilute H_2SO_4 (Fisher-Scientific) (pH 2). U(VI) oxidation experiments were performed following reduction of U(VI) and anaerobic incubation overnight. Following bubbling with 150 mL ambient air and aerobic incubation for 5 hours, U(VI) concentration was measured.

Acknowledgements:

This chapter is modified from work published in *Environmental Microbiology* on January 27, 2015 (DOI: 10.1111/1462-2920.12673). Permission to reuse this content for this dissertation was obtained from John Wiley and Sons under the license number 3770301179040.

Authors involved in this work include:

Otwell, A.E.[1], Sherwood, R.W.[2], Zhang, S.[2], Nelson, O.D.[3], Li, Z.[3], Lin, H.[3], Callister, S.J.[4], Richardson, R.E.[5]

[1]Department of Microbiology, Cornell University, Ithaca, NY

[2]Proteomics and Mass Spectrometry Facility, Cornell University, Ithaca, NY

[3]Department of Chemistry and Chemical Biology, Cornell University, Ithaca, NY

[4]Pacific Northwest National Laboratory, Richland, WA

[5]Department of Civil and Environmental Engineering, Cornell University, Ithaca, NY

References:

Bird, L.J., Bonnefoy, V., and Newman, D.K. (2011) Bioenergetic challenges of microbial iron metabolisms. *Trends in microbiology* **19**: 330–340.

Bradford, M.M. (1976) A rapid and sensitive method for the quantitation of microgram quantities of protein utilizing the principle of protein-dye binding. *Analytical Biochemistry* **72**: 248–254.

Cardenas, E., Wu, W.-M., Leigh, M.B., Carley, J., Carroll, S., Gentry, T., et al. (2010) Significant Association between Sulfate-Reducing Bacteria and Uranium-Reducing Microbial Communities as Revealed by a Combined Massively Parallel Sequencing-Indicator Species Approach. *Applied and Environmental Microbiology* **76**: 6778–6786.

Carlson, H.K., Iavarone, A.T., Gorur, A., Yeo, B.S., Tran, R., Melnyk, R.A., et al. (2012) Surface multiheme c-type cytochromes from *Thermincola potens* and implications for respiratory metal reduction by Gram-positive bacteria. *Proceedings of the National Academy of Sciences*.

Dalla Vecchia, E., Suvorova, E.I., Maillard, J., and Bernier-Latmani, R. (2014) Fe(III) reduction during pyruvate fermentation by *Desulfotomaculum reducens* strain MI-1. *Geobiology* **12**: 48–61.

Elias, D.A., Yang, F., Mottaz, H.M., Beliaev, A.S., and Lipton, M.S. (2007) Enrichment of functional redox reactive proteins and identification by mass spectrometry results in several terminal Fe(III)-reducing candidate proteins in *Shewanella oneidensis* MR-1. *Journal of microbiological methods* **68**: 367–375.

Fontecave, M., Coves, J., and Pierre, J.-L. (1994) Ferric reductases or flavin reductases? *Biometals* **7**:

Gaspard, S., Vazquez, F., and Holliger, C. (1998) Localization and Solubilization of the Iron(III) Reductase of *Geobacter sulfurreducens*. *Appl. Envir. Microbiol.* **64**: 3188–3194.

Gavrilov, S.N., Lloyd, J.R., Kostrikina, N.A., and Slobodkin, A.I. (2012) Fe(III) Oxide Reduction by a Gram-positive Thermophile: Physiological Mechanisms for Dissimilatory Reduction of Poorly Crystalline Fe(III) Oxide by a Thermophilic Gram-positive Bacterium *Carboxydothermus ferrireducens*. *Geomicrobiology Journal* **29**: 804–819.

Golmohammadi, H., Rashidi, A., and Safdari, S.J. (2012) Simple and rapid spectrophotometric method for determination of uranium (VI) in low grade uranium ores using arsenazo (III) . *Chemistry & Chemical Technology* **6**: 245–249.

Hubbard, P.A., Liang, X., Schulz, H., and Kim, J.-J.P. (2003) The crystal structure and reaction mechanism of *Escherichia coli* 2,4-dienoyl-CoA reductase. *The Journal of biological chemistry* **278**: 37553–60.

Junier, P., Frutschi, M., Wigginton, N.S., Schofield, E.J., Bargar, J.R., and Bernier-Latmani, R. (2009) Metal reduction by spores of *Desulfotomaculum reducens*. *Environmental microbiology* **11**: 3007–3017.

Junier, P., Junier, T., Podell, S., Sims, D.R., Detter, J.C., Lykidis, A., et al. (2010) The genome of the Gram-positive metal- and sulfate-reducing bacterium *Desulfotomaculum reducens* strain MI-1. *Environmental microbiology* **12**: 2738–2754.

Junier, P., Vecchia, E.D., and Bernier-Latmani, R. (2011) The Response of *Desulfotomaculum reducens* MI-1 to U(VI) Exposure: A Transcriptomic Study. *Geomicrobiology Journal* **28**: 483–496.

Kim, S.-H., Harzman, C., Davis, J.K., Hutcheson, R., Broderick, J.B., Marsh, T.L., and Tiedje, J.M. (2012) Genome sequence of *Desulfitobacterium hafniense* DCB-2, a Gram-positive anaerobe capable of dehalogenation and metal reduction. *BMC Microbiology* **12**: 21.

Lovley, D.R. and Phillips, E.J.P. (1987) Rapid Assay for Microbially Reducible Ferric Iron in Aquatic Sediments. *Applied and Environmental Microbiology* **53**: 1536–1540.

Lovley, D.R., Roden, E.E., Phillips, E.J.., and Woodward, J.. (1993) Enzymatic iron and uranium reduction by sulfate-reducing bacteria. *Marine Geology* **113**: 41–53.

Magnuson, T.S., Hodges-Myerson, A.L., and Lovley, D.R. (2000) Characterization of a membrane-bound NADH-dependent Fe3+ reductase from the dissimilatory Fe3+-reducing bacterium *Geobacter sulfurreducens*. *FEMS Microbiology Letters* **185**: 205–211.

Magnuson, T.S., Isoyama, N., Hodges-Myerson, A.L., Davidson, G., Maroney, M.J., Geesey, G.G., and Lovley, D.R. (2001) Isolation, characterization and gene sequence analysis of a membrane-associated 89 kDa Fe(III) reducing cytochrome c from *Geobacter sulfurreducens*. *Biochemical Journal* **359**: 147–152.

Mazoch, J., Tesařík, R., Sedláček, V., Kučera, I., and Turánek, J. (2004) Isolation and biochemical characterization of two soluble iron(III) reductases from *Paracoccus denitrificans*. *European Journal of Biochemistry* **271**: 553–562.

Mohapatra, B.R., Dinardo, O., Gould, W.D., and Koren, D.W. (2010) Biochemical and genomic facets on the dissimilatory reduction of radionuclides by microorganisms – A review. *Minerals Engineering* **23**: 591–599.

Newsome, L., Morris, K., and Lloyd, J.R. (2014) The biogeochemistry and bioremediation of uranium and other priority radionuclides. *Chemical Geology* **363**: 164–184.

Nielsen, F.S., Andersen, P.S., and Jensen, K.F. (1996) The B form of dihydroorotate dehydrogenase from *Lactococcus lactis* consists of two different subunits, encoded by the pyrDb and pyrK genes, and contains FMN, FAD, and [FeS] redox centers. *The Journal of biological chemistry* **271**: 29359–65.

Nørager, S., Jensen, K.F., Björnberg, O., and Larsen, S. (2002) *E. coli* dihydroorotate dehydrogenase reveals structural and functional distinctions between different classes of dihydroorotate dehydrogenases. *Structure (London, England : 1993)* **10**: 1211–23.

Petrie, L., North, N.N., Dollhopf, S.L., Balkwill, D.L., and Kostka, J.E. (2003) Enumeration and Characterization of Iron(III)-Reducing Microbial Communities from Acidic Subsurface Sediments Contaminated with Uranium(VI). *Applied and Environmental Microbiology* **69**: 7467–7479.

Sharma, S., Cavallaro, G., and Rosato, A. (2010) A systematic investigation of multiheme c-type cytochromes in prokaryotes. *JBIC Journal of Biological Inorganic Chemistry* **15**: 559–571.

Shevchenko, A., Wilm, M., Vorm, O., and Mann, M. (1996) Mass spectrometric sequencing of proteins silver-stained polyacrylamide gels. *Analytical chemistry* **68**: 850–8.

Shi, L., Richardson, D.J., Wang, Z., Kerisit, S.N., Rosso, K.M., Zachara, J.M., and Fredrickson, J.K. (2009) The roles of outer membrane cytochromes of *Shewanella* and *Geobacter* in extracellular electron transfer. *Environmental Microbiology Reports* **1**: 220–227.

Strocchi, A., Furne, J.K., and Levitt, M.D. (1992) A modification of the methylene blue method to measure bacterial sulfide production in feces. *Journal of Microbiological Methods* **15**: 75–82.

Suzuki, Y., Kelly, S.D., Kemner, K.M., and Banfield, J.F. (2004) Enzymatic U(VI) reduction by *Desulfosporosinus* species. *Radiochimica Acta* **92**: 11–16.

Suzuki, Y., Kelly, S.D., Kemner, K.M., and Banfield, J.F. (2003) Microbial Populations Stimulated for Hexavalent Uranium Reduction in Uranium Mine Sediment. *Applied and Environmental Microbiology* **69**: 1337–1346.

Tebo, B.M. and Obraztsova, A.Y. (1998) Sulfate-reducing bacterium grows with Cr(VI), U(VI), Mn(IV), and Fe(III) as electron acceptors. *FEMS Microbiology Letters* **162**: 193–198.

Urone, P.F. (1955) Stability of Colorimetric Reagent for Chromium, s-Diphenylcarbazide, in Various Solvents. *Analytical Chemistry* **27**: 1354–1355.

Vadas, A., Monbouquette, H.G., Johnson, E., and Schröder, I. (1999) Identification and characterization of a novel ferric reductase from the hyperthermophilic Archaeon *Archaeoglobus fulgidus*. *The Journal of biological chemistry* **274**: 36715–36721.

Wall, J.D. and Krumholz, L.R. (2006) Uranium reduction. *Annual review of microbiology* **60**: 149–166.

Weber, K.A., Achenbach, L.A., and Coates, J.D. (2006) Microorganisms pumping iron: anaerobic microbial iron oxidation and reduction. *Nature reviews. Microbiology* **4**: 752–64.

Williams, R.E. and Bruce, N.C. (2002) "New uses for an Old Enzyme" - the Old Yellow Enzyme family of flavoenzymes. *Microbiology* **148**: 1607–1614.

Williamson, A.J., Morris, K., Shaw, S., Byrne, J.M., Boothman, C., and Lloyd, J.R. (2013) Microbial reduction of Fe(III) under alkaline conditions relevant to geological disposal. *Applied and environmental microbiology* **79**: 3320–6.

Yu, N.Y., Wagner, J.R., Laird, M.R., Melli, G., Rey, S., Lo, R., et al. (2010) PSORTb 3.0: improved protein subcellular localization prediction with refined localization subcategories and predictive capabilities for all prokaryotes. *Bioinformatics (Oxford, England)* **26**: 1608–15.

Zhang, S., Van Pelt, C.K., and Henion, J.D. (2003) Automated chip-based nanoelectrospray-mass spectrometry for rapid identification of proteins separated by two-dimensional gel electrophoresis. *Electrophoresis* **24**: 3620–32.

Supplementary Figures and Tables:

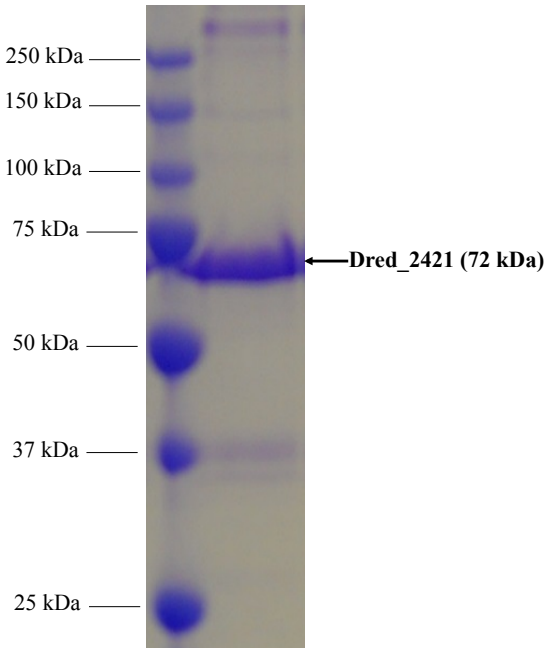

Supplementary Figure 2.1: Expression and purification of Dred_2421: SDS-PAGE analysis of recombinant Dred_2421 following expression and affinity purification shows highly purified protein at expected size of 72 kDa.

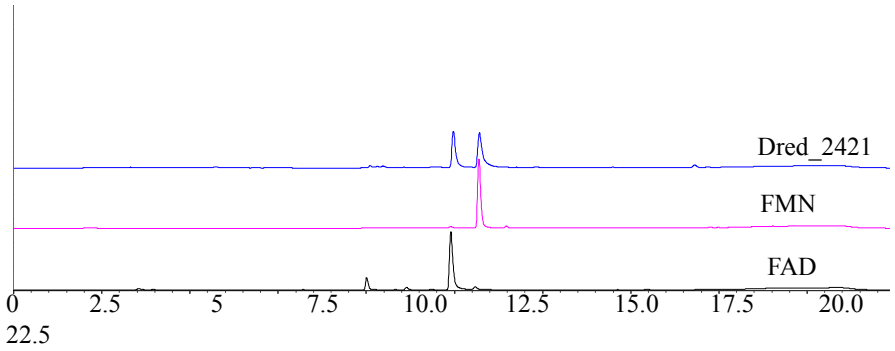

Supplementary Figure 2.2: Dred_2421 contains bound flavin in the form of FMN and FAD. To examine the cofactors bound to Dred_2421, the protein was boiled at 95°C for 5 minutes and then spun down to remove the precipitation. The supernatant was analyzed by reversed-phase HPLC at 260nm and standards for FMN (flavin mononucleotide) and FAD (flavin adenine dinucleotide) were run. Elution time in minutes is displayed on the x-axis. Both flavins were identified in Dred_2421.

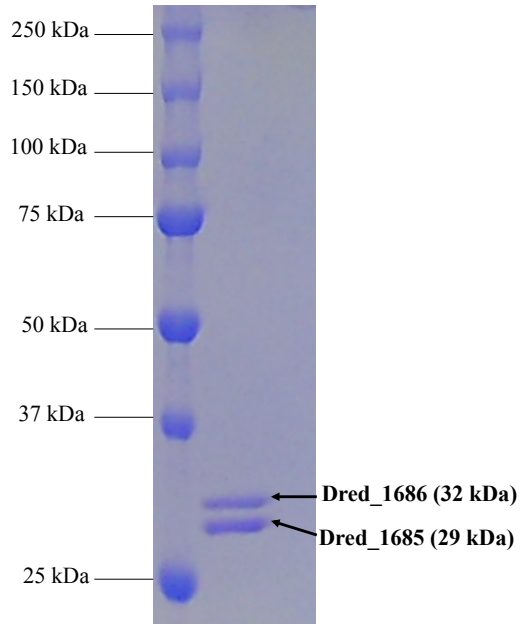

Supplementary Figure 2.3: **Co-expression and purification of Dred_1685 and Dred_1686:** SDS-PAGE analysis of recombinant Dred_1685-1686 complex following pETDuet co-expression, affinity purification, and size exclusion chromatography. The presence of two bands at predicted sizes for Dred_1685 and Dred_1686 provides evidence for the formation of the Dred_1685-1686 complex, as only Dred_1685 contained a His_6-tag.

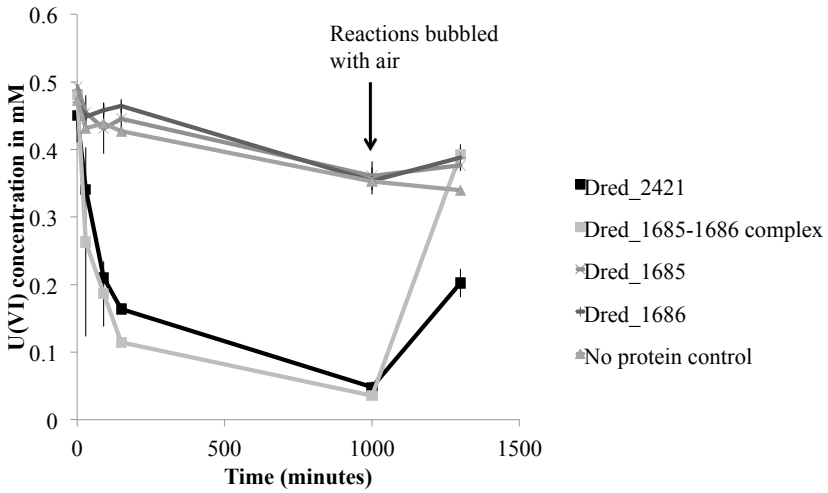

Supplementary Figure 2.4: Reoxidation of reduced U(VI) provides evidence for U(VI) reduction: Following reduction of U(VI) and anaerobic incubation overnight, reactions were bubbled with 150mL ambient air and left in an aerobic environment for 5 hours. Subsequent measures of U(VI) show oxidization of the uranium back to U(VI) in the reactions containing discovered uranium reductases, Dred_2421 and Dred_1685-1686 complex. Individual Dred_1685 and Dred_1686 proteins resembled the no protein control.

a.

Locus Tag	Annotation	Protein Score	Protein Mass	Unique peptides identified	emPAI	Expressed and purified?
Dred_2421	NADH:flavin oxidoreductase	1502	72319	35	3.72	Yes
Dred_2457	oligoendopeptidase F	478	69310	13	0.83	No
Dred_1784	acetyl-CoA acetyltransferase	412	41203	11	1.16	No
Dred_0635	sulfate adenylyltransferase	85	44129	4	0.33	No

b.

Locus Tag	Annotation	Protein Score	Protein Mass	Unique peptides identified	emPAI	Expressed and purified?
Dred_1685	oxidoreductase FAD/ NAD(P)-binding subunit	431	28894	14	3.13	Yes
Dred_1686	dihydroorotate dehydrogenase 1B	259	32012	7	0.81	Yes
Dred_0137	4Fe-4S ferredoxin	150	111909	6	0.19	No *
Dred_0047	pyruvate flavodoxin/ ferredoxin oxidoreductase domain-containing protein	78	40112	2	0.17	Yes

c.

Locus Tag	Name	Protein Score	Protein Mass	Unique peptides identified	emPAI	Expressed and purified?
Dred_3152	ATP synthase F1 subunit alpha	154	54403	5	0.34	No
Dred_1686	dihydroorotate dehydrogenase 1B	143	32012	3	0.35	Yes
Dred_0095	GntR family transcriptional regulator	141	25831	4	0.63	No
Dred_1685	oxidoreductase FAD/NAD(P)-binding subunit	130	28894	5	0.73	Yes
Dred_0637	adenylylsulfate reductase subunit alpha	66	69579	2	0.1	No

Supplementary Table 2.1: Proteins identified from excised iron-reduction active gel bands. Following LC-MS/MS analysis, proteins identified by at least two unique peptides from excised iron-reduction active gel bands are reported. Potential iron reduction proteins, based on protein score and annotation, were heterologously expressed and purified in *E. coli* for further characterization. **a)** is from separations involving *D. reducens* soluble fraction SAX Peak 1 (see Figure 3b). **b)** is from separations involving *D. reducens* soluble fraction SAX Peak 2 (see Figure 3c). **c)** is from separations involving *D. reducens* insoluble fraction (see Figure 4). Values in this table were derived from analysis with Mascot. Protein score is a relative number assigned to rank reported proteins within a single analysis, defined as the sum of the highest ions score for each distinct sequence. The Exponentially Modified Protein Abundance Index (emPAI) provides an approximate, label-free, relative quantitation of the proteins in the mixture based on protein coverage by the peptide matches in the database search result (Ishihama et al., 2005) (Mascot database, Matrix Science, http://www.matrixscience.com). The final column denotes whether the protein was heterologously expressed and purified in *E. coli*. *Dred_0137 was selected for expression, but mutations accumulated during the cloning process prevented creation of an expression vector.

Chapter 3

Identification of a Soluble Fe(III) Reductase from *Geobacter sulfurreducens* PCA and Preliminary *in vitro/in vivo* Characterization

Summary

In order to validate any *in vivo* role for the metal reductases from *Desulfotomaculum reducens* MI-1 described in the previous chapter, we ideally would have created knockout mutations of the genes encoding for the identified proteins. However, *D. reducens* is poorly characterized and there is no described genetic system for any organism within the *Desulfotomaculum* genus. In parallel with top-down proteomic-based screens of *D. reducens*, the proteome of *Geobacter sulfurreducens* PCA was also screened for Fe(III)-reductase activity. Interestingly, an Fe(III)-reductase (GSU1371) was identified from the soluble protein fraction of *G. sulfurreducens* that is an ortholog to Dred_2421, one of the *D. reducens* proteins described in the previous chapter. The identification, *in vitro* characterization, and attempts at *in vivo* characterization of GSU1371 (annotated as an NADPH-dependent enal/enone/nitroreductase, Old Yellow Enzyme family) is described here.

Introduction

In the late 1980's, two microorganisms were isolated that advanced understanding of the diverse metabolisms supporting life on this planet. Now classified as *Geobacter* and *Shewanella* species, researchers studying these isolates proved for the first time that Fe(III) and Mn(IV) could be used as sole terminal electron acceptors during oxidation of organic compounds (Lovley and Phillips, 1988; Myers and Nealson, 1988). As Fe(III) and Mn(IV) metals are most commonly insoluble oxides in the environment, this discovery led to a new field, aiming to elucidate pathways of extracellular electron transfer. While the number of species described as dissimilatory metal-reducing microorganisms (DMRM) is continually expanding, *Geobacter* and *Shewanella* species continue to serve as the major model organisms in the field.

In both bacteria, the major class of proteins that has been implemented in the extracellular reduction of metals is multiheme c-type cytochromes (MHCs). The genome of *G. sulfurreducens* encodes 111 predicted c-type cytochromes, whereas *Shewanella oneidensis* encodes 42 (Shi et al., 2009). Before the development of a genetic system in *G. sulfurreducens*, a number of studies were conducted in search of proteins involved in the metal reduction pathway, with a specific focus on MHCs. The first MHC shown to play an *in vivo* role in Fe(III) reduction in *G. sulfurreducens*, OmcB, was initially identified using protein purification-based functional assays (Magnuson et al., 2000, 2001). Following the development of a genetic system, the ability to create gene knockouts allowed for confirmation of MHCs in the pathway of Fe(III) reduction, including OmcB (Coppi et al., 2001; Leang et al., 2003). Gene deletions of multiple MHCs have been created in *G. sulfurreducens,* including *ppcA*, *omcE*, *omcF*, *omcT*, *omcS* and *omcZ* knockout strains (Aklujkar et al., 2013; Inoue et al., 2010; Kim et al., 2005; Lloyd et al., 2003; Qian et al., 2011; Shi et al., 2007, 2009). Likely due to functional redundancy of MHCs in the genome of *G. sulfurreducens*, knockout studies are not straightforward. For instance, mutants often adapt to regain Fe(III) reduction activity (Kim et al., 2005). Regaining complete wild-type phenotype through complementation has also proven difficult (Afkar et al., 2005; Butler et al., 2004; Leang et al., 2003).

Nearly all knockout studies aimed towards elucidating pathways of electron transfer in *G. sulfurreducens* have targeted membrane proteins, which is logical based on our current knowledge of extracellular electron transfer. One study targeted a soluble protein based on identification of this protein during assays for Fe(III) reduction activity in the soluble proteome using NADPH as electron donor (Kaufmann and Lovley, 2001). By comparison of the mutant with wild-type *G. sulfurreducens*, it was determined that this soluble protein was not involved in

metal reduction, but rather in acetate metabolism (Coppi et al., 2007). As NADPH is most commonly an electron donor for anabolic reactions, this result is not surprising. The report demonstrates the importance of *in vivo* phenotypic tests following protein purification-based identification and *in vitro* characterization.

Along with MHCs, flavins have been found to play an important role in Fe(III) reduction in both *Shewanella* and *Geobacter* species. In *Shewanella*, it has been accepted for some time that soluble flavins (including riboflavin and FMN) mediate extracellular electron transfer, serving as a shuttle between the cell and the insoluble metal (von Canstein et al., 2008; Coursolle et al., 2010; Marsili et al., 2008). In this scenario, the flavins reduce the metal in a two-electron transfer event. This type of flavin-based shuttling does not occur in *Geobacter*, and so flavins were thought to not play a critical role in Fe(III) reduction in this organism (Nevin and Lovley, 2000). However, recent studies have shown that in both *Shewanella* and *Geobacter*, self-secreted flavins serve as redox cofactors bound to outer membrane MHCs. These bound flavins participate in one-electron transfer reactions, enhancing the rates of extracellular electron transfer (Okamoto et al., 2013, 2014a, 2014b). These studies expand understanding of Fe(III) reduction and show even greater pathway similarity between model organisms *Shewanella* and *Geobacter* than previously thought.

In this study, we separated and fractionated the soluble and insoluble proteomes of *G. sulfurreducens*, assaying for Fe(III) reduction activity with NADH as electron donor. Across multiple attempts, the soluble protein GSU1371, described as an NADPH-dependent enal/enone/nitroreductase, Old Yellow Enzyme family protein, was identified with the highest specific Fe(III) reductase activity. Following heterologous expression, GSU1371 was confirmed as an *in vitro* Fe(III) reductase and was described as an *in vitro* Cr(VI) reductase. GSU1371 is an

ortholog of Dred_2421, described in Chapter 2 as an *in vitro* Fe(III), U(VI), and Cr(VI) reductase from *D. reducens*, a bacterium that lacks a genetic system (Otwell et al., 2015). Based on these findings, we created a GSU1371-knockout (KO) strain. Phenotypes of this strain were compared with the *G. sulfurreducens* wild-type (WT).

Methods

Culturing

Geobacter sulfurreducens PCA was purchased from the DSMZ (Deutsche Sammlung von Mikroorganismen und Zellkulturen) and cultivated at 30° C in batch culture with an 80/20 N_2/CO_2 headspace. *Geobacter* freshwater media, as described by the American Type Culture Collection (ATCC) was used for all phenotypic studies reported. Electron acceptor was either 50 mM sodium fumarate, 50mM Fe(III)-citrate, or 100mM Fe(III)-oxide particles, with 20 mM sodium acetate as electron donor. NBAFYE media was used for preparation of electrocompetent cells, as described (Coppi et al., 2001). 200 µg kanamycin was added when appropriate. Plating and incubations on solid NBAFYE media, containing 15 g/L of agar, was performed inside an anaerobic chamber.

Protein extraction, fractionation, iron reduction activity assay, and protein identification

The soluble and insoluble proteomes of *G. sulfurreducens* were prepared as described in Chapter 2. The functional proteomes were subjected to strong anion exchange (SAX) chromatography, size exclusion chromatography (SEC) and native gel electrophoresis as described in Chapter 2. Ferrozine-based iron reduction activity assays and in-gel activity assays were also performed as described in Chapter 2. Following detection of Fe(III) reduction activity, proteins were identified using tandem mass spectrometry as described in Chapter 2.

Heterologous expression, in vitro and in vivo activity assays

In order to confirm Fe(III) reduction activity in GSU1371, the protein was heterologously expressed and purified in *Escherichia coli* as described previously (Li et al., 2015). *In vitro* and *in vivo* Fe(III) reduction was measured using the ferrozine assay as described in Chapter 2. *In vitro* and *in vivo* Cr(VI) reduction activity was measured using the diphenylcarbazide method as described in Chapter 2.

Preparation of electrocompetent cells and transformation

For creation of the GSU1371-knockout (KO) strain, *G. sulfurreducens* electrocompetent cells were prepared as described (Coppi et al., 2001). Careful attention was made to keeping all materials anaerobic and on ice throughout the procedure. Electrocompetent cells were frozen immediately with liquid nitrogen at stored at -80° C for later use. The construct used to knock-out GSU1371 was created using an *E. coli*-mediated DNA assembly technique, which is the content of Chapter 4 (Kostylev et al., 2015). Electroporation was carried out using a Cell-Porator (Life Technologies) and performed as described (Coppi et al., 2001). 4 μL of DNA (concentration ~100 ng/μL) was added to 25 μL of electrocompetent cells for each transformation. Following electroporation, cells were collected by pipetting gently into the electroporation chamber with 1 mL of room temperature phosphate-buffered NBAF, and then transferred by syringe into a pre-warmed anaerobic pressure tube containing 9 mL of NBAFYE. Cells were allowed to recover for 8 hours at 30° C, followed by plating in the anaerobic chamber. The GSU1371-KO was regularly maintained with addition of kanamycin. Tests were performed without kanamycin to confirm that addition of the antibiotic was not responsible for observed phenotypes.

Results

I. Identification and in vitro confirmation of GSU1371 as an Fe(III) reductase

In commencing functional proteomic-based studies of *G. sulfurreducens*, one goal was to develop a workflow to then implement to study less-characterized organisms, such as *D. reducens*. In search for Fe(III) reductases of *G. sulfurreducens*, we expected similar findings as previous studies have had (i.e. identification of membrane-associated c-type cytochromes) (Magnuson et al., 2000, 2001). However, across multiple attempts, the soluble proteome of *G. sulfurreducens* contained higher specific Fe(III) reduction activity than the insoluble proteome with our assay, and activity was only maintained upon liquid chromatography and gel-based separations in the soluble proteome. One dominant peak of Fe(III) reduction activity consistently remained following three phases of non-denaturing separations (strong anion exchange (SAX) chromatography, size exclusion chromatography (SEC), and native gel electrophoresis). In this peak, GSU1371 was identified with tandem mass spectrometry **(Figure 3.1)**. This protein is annotated as an NADPH-dependent enal/enone/nitroreductase, Old Yellow Enzyme (OYE) family and is ~40 kDa in size. It was identified from a pink band in the native gel (signifying Fe(III) reduction activity) located at ~240 kDa, suggesting that it functions as a hexamer. Our group performed heterologous expression and purification of the protein in *E. coli* and confirmed its Fe(III) reduction activity, as described in Li et al., 2015.

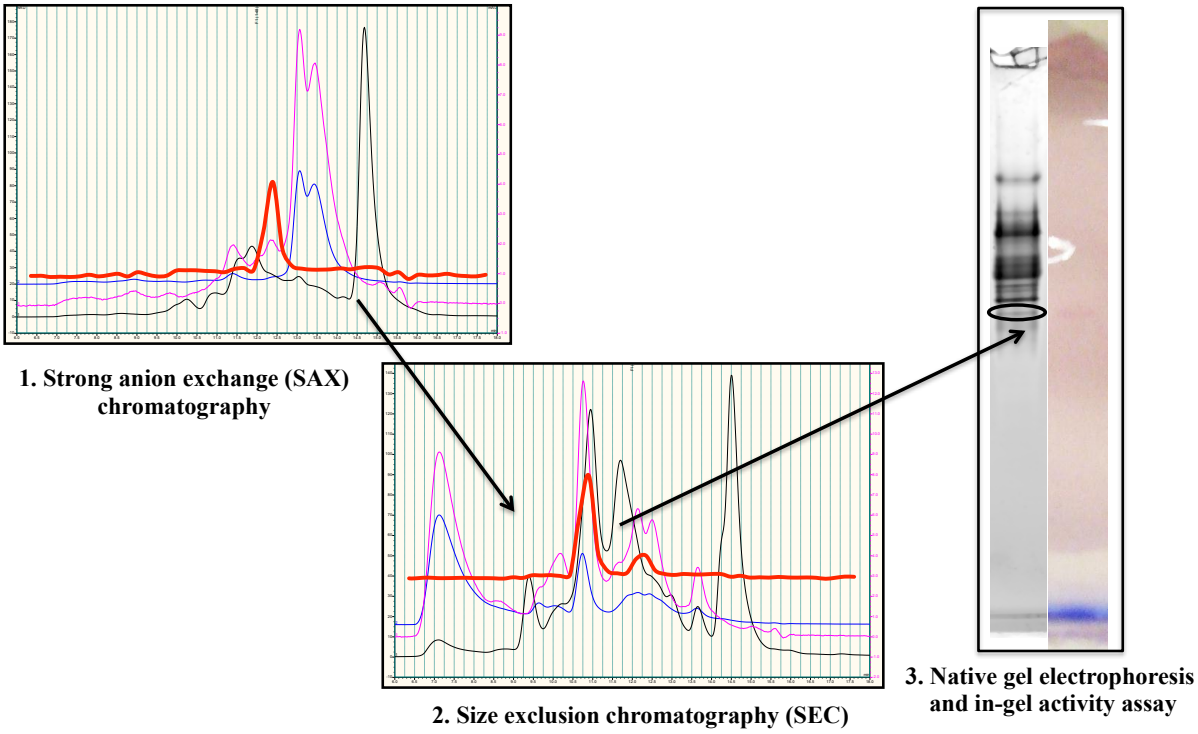

Figure 3.1: GSU1371 was identified from the fractionated proteome of *Geobacter sulfurreducens* using an Fe(III) reduction activity assay. Three phases of non-denaturing separation were employed including 1) Strong anion exchange (SAX) chromatography, 2) Size exclusion chromatography (SEC), and 3) native gel electrophoresis. Following each phase of separation, a ferrozine-based Fe(III) reduction activity assay was employed, which allowed for selection and further separation of the active fraction. Once an active band was identified in the native gel, tandem mass spectrometry was employed in order to identify the protein GSU1371, an NADPH-dependent enal/enone/nitroreductase, Oye family.

GSU1371 is an ortholog of the OYE Dred_2421 identified in Chapter 2 (Otwell et al., 2015). Dred_2421 contains an N-terminal and C-terminal domain and is 668 amino acids in length, and GSU1371 (365 amino acids) shares 32% identity with the N-terminal domain (http://blast.ncbi.nlm.nih.gov). Cr(VI) reduction activity was tested for GSU1371 and found to be significantly more efficient than in Dred_2421 **(Figure 3.2).** Upon further investigation, it was found that GSU1371 shares high similarity (56% sequence identity across 99% query) with the most active soluble Cr(VI) reductase discovered to date, now annotated as ChrR (chromate reductase) (http://blast.ncbi.nlm.nih.gov). This reductase was identified from *Thermus scotoductus* using protein purification and assay-based methods similar to those described here.

No *in vivo* characterization was performed (Opperman et al., 2008). For this reason, along with our interest in Dred_2421 but inability to test for *in vivo* functions, we created a GSU1371-KO strain.

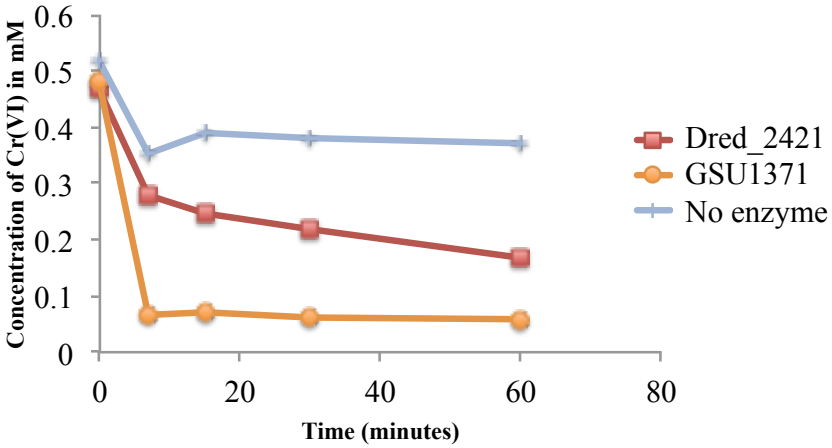

Figure 3.2: GSU1371 is an efficient Cr(VI) reductase with NADH as electron donor. Reduction of Cr(VI) was tested using the diphenylcarbazide method (see Chapter 2). Dred_2421 was tested at a concentration of 5.4 micromolar, while GSU1371 was at a concentration of 0.6 micromolar. The higher Cr(VI) reduction capability of GSU1371 at significantly lower concentrations than Dred_2421 suggests that GSU1371 is a highly efficient *in vitro* Cr(VI) reductase. In fact, GSU1371 is a close ortholog (56% sequence identity across 99% query) to the most active soluble chromate reductase reported to date, which was isolated from *Thermus scotoductus*.

II. In vivo characterization of GSU1371

The GSU1371-KO construct was assembled using *E. coli*-mediated assembly as described in Chapter 4 (Kostylev et al., 2015). In order to confirm correct integration of the construct into the chromosome, primers were designed upstream and downstream of the target sites. PCR confirmed successful integration of the construct into the genome of *G. sulfurreducens*. The ability of the mutant, but not the *G. sulfurreducens* WT, to grow on kanamycin further supported creation of the desired GSU1371-KO strain.

II.a. The GSU1371-KO displays a faster growth phenotype on fumarate and acetate

With the goal of characterizing potential phenotypic differences resulting from deletion of GSU1371, multiple studies were performed comparing the WT and GSU1371-KO. A critical initial step was to confirm that the mutation did not cause any growth defects in the organism. Growth studies were performed comparing the WT and KO growing on fumarate and acetate, common cultivation conditions for the organism. Surprisingly, across multiple experiments, the GSU1371-KO grew faster on these conditions **(Figure 3.3).** Cultivating the KO with or without kanamycin did not affect this result.

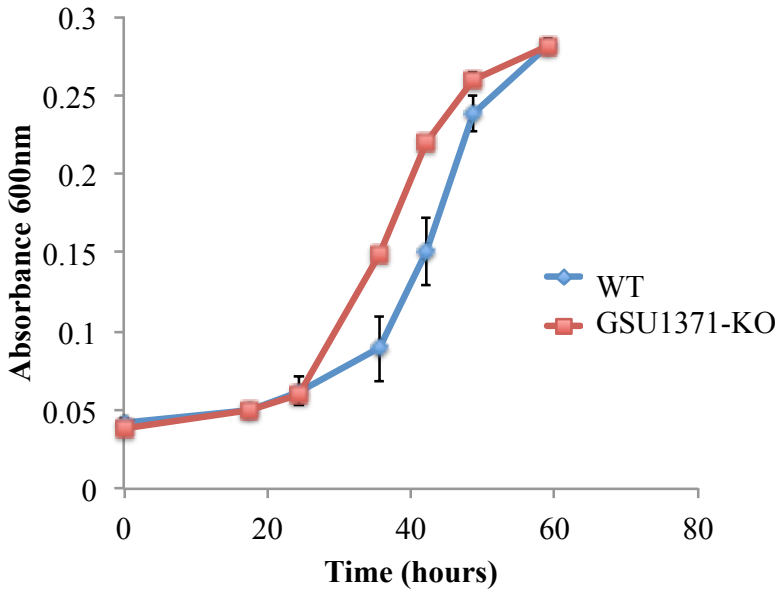

Figure 3.3: The GSU1371-KO displays a faster growth phenotype on fumarate/acetate conditions than the *G. sulfurreducens* WT. Growth of the *G. sulfurreducens* and the GSU1371-KO was compared on the fumarate/acetate condition in order to test for any growth defects in the mutant. Unexpectedly, the GSU1371-KO consistently demonstrated an enhanced growth phenotype on these conditions. Absorbance at 600nm was monitored in a plate reader (Tecan Infinite 200 series microplate reader, Tecan Group Ltd, Männedorf, Switzerland). Cell counts were also monitored, and correlated closely with absorbance readings.

II.b. The GSU1371-KO has reduced ability to reduce Fe(III)-citrate

GSU1371 was originally isolated using based on its ability to reduce soluble Fe(III)-citrate, so comparisons of *in vivo* Fe(III)-reduction activity were performed. The KO was still able to reduce Fe(III)-citrate, which is not surprising as even knockouts of MHCs known to be Fe(III)-reductases do not completely eliminate this activity (Kim et al., 2005; Lloyd et al., 2003). However, the WT and the mutant display different phenotypes while growing on Fe(III)-citrate. Specifically, GSU1371-KO cultures reduce the Fe(III) slower than the WT and display a longer lag phase. This lag phase was consistently more variabile in the KO than in the WT **(Figure 3.4).** Tests were also performed to compare insoluble Fe(III)-oxide reduction phenotypes, but no significant differences were found between the WT and mutant.

II.c. No significant differences are observed in Cr(VI)-reduction phenotype

As *in vitro* Cr(VI)-reduction activity was found in GSU1371, (and its ortholog in *T. scotoductus*) we were interested to test Cr(VI) reduction ability of the mutant compared to the WT. It was assumed that *G. sulfurreducens* can reduce Cr(VI) due to its other metal reduction capabilities, but actual reports of Cr(VI) reduction by the organism were not found in the literature. Therefore, cell suspensions of fumarate-grown *G. sulfurreducens* were tested for Cr(VI)-reduction ability with acetate as electron donor (**Supplementary Figure 3.1)**. The cells were capable of reducing Cr(VI) even without the addition of electron donor, which is not surprising as *G. sulfurreducens* has been reported to store electrons in their MHCs (Esteve-Núñez et al., 2008).

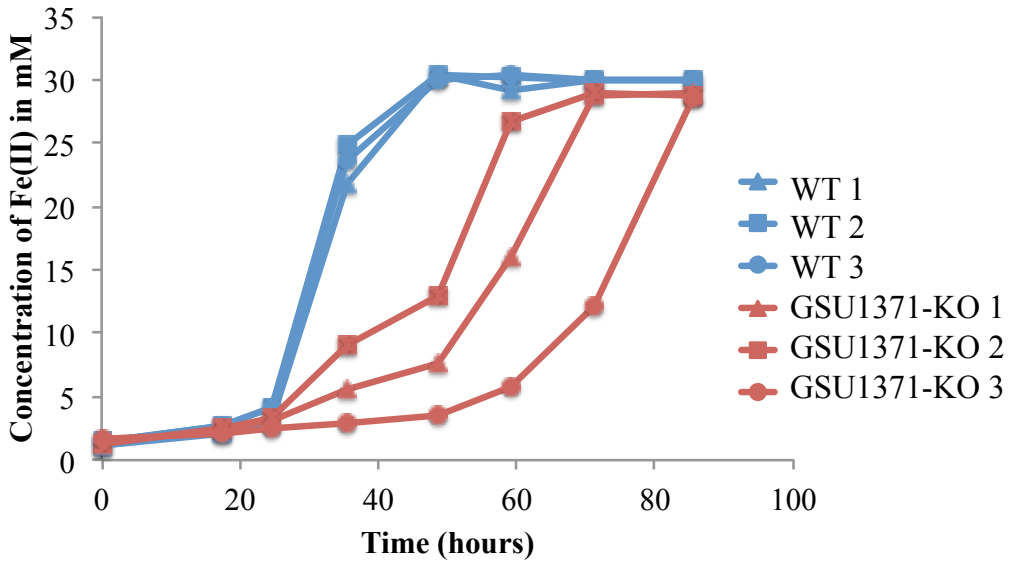

Figure 3.4: The GSU1371-KO displays a delayed Fe(III)-citrate reduction phenotype as compared to the *G. sulfurreducens* WT. Ability to reduce soluble Fe(III)-citrate was compared in the WT and GSU1371-KO. Overall, the mutant displayed an increased lag phase compared with the WT. Furthermore, while the WT culture replicates clustered tightly, the mutant exhibited variability in the length of its lag phase, and therefore triplicates show great variability. For this reason, triplicate cultures are displayed separately in order to most accurate depict separate growth curves. Accumulation of Fe(II) was monitored with the ferrozine assay (see Chapter 2).

4

Following confirmation of Cr(VI) reductase activity in whole cells of *G.* sulfurreducens, a variety of phenotypic studies were performed in order to compare Cr(VI)-reduction capabilities of the *G. sulfurreducens* WT and GSU1371-KO. None of the studies displayed decreased Cr(VI) reduction ability in the KO, suggesting that GSU1371 is not involved in *in vivo* Cr(VI) reduction. Studies included cell suspension experiments testing the reduction of Cr(VI) with acetate as electron donor (similar to **Supplementary Figure 3.1**), addition of Cr(VI) to cultures growing on fumarate and acetate to test reduction capability **(Figure 3.5a)**, and Cr(VI) toxification tests **(Figure 3.5b)**. Toxification tests were developed based on studies in *Pseudomonas putida*, which found greater cell growth inhibition in strains where a soluble chromate reductase had been knocked out (Gonzalez et al., 2003). In our study, however, the *G. sulfurreducens* WT was

actually more sensitive to increasing Cr(VI) concentrations during cell growth. In one final test, cells were transferred to fresh fumarate/acetate media following Cr(VI) reduction and toxicity experiments in order to see if growth phenotypes following Cr(VI) were altered. This was not the case, however, as growth phenotypes following Cr(VI) exposure resembled those displayed in **Figure 3.3.**

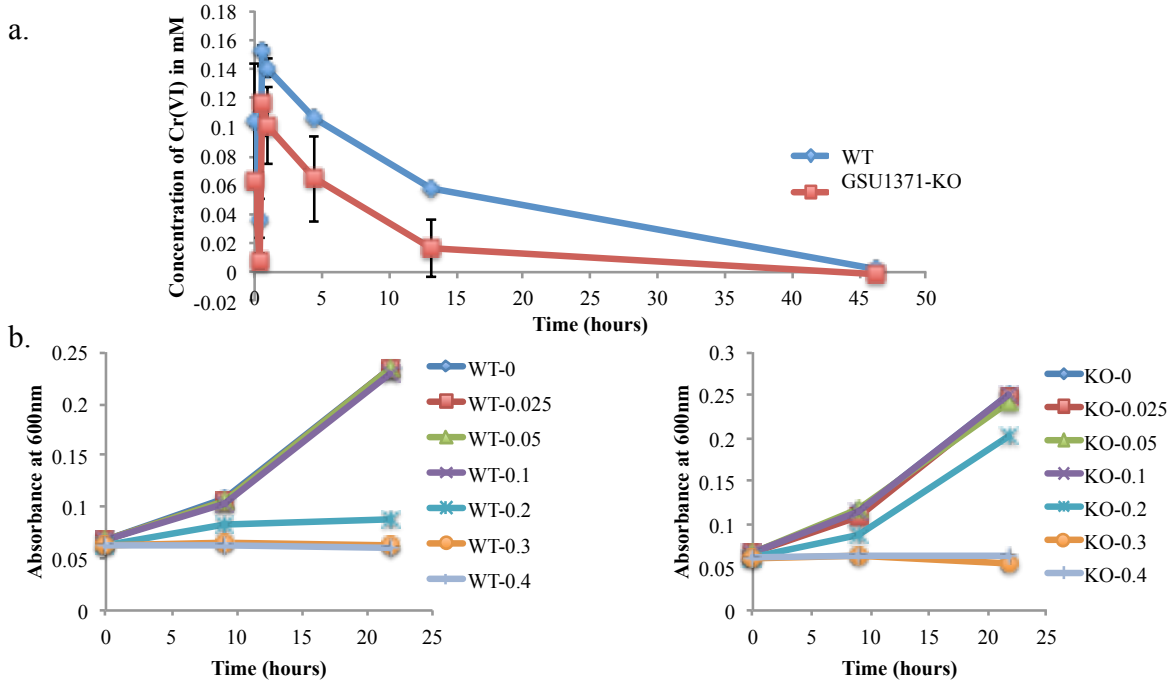

Figure 3.5: A reduced Cr(VI) reduction phenotype is not observed in the GSU1371-KO. A variety of phenotypic tests for Cr(VI) reduction capability were performed, and overall the KO does not have impaired Cr(VI) reduction ability. This suggests that GSU1371 is not involved in *in vivo* Cr(VI) reduction. **a.** Cells were grown on fumarate and acetate conditions to an absorbance of ~0.2 at 600nm. 0.1 mM of Cr(VI) was then injected and disappearance of Cr(VI) was monitored. After 10 minutes, an additional 0.1 mM of Cr(VI) was injected. At all timepoints, the KO had reduced more Cr(VI). **b.** Various concentrations of Cr(VI) (0 to 0.4 mM) were added during inoculation of cultures in order to compare effects of Cr(VI) toxicity in the WT and GSU1371-KO. An addition of 0.2 mM Cr(V) greatly inhibited growth of the wild-type, whereas the same concentration had minor effects on the mutant. Culture conditions contained 50mM fumarate and 20mM acetate. In all studies, the disappearance of Cr(VI) was quantified as described in Chapter 2, and when applicable, cell concentrations were normalized based on absorbance at 600nm.

II.d. Biofilm phenotype

An additional observation regarding the GSU1371-KO was a consistently decreased biofilm-formation phenotype compared to the *G. sulfurreducens* WT when cultivated on fumarate/acetate conditions. A pink biofilm forms early in the growth phase of *G. sulfurreducens*,

which grows thick by late stationary phase **(Supplementary Figure 3.2)**. Qualitative differences were observed both in early-stage biofilm formation **(Supplementary Figure 3.2a)** and late-stage biofilm phenotype **(Supplementary Figure 3.2b)** between the KO and WT. Attempts were made to quantify this difference through a 96-well plate-based biofilm assay. In this assay, biofilms are stained with crystal violet and destained with acetic acid. Absorbance is then measured, which is correlated to the thickness of the biofilm (O'Toole et al., 1999; Rollefson et al., 2009). However, experiments carried out in plates incubated in both an anaerobic chamber and anaerobic plate reader failed to grow, likely due to oxygen exposure. Interestingly, besides two other proteins from *Geobacter* species, the closest orthologs to GSU1371 are from various *Pseudomonas* species, including strains of *Pseudomonas aeruginosa* (http://blast.ncbi.nlm.nih.gov). Biofilm formation is an important focus in the study of the pathogen *P. aeruginosa*, which colonizes the lungs of patients with cystic fibrosis, and so any relevance for this type of protein in biofilm formation should be further explored (Tolker-Nielsen, 2014).

Discussion

GSU1371 was the single protein confidently identified as an Fe(III) reductase from *G. sulfurreducens* across >10 studies of the extracted proteome. In fact, in all of these studies, the signal for this protein at every stage of separation (following SAX, SEC, and/or in-gel activity assay) had the highest Fe(III) reduction specific activity that we observed. While a soluble protein was not the result that we expected, given our relatively unbiased approach and the consistency of the result, we decided to explore the finding further. Interestingly, in talking with the author of two of the initial *G. sulfurreducens* MHC papers (which led to the identification of OmcB), it was disclosed that in their studies they also identified a soluble flavin oxidoreductase.

At the time, the Lovley lab was pursuing MHC research, however, so it was not reported (Magnuson personal communication).

Additional support for our interest in GSU1371 came from comparative proteomic analysis, where we utilized iTRAQ (isobaric tag for relative and absolute quantitation) to analyze the global proteomes of *G. sulfurreducens* grown on Fe(III)-citrate and fumarate conditions (both with acetate as electron donor). GSU1371 increased in abundance ~2 fold during Fe(III)-citrate reduction relative to fumarate (Otwell and Richardson, unpublished data). With additional interest in GSU1371 derived from its shared homology with Dred_2421 (from *D. reducens*) and an annotated chromate reductase (from *T. scotoductus)*, we decided to knock the gene out of the genome of *G. sulfurreducens* and investigate *in vivo* phenotypes (Opperman et al., 2008; Otwell et al., 2015).

Our *in vivo* results demonstrate an enhanced growth rate of the GSU1371-KO during cultivation with fumarate along with a decreased rate of Fe(III)-citrate reduction. This suggests that GSU1371 plays an *in vivo* role in soluble Fe(III) reduction. While some Fe(III) reduction-related mutants of *G. sulfurreducens* show gradual reversion back to a regular Fe(III) reduction phenotype, the GSU1371-KO displayed a similar growth phenotype upon successive transfers. The literature on the importance of flavins in the pathway of Fe(III)-reduction in *Shewanella* and *Geobacter* species is expanding (Okamoto et al., 2013, 2014a, 2014b). While GSU1371 is annotated as NADPH-dependent enal/enone/nitroreductase, it is an NADH:flavin oxidoreductase in the OYE family and contains bound FMN (Li et al., 2015). It is possible that GSU1371 is involved in the reduction of flavins destined for secretion, which bind to MHCs and enhance rates of Fe(III) reduction (Okamoto et al., 2014a). It is not clear how an enhanced growth rate on fumarate might relate to an *in vivo* role for GSU1371. One simple explanation would be that it is

an energetically expensive protein to produce, and therefore interrupting its production enhances the growth rate on a non-Fe(III) substrate. If GSU1371 is involved in reduced flavin generation for the purposes of Fe(III) reduction, and *Geobacter* is an organism majorly reducing Fe(III) under environmental conditions, it makes sense that this protein would always be expressed. During laboratory-based cultivation with fumarate, however, the protein would not be necessary.

Another important finding from this study is that GSU1371 does not appear to be a true chromate reductase, which suggests that the annotated chromate reductase from *T. scotoductus* (ChrR) is likely not either. *In vitro* Cr(VI) reductase ability is likely fortuitous, for instance due to similar reduction potentials between Cr(VI) and its physiological electron acceptor. If anything, the GSU1371-KO strain appears to more actively reduce Cr(VI) **(Figure 3.5).** The cells were prepared for Cr(VI) reduction studies on fumarate rather than Fe(III) due to the ability for Fe(II) to abiotically reduce Cr(VI). Therefore, increased Cr(VI) reduction activity in the KO could be a confounding effect of the enhanced growth phenotype of the mutant on fumarate conditions. Due to limited time and resources for anaerobic genetic manipulation experiments, we decided to not pursue further testing of the GSU1371-KO, including complementation. More research is needed in order to support or refute the findings and hypotheses generated in this study and further elucidate the *in vivo* role of GSU1371.

Acknowledgements

Authors involved in this work include:

Anne E. Otwell[1], Robert W. Sherwood[2], Sheng Zhang[2], Zhi Li[3], Hening Lin[3], Ruth E. Richardson[4]

[1]Department of Microbiology, Cornell University, Ithaca, NY
[2]Proteomics and Mass Spectrometry Facility, Cornell University, Ithaca, NY
[3]Department of Chemistry and Chemical Biology, Cornell University, Ithaca, NY
[4]Department of Civil and Environmental Engineering, Cornell University, Ithaca, NY

References

Afkar, E., Reguera, G., Schiffer, M., and Lovley, D. R. (2005). A novel Geobacteraceae-specific outer membrane protein J (OmpJ) is essential for electron transport to Fe(III) and Mn(IV) oxides in Geobacter sulfurreducens. *BMC Microbiol.* 5, 41. doi:10.1186/1471-2180-5-41.

Aklujkar, M., Coppi, M. V., Leang, C., Kim, B. C., Chavan, M. A., Perpetua, L. A., et al. (2013). Proteins involved in electron transfer to Fe(III) and Mn(IV) oxides by Geobacter sulfurreducens and Geobacter uraniireducens. *Microbiology* 159, 515–535. doi:10.1099/mic.0.064089-0.

Butler, J. E., Kaufmann, F., Coppi, M. V., Nunez, C., and Lovley, D. R. (2004). MacA, a Diheme c-Type Cytochrome Involved in Fe(III) Reduction by Geobacter sulfurreducens. *J. Bacteriol.* 186, 4042–4045. doi:10.1128/JB.186.12.4042-4045.2004.

von Canstein, H., Ogawa, J., Shimizu, S., and Lloyd, J. R. (2008). Secretion of flavins by Shewanella species and their role in extracellular electron transfer. *Appl. Environ. Microbiol.* 74, 615–623. doi:10.1128/AEM.01387-07.

Coppi, M. V, Leang, C., Sandler, S. J., and Lovley, D. R. (2001). Development of a genetic system for Geobacter sulfurreducens. *Appl. Environ. Microbiol.* 67, 3180–7. doi:10.1128/AEM.67.7.3180-3187.2001.

Coppi, M. V, O'neil, R. A., Leang, C., Kaufmann, F., Methé, B. A., Nevin, K. P., et al. (2007). Involvement of Geobacter sulfurreducens SfrAB in acetate metabolism rather than intracellular, respiration-linked Fe(III) citrate reduction. *Microbiology* 153, 3572–85. doi:10.1099/mic.0.2007/006478-0.

Coursolle, D., Baron, D. B., Bond, D. R., and Gralnick, J. A. (2010). The Mtr respiratory pathway is essential for reducing flavins and electrodes in Shewanella oneidensis. *J. Bacteriol.* 192, 467–474. doi:10.1128/JB.00925-09.

Esteve-Núñez, A., Sosnik, J., Visconti, P., and Lovley, D. R. (2008). Fluorescent properties of c-type cytochromes reveal their potential role as an extracytoplasmic electron sink in Geobacter sulfurreducens. *Environ. Microbiol.* 10, 497–505. doi:10.1111/j.1462-2920.2007.01470.x.

Gonzalez, C. F., Ackerley, D. F., Park, C. H., and Matin, A. (2003). A Soluble Flavoprotein Contributes to Chromate Reduction and Tolerance byPseudomonas putida. *Acta Biotechnol.* 23, 233–239. doi:10.1002/abio.200390030.

Inoue, K., Qian, X., Morgado, L., Kim, B.-C., Mester, T., Izallalen, M., et al. (2010). Purification and Characterization of OmcZ, an Outer-Surface, Octaheme c-Type Cytochrome Essential for Optimal Current Production by Geobacter sulfurreducens. *Appl. Environ. Microbiol.* 76, 3999–4007. doi:10.1128/AEM.00027-10.

Kaufmann, F., and Lovley, D. R. (2001). Isolation and Characterization of a Soluble NADPH-Dependent Fe(III) Reductase from Geobacter sulfurreducens. *J. Bacteriol.* 183, 4468–4476. doi:10.1128/JB.183.15.4468-4476.2001.

Kim, B.-C., Leang, C., Ding, Y.-H. R., Glaven, R. H., Coppi, M. V, and Lovley, D. R. (2005). OmcF, a putative c-Type monoheme outer membrane cytochrome required for the expression of other outer membrane cytochromes in Geobacter sulfurreducens. *J. Bacteriol.*

187, 4505–13. doi:10.1128/JB.187.13.4505-4513.2005.

Kostylev, M., Otwell, A. E., Richardson, R. E., and Suzuki, Y. (2015). Cloning Should Be Simple: Escherichia coli DH5α-Mediated Assembly of Multiple DNA Fragments with Short End Homologies. *PLoS One* 10, e0137466. doi:10.1371/journal.pone.0137466.

Leang, C., Coppi, M. V., and Lovley, D. R. (2003). OmcB, a c-Type Polyheme Cytochrome, Involved in Fe(III) Reduction in Geobacter sulfurreducens. *J. Bacteriol.* 185, 2096–2103. doi:10.1128/JB.185.7.2096-2103.2003.

Li, Z., Kim, D. D., Nelson, O. D., Otwell, A. E., Richardson, R. E., Callister, S. J., et al. (2015). Molecular dissection of a putative iron reductase from Desulfotomaculum reducens MI-1. *Biochem. Biophys. Res. Commun.* 467, 503–8. doi:10.1016/j.bbrc.2015.10.016.

Lloyd, J. R., Leang, C., Hodges Myerson, A. L., Coppi, M. V, Cuifo, S., Methe, B., et al. (2003). Biochemical and genetic characterization of PpcA, a periplasmic c-type cytochrome in Geobacter sulfurreducens. *Biochem. J.* 369, 153–161. doi:10.1042/BJ20020597.

Lovley, D. R., and Phillips, E. J. P. (1988). Novel Mode of Microbial Energy Metabolism: Organic Carbon Oxidation Coupled to Dissimilatory Reduction of Iron or Manganese. *Appl. Environ. Microbiol.* 54, 1472–1480. Available at: http://www.ncbi.nlm.nih.gov/pmc/articles/PMC202682/.

Magnuson, T. S., Hodges-Myerson, A. L., and Lovley, D. R. (2000). Characterization of a membrane-bound NADH-dependent Fe3+ reductase from the dissimilatory Fe3+-reducing bacterium Geobacter sulfurreducens. *FEMS Microbiol. Lett.* 185, 205–211. doi:10.1111/j.1574-6968.2000.tb09063.x.

Magnuson, T. S., Isoyama, N., Hodges-Myerson, A. L., Davidson, G., Maroney, M. J., Geesey, G. G., et al. (2001). Isolation, characterization and gene sequence analysis of a membrane-associated 89 kDa Fe(III) reducing cytochrome c from Geobacter sulfurreducens. *Biochem. J.* 359, 147–152. Available at: http://www.ncbi.nlm.nih.gov/pmc/articles/PMC1222130/.

Marsili, E., Baron, D. B., Shikhare, I. D., Coursolle, D., Gralnick, J. A., and Bond, D. R. (2008). Shewanella secretes flavins that mediate extracellular electron transfer. *Proc. Natl. Acad. Sci.* 105, 3968–3973. doi:10.1073/pnas.0710525105.

Myers, C. R., and Nealson, K. H. (1988). Bacterial Manganese Reduction and Growth with Manganese Oxide as the Sole Electron Acceptor. *Science (80).* 240, 1319–1321. doi:10.1126/science.240.4857.1319.

Nevin, K. P., and Lovley, D. R. (2000). Lack of production of electron-shuttling compounds or solubilization of Fe(III) during reduction of insoluble Fe(III) oxide by Geobacter metallireducens. *Appl. Environ. Microbiol.* 66, 2248–2251. Available at: http://www.ncbi.nlm.nih.gov/pubmed/10788411.

O'Toole, G. A., Pratt, L. A., Watnick, P. I., Newman, D. K., Weaver, V. B., and Kolter, R. (1999). Genetic approaches to study of biofilms. *Methods Enzymol.* 310, 91–109. Available at: http://www.ncbi.nlm.nih.gov/pubmed/10547784 [Accessed January 8, 2016].

Okamoto, A., Hashimoto, K., Nealson, K. H., and Nakamura, R. (2013). Rate enhancement of bacterial extracellular electron transport involves bound flavin semiquinones. *Proc. Natl. Acad. Sci.* 110, 7856–7861. doi:10.1073/pnas.1220823110.

Okamoto, A., Nakamura, R., Nealson, K. H., and Hashimoto, K. (2014a). Bound Flavin Model

Suggests Similar Electron-Transfer Mechanisms in Shewanella and Geobacter. *ChemElectroChem* 1, 1808–1812. doi:10.1002/celc.201402151.

Okamoto, A., Saito, K., Inoue, K., Nealson, K. H., Hashimoto, K., and Nakamura, R. (2014b). Uptake of self-secreted flavins as bound cofactors for extracellular electron transfer in Geobacter species. *Energy Environ. Sci.* 7, 1357. doi:10.1039/c3ee43674h.

Opperman, D. J., Piater, L. A., and van Heerden, E. (2008). A Novel Chromate Reductase from Thermus scotoductus SA-01 Related to Old Yellow Enzyme. *J. Bacteriol.* 190, 3076–3082. doi:10.1128/JB.01766-07.

Otwell, A. E., Sherwood, R. W., Zhang, S., Nelson, O. D., Li, Z., Lin, H., Callister, S. J. and Richardson, R. E. (2015), Identification of proteins capable of metal reduction from the proteome of the Gram-positive bacterium *Desulfotomaculum reducens* MI-1 using an NADH-based activity assay. Environ Microbiol, 17: 1977–1990. doi:10.1111/1462-2920.12673.

Qian, X., Mester, T., Morgado, L., Arakawa, T., Sharma, M. L., Inoue, K., et al. (2011). Biochemical characterization of purified OmcS, a c-type cytochrome required for insoluble Fe(III) reduction in Geobacter sulfurreducens. *Biochim. Biophys. Acta - Bioenerg.* 1807, 404–412. doi:10.1016/j.bbabio.2011.01.003.

Rollefson, J. B., Levar, C. E., and Bond, D. R. (2009). Identification of genes involved in biofilm formation and respiration via mini-Himar transposon mutagenesis of Geobacter sulfurreducens. *J. Bacteriol.* 191, 4207–17. doi:10.1128/JB.00057-09.

Shi, L., Richardson, D. J., Wang, Z., Kerisit, S. N., Rosso, K. M., Zachara, J. M., et al. (2009). The roles of outer membrane cytochromes of Shewanella and Geobacter in extracellular electron transfer. *Environ. Microbiol. Rep.* 1, 220–227. doi:10.1111/j.1758-2229.2009.00035.x.

Shi, L., Squier, T. C., Zachara, J. M., and Fredrickson, J. K. (2007). Respiration of metal (hydr)oxides by Shewanella and Geobacter: a key role for multihaem c-type cytochromes. *Mol. Microbiol.* 65, 12–20. doi:10.1111/j.1365-2958.2007.05783.x.

Tolker-Nielsen, T. (2014). Pseudomonas aeruginosa biofilm infections: from molecular biofilm biology to new treatment possibilities. *APMIS. Suppl.*, 1–51. doi:10.1111/apm.12335.

Supplementary Figures:

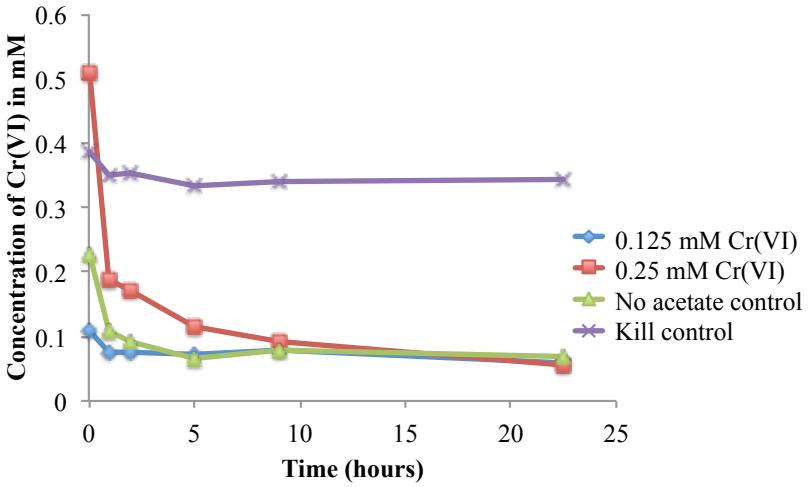

Supplementary Figure 3.1: *Geobacter sulfurreducens* is capable of Cr(VI) reduction. Fumarate/acetate grown cells were prepared in cell suspensions by washing and resuspending to equal cell density in Elias activity buffer minus NADH and ferrozine (see Chapter 2). Cr(VI) concentrations of 0.125 and 0.25 mM were tested (both with 3.3 mM acetate) and a no acetate control was prepared with 0.125 mM Cr(VI). A kill control was prepared by boiling cells for 10 minutes. 0.125 mM Cr(VI) and 3.3 mM acetate were added to the kill control. Disappearance of Cr(VI) was monitored with the diphenylcarbazide assay (see Chapter 2).

a. b.

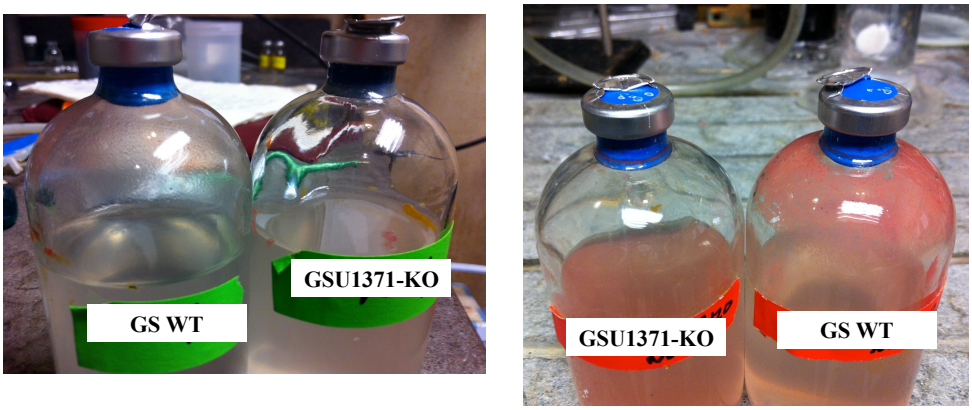

Supplementary Figure 3.2: Decreased biofilm phenotype is observed in GSU1371-KO as compared to WT in both early and late growth phase cultures. During growth on fumarate/acetate conditions, the *G. sulfurreducens* WT displays formation of a biofilm attached to the bottle (inverted during growth) during early growth phase **(a)**. By late growth phase, the attached biofilm can become thick and dark pink **(b)**. In comparison to the WT, the GSU1371-KO displays a decreased biofilm formation phenotype.

Chapter 4

Cloning Should Be Simple:

Escherichia coli DH5α-Mediated Assembly of

Multiple DNA Fragments with Short End Homologies

Prelude

During my last two years at Cornell, I had the opportunity to spend multiple weeks working with the Synthetic Biology and Bioenergy group at J. Craig Venter Institute. While creating constructs for the heterologous expression of certain old yellow enzymes for my work on microbial metal reduction, we began developing a technique for *in vivo E. coli*-mediated DNA assembly. We found the technique to work exceptionally well for the type of two-fragment assemblies necessary for creating a heterologous expression construct. When we decided to delete GSU1371 from the genome of *G. sulfurreducens* (described in the previous chapter), Maxim Kostylev and I decided to attempt to construct the four-fragment construct necessary for creating a GSU1371-knockout. The *E. coli*-mediated DNA assembly technique worked impressively well, quickly and efficiently assembling the multi-fragment construct without the need for exogenous enzymes. The characterization of this technique is the content of this chapter.

Summary

Numerous DNA assembly technologies exist for generating plasmids for biological studies. Many procedures require complex *in vitro* or *in vivo* assembly reactions followed by plasmid propagation in recombination-impaired *Escherichia coli* strains such as DH5α, which are optimal for stable amplification of the DNA materials. Here we show that despite its utility as a cloning strain, DH5α retains sufficient recombinase activity to assemble up to six double-stranded DNA fragments ranging in size from 150 bp to at least 7 kb into plasmids *in vivo*. This process also requires surprisingly small amounts of DNA, potentially obviating the need for upstream assembly processes associated with most common applications of DNA assembly. We demonstrate the application of this process in cloning of various DNA fragments including synthetic genes, preparation of knockout constructs, and incorporation of guide RNA sequences

in constructs for clustered regularly interspaced short palindromic repeats (CRISPR) genome editing. This consolidated process for assembly and amplification in a widely available strain of *E. coli* may enable productivity gain across disciplines involving recombinant DNA work.

Introduction

Recombinant DNA technologies have been critical for driving biotechnological advances and facilitating studies aimed at understanding basic biological principles. Despite its limitations, restriction digestion- and ligation-based cloning is still widely used to generate DNA constructs for a variety of molecular biology applications. At the same time, techniques for the seamless assembly of DNA have been rapidly expanding, enabling more precise genetic manipulation in synthetic biology and metabolic engineering. Many of these methods rely on the annealing of strands from neighboring DNA fragments, allowing for assembly of fragments with overlapping ends. Both *in vitro* [1–10] and *in vivo* [11–21] techniques have been developed for this purpose.

A particular advantage of *in vivo* techniques is that they do not require externally added purified enzymes. The yeast *Saccharomyces cerevisiae* is used as a host organism for *in vivo* DNA assembly due to its ability to efficiently repair double-strand breaks. Multiple linear DNA fragments can be taken up and accurately assembled via homologous recombination in yeast [11–15]. However, relative to *S. cerevisiae*, *Escherichia coli* offers a number of strengths as a host organism for *in vivo* DNA assembly including faster growth rates, higher plasmid yields, and greater transformation efficiency. A number of studies have led to the development of *in vivo* DNA assembly methods in *E. coli*, primarily utilizing the RecA-independent λ phage- and Rac prophage-based systems (λ Red and RecET, respectively) [16–18]. *E. coli* also has been shown to contain endogenous RecA-independent homologous recombination activities, but the mechanisms remain to be fully characterized [2,21–24].

One of the most common laboratory *E. coli* strains used to maintain and amplify small plasmid DNA is K-12 derived DH5α. Typical DNA assembly and cloning procedures involve as their last step transformation of the constructed plasmid into competent DH5α cells. Even for λ Red- and RecET-based methods, it is recommended that the *in vivo* assembled plasmid be transferred into a cloning strain such as DH5α to ensure stability of the DNA product [18]. It has been previously shown that DH5α cells have some ability to recombine *in vivo* heterologous DNA fragments with homologous ends, albeit at relatively low efficiency [19–21,25]. We therefore explored the ability of this strain to recombine DNA for the purpose of simplifying basic DNA cloning and multi-fragment assembly.

Our scheme for *E. coli* DH5α-mediated DNA assembly involves only two basic steps: preparation of DNA fragments to be assembled and introduction of the fragments into competent cells **(Fig 4.1)**. When PCR is used to generate these fragments from plasmids that share the marker used for the final transformant selection, the PCR templates can contribute to false positives where transformants contain no assembled products. These templates can be conveniently removed using DpnI restriction enzyme, which specifically destroys *E. coli*-derived templates at methylated GATC sequences while not affecting non-methylated PCR fragments. After the fragments are prepared, they are directly introduced into DH5α cells. DNA amplification, DpnI digestion, and transformation can be completed in one day. This is a simple and rapid DNA assembly technique that can be employed for a variety of applications.

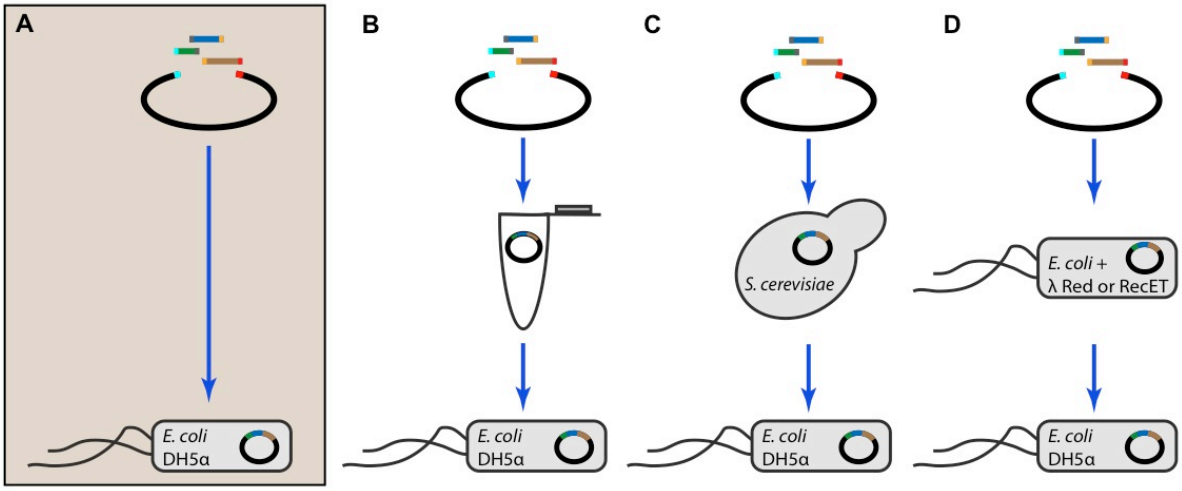

Figure 4.1: *In vivo* DNA assembly and cloning in *E. coli* DH5α
(A)E. coli DH5α-mediated DNA assembly involves only two basic steps: 1) preparation of fragments with homologous ends and 2) introduction of the fragments into competent cells. This approach minimizes the time and reagents required for DNA assembly in comparison to other common methods, which contain a separate assembly step before the introduction of the constructed plasmid into a recombination-impaired cloning strain such as DH5α (**B-D**). Assembly is typically carried out either with added enzymes *in vitro* (**B**), or *in vivo*, using as a host *S. cerevisiae* (**C**) or specialized *E. coli* strains expressing the λ Red or RecET phage-based systems (**D**).

Materials and Methods

Bacterial strains

The following commercial products were used: Max Efficiency DH5α (Life Technologies, Carlsbad, CA; chemically competent, ~109 colony-forming unit or CFU / μg pUC19), High Efficiency NEB 5-alpha (New England Biolabs, Ipswich, MA; chemically competent, CFU ~109/μg pUC19), and NEB 5-alpha Electrocompetent *E. coli* (New England Biolabs, CFU ~1010/μg pUC19).

DNA

Original pUC19 and pBR322 vectors were used for most assemblies. For the cloning of cellulase genes, a vector derived from pYOGM081 [26] was used. The following modifications were made (T. Hanly, M.K., and Y.S., unpublished result). The att sites for Gateway cloning (Life Technologies) were removed and GAL1-10 promoter for expressing an exogenous gene was replaced with ENO1 promoter, followed by sequences encoding the 19-amino acid signal sequence of *S. cerevisiae* mating factor alpha 1, Ala-Gly dipeptide, human influenza hemagglutinin epitope tag, 17-amino acid Gly-Ser linker (codon-optimized for *S. cerevisiae*; DNA 2.0, Inc., Menlo Park, CA), Ser-Thr linker (codon-optimized for *S. cerevisiae*; DNA 2.0, Inc.), and dockerin from *Ruminococcus flavefaciens* cel44A gene (codon-optimized for *S. cerevisiae*; DNA 2.0, Inc.). Between the sequences for the Gly-Ser linker and the Ser-Thr linker is the cellulase insertion site. For gRNA plasmid alteration experiments, p426-SNR52p-gRNA.CAN1.Y-SUP4t (6.3 kb; [27]) and PTRC gRNA pUC (3.2 kb; P. Weyman and K. Schmitz, unpublished result) plasmids were used.

Cellulase genes **(S4.1 Table)** were synthesized using BioXp 3200 system (SGI-DNA, La Jolla, CA). All the fragments contained at their 5' and 3' ends 40-bp homology to the insertion site of the above vector, as well as so-called Gibson ends outside of the user defined sequences. Gel-purification is recommended in the manufacturer protocol to remove intermediate by-products (SGI-DNA). To aid with high-throughput assembly of 29 constructs, we modified the protocol by replacing gel-purification with PCR amplification. The synthesized genes were PCR-amplified using the primers that matched the 5' and 3' homologous sequences **(S4.2 Table)** and purified using Nucleospin Gel and PCR Clean-Up kit (Macherey-Nagel, Bethlehem, PA). The sequence encoding a 17-amino acid Gly-Ser linker and three cohesin domains of *Clostridium thermocellum* cipA gene was codon-optimized (Integrated DNA Technologies, Coralville, IA)

for expression in *S. cerevisiae* and synthesized as 3 gBlocks fragments 966, 499, and 987 bp in length (Integrated DNA Technologies).

All DNA fragments, including the synthesized fragments, were PCR-amplified using high-fidelity DNA polymerases PrimeSTAR Max (2× Master Mix, Takara Bio, Mountain View, CA) or Q5 (Hot-Start 2× Master Mix, New England Biolabs). Primers and templates are listed in **S4.2 Table**. When applicable, PCR products were subjected to DpnI digest (New England Biolabs; CutSmart buffer was added to final concentration of 1× for all digests) for ~2 hours at 37°C. Nucleospin Gel and PCR Clean-Up kit (Macherey-Nagel) was used for PCR product purification.

Transformation of E. coli and assembly verification

Transformation of Max Efficiency DH5α competent cells was modified from the manufacturer's protocol as follows. 25 µl of cells were used per transformation, corresponding to one fourth of the recommended cell volume. Cells were transferred to 2 ml polypropylene tubes (Axygen, Union City, CA). DNA was diluted and mixed in Milli-Q purified sterile water and 2.5 µl was added per transformation. No difference in transformation efficiency was observed when the DNA was prepared in 10 mM Tris-HCl buffer, pH 8.5, with or without 1 mM EDTA. Cells and DNA were incubated on ice for 30 minutes and then placed in a 42°C water bath for 45 seconds. Following a two- to five-minute incubation on ice, 225 µl of room temperature SOC medium (Life Technologies) was added to the tubes, and the cells were allowed to recover at 37°C with shaking at 250 rpm for one hour. Cells were then plated on LB-agar plates with appropriate antibiotics (100 µg/ml ampicillin, 60µg/ml kanamycin) and X-gal/IPTG, when applicable. Plates were incubated at 37°C overnight. Transformation of NEB 5-alpha chemically competent cells was the same as above with the following modifications. 25 µl of cells

corresponded to half of the recommended cell volume per transformation. The cells were placed at 42°C for 30 seconds and were allowed to recover in 450 µl of SOC medium. Transformation of NEB 5-alpha electrocompetent cells was performed following the manufacturer's protocol.

For p426-SNR52p-gRNA.CAN1.Y-SUP4t self-closure experiments 1 ng of the original gRNA plasmid was used as template DNA in a 50-µl PCR reaction. PrimeSTAR Max polymerase (2× Master Mix, Takara Bio) was used to generate both altered plasmids. PCR reactions were digested with DpnI for ~2 hours at 37°C and purified with Nucleospin Gel and PCR Clean-Up kit (Macherey-Nagel). 1 µl of the purified product (125–150 ng DNA) was combined with 25 µl NEB 5-alpha chemically competent cells and transformation was performed as above. For the PTRC gRNA pUC alteration, PCR was carried out using 0.4 ng of the original gRNA plasmid and PrimeSTAR Max polymerase in a 20-µl reaction. PCR product was purified (without DpnI digest). When 1 µl (38 ng) of the purified product was combined with 10 µl NEB 5-alpha chemically competent cells, ~1,000 colonies formed on an ampicillin plate.

To verify correct assembly of the plasmids (not including those in plasmid-alteration experiments), colony PCR was performed with Quickload OneTaq polymerase (2× Master Mix, New England Biolabs) using primers outside of the insertion junctions **(S4.2 Table)**. For Sanger sequencing, colonies were cultured in LB medium containing the appropriate antibiotics and the DNA was isolated using a miniprep kit (Qiagen, Valencia, CA).

Results

Single-fragment cloning

If DNA constructs can be generated and propagated in a single organism, the overall workflow in molecular biology can be considerably simplified with far-reaching impacts on scientific advances. According to published data, *E. coli* is able to recombine DNA fragments

that share more than ~20-base end homology and the efficiency increases with increasing homology length regardless of the recombination mechanism [2,16,22,23,25,28]. We chose ~50-bp end homology for most of the experiments described here because this length is readily attainable using standard commercially available DNA primers. Reasoning that transformation efficiency may play an important role in the overall cloning efficiency, we chose commercially available, highly competent (~109 colony-forming unit or CFU / μg pUC19) DH5α cells. In preliminary experiments we determined that chemically competent cells are more efficient than electrocompetent ones **(Table 4.1)**.

***E. coli* strain**	**Expected transformation efficiency (CFU/μg pUC19)**	**Blue colonies per 25 μl cells[a,b]**	**Viable cell counts per 25 μl cells**	**Blue colonies per 10^9 viable cells**
Max Efficiency DH5α™, chemically competent (Life Technologies)	>1 x 10^9	821	3 × 10^9	243
High efficiency NEB 5-alpha, chemically competent (New England Biolabs)	1–3 x 10^9	619	2 × 10^9	292
NEB 5-alpha, electrocompetent (New England Biolabs)	>1 x 10^{10}	507	4 × 10^{10}	13

[a] 1 ng vector was used per transformation with a molar insert-to-vector ratio of 5:1.

[b] 25 μl cells corresponds to 1/4, 1/2, and 1 recommended transformation cell volume in rows 1, 2, and 3, respectively.

Table 4.1. Assembly of pUC19 by different commercial strains.

To determine the efficiency and fidelity of DH5α-mediated *in vivo* assembly and cloning, we designed a pUC19 plasmid-based screen **(Fig 4.2A)**. In this work, efficiency is defined as the number of colonies obtained per quantity of added DNA. Fidelity is defined as the presence of all introduced fragments in a generated construct. Two fragments of pUC19 were PCR-amplified to create an insert and a vector (544 bp and 2,241 bp, respectively) with 50 bp of homology at their ends. The insert contained the coding sequence of the lacZα gene starting at nucleotide position five, as well as some of the downstream pUC19 plasmid sequence, while the vector contained the rest of the plasmid, including the ampicillin (Amp) resistance gene (bla) and the origin of replication. This design was employed for two reasons. Primarily, it allowed for efficient screening of correctly assembled plasmids, identified as blue colonies on X-gal-containing agar plates **(S4.1 Fig)**. In addition, it enabled us to determine whether the few colonies observed in vector-only (negative control) transformations were due to template plasmid carryover (blue colonies) or other events such as self-closure and chromosomal integration of the vector (mostly white colonies), potentially mediated by non-homologous end joining or microhomology-based recombination [29].

To determine the effect of DNA quantity on transformation efficiency, we tested a range of 0.1 to 10 ng vector DNA per ~3 × 109 cells (25 µl cell suspension, corresponding to ¼ of the recommended transformation volume), maintaining an insert-to-vector molar ratio of 5:1 **(Fig 4.2B)**. At low DNA concentrations, the number of colonies depended strongly on the amount of DNA added to each transformation, but the effect became less pronounced at higher DNA concentrations. Importantly, nearly all colonies were blue, indicating correct assembly of the plasmid. The few white colonies accounted for less than 1% of the total colony number **(S4.3 Table)**. Negative control transformations using either the insert or the vector alone were done to

quantify the amount of undigested pUC19 template DNA from DpnI digest. As expected, very few colonies were observed even at the highest DNA concentrations used **(S4.3 Table)**. Altogether, the colony numbers on the negative control plates and the white colonies present on the experimental plates accounted for less than 1% of the total colony numbers. Sanger sequencing of DNA from ten colonies confirmed correct coding and junction sequences in all cases.

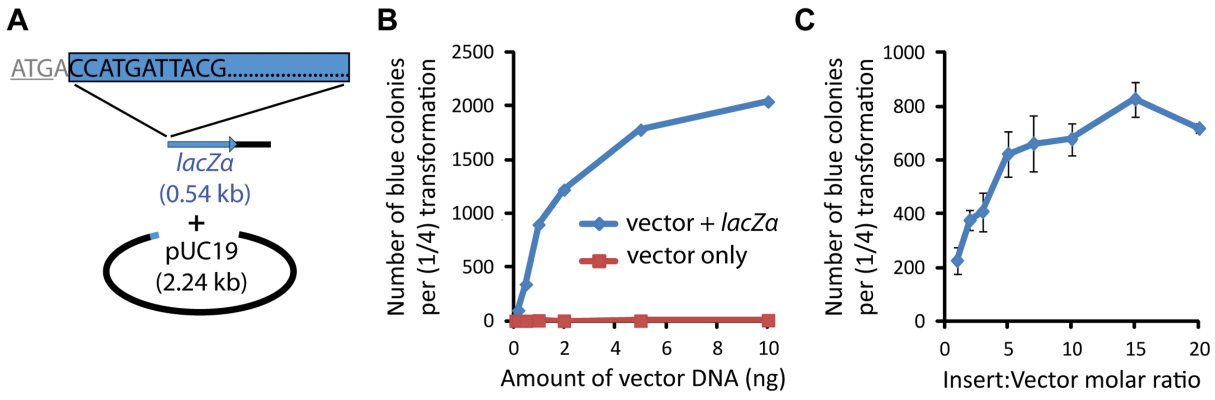

Figure 4.2: pUC19-*lacZα* assembly assay
(**A**) Two fragments were PCR-amplified from the pUC19 vector to create an efficient screen for DNA assembly capability. The smaller "insert" fragment contained the coding sequence of the *lacZα* gene starting at position five and some downstream vector sequence. The larger "vector" fragment contained the rest of the plasmid, including the Amp resistance gene (*bla*) and the origin of replication. The fragments shared 50-bp homology at both ends. (**B**) Blue colony formation as a function of DNA concentration. Very few white colonies were observed on any of the plates **(Supplementary Table 4.3).** Small numbers of blue colonies present in the vector-only transformations are indicative of the small amount of contaminating circular template pUC19 used in PCR-mediated linearization of the vector and undigested during DpnI treatment. Insert-to-vector molar ratio was maintained at 5:1, and 25 µl of cells were used, corresponding to ¼ of the recommended volume. (**C**) Effect of insert-to-vector molar ratio on assembly efficiency. The vector DNA quantity was maintained at 0.5 ng. Error bars indicate standard deviation from two independent sets of experiments.

In some DNA assembly techniques, the molar ratios of DNA fragments can affect assembly efficiency, with an excess of small fragments leading to maximal efficiency [2,10,30]. To determine whether this is the case for the current method, we tested insert-to-vector molar

ratios in the range of 1:1 to 20:1 with the pUC19 plasmid-based screen **(Fig 4.2C)**. Vector DNA concentration was maintained at 0.5 ng. Increasing the insert-to-vector molar ratio resulted in an increased number of colonies, with the effect being most evident at lower ratios and hitting the point of diminishing returns around 5:1.

Transformation efficiency decreases with increasing plasmid size [31] and pUC19 is one of the smallest commonly used cloning vectors. To verify that the results obtained in the pUC19-based experiments apply to the generation of larger plasmids, we tested the ability of DH5α to assemble a 1.4-kb cellulase gene (cbhA) from Aspergillus niger, codon-optimized for *S. cerevisiae* [32], with a custom 7-kb high-copy vector (containing the pBluescript SK+ backbone) derived from the plasmid pYOGM081 [26]. The two fragments, designed to share 50 bp of homology at each end, were amplified using PCR. We tested 0.1–100 ng vector DNA with insert-to-vector molar ratio of 5:1 and observed a similar pattern as that seen for pUC19 **(S4.2 Fig)**. The efficiency of assembly, quantified as colony number, was lower than that observed with pUC19, presumably due to the larger size of the DNA fragments. Seven to 852 colonies were obtained for the tested DNA concentrations. Thirty colonies were analyzed using colony PCR, and all showed the insert of the correct size **(S4.3 Fig)**. Sanger sequencing of 20 junctions confirmed correct assembly in all but one case, where a one-base deletion was identified. This may be due to an erroneous primer having been incorporated in the PCR amplification of the fragments to be assembled.

Based on the results obtained with the cbhA construct assembly, we used this method to assemble a library of 29 cellulase genes into the same custom vector, for use in a different project in our group. Bacterial and fungal cellulase genes were chosen from the CAZy database (www.cazy.org), codon-optimized for yeast expression [32], and synthesized in-house using the

BioXpTM 3200 system (SGI-DNA, La Jolla, California). All synthesized fragments were PCR-amplified using primers that matched part of the universal sequences upstream and downstream of the gene (See **Materials and Methods**; **S4.2 Table)**. All amplified fragments contained at each end 40-bp sequences homologous to the vector. To enable high-throughput assembly, the transformation was scaled in half (~1.5 × 109 cells, corresponding to ⅛ of the recommended cell suspension volume) and carried out in PCR strips. For each assembly, 5 ng vector was mixed with 5 ng cellulase fragment, resulting in an insert-to-vector molar ratio between 5:1 and 9:1.

Transformations produced four to 112 colonies per reaction **(S4.1 Table)**, indicating that sequence length, composition, or structure of the insert may significantly affect assembly efficiency. We also observed a batch effect, where one group of assemblies produced substantially more colonies than the other (**S4.1 Table**, reactions 1–16 vs. 17–29). This may have been caused by slight differences between batches of cells and/or experimental techniques. One to three colonies were picked for each construct and tested using colony PCR, and the desired construct was obtained in all attempted assemblies. A great majority of tested colonies (47 out of 54) showed the insert of the expected size, and in most cases, incorrect assemblies correlated with PCR products that showed abnormalities (e.g., the presence of non-specific bands and smears; **S4.1 Table**). Altogether, our results demonstrate the utility of *E. coli*-mediated assembly for high-throughput cloning in an efficient and cost effective manner, requiring small amounts of DNA and minimal screening.

Multi-fragment cloning

In many instances, it is necessary to assemble several DNA fragments, such as in the construction of fusion proteins, gene knockout cassettes, and large genes from smaller synthesized fragments. To explore whether DH5α is able to combine *in vivo* several fragments in

one transformation event, we attempted the assembly of a gene knockout construct using three PCR-amplified fragments and a PCR-linearized pBR322 vector. The knockout cassette was designed to delete gene GSU 1371 from *Geobacter sulfurreducens*. 0.5-kb sequences upstream and downstream of GSU 1371 were PCR-amplified from *G. sulfurreducens* genomic DNA, and the kanamycin (Kan) cassette was amplified from the pET28a vector **(Fig 4.3A)**. An important advantage of knockout cassette assembly is the option to apply double selection to the transformed colonies (when the marker for knockout, in addition to the one for plasmid maintenance, is functional in *E. coli*), which promotes high fidelity of the obtained constructs. Furthermore, when using double selection, we found it unnecessary to remove residual template vector DNA with DpnI **(S4.4 Table)**, which further simplifies the overall assembly protocol.

Similar to the single-fragment experiments, we tested the effect of added DNA quantity, ranging from 1 to 100 ng, on the efficiency of multi-fragment assemblies (quantified as colony numbers obtained per transformation; **Fig 4.3B**). The molar ratios of all "insert" fragments with respect to the vector were maintained at 5:1. As for single-fragment cloning, increasing the amount of added DNA resulted in an increased number of colonies, with the effect more pronounced at low DNA concentrations. PCR analysis of 30 colonies confirmed the presence of an insert of the correct size **(S4.4 Fig)**, and restriction analysis of five colonies resulted in the expected pattern in all cases. The assembled knockout cassette was successfully used to remove GSU 1371 from *G. sulfurreducens* (A.E.O and R.E.R., unpublished result).

It is likely that sizes of DNA fragments affect efficiency and accuracy of assembly. In addition to absolute sizes of fragments, relative sizes or differences in size among the fragments may affect DNA assembly. To evaluate the effect of fragment size on DNA assembly efficiency, we varied the length of the fragments upstream and downstream of GSU 1371 (targeting

fragments) from 150 to 1,150 bp (including the overlap regions), working with 10 ng vector DNA and insert-to-vector molar ratios of 5:1 **(Fig 4.3C)**. Assemblies with 150- and 250-bp targeting fragments resulted in significantly reduced colony numbers compared to those with targeting sequences 350 bp and longer. Since the efficiency of cellular entry is not expected to be reduced for smaller DNA fragments [31], our results suggest that processes subsequent to this step are unfavorable to incorporating short fragments. It is possible that such fragments are more easily degraded by exonuclease action before they are able to recombine with a neighboring fragment [23].

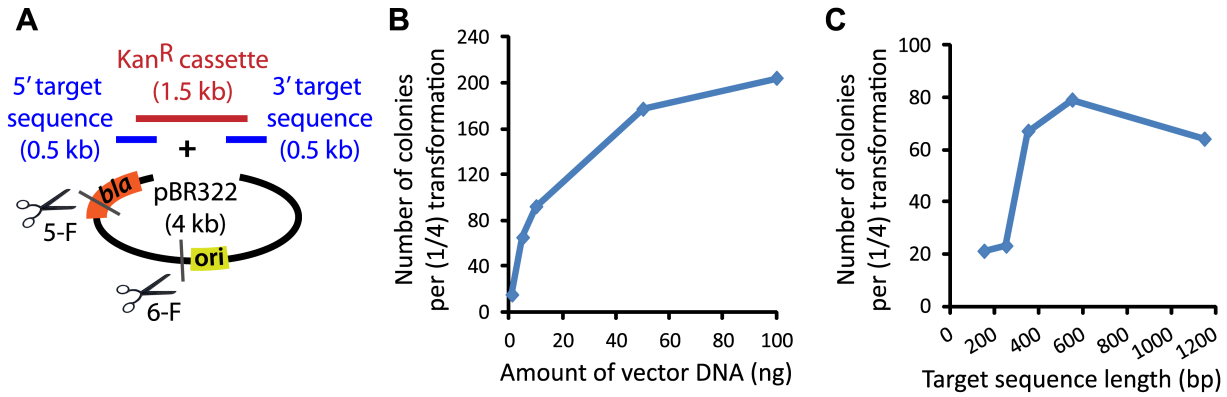

Figure 4.3: Knockout cassette assembly for the deletion of GSU 1371 from *Geobacter sulfurreducens*

(A) The GSU 1371 knockout construct was assembled from four fragments including 0.5-kb sequences upstream and downstream of GSU 1371, the kanamycin cassette (amplified from pET28a), and the PCR-linearized pBR322 vector. All adjacent fragments shared 50-bp end homology. In five- and six-fragment assembly experiments, a fifth site (5-F) and both the fifth and sixth sites (5-F and 6-F), respectively, were used to make additional junctions with homology for assembly. (**B**) Assembly efficiency as a function of DNA concentration was examined using plates containing both Kan and Amp. Colony PCR confirmed the correct insertion in 30/30 transformants tested (**Supplementary Figure 4.4**). (**C**) The size of the fragments upstream and downstream of GSU 1371 was varied to test the effect on DNA assembly efficiency. Reducing the length of fragments to 250 bp and less resulted in a substantially lower number of colonies. Molar ratio of insert fragments-to-vector was maintained at 5:1 in all experiments.

While double selection is an inherent advantage in the assembly of gene knockout constructs, this option is not available in many other DNA assembly applications. To compare the effect of single and double selection on fidelity, we repeated the knockout construct assembly using PCR-amplified vector DNA that had been treated with DpnI, and plated transformed cells on medium containing either both Kan and Amp or only Amp (matching the resistance on vector). Fidelity of the constructs was quantified as the fraction of colonies showing a correct band in colony PCR. Selection on Amp alone resulted in about twice as many colonies as that on both antibiotics, while fidelity of the assembled constructs decreased to 77% (27/35 colonies; **S4.5 Table** and **S4.5 Fig**). We observed similar results in the assembly of another construct. Codon-optimized scaffoldin gene cipA from *Clostridium thermocellum* was synthesized in three fragments, which were then used as templates to generate three PCR fragments. These were assembled into a pUC19 vector and selected on Amp plates. Colony numbers and fidelity are comparable to those obtained with the knockout construct assembly **(S4.6 Table and S4.6 Fig)**, suggesting that the presented method can be used successfully for a variety of multi-fragment assemblies.

To explore the limits of the number of fragments that can be assembled in *E. coli*, we split the pBR322 vector in either two or three fragments and repeated the knockout construct assemblies, now with a total of five or six fragments **(Fig 4.3A)**. For the five-fragment assembly, the vector was split within the Amp resistance gene, generating 765- and 3,320-bp fragments with 50-bp overlaps. For the six-fragment assembly, the 3,320 bp fragment was further split, generating 1,567- and 1,803-bp fragments. For both assemblies, all of the fragments were mixed in equimolar ratios such that the total amount of DNA from all fragments combined was ~125 ng (~30 fmol of each fragment) per transformation reaction. Transformants were selected on plates

containing either Amp alone or both Kan and Amp, and a subset of colonies was analyzed using colony PCR **(S4.7 Table)**. As expected, the colony numbers decreased significantly with the increasing number of fragments. For the five-fragment assembly, 10 (Kan-Amp) and 19 (Amp) colonies were obtained, whereas the six-fragment assembly resulted in only four (Kan-Amp) and 14 (Amp) colonies. As was the case for the four-fragment assembly with double-selection, all of the tested colonies for both five- and six-fragment assemblies selected on Kan-Amp plates had the correct knockout cassette as determined using colony PCR. Fidelity dropped to ~50–75% of the tested colonies from Amp-only plates **(S4.7 Table)**. Furthermore, restriction analysis performed on plasmids isolated from three colonies revealed the expected band pattern, confirming that the DH5α-mediated method is effective for multi-fragment DNA assembly.

Plasmid alteration via self-closure

Along with the assembly of one or more fragments into a vector, it is sometimes useful to alter existing plasmids. Common applications include the introduction of a point mutation in a cloned gene or deletion of a coding or regulatory region already in a plasmid. Presently, a powerful, targeted genome editing technique based on clustered regularly interspaced, short palindromic repeats (CRISPR) is emerging. The most studied and developed system uses CRISPR-associated protein 9 (Cas9) from *Streptococcus pyogenes* to create a double-stranded DNA break at a specified sequence [33]. Cas9 is targeted to a specific 20-bp sequence by a matching protospacer sequence of a guide RNA (gRNA), which is typically encoded on a plasmid. Once Cas9 and gRNA plasmids are constructed for engineering of an organism, Cas9 activity can be targeted to any new region of the genome simply by introducing an appropriate 20-bp gRNA sequence on the already constructed plasmid. Based on the demonstrated ability of DH5α to recombine DNA with homologous overlaps, we tested our method for the simple

replacement of short sequences in two different plasmids for expressing gRNA (see Materials and Methods). In one case, two new plasmids were derived from a 6.3-kb plasmid p426-SNR52p-gRNA.CAN1.Y-SUP4t [27] for the engineering of previously published *S. cerevisiae* GMToolkit-a and GMToolkit-α strains [34]. One plasmid was altered to target neutral locus YGR176W while the other to target a component of the GMToolkit module [34] not needed in subsequent applications. In another case, we altered a sequence in a 3.2-kb plasmid, PTRC gRNA pUC, for expressing gRNA in *Klebsiella pneumoniae* (P. Weyman and K. Schmitz, unpublished result) to target fepC, which encodes a ferric enterobactin transport ATP-binding protein [35]. In each case, the original gRNA-encoding plasmid was PCR-linearized using primers that contained the new 20-bp target sequence **(S4.2 Table)**. The resultant linear products, containing ends with 25- or 20-base homologous overlaps, were introduced into *E. coli*. Two colonies were picked for each of the p426-SNR53p-gRNA-based plasmids, and the correct new target sequence was confirmed in all using Sanger sequencing. PTRC gRNA pUC-based plasmids were purified from five colonies. All plasmids were of the expected size for a correctly recircularized plasmid, as assayed using agarose gel electrophoresis, and all plasmids contained the intended sequence in the gRNA region based on data from Sanger sequencing. The success of these experiments indicates that *E. coli*-mediated assembly can be readily integrated in existing CRISPR genome editing protocols for the quick alteration of constructed gRNA plasmids.

Discussion

Reducing the number of steps in DNA assembly has several important advantages. It can minimize the time and cost associated with the process, as well as with training for the technique and troubleshooting (because the sources and chance of errors can be simultaneously reduced). It

can also promote rapid adoption of the developed methods by the research community. To this end, we demonstrate what we believe to be the simplest and fastest method for the accurate assembly of DNA ranging from 150 to several thousand base pairs.

Bubeck et al. previously showed that *E. coli* DH5α has the ability to recombine linear DNA fragments sharing short homologous ends, thus making it possible to carry out simple *in vivo* fragment assembly [25]. However, the utility of this earlier published effort was limited by the cloning efficiency and fidelity. The low efficiency was likely due to the CaCl2 method with relatively low cell competence (~106 CFU / μg pBluescript SK- [25]). The perceived low fidelity was probably due to circular vector carryover, and this is indicated by high numbers of colonies observed in negative control vector-only transformations. To improve on these limitations, we used highly competent cells (~109 CFU / μg pUC19) and linearized the vector using PCR followed by a DpnI digest. Using highly competent cells helps ensure that a sufficient number of cells take up all of the DNA fragments that are required for correct assembly even at low concentrations of DNA. Compared to a traditional approach of vector linearization using restriction digest, PCR-mediated amplification of a linearized vector from a minute quantity of template plasmid DNA followed by the elimination of the methylated template ensures a purer sample of the linearized vector with little circular vector DNA. Our results show that for single-fragment cloning, using small amounts of DNA (<1–10 ng), it is possible to obtain hundreds to thousands of colonies, nearly all of which carry the correctly assembled recombinant plasmid. In subsequent DNA assemblies in our group, we have found that for single-fragment cloning, the DpnI digest of template plasmid DNA (used in sub-nanogram quantities for PCR) can be optionally skipped with only a small reduction in the fidelity due to the high cloning efficiency of such constructs. We also expanded the applications of DH5α-mediated cloning to multi-

fragment *in vivo* DNA assembly and to the alteration of existing plasmids, in particular for use with CRISPR-Cas9 genome editing protocols.

An approach very similar to ours, describing DH5α-mediated DNA assembly and cloning, was published [21] during the writing stage of this manuscript. In that study, up to three DNA fragments, prepared using PCR, were introduced into chemically-competent cells and the majority of the selected colonies carried the desired DNA construct. However, the cloning efficiency was up to 100 times lower than that reported in our experiments. For example, in single-fragment cloning experiments using 25 ng of pUC19 and molar insert-to-vector ratio of 2:1, only ~40 colonies were reported. Importantly, the higher cloning efficiencies observed with our method make it possible to assemble more fragments (up to six in our experiments) and simplify high-throughput cloning due to substantially lower requirements for DNA concentrations. Based on the experimental descriptions provided in the other study, we believe that several factors may explain the discrepancy. The authors used 30 bp homologous overlaps in most of their experiments, while we designed 40–50 bp overlaps for all of the reported assemblies. The transformation efficiency of the competent cells (prepared in-house using rubidium chloride method [36]) was not stated and it is possible that it was substantially lower than that of the commercial cells used in our work. Finally, the differences in the transformation protocols may also affect the overall cloning efficiency in our methods, although it is likely that the protocols should be optimized for the specific cells used. Three other efforts, relying on the same basic principle of introducing PCR-amplified DNA products into *E. coli* had been previously published [19,20,30]. In these studies the cloning efficiency is also relatively low and in two of them [19,20] the proposed basis of assembly was attributed to the annealing of complementary single stranded DNA overhangs common to PCR products. However, in the

study by Jacobus and Gross [21], this hypothesis is disproven in cloning experiments using restriction enzyme digested products, which show definitively that the assembly of the DNA fragments occurs *in vivo*. Together, our study along with those mentioned above demonstrate the applicability of *in vivo* cloning in *E. coli* DH5α, while the experimental differences provide a basis for balancing the cost and cloning efficiency for user-specific experimental needs.

In the pUC19-lacZ experiments, only a few white colonies were observed in both experimental and vector-only transformations, suggesting that non-homologous end joining was extremely rare in the *E. coli* DH5α strain. It is therefore somewhat surprising that the fidelity of the multi-fragment assembly (frequency of colonies containing a correctly assembled plasmid among colonies tested) is lower with single antibiotic selection than that observed for single fragment cloning, and the reason for this is not clear. One possible explanation is that the greater variety of sequences at double-strand breaks increases the chance of having unintended end-microhomologies that may be able to recombine [29], forming unwanted products.

Plasmid DNA is commonly transformed into *E. coli* rendered competent either by chemical treatment or electroporation, with the latter method generally yielding higher transformation efficiencies, as measured by CFU per amount added DNA. However, our preliminary results indicated that highly competent chemically-prepared cells (~109 CFU/μg pUC19) produce substantially more colonies than electroporated cells (~1010 CFU/μg pUC19) in the pUC19-lacZ assemblies **(Table 4.1)**. This result was supported by other assembly transformations attempted in our group and may be consistent with the previously described lack of recombinants using electroporation for DNA assembly in DH5α [25,28]. We hypothesize that the observed difference in assembly efficiency can be explained by the different mechanisms of DNA transport in the two approaches. The conditions employed for the transformation of

chemically competent cells are believed to promote the formation of multiple channels per cell as well as DNA crowding at the cell membranes. Uptake of one DNA molecule does not affect uptake of additional DNA, and multiple DNA molecules are commonly introduced into the same cell [31]. On the other hand, in electroporation-induced transformation, the DNA appears to enter the cells in a stochastic manner through the pores formed during the short electrical pulse. At the DNA concentrations employed in our experiments (1–10 ng DNA / ~4×1010 cells), not all viable cells are likely to be transformed due to the limited DNA present [37]. Thus, the probability that the same viable competent cell will take up all DNA fragments required for the correct assembly would decrease exponentially with each additional fragment. Based on the observations of Koskela and Frey, [30] it is also possible that in the transformation method of chemically-induced cells, DNA fragments to be assembled begin to interact during the incubation of DNA with competent cells before heat shock, further enhancing the efficiency of this method in comparison to electroporation-induced transformation. *E. coli*-mediated *in vivo* assembly methods employing the λ Red and RecET systems rely on electroporation for the co-transformation of DNA fragments to be assembled and usually call for relatively high DNA concentrations of 100 ng or more of each PCR fragment per transformation [16,18,38]. It is not clear whether a similar comparison between highly competent chemically induced cells and electroporation-induced cells has been performed in the published experiments.

Many studies have focused on mechanisms of homologous recombination in *E. coli*. RecA is the major bacterial recombination protein, essential for repair and maintenance of DNA in the cell [39]. RecA-dependent *in vivo* cloning with linear DNA fragments has been demonstrated in *E. coli*, but the assembly of fragments with short end-homology had low efficiency [40]. This was later supported by Lovett et al., showing that RecA-dependent

recombination is optimal with homologous regions longer than ~150 bp [22]. The phage-based λ Red and RecET systems are the major mechanisms of RecA-independent homologous recombination that have been studied *in E. coli*. Both systems have shown promise for *in vivo* assembly with short regions of homology (<50 bp [18]). The Red system has been studied and employed mainly for engineering of the *E. coli* chromosome and BACs, while the RecET system has shown greater utility for *in vivo* assembly of linear fragments [16,17,38]. Established procedures call for specialized strains expressing the Red or RecET systems and recommend a second transformation step into a recA- laboratory strain subsequent to "recombineering" in the specialized strain [18]. Based on current literature, DH5α does not contain an active form of either phage-encoded system. Other mechanisms of RecA-independent recombination have been identified in *E. coli*, both for recombination of double- and single-stranded DNA, but have not been fully characterized [22,24]. For double-stranded DNA, RecA-independent mechanisms have been found to be dominant for recombination of short homologous sequences (<50 bp) and to be limited by exonuclease activity [22,23]. We hypothesize that one of these mechanisms enables DH5α to efficiently assemble DNA fragments, as shown here. The observed frequency of recombinants for two-fragment assemblies in DH5α is ~10−7 per viable cell **(Table 4.1)**, which is substantially lower than that for either RecET (~10−3–10−4) or λ Red (~10−5) systems [18]. Nevertheless, as demonstrated here, sufficient colony numbers for many applications are obtained through transformation in highly competent DH5α cells, even for multi-fragment DNA assemblies. The lower recombination efficiency thus becomes an advantage, as it allows the same cell to be used to assemble, clone, and amplify the recombinant DNA.

As with any method, *E. coli*-mediated DNA assembly has some limitations. Based on the early Bubeck et al. study [25] and the colony numbers obtained in our experiments, it seems essential to use highly competent cells. While we have not fully explored the size limitation for DNA fragments used for assembly, results obtained with the GSU 1371 knockout construct suggest that the use of fragments smaller than ~350 bp may significantly reduce assembly efficiency. It is also known that transformation efficiency decreases with size [31], and it is likely that assembly of fragments larger than 20–30 kb will be challenging. Furthermore, our results suggest that assembly of more than five fragments is difficult and fidelity decreases with increasing number of fragments. Based on the trends observed in our experiments, it is likely that larger transformation volumes and/or greater amounts of DNA would help with at least some difficult assemblies.

Despite the stated limitations, the method described here should be pertinent to most biological applications that require recombinant DNA. Its power is in its simplicity, as it reduces cloning to two basic steps of DNA preparation and transformation of commercially available *E. coli* DH5α, with minimal requirements of reagents and time. It can be readily integrated into a wide range of experimental workflows.

Acknowledgements

This chapter is modified from work published in *PLoS ONE* on September 8, 2015. As is the open access policy of PLoS ONE, permission is not required for reuse of content.

Citation:

Kostylev M.,[*1] Otwell A.E.,[*2] Richardson R.E.[3], Suzuki Y[1]. (2015). Cloning Should Be Simple: *Escherichia coli* DH5α-Mediated Assembly of Multiple DNA Fragments with Short End Homologies. PLoS ONE 10(9): e0137466. doi: 10.1371/journal.pone.0137466

[*]Co first-authors
[1]Department of Synthetic Biology and Bioenergy, J. Craig Venter Institute, La Jolla, California, United States of America
[2]Department of Microbiology, Cornell University, Ithaca, New York, United States of America

[3]School of Civil and Environmental Engineering, Cornell University, Ithaca, New York, United States of America

References

1. Horton RM, Hunt HD, Ho SN, Pullen JK, Pease LR. Engineering hybrid genes without the use of restriction enzymes: gene splicing by overlap extension. Gene. 1989; 77: 61–68. doi: 10.1016/0378-1119(89)90359-4. pmid:2744488

2. Zhang Y, Werling U, Edelmann W. SLiCE: a novel bacterial cell extract-based DNA cloning method. Nucleic Acids Res. 2012; 40: e55. doi: 10.1093/nar/gkr1288. pmid:22241772

3. Quan J, Tian J. Circular polymerase extension cloning of complex gene libraries and pathways. PLoS One. 2009; 4: e6441. doi: 10.1371/journal.pone.0006441. pmid:19649325

4. Li MZ, Elledge SJ. Harnessing homologous recombination in vitro to generate recombinant DNA via SLIC. Nat Methods. 2007; 4: 251–256. doi: 10.1038/nmeth1010. pmid:17293868

5. Smith C, Day PJ, Walker MR. Generation of cohesive ends on PCR products by UDG-mediated excision of dU, and application for cloning into restriction digest-linearized vectors. PCR Methods Appl. 1993; 2: 328–32. pmid:8324507 doi: 10.1101/gr.2.4.328

6. Wang R-Y, Shi Z-Y, Guo Y-Y, Chen J-C, Chen G-Q. DNA fragments assembly based on nicking enzyme system. PLoS One. 2013; 8: e57943. doi: 10.1371/journal.pone.0057943. pmid:23483947

7. Colloms SD, Merrick CA, Olorunniji FJ, Stark WM, Smith MCM, Osbourn A, et al. Rapid metabolic pathway assembly and modification using serine integrase site-specific recombination. Nucleic Acids Res. 2014; 42: e23. doi: 10.1093/nar/gkt1101. pmid:24225316

8. You C, Zhang X-Z, Zhang Y-HP. Simple cloning via direct transformation of PCR product (DNA Multimer) to *Escherichia coli* and *Bacillus subtilis*. Appl Environ Microbiol. 2012; 78: 1593–5. doi: 10.1128/AEM.07105-11. pmid:22194286

9. Cao P, Wang L, Zhou G, Wang Y, Chen Y. Rapid assembly of multiple DNA fragments through direct transformation of PCR products into *E. coli* and *Lactobacillus*. Plasmid. 2014; 76C: 40–46. doi: 10.1016/j.plasmid.2014.09.002. pmid:25261623

10. Gibson DG. Enzymatic assembly of overlapping DNA fragments. Methods Enzymol. 1st ed. Elsevier Inc.; 2011; 498: 349–361. doi: 10.1016/B978-0-12-385120-8.00015-2. pmid:21601685

11. Szostak JW, Orr-Weaver TL, Rothstein RJ, Stahl FW. The double-strand-break repair model for recombination. Cell. 1983; 33: 25–35. pmid:6380756 doi: 10.1016/0092-8674(83)90331-8

12. Ma H, Kunes S, Schatz PJ, Botstein D. Plasmid construction by homologous recombination in yeast. Gene. 1987; 58: 201–16. pmid:2828185 doi: 10.1016/0378-1119(87)90376-3

13. Noskov V. A genetic system for direct selection of gene-positive clones during recombinational cloning in yeast. Nucleic Acids Res. 2002; 30: 8e–8. doi: 10.1093/nar/30.2.e8.

14. Gibson DG, Benders GA, Axelrod KC, Zaveri J, Algire MA, Moodie M, et al. One-step assembly in yeast of 25 overlapping DNA fragments to form a complete synthetic *Mycoplasma genitalium* genome. Proc Natl Acad Sci U S A. 2008; 105: 20404–9. doi: 10.1073/pnas.0811011106. pmid:19073939

15. Mitchell LA, Chuang J, Agmon N, Khunsriraksakul C, Phillips NA, Cai Y, et al. Versatile genetic assembly system (VEGAS) to assemble pathways for expression in S. cerevisiae. Nucleic Acids Res. 2015; doi: 10.1093/nar/gkv466.

16. Zhang Y, Buchholz F, Muyrers JP, Stewart AF. A new logic for DNA engineering using recombination in *Escherichia coli*. Nat Genet. 1998; 20: 123–8. doi: 10.1038/2417. pmid:9771703

17. Yu D, Ellis HM, Lee EC, Jenkins NA, Copeland NG, Court DL. An efficient recombination system for chromosome engineering in *Escherichia coli*. Proc Natl Acad Sci U S A. 2000; 97: 5978–83. doi: 10.1073/pnas.100127597. pmid:10811905

18. Thomason LC, Sawitzke JA, Li X, Costantino N, Court DL. Recombineering: genetic engineering in bacteria using homologous recombination. Curr Protoc Mol Biol. 2014; 106: 1.16.1–1.16.39. doi: 10.1002/0471142727.mb0116s106.

19. Klock HE, Koesema EJ, Knuth MW, Lesley SA. Combining the polymerase incomplete primer extension method for cloning and mutagenesis with microscreening to accelerate structural genomics efforts. Proteins. 2008; 71: 982–94. doi: 10.1002/prot.21786. pmid:18004753

20. Li C, Wen A, Shen B, Lu J, Huang Y, Chang Y. FastCloning: a highly simplified, purification-free, sequence- and ligation-independent PCR cloning method. BMC Biotechnol. 2011; 11: 92. doi: 10.1186/1472-6750-11-92. pmid:21992524

21. Jacobus AP, Gross J. Optimal Cloning of PCR Fragments by Homologous Recombination in *Escherichia coli*. PLoS One. 2015; 10: e0119221. doi: 10.1371/journal.pone.0119221. pmid:25774528

22. Lovett ST, Hurley RL, Sutera VA, Aubuchon RH, Lebedeva MA. Crossing over between regions of limited homology in *Escherichia coli*. RecA-dependent and RecA-independent pathways. Genetics. 2002; 160: 851–9. pmid:11901106

23. Dutra BE, Sutera VA, Lovett ST. RecA-independent recombination is efficient but limited by exonucleases. Proc Natl Acad Sci U S A. 2007; 104: 216–21. doi: 10.1073/pnas.0608293104. pmid:17182742

24. Swingle B, Markel E, Costantino N, Bubunenko MG, Cartinhour S, Court DL. Oligonucleotide recombination in Gram-negative bacteria. Mol Microbiol. 2010; 75: 138–48. doi: 10.1111/j.1365-2958.2009.06976.x. pmid:19943907

25. Bubeck P, Winkler M, Bautsch W. Rapid cloning by homologous recombination in vivo. Nucleic Acids Res. 1993; 21: 3601–2. pmid:8346047 doi: 10.1093/nar/21.15.3601

26. Labunskyy VM, Suzuki Y, Hanly TJ, Murao A, Roth FP, Gladyshev VN. The Insertion Green Monster (iGM) Method for Expression of Multiple Exogenous Genes in Yeast. G3 (Bethesda). 2014; 4: 1183–91. doi: 10.1534/g3.114.010868.

27. Dicarlo JE, Norville JE, Mali P, Rios X, Aach J, Church GM. Genome engineering in *Saccharomyces cerevisiae* using CRISPR-Cas systems. Nucleic Acids Res. 2013; 41: 4336–4343. doi: 10.1093/nar/gkt135. pmid:23460208

28. Oliner JD, Kinzler KW, Vogelstein B. In vivo cloning of PCR products in *E. coli*. Nucleic Acids Res. 1993; 21: 5192–7. pmid:8255776 doi: 10.1093/nar/21.22.5192

29. Chayot R, Montagne B, Mazel D, Ricchetti M. An end-joining repair mechanism in Escherichia coli. Proc Natl Acad Sci U S A. 2010; 107: 2141–2146. doi: 10.1073/pnas.0906355107. pmid:20133858

30. Koskela E, Frey A. Homologous Recombinatorial Cloning Without the Creation of Single-Stranded Ends: Exonuclease and Ligation-Independent Cloning (ELIC). Mol Biotechnol. Springer US; 2015; 57: 233–240. doi: 10.1007/s12033-014-9817-2. pmid:25370826

31. Hanahan D. Studies on Transformation of *Escherichia coli* with Plasmids. J Mol Biol. 1983; 166: 557–580. pmid:6345791 doi: 10.1016/s0022-2836(83)80284-8

32. Lanza AM, Curran K a, Rey LG, Alper HS. A condition-specific codon optimization approach for improved heterologous gene expression in *Saccharomyces cerevisiae*. BMC Syst Biol. 2014; 8: 33. doi: 10.1186/1752-0509-8-33. pmid:24636000

33. Sander JD, Joung JK. CRISPR-Cas systems for editing, regulating and targeting genomes. Nat Biotechnol. 2014; 32: 347–55. doi: 10.1038/nbt.2842. pmid:24584096

34. Suzuki Y, Onge RP, Mani R, King OD, Heilbut A, Labunskyy VM, et al. Knocking out multigene redundancies via cycles of sexual assortment and fluorescence selection. Nat Methods. 2011; 8: 159–164. doi: 10.1038/nmeth.1550. pmid:21217751

35. Wright MS, Perez F, Brinkac L, Jacobs MR, Kaye K, Cober E, et al. Population structure of KPC-producing *Klebsiella pneumoniae* isolates from midwestern U.S. hospitals. Antimicrob Agents Chemother. 2014; 58: 4961–4965. doi: 10.1128/AAC.00125-14. pmid:24913165

36. Maniatis T, Frisch E, Sambrook J. Molecular Cloning: A laboratory manual. Cold Spring Harbor, NY: Cold Spring Harbor Laboratory Press; 1982.

37. Dower WJ, Miller JF, Ragsdale CW. High efficiency transformation of *E. coli* by high voltage electroporation. Nucleic Acids Res. 1988; 16: 6127–6145. pmid:3041370 doi: 10.1093/nar/16.13.6127

38. Fu J, Bian X, Hu S, Wang H, Huang F, Seibert PM, et al. Full-length RecE enhances linear-linear homologous recombination and facilitates direct cloning for bioprospecting. Nat Biotechnol. 2012; 30: 440–6. doi: 10.1038/nbt.2183. pmid:22544021

39. Kowalczykowski SC, Dixon DA, Eggleston AK, Lauder SD, Rehrauer WM. Biochemistry of homologous recombination in *Escherichia coli*. Microbiol Rev. 1994; 58: 401–65. pmid:7968921

40. Degryse E. In vivo intermolecular recombination in *Escherichia coli*: application to plasmid constructions. Gene. 1996; 170: 45–50. doi: 10.1016/0378-1119(95)00858-6. pmid:8621087

Supplementary Figures and Tables:

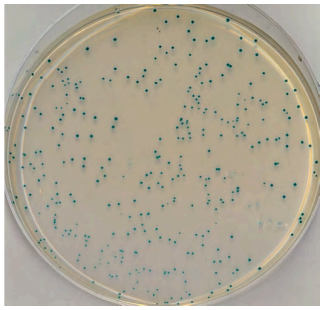

Supplementary Figure 4.1: pUC19-LacZα assembly screen. Following transformation and recovery, cells were plated on LB agar plates containing ampicillin, X-gal, and IPTG. Blue colonies indicate correct assembly of the pUC19 construct. Shown is a plate from an experiment testing the effect of DNA quantity on transformation efficiency, quantified as the number of blue colonies (see **Figure 4.2** and **Supplementary Table 4.3**). 0.5 ng of linearized pUC19 was used.

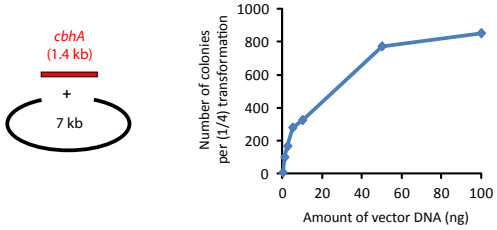

Supplementary Figure 4.2: Assembly of Aspergillus niger cbhA into a custom vector. Fragments shared 50 bp of homology at their ends (see **Materials and Methods**). A range of vector DNA concentrations was tested while maintaining the insert-to-vector ratio at 5:1. Colony PCR confirmed the presence of the correct insert in 30/30 transformants tested, and Sanger sequencing of 20 junctions confirmed correct assembly in all but one case, where a one-base deletion was identified.

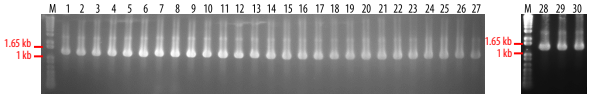

Supplementary Figure 4.3: Colony PCR of A. niger cbhA assembly. Thirty colonies were tested using primers 5-F and 5-R (**Supplementary Table 2**). Expected band size was 1.4 kb.

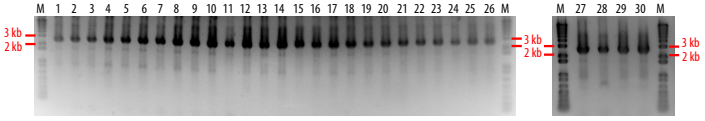

Supplementary Figure 4.4: Colony PCR of G. sulfurreducens GSU1371 knockout construct assembly, selected on Kan-Amp. Thirty colonies were tested using primers pBR-F and pBR-R (**Supplementary Table 2**). Expected band size was 2.52 kb.

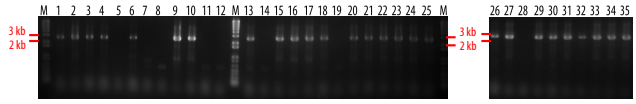

Supplementary Figure 4.5: Colony PCR of G. sulfurreducens GSU1371 knockout construct assembly, selected on Amp only. Thirty five colonies were tested using primers pBR-F and pBR-R (**Supplementary Table 2**). Expected band size was 2.52 kb.

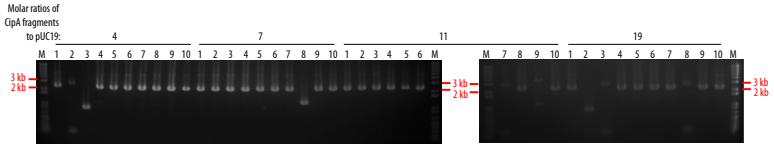

Supplementary Figure 4.6: Colony PCR of C. thermocellum cipA assembly. Ten colonies from each molar ratio experiment (see **Supplementary Table 6**) were tested using primers M13-F(-40) and M13-R (**Supplementary Table 6**). Expected band size was 2.47 kb.

S4.1 Table: High-throughput cloning of cellulase and other carbohydrate-active enzyme genes.

Reaction ID	Species	Family	Fragment size (bp)[a]	Colonies per transformation[b]	Correct band in colony PCR	Issues with PCR?
1	*Talaromyces emersonii*	GH6	1411	18	2/3	multiple bands
2	*Neurospora crassa*	AA9	769	45	3/3	smear
3	*Thermobifida fusca*	AA10	658	31	1/1	-
4	*Chrysosporium lucknowense*	GH7	1282	54	2/3	multiple bands
5	*Acidothermus cellulolyticus*	GH12	769	100	1/1	-
6	*Chaetomium thermophilum*	GH7	1456	35	1/3	multiple bands
7	*Neosartorya fischeri*	GH7	1456	43	1/1	multiple bands
8	*Clostridium termitidis*	GH8	1216	56	1/1	-
9	*Gibberella zeae*	GH45	1003	125	1/1	-
10	*Trichoderma viride*	GH5	1357	130	1/1	-
11	*Paenibacillus barcinonensis*	GH5	1201	112	1/1	-
12	*Talaromyces stipitatus*	GH5	1063	87	1/1	multiple bands
13	*Talaromyces cellulolyticus*	GH6	1201	69	3/3	multiple bands
14	*Talaromyces marneffei*	GH7	1435	65	1/1	-
15	*Saccharophagus degradans*	GH5	943	42	1/1	-
16	Uncultured organism	GH5	1024	80	1/1	-
17	*Aureobasidium pullulans*	GH5	1000	24	2/2	multiple bands
18	*Trichoderma koningii*	GH6	1162	14	2/2	-
19	*Cytophaga hutchinsonii*	GH5	913	30	2/2	-
20	*Trichoderma koningii*	GH12	754	11	2/2	-
21	Uncultured organism	GH5	997	5	2/2	-
22	*Thielavia terrestris*	GH7	1459	5	1/2	multiple bands
23	*Myceliophthora thermophila*	GH5	985	16	2/2	-
24	*Thielavia terrestris*	GH1	1525	16	2/2	-
25	*Thielavia terrestris*	GH6	1189	25	2/2	-
26	*Trichoderma reesei*[c]	GH6	1447	8	1/2	multiple bands
27	*Trichoderma reesei*	GH6	1447	19	2/2	-
28	*Trichoderma reesei*[c]	GH5	1297	24	3/3	-
29	*Trichoderma reesei*	GH5	1297	4	2/3	-

[a] All fragments contained 40 bp of overlapping sequences with the vector at each end; coding sequences were codon-optimized using a published algorithm (Lanza et al., 2014), synthesized with BioXp™ 3200 (SGI-DNA), and PCR-amplified with PrimeSTAR Max polymerase (Takara Bio).
[b] 5 ng of a 7-kb custom vector was cotransformed with 5 ng insert, giving molar insert-to-vector ratio between 5:1 and 9:1.
[c] Native rather than codon-optimized cellulase sequences were used in these reactions.

S4.2 Table: Primers used for PCR amplification and DNA assembly verification.

Fragment	Primer name	Primer sequence	Template	Final construct
vector (LacZ)	1-F	TTATAGGTTAATGTCATGATAATAATGGTTTCTTAGAC	pUC19	pUC19 (reassembled)
	1-R	GGATCTCTAGAGTCGACCTG		
LacZ	2-F	CCATGATTACGCCAAGCTTGCATG	pUC19	
	2-R	GTGCCACCTGACGTCTAAGAAACC		
vector (AnCbhA)	3-F	ATTCAACTTTCAGTGCTTCTGCGGGGTGAAGCTCCAAAAGTTACCAC	pYOGM081-Cel	pYOGM081-Cel-AnCbhA
AnCbhA	3-R	TAAGAGTACCGGCTTGCTGAGAGCCACCTCCACCGGAAC		
	3-F	AGGAGGTGGCGGTTCCGGTGGAGGTGGCTCTCAGCAAG	synthetic DNA (BioXP™ 3200)	
	3-R	TGTAGTGGTAACTTTGGAGCTTCAC		
vector (cellulase)	4-F	CAAAAGTTACCACTACAACAACTTCCTCTG	pYOGM081-Cel	pYOGM081-Cel-Cellulase
	4-R	CCACCGGAACCGCCACCTCCTGAG		
Cellulase	5-F	CTTCAGGAGGGGGTGGCTC	synthetic DNA (BioXP™ 3200)	
	5-R	GTTGTGACGGCAGAGGAAG		
Kan-cassette	6-F	ATGAACCACCAGCCAAGGAGGCACGCCGTATCTCAGTTCGGTGTAGGTCG	pET28a	All KO constructs
	6-R	TAGTTTCGCGTGCGGTTCACGGCTACAATTTCAGGTGCACTTTTCG		
vector-KO-1150	7-F	GAATTCTGCAGCAAAGCCATGGAAACGGTGGGATCTCTACGCCGGACGCA	pBR322	KO-1150
	7-R	TGCCGAAATAGTGCCTGATCCTGTCGAAAGACGAAAGGGCCTCGTGATACG		
5'-1150	8-F	GTATCACGAGGCCCTTTCGTCTTTCGACAGGATCAGGCACTATTTCG	*G. sulfurreducens* gDNA	
	8-R	GAACGACCTACACCGAACTGAGATACGGCGTCGCCTCCTTGGCTGGTG		
3'-1150	9-F	TTTCCCCGAAAAGTGCCACCTGAAATTGTAGCCGTGAACCGCACGCGAAAC	*G. sulfurreducens* gDNA	
	9-R	ACGATGCGTCCGGCGTAGAGGATCCCACCGTTTCCATGGCTTTGC		
vector-KO-550	10-F	AGCTGCACGAGATCGCCCAGGAAAAGGACTGGATCCTCTACGCCGGACGCA	pBR323	KO-550
	10-R	TCGCCCAGGTGGAGGCATTTCTTGCGAAAGACGAAAGGGCCTCGTGATACG		
5'-550	11-F	GTATCACGAGGCCCTTTCGTCTTTCGCAAGAAATGCCTCCACCTGGGCGAG	*G. sulfurreducens* gDNA	
	8-R	GAACGACCTACACCGAACTGAGATACGGCGTCGCCTCCTTGGCTGGTG		
3'-550	9-F	TTTCCCCGAAAAGTGCCACCTGAAATTGTACCCGTGAACCGCACGCGAAAC	*G. sulfurreducens* gDNA	
	12-R	ACGATGCGTCCGGGGTAGAGGATCCAGTCCTTTTCCTGGGCGATCTGG		
vector-KO-350	13-F	CCGGGGGATCACCTTCTTCGACACGGGATCCTCTACGCCGGACGCA	pBR323	KO-350
	13-R	GGGAATTCACCGCTCAGGAGCATCTGAAGACGAAAGGGCCTCGTGATACG		
5'-350	14-F	GTATCACGAGGCCCTTTCGTCTTTCAGATGCTCCTGAGCGGTGAATTCC	*G. sulfurreducens* gDNA	
	8-R	GAACGACCTACACCGAACTGAGATACGGCGTCGCCTCCTTGGCTGGTG		
3'-350	9-F	TTTCCCCGAAAAGTGCCACCTGAAATTGTAGCCGTGAACCGCACGCGAAAC	*G. sulfurreducens* gDNA	
	15-R	ACGATGCGTCCGGCGTAGAGGATCCCGTGTCGAAGAAGGTGATCC		
vector-KO-250	16-F	CTCGGTTCGACCGGGCTGACCGTTTGGATCCTCTACGCCGGACGCA	pBR324	KO-250
	16-R	TCGTTGGCCGTGGCCGCCGCCGTGGAGAAAGCGAAAGGGCCTCGTGATACG		
5'-250	17-F	GTATCACGAGGCCCTTTCGTCTTTCTCCACGGCGCCGCCACGGCCAAC	*G. sulfurreducens* gDNA	
	8-R	GAACGACCTACACCGAACTGAGATACGGCGTCGCCTCCTTGGCTGGTG		
3'-250	9-F	TTTCCCCGAAAAGTGCCACCTGAAATTGTAGCCGTGAACCGCACGCGAAAC	*G. sulfurreducens* gDNA	
	18-R	ACGATGCGTCCGGCGTAGAGGATCCAACGGTCAGCCCGGTCGAAC		
vector-KO-150	19-F	CGGGTGCCGGGGCGTTCAGCCCTCCTCGCCAGGATCCTCTACGCCGGACGCA	pBR325	KO-150
	19-R	CCCCGGCAGGAATGGCGCTACTCCAGAAAGACGAAAGGGCCTCGTGATACG		
5'-150	20-F	GTATCACGAGGCCCTTTCGTCTTTCTGGAGTAGCGCCATTCCTGC	*G. sulfurreducens* gDNA	
	8-R	GAACGACCTACACCGAACTGAGATACGGCGTCGCCTCCTTGGCTGGTG		
3'-150	9-F	TTTCCCCGAAAAGTGCCACCTGAAATTGTAGCCGTGAACCGCACGCGAAAC	*G. sulfurreducens* gDNA	
	21-R	GAACGACCTACACCGAACTGAGATACGGCGTCGCCTCCTTGGCTGGTG		
vector-CipA	22-F	ACAATAAGCGAATTTCTTATGATTTATGGATCCTCTAGAGTCGACCTGC	pUC19	pUC19-CiCipA
	22-R	GAGCCACCCCCTCCTGAAGCCGGGTACCGAGCTCGAATTC		
CipA-F1	23-F	GACGGCCAGTGAATTCGAGCTCGGTACCCGGCTTCAGGAGGGGGTGGCTCAG	synthetic DNA (gBlocks®, IDT)	
	23-R	CGTAGGGGTCGCGCCCTTAG		
CipA-F2	24-F	GTGGAGTAAACGTTGGAAATGCAAC	synthetic DNA (gBlocks®, IDT)	
	24-R	TTTTTAGCAAAACGTCCCTGAATCTG		
CipA-F3	25-F	ACTTTAGAACCTGGAGCTCACGTG	synthetic DNA (gBlocks®, IDT)	
	25-R	TGCAGGTCGACTCTAGAGGATCCATAAATCATAAGAAATTCGCTTATTGTGC		
p426-gRNA-GMTK-KO	26-F	TGGCCCTTGGAATTGACGAGTAGTTTTAGAGCTAGAAATAGCAAG	p426-SNR52p-gRNA-CAN1.Y-SUP4t	p426-gRNA-GMTK-KO
	26-R	AACTACTCGTCAATTCCAAGGGCGATCATTTATCTTTCACTGCGGAG		
p426_gRNA-YGR176W	27-F	TCCTCGTAGTCGATGCATGCCGGTTTTAGAGCTAGAAATAGCAAG	p426-SNR52p-gRNA-CAN1.Y-SUP4t	p426_gRNA-YGR176W
	27-R	AACCGGCATGCATCGACTACGAGGATCATTTATCTTTCACTGCGGAG		
P_{tet}_gRNA_pUC-FEPC	28-F	GTAAAGAGGTTGCTCGCCGCCGGTGTGTGTGAAATTGTTATCC	P_{tet}_gRNA_pUC	P_{tet}_gRNA_ pUC-FEPC
	28-R	GCGGCCGAGCAACCTCTTTACGTTTTAGAGCTAGAAATAGCAAGTTAAAATAAGG		
Sequencing / verification	M13-F(-40)	GTTTTCCCAGTCACGAC	pUC19-based and p426-SNR52p-gRNA-based constructs	N/A
	M13-R	CAGGAAACAGCTATGAC		
	pBR-F	AAAGTGCCACCTGACGTCTAAG	pBR322-based constructs	
	pBR-R	ATCTTCCGCATCGGTGATGTCG		
	5-F	CTTCAGGAGGGGGTGGCTC	pYOGM081-Cel-AnCbhA	
	5-R	GTTGTGACGGCAGAGGAAG		
	Cel-F	CTTGTAATCCCTTATTCCTTCTAGC	Cellulase constructs (except pYOGM081-Cel-AnCbhA)	
	Cel-R	CATCTGGGCAGATGATGTCGAG		
	Seq_CR	CTCTCATCCGCCAAAACAGC	P_{tet}_gRNA_pUC-FEPC	

S4.3 Table: pUC19-*lacZα* assembly assay

Vector added (ng)	Insert added (ng)[a]	Blue colonies[b]	White colonies
0.1	0.12	24	0
0.2	0.24	98	0
0.5	0.6	340	3
1	1.2	896	4
2	2.4	1220	2
5	6	1778	5
10	12	2040	1
0.1	0	0	0
0.2	0	0	1
0.5	0	0	1
1	0	4	1
2	0	1	1
5	0	2	2
10	0	6	2
0	6	5	0
0	12	10	0

[a] The insert-to-vector molar ratio was 5:1 for all reactions.
[b] Shown are colony numbers per 25 µl cells, which corresponds to 1/4 recommended transformation cell volume.

S4.4 Table: *In vivo* assembly of the knockout cassette for gene 1371 in *Geobacter sulfurreducens* from three fragments into a pBR322 vector.

Vector added (ng)[a]	5' target sequence added (ng)	Kanamycin cassette added (ng)[a]	3' target sequence added (ng)	Colonies on Kan-Amp	Colonies on Kan[b]	Colonies on Amp[b]
1	0.68	1.8	0.68	15	ND	ND
5	3.4	9.1	3.4	65	ND	ND
10	6.8	18	6.8	92	ND	ND
50	34	91	34	177	ND	ND
100	68	182	68	204	ND	ND
10[c]	0	18	0	0	93	556

[a] DpnI digest after PCR was omitted because the contaminating template plasmid with only the Amp marker or the Kan marker is unable to produce colonies in double selection.
[b] ND = Not determined
[c] A control sample lacking fragments for bridging the fragments carrying antibiotics resistance markers confirmed that no colony is generated with contaminating template plasmids in double selection in the absence of correct assembly.

S4.5 Table: Comparison of single and double selections on colony number and the fidelity of the GSU 1371 knockout construct.

Sample	Selection	Colonies per transformation	Correct band in colony PCR
Vector only[a]	Amp	4	N/A
Assembly[b]	Amp/Kan	61	10/10
Assembly[b]	Amp	126	27/35
Assembly[b]	Kan[c]	68	10/10

[a] Only the vector fragment (10 ng) was introduced into 25 µl of cells as a negative control.
[b] The insert DNA fragments were first combined with 10 ng of the vector fragment at a 5:1 molar ratio for insert and vector, and then with 25 µl of cells.
[c] Although Kan was the only antibiotic used, this selection was equivalent to double selection because the origin of replication needed in the final product was provided by the vector fragment.

S4.6 Table: *In vivo* assembly of *Clostridium thermocellum cipA* from three fragments into pUC19.

Molar ratio of *cipA* fragments to pUC 19[a]	Colonies per transformation[b]	Correct band in colony PCR
4	66	8/10
7	96	9/10
11	95	8/10
19	39	7/10
0	4	N/A

[a] *cipA* fragments were 996, 499, and 1009 bp.
[b] 10 ng of vector was used in all transformations.

S4.7 Table: Effect of fragment number on the assembly of a pBR322-based knockout construct for the deletion of gene GSU 1371 in *Geobacter sulfurreducens*

	Kan-Amp selection		Amp selection	
Number of fragments[a]	Colonies per transformation[b]	Correct band in colony PCR	Colonies per transformation[b]	Correct band in colony PCR
5	10	5/5	19	5/10
6	4	4/4	14	6/8

[a] Fragment sizes were 551, 1,466, 555, 3,320, and 765 bp for five-fragment assembly; and 551, 1,466, 555, 1,803, 1,567, and 765 bp for six-fragment assembly.
[b] Fragments were added at an equimolar ratio to the collective amount of ~125 ng per 25 µl transformation.

Chapter 5

Comparative Proteomic Analysis of *Desulfotomaculum reducens* MI-1: Insights into the Metabolic Versatility of a Gram-positive Sulfate- and Metal-reducing Bacterium

Summary

The proteomes of the metabolically versatile and poorly characterized Gram-positive bacterium *Desulfotomaculum reducens* MI-1 were compared across four cultivation conditions including sulfate reduction, soluble Fe(III) reduction, insoluble Fe(III) reduction, and pyruvate fermentation. Collectively across conditions, we observed at high confidence ~38% of genome-encoded proteins. Here, we focus on proteins that display significant differential abundance on conditions tested. To the best of our knowledge, this is the first full-proteome study focused on a Gram-positive organism cultivated either on sulfate or metal-reducing conditions. Several proteins with uncharacterized function encoded within heterodisulfide reductase (*hdr*)-containing loci were upregulated on either sulfate (Dred_0633-4, Dred_0689-90, and Dred_1325-30) or Fe(III)-citrate-reducing conditions (Dred_0432-3 and Dred_1778-84). Two of these *hdr*-containing loci display homology to recently described flavin-based electron bifurcation (FBEB) pathways (Dred_1325-30 and Dred_1778-84). Additionally, we propose that a cluster of proteins, which is homologous to a described FBEB lactate dehydrogenase (LDH) complex, is performing lactate oxidation in *D. reducens* (Dred_0367-9). Analysis of the putative sulfate reduction machinery in *D. reducens* revealed that most of these proteins are constitutively expressed across cultivation conditions tested. In addition, peptides from the single multiheme c-type cytochrome (MHC) in the genome were exclusively observed on the insoluble Fe(III) condition, suggesting that this MHC may play a role in reduction of insoluble metals.

Introduction

Microbial sulfate and metal reduction are thought to be ancient processes that today are major drivers of nutrient cycles in anaerobic environments (Bird et al., 2011; Hori et al., 2015; Pereira et al., 2011). Decades of research have focused on understanding the proteins involved in these electron transfer pathways, and Gram-negative bacteria have mainly served as model organisms in studies. However, it is becoming increasingly understood that sulfate-reducing organisms (SROs) and dissimilatory metal-reducing organisms (DMROs) are phylogenetically diverse, and Gram-positive bacteria are suspected to be major contributors to these processes in natural settings (Cardenas et al., 2010; Newsome et al., 2014; Petrie et al., 2003; Suzuki et al., 2003; Williamson et al., 2013).

Studies on the Gram-negative genus *Desulfovibrio* have been foundational in elucidating mechanisms involved in microbial sulfate reduction. Core proteins in the sulfate reduction pathway (sulfate adenyltransferase, APS reductase, sulfite reductase) are conserved amongst SROs. However, several other proteins described in the pathway of sulfate reduction in *Desulfovibrio* do not contain homologs in the genomes of Gram-positive SROs, implying that divergent mechanisms are involved (Grein et al., 2013; Pereira et al., 2011). Even less is understood regarding metal reduction in Gram-positive bacteria. Studies on Gram-negative metal-reducing representatives, namely *Geobacter* and *Shewanella* species, have defined the current understanding of microbial metal reduction. A critical trait for metal reduction shared amongst model metal reducers is an abundance of genes encoding multiheme c-type cytochromes (MHCs) (Sharma et al., 2010; Shi et al., 2009; Wall and Krumholz, 2006). Gram-positive bacteria, however, rarely contain multiple MHCs (Sharma et al., 2010).

The *Desulfotomaculum* genus is composed of anaerobic, Gram-positive, endospore-forming SROs. These Peptococcaceae are widely distributed in the environment, and the number of

identified species as well as sequenced genomes is continually expanding (Aüllo et al., 2013; Kuever et al., 2014; Visser et al., 2014). Characterized species display considerable metabolic versatility, and some have been shown to reduce metals (Barton et al., 2015; Haouari et al., 2008; Tebo and Obraztsova, 1998). Certain *Desulfotomaculum* species completely oxidize organic substrates to CO_2, whereas others are incomplete oxidizers. The sulfite reductases from these two groups are phylogenetically distinct, and it has been suggested that complete oxidizers acquired their sulfite reductase laterally from a deltaproteobacterial donor (Klein et al., 2001; Zverlov et al., 2005).

Desulfotomaculum reducens MI-1 was isolated from a heavy-metal contaminated site and is a species of marked interest as a Gram-positive SRO that also has the capability to reduce metals including Fe(III) and Mn(IV) (Tebo and Obraztsova, 1998). As one of only a few organisms reported to conserve energy from utilization of U(VI) and Cr(VI) as electron acceptors, *D. reducens* is also of interest for bioremediation applications (Barton et al., 2015; Tebo and Obraztsova, 1998; Wall and Krumholz, 2006). Previous work in *D. reducens* has helped to elucidate the mechanism of Fe(III) reduction. It was proposed that Fe(III)-oxide reduction during pyruvate fermentation occurs through a soluble electron shuttle, as direct contact was found to not be required for Fe(III) reduction on this condition (Dalla Vecchia et al., 2014b). Conversely, direct contact was found to be required for Fe(III)-oxide reduction with lactate as electron donor and is therefore not mediated by a soluble shuttle (Dalla Vecchia et al., 2014a). Understanding of the proteins involved in Fe(III) reduction in *D. reducens* is less developed. The genome contains one annotated MHC (Dred_0700-1, nitrite reductase), a likely candidate for Fe(III) reduction (Junier et al., 2010). However, studies have analyzed its expression levels and found it to not be induced in the presence of soluble Fe(III) or U(VI) relative to pyruvate fermentation conditions

(Dalla Vecchia et al., 2014a, 2014b; Junier et al., 2011). One of these studies also analyzed the surface proteins (or surfaceome) of *D. reducens* while fermenting pyruvate or reducing soluble Fe(III) with lactate as electron donor and identified no peptides for the MHC (Dalla Vecchia et al., 2014a). However, no mRNA/protein-based analyses of the MHC during insoluble Fe(III) reduction have been performed.

In this study, we compared the proteomes of *D. reducens* during sulfate, soluble Fe(III), and insoluble Fe(III) reduction (all with lactate as electron donor), and pyruvate fermentation. The genome of *D. reducens* was sequenced in 2010, allowing for genomic predictions to be tested with proteomic measurements (Junier et al., 2010). The *D. reducens* genome contains an abundance of proteins that contain oxidoreductase-related annotations but lack specific functional annotations. There is increasing understanding of the types of domains and proteins that drive anaerobic respiration (Grein et al., 2013). In *D. reducens,* however, experimental information is not available in order to determine the function of many predicted redox proteins. Furthermore, in recent years, pathways of flavin-based electron bifurcation (FBEB) have been described in anaerobic microorganisms. FBEB is now regarded as a third mode of energy conservation, along with respiration and fermentation (Buckel and Thauer, 2013; Herrmann et al., 2008). The *D. reducens* genome contains homology to described FBEB pathways, and comparative proteomic analysis provides a tool for predicting whether these pathways are contributing to the metabolism of *D. reducens.* We report here the first global proteomic comparison of a *Desulfotomaculum* species. In fact, to the best of our knowledge this is the first full-proteome comparative analysis of any Gram-positive organism focused on either sulfate or metal-reducing conditions.

Materials and Methods

Biomass preparation

Desulfotomaculum reducens MI-1 was purchased from the American Type Culture Collection (ATCC® BAA-1160™) and grown anaerobically at 30° C in batch culture with an 80/20 N_2/CO_2 headspace in Widdel Low Phosphate (WLP) media (pH 7) as described (Otwell et al., 2015). Cultures were grown with either 28 mM sodium sulfate, 25 mM Fe(III)-citrate, or 35 mM Fe(III)-oxide with 20 mM sodium lactate as electron donor. Fermentation cultures were grown with 20 mM pyruvic acid. Lactate only and Fe(III)-citrate only controls did not exhibit growth. For each cultivation condition analyzed, *D. reducens* was transferred to fresh growth medium at least three times prior to harvesting in order to ensure accurate representation of the proteome for the given cultivation condition. Cell growth was tracked with fluorescence microscopy by staining with acridine orange and the ferrozine assay for quantification of Fe(II) or the Cline assay for quantification of sulfide when appropriate (Lovley and Phillips, 1987; Strocchi et al., 1992). Representative growth curves for each culture condition are displayed in **Supplemental Figure 5.1**. Cells were harvested anaerobically using an anaerobic glove bag during mid-late exponential phase and cell pellets were stored at -80° until protein extraction.

Protein Extraction and Digestion

Harvested cell pellets were suspended in 50 mM NH_4HCO_3 (pH 8) and lysed in the presence of 100-200 µL of 0.1 mm zirconia/silica beads (BioSpec Products, Bartlesville, OK) as described (Callister et al., 2006) with the following modifications. Bead beating was performed using a Bullet Blender (Next Advance, Averill Park, NY) operated for 3 minutes at speed 8. The lysate was collected at 4,500*g* for 5 minutes at 4°C and the beads were rinsed with 100 µL of 50 mM NH_4HCO_3 (pH 8). The combined lysates were transferred to a 1.5-mL microcentrifuge tube and cellular debris was separated from soluble lysate material by centrifuging at 10,000*g* for 15

minutes at 4^{o}C. Protein concentrations within the soluble lysate were measured using the Bicinchoninic Acid (BCA) Protein Assay and then normalized to equal concentration (Smith et al., 1985). Proteins were denatured and digested by following the FASP digest method (Wiśniewski et al., 2009) without alkylation, then washed using C18 SPE chromatography according to previously established protocols (Callister et al., 2008). Equal portions of peptides (100 μg) from biological replicates acquired for each cultivation condition were pooled, then separated using C18 reverse phase high pH fractionation according to previously published protocols (Wang et al., 2011). Ninety-six fractions were collected from each pooled sample and dried overnight in a SpeedVac. Peptides within each well were suspended in 100 ml of 50% methanol and combined into 12 fractions, concentrated to dryness then suspended in nanopure water to achieve a final concentration of 0.1 mg/ml. Additionally, peptides from the unfractionated samples were transferred to MicroSolv ALS vials and diluted with nanopure water to a final concentration of 0.1 μg/μL.

Proteomic Data Generation

Mass spectra were generated for both fractionated (60 fractions in total) and unfractionated peptide samples (30 samples originating from 2 to 3 biological replicates per cultivation condition and 3 technical replicates per biological replicate). The unfractionated samples were randomized and blocked prior to data generation. For both sample types 7 mg of peptides was injected to an Agilent LC system (Agilent Technologies, Santa Clara, CA) coupled to a hybrid ion trap Orbitrap Velos mass spectrometer (Thermo Scientific, San Jose, CA) equipped with an ion funnel and electrospray ionization (ESI) interface. Conditions for peptide separation and HPLC operating conditions have been previously published (Robidart et al., 2013; Sowell et al., 2008). Orbitrap spectra were collected from 400 to 2,000 m/z at a resolution of

100k followed by data-dependent ion trap tandem mass (MS/MS) spectra generation of the six most abundant ions using 35% collision energy (CID). Additional mass spectrometer operating conditions have been previously described (Robidart et al., 2013; Sowell et al., 2008).

Data analysis

Peptide sequences were assigned to MS/MS spectra using the MSGF search algorithm (Kim et al., 2008) and the translated *Desulfotomaculum reducens* MI-1 annotated genome sequence downloaded (September 18, 2012) from the U.S. Department of Energy's Joint Genome Institute's (JGI) IMG database (Markowitz et al., 2014). From measured peptides, an empirical peptide database was generated for use as a library to match high-resolution parent ion spectra (i.e. AMT tag approach (Lipton et al., 2002)) generated by the Orbitrap Velos instrument from the unfractionated samples. These unfractionated peptide samples were used to obtain label-free abundance measurements for use in relative quantification comparisons. The area under each peptide peak, constructed from ion intensities (ion current) measured across instrument scans, was used to represent the arbitrary abundances of peptides (Lipton et al., 2002; Sowell et al., 2008). The dataset of peptides and their associated abundances, resulting from matching to the library, was filtered to achieve a false discovery rate of $\leq 5\%$ using established protocols (Stanley et al., 2011). Peptides matching to multiple proteins were filtered out unless the matched proteins were identical, duplicated genes. Peptide abundances were log transformed (base 2) and protein abundance was estimated as the mean of its measured peptides' log-transformed abundances across replicates. A protein was considered positively observed if identified by at least two unique peptide sequences in replicates from a given cultivation condition. If detected, the protein's mean abundance was compared between different cultivation conditions and p-values assigned using ANOVA; part of the InfernoRDN (previously known as

DAnTE, (Polpitiya et al., 2008)) proteomics analysis software tools (http://omics.pnl.gov/software/InfernoRDN). Abundance measurements for a protein were required to be present in at least 50% of replicates in order for its means to be compared. Proteins were considered differentially abundant if their mean peptide intensity had a >2-fold change calculated as the difference between means across the conditions being compared, with a p-value of ≤ 0.05. Along with the cultivation conditions described, the AMT tag approach was used to analyze Fe(III)-oxide cultures harvested at eight days. This data was excluded from the analysis as the six-day samples matched closer with the growth phase of the other conditions. All raw data is deposited and publicly available in MassIVE (Mass spectrometry Interactive Virtual Environment) with accession number MSV000079501 and ProteomeXchange with accession number PXD003605. The endospore proteome of *D. reducens* was also analyzed. Proteins significantly increased in the endospore proteome relative to pyruvate are provided in **Appendix Table 1.** Proteins exclusively detected in the endospore proteome (i.e. not detected on any of the cultivation conditions described here) are provided in **Appendix Table 2.**

Results: Global proteome of *D. reducens*

The genome of *D. reducens* encodes 3324 predicted proteins, and across the four conditions analyzed in our study, 1268 proteins were confidently identified, representing ~38% of predicted proteins. This includes 1064 proteins with functional annotations and 204 hypothetical proteins. **Table 5.1** displays a global overview of the proteomic data presented.

Table 5.1: Global overview of *D. reducens* comparative proteomic analysis

Cultivation condition	Total proteins identified	Average $\log_2$ peptide ion intensity	Proteins unique to condition	Proteins significantly increased compared to pyruvate
Pyruvate fermentation	1104	19.87 (SD 1.49)	113 (Supp. Table 5.1a)	NA
Sulfate reduction (lactate as ED)	1046	19.85 (SD 1.63)	81 (Supp. Table 5.1b)	109 (Supp. Table 5.2a)

Fe(III)-citrate reduction (lactate as ED)	582	19.11 (SD 1.69)	23 (Supp. Table 5.1c)	29 (Supp. Table 5.2b)
Fe(III)-oxide reduction (lactate as ED)	724	19.58 (SD 1.66)	35 (Supp. Table 5.1d)	54 (Supp. Table 5.2c)

Biological and technical replicates of each condition cluster tightly together when visualizing full-proteome relatedness in a hierarchical clustering-based heat map, demonstrating consistency in the data **(Figure 5.1)**. A Venn diagram shows overlap of observed proteins across conditions tested, and displays a 'core' proteome of 465 proteins identified on every condition (created in Venny 2.0: Oliveros, J.C., 2007, VENNY. An interactive tool for comparing lists with Venn Diagrams, http://bioinfogp.cnb.csic.es/tools/venny/index.html) **(Supplementary Figure 5.2)**. In evaluating the number of proteins observed for each cultivation condition, more total proteins were identified on the pyruvate fermentation and sulfate reduction conditions than on the Fe(III) reduction conditions, as there are 1104, 1046, 582, and 724 total proteins observed on pyruvate, sulfate, Fe(III)-citrate, and Fe(III)-oxide respectively **(Table 5.1)**. 113 proteins were observed solely on the pyruvate condition, 81 on sulfate, 23 on Fe(III)-citrate, and 35 on Fe(III)-oxide **(Table 5.1)**. These proteins observed exclusively on a single condition are displayed in **Supplementary Table 5.1**. Research on model metal-reducing organisms has identified oxidoreductases as well as porin-like proteins that together function as a conduit for extracellular electron transfer, and therefore proteins with either of these predicted functions are highlighted for the Fe(III) reduction conditions (Liu et al., 2014; Richardson et al., 2012; Shi et al., 2012). Proteins that display significant fold increases (>2-fold change, p-value <0.05) relative to pyruvate during sulfate, Fe(III)-citrate, and Fe(III)-oxide reduction conditions are provided in **Supplementary Table 5.2.** This includes 109 proteins significantly increased on sulfate relative to pyruvate, 29 on Fe(III)-citrate, and 54 on Fe(III)-oxide. Again, potential oxidoreductases and

porin-like proteins are highlighted for the Fe(III) reduction conditions. A summary of all proteomic data presented in supplementary tables is displayed in **Table 5.2.**

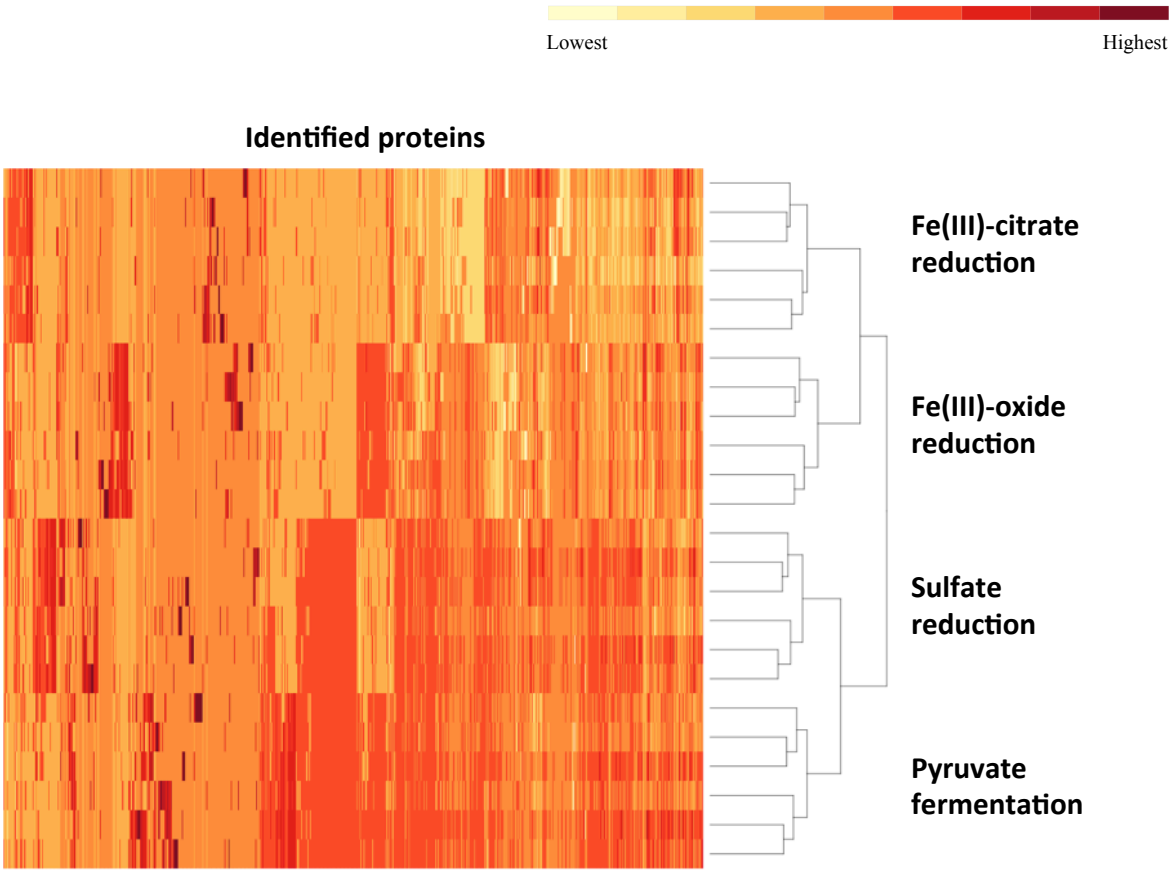

Figure 5.1: A heat map of the proteomes generated for *D. reducens*. Replicates grouped together based on hierarchical clustering using the heat map command in R. The two Fe(III) reduction conditions form clusters that are more similar to each other than to any other condition. A similar relationship is observed for the pyruvate fermentation and sulfate reduction condition. Data input for each replicate (two biological duplicates and three technical triplicates per condition) consisted of the average ion intensity for all proteins observed, and data for all detected peptides was included. Identified proteins are displayed across the horizontal axis and ordered by hierarchical clustering with complete linkage. Relative average ion intensity is displayed from yellow (lowest) to red (highest). Citation: R Development Core Team (2012), R: A Language and Environment for Statistical Computing. Vienna, Austria : the R Foundation for Statistical Computing. ISBN: 3-900051-07-0. Available online at http://www.R-project.org/.

Table 5.2: Summary of proteomic data presented in Supplementary Tables

Supplementary Table #	Content
5.1a-d	List of proteins unique to each cultivation condition
5.2a-c	Abundance comparisons for proteins significantly increased compared to pyruvate
5.3	Abundance comparisons for proteins potentially involved in lactate and/or pyruvate utilization.
4	Abundance comparisons for annotated hydrogenases
5	Abundance comparisons for putative respiration-related proteins
6	Abundance comparisons for additional clusters of proteins significantly increased during sulfate reduction

Along with lower total protein numbers on the Fe(III) reduction conditions, average ion intensities are lower compared to the sulfate and pyruvate conditions. Comparing average $\log_2$ fold change of average ion intensities across all proteins observed on both pyruvate and sulfate conditions yields a value of ~0.03 (pyruvate to sulfate), demonstrating that neither condition displayed significantly higher ion intensities. However, the average $\log_2$ fold change of all proteins identified on pyruvate and Fe(III)-citrate is 1.34 (pyruvate to Fe(III)-citrate), showing that overall, abundances are >2-fold lower on Fe(III)-citrate. The average $\log_2$ fold change between the pyruvate and Fe(III)-oxide conditions is 0.78 (pyruvate to Fe(III)-oxide). These differences are reflected in the average ion intensity ($\log_2$) for all proteins detected, which is 19.87 (SD 1.49) for the pyruvate condition, 19.85 (SD 1.63) for sulfate, 19.11 (SD 1.69) for Fe(III)-citrate, and 19.58 (SD 1.66) for Fe(III)-oxide **(Table 5.1)**. Also reflecting this variance between conditions are abundance patterns of certain housekeeping genes, including the RNA polymerase. For instance, RpoB (Dred_0207) is increased on pyruvate 1.8-fold (p-value <0.01) relative to sulfate, 5.8-fold (p-value <0.01) relative to Fe(III)-citrate, and 3.0-fold (p-value

<0.01) relative to Fe(III)-oxide. The β' (Dred_0208) and α (Dred_0243) subunits display similar abundance patterns. The 36 ribosomal proteins encoded in this region are nearly equal in abundance on pyruvate and sulfate (1.1-fold increased on pyruvate relative to sulfate on average), but significantly decreased in abundance on Fe(III) conditions. These ribosomal proteins are increased on average 5.8-fold on pyruvate conditions relative to Fe(III)-citrate and 1.6-fold relative to Fe(III)-oxide. This is likely a reflection of the slower growth rates observed on Fe(III)-reduction conditions compared with sulfate reduction and pyruvate fermentation **(Supplementary Figure 5.1**).

Our comparative proteomic analysis has revealed many potentially redox-related proteins from *D. reducens.* For instance, seven heterodisulfide reductase (*hdr*)-containing loci were identified in the genome, which are genomic regions rich with other predicted redox-related proteins including ferredoxins, proteins with iron-sulfur binding domains, proteins with flavin-binding domains, and annotated oxidoreductases (Junier et al., 2010). High numbers of unique peptides and differential protein abundance patterns across conditions were observed for proteins encoded within the *hdr*-containing loci. Identification patterns of proteins within these loci are displayed in **Figure 5.2**, and abundance comparisons for proteins of interest are displayed in **Table 5.4**. Proteomic data from various proteins, including proteins within these *hdr*-containing loci, are discussed below.

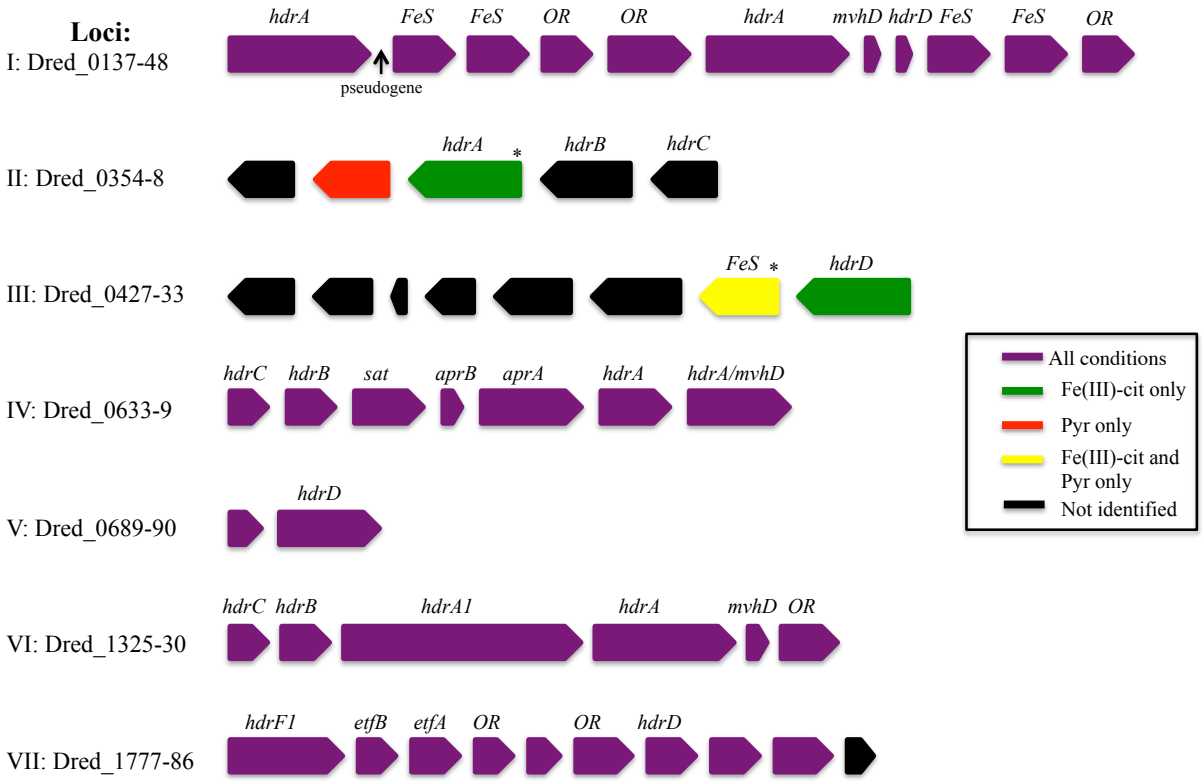

Figure 5.2: Identification of proteins encoded within heterodisulfide reductase (*hdr*)-containing loci. A number of proteins within hdr-containing loci were identified during proteomic analysis of *D. reducens* and many displayed differential abundance across cultivation conditions. Gene name abbreviations stand for iron sulfur proteins (*FeS*), methyl viologen hydrogenase, delta subunit (*mvhD*), annotated oxidoreductases (OR), electron transfer flavoproteins (*etfA* and *etfB*), sulfate adenyltransferase (*sat*), and APS reductase (*aprA* and *aprB*). Subunits of heterodisulfide reductases (*hdr*) are also shown. This figure is modified from an image published in the *D. reducens* genome paper and loci have been renumbered to match with locus tag position in the genome (Junier *et al*., 2010). *Refers to identification by only one unique peptide in at least half of the replicates.

Discussion

I. Energy production and catabolism of organic carbon in *D. reducens*

A novel method of lactate metabolism involving a FBEB complex in *Acetobacterium woodii* (Awo_c08730, 20, and 10) was recently described (Weghoff et al., 2015). The researchers suggested that the complex has the same role in many anaerobes, and Dred_0367-9 is

the homologous region in *D. reducens.* These proteins are currently annotated as the beta and alpha subunits of electron transfer flavoproteins (Dred_0367-8) and an FAD-linked oxidase domain-containing protein (Dred_0369). A high number of unique peptides for each of these proteins was detected on all conditions, with the lowest number observed on pyruvate. The average ion intensity of each protein in the operon Dred_0367-9 is higher on lactate-fed sulfate reduction cultures than pyruvate fermentation cultures, with p-values <0.002, 0.08, and 0.03 respectively. Abundance comparisons for all conditions are displayed in **Supplementary Table 5.3**. The annotated pathway for lactate oxidation in the *D. reducens* genome contains lactate dehydrogenase (LDH) Dred_2797, but no peptides for this protein were observed in our study. Based on the lack of detection of the annotated LDH, the high sequence similarity between Dred_0367-9 and the FBEB LDH complex, and the confident identification of these proteins in lactate-grown cultures, we propose that Dred_0367-9 is how *D. reducens* oxidizes lactate to pyruvate, producing NADH in the process **(Figure 5.3a).** It is important to note that in *A. woodii*, it was proposed that reduced ferredoxin is regenerated from NADH by reverse electron transfer, mediated by the Rnf complex (Weghoff et al., 2015). As the genome of *D. reducens* does not encode this complex, however, reduced ferredoxin would need to be regenerated through other means (see below).

Three potential pathways for pyruvate utilization are predicted in the annotated genome of *D. reducens*, encoded by genes Dred_0047-50, Dred_2750-3, and Dred_1893 (Junier et al., 2010). Proteomic data revealed that the pyruvate-ferredoxin oxidoreductase pathway (Dred_0047-50) is expressed during both lactate oxidation and pyruvate fermentation and that the pyruvate-formate lyase pathway (Dred_2750-3) is expressed only during pyruvate fermentation. The third predicted pathway, through the annotated pyruvate dehydrogenase

Dred_1893 (a pseudogene), was not observed **(Figure 5.3b, Supplementary Table 5.3)**. The pyruvate-ferredoxin oxidoreductase pathway (Dred_0047-50) yields acetate, CO_2, and H_2 during fermentative growth. H_2 is not produced during lactate oxidation, and instead this pathway is proposed to produce reduced ferredoxin, which could feed into the LDH complex described above (Junier et al., 2010). High numbers of unique peptides were observed for Dred_0047-9 on both lactate and pyruvate-fed cultures and the proteins do not display strong differential abundance patterns across conditions **(Supplementary Table 5.3).** Peptides from Dred_0050, an annotated 4Fe-4S ferredoxin, are detected in every condition (and are the highest in abundance on Fe(III)-citrate conditions), but these peptides are also present in another annotated 4Fe-4S ferredoxin (Dred_2822) and therefore cannot be distinguished. The monomeric hydrogenase Dred_1794 was identified as a likely candidate for production of hydrogen during pyruvate fermentation based on transcriptome patterns, and our proteomic data support this hypothesis (Junier et al., 2010). Dred_1794 is significantly increased on pyruvate relative to all other conditions (5-8-fold increase, p-value <0.01). Abundance ratios for this hydrogenase, as well as all six hydrogenases annotated in the genome of *D. reducens*, are displayed in **Supplementary Table 5.4.** Our data suggest that the second predicted pyruvate utilization pathway, the acetate and formate yielding pyruvate-formate lyase pathway (Dred_2750-3) is active during pyruvate fermentation. Previously reported experimental evidence supports this finding, as small amounts of formate are shown to accumulate during pyruvate fermentation (Dalla Vecchia et al., 2014b). Dred_2751 is detected only on the pyruvate condition and Dred_2750 and Dred_2752 are most abundant during fermentative growth relative to all other conditions (~3 and 2-fold increased relative to sulfate conditions, p-values <0.01 and 0.1 respectively). Peptides from Dred_2753 were not detected on any condition **(Supplementary Table 5.3)**. A model illustrating lactate

and/or pyruvate oxidation in *D. reducens* based on proteomic findings is presented in **Figure 5.3b.**

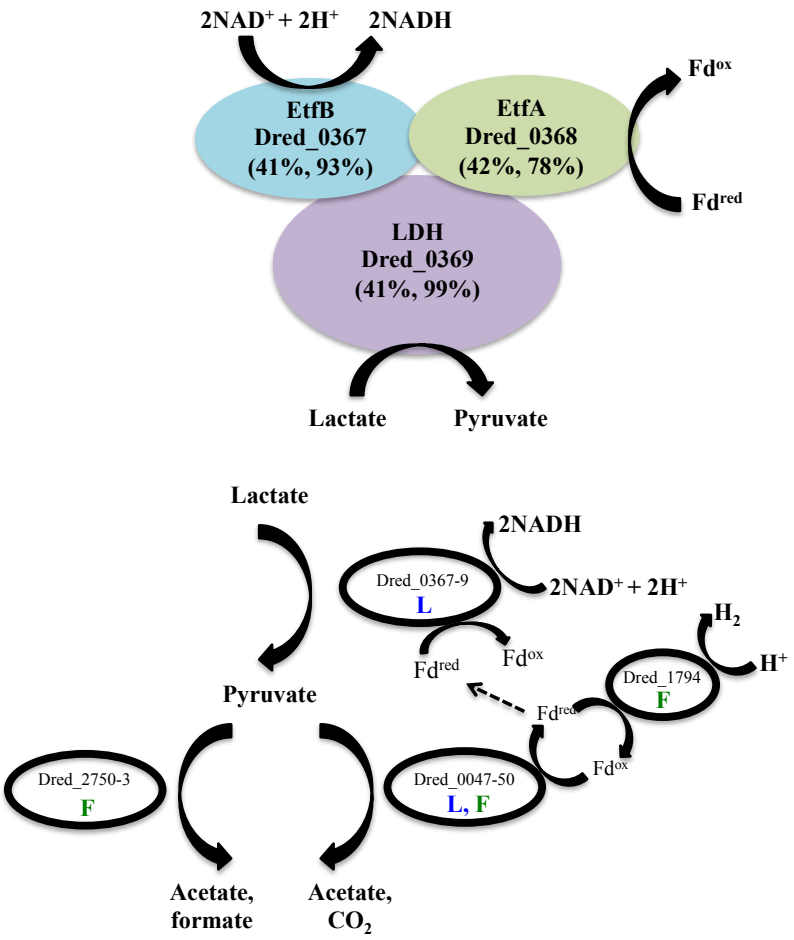

Figure 5.3: Predicted pathways of lactate and pyruvate utilization in *D. reducens* based on proteomic analysis.

5.3a: Dred_0367-9 is proposed to perform lactate oxidation in *D. reducens*. These proteins share similarity with a lactate-oxidizing complex recently described in *Acetobacterium woodii* to operate through flavin-based electron bifurcation (FBEB) (Awo_c08730, 20, and 10) (Weghoff *et al*., 2015). Similarity between *D. reducens* proteins and those from *A. woodii* is displayed as percent sequence identity across percent query coverage (http://blast.ncbi.nlm.nih.gov).

5.3b. Model of lactate and/or pyruvate utilization in *D. reducens*. In lactate-fed cultures, lactate is oxidized to pyruvate. Pyruvate is then converted to acetate (along with CO_2 or formate), and H_2 is produced during pyruvate fermentation. In lactate-fed conditions, H_2 is not formed, and instead reduced ferredoxin could be utilized in other pathways, including the lactate oxidation pathway. Pathways predicted to be involved in lactate-fed cultures are denoted with a blue L. Pathways predicted to be involved in pyruvate-fed fermentative cultures are denoted with a green F. Abundance comparisons for proteins displayed are in **Supplementary Table 5.3.**

The genome of *D. reducens* contains an eleven-subunit, proton-translocating NADH: quinone oxidoreductase (Nuo, Dred_2036-46), predicted to be involved in NADH oxidation for cellular respiration (Junier et al., 2010). On sulfate reduction conditions as well as pyruvate fermentation, four of the subunits were identified (B, C, D, and I), while only the D subunit was observed on Fe(III)-oxide. During Fe(III)-citrate reduction, not a single subunit of Nuo was identified with any confidence, providing evidence that the Nuo complex is not being utilized during this type of growth in *D. reducens.* Cellular respiration generates ATP by ATP synthase, and all but two subunits of the F-type H+-transporting ATPase were identified in our study. The six identified proteins of the ATP synthase (Dred_3149-56) were most abundant during the sulfate reduction condition and decreased in abundance on Fe(III)-citrate relative to all other conditions (**Supplementary Table 5.5**). While Fe(III) was initially reported to serve as an electron acceptor for *D. reducens*, more recent reports have suggested that Fe(III) acts as an electron dump rather than a true respiratory electron acceptor (Dalla Vecchia et al., 2014a, 2014b). Our proteomic findings on the Nuo complex as well as the ATP synthase support the idea that *D. reducens* may not be truly respiring Fe(III). We propose that the downregulation of energy production-related proteins during Fe(III) reduction in *D. reducens* indicates that Fe(III) serves as a less suitable cultivation condition for *D. reducens* than sulfate reduction or pyruvate fermentation. This is supported by less vigorous growth of *D. reducens* on Fe(III), as evidenced by substantially lower growth rates and biomass yields **(Supplementary Figure 5.1)**.

II. Proteome of *D. reducens* during sulfate reduction

Our proteomic analysis revealed that core proteins involved in sulfate reduction in *D. reducens* (and conserved between Gram-negative and Gram-positive SROs) are consistent in abundance across conditions. Furthermore, we have identified key clusters of proteins that are

highly abundant on sulfate relative to other conditions, and we hypothesize that these are involved in the respiratory process. Some of these clusters include the *hdr*-containing loci introduced previously **(Figure 5.2)**. **Figure 5.4** summarizes the predicted pathway of electron transfer during sulfate reduction in *D. reducens* based on proteomic evidence.

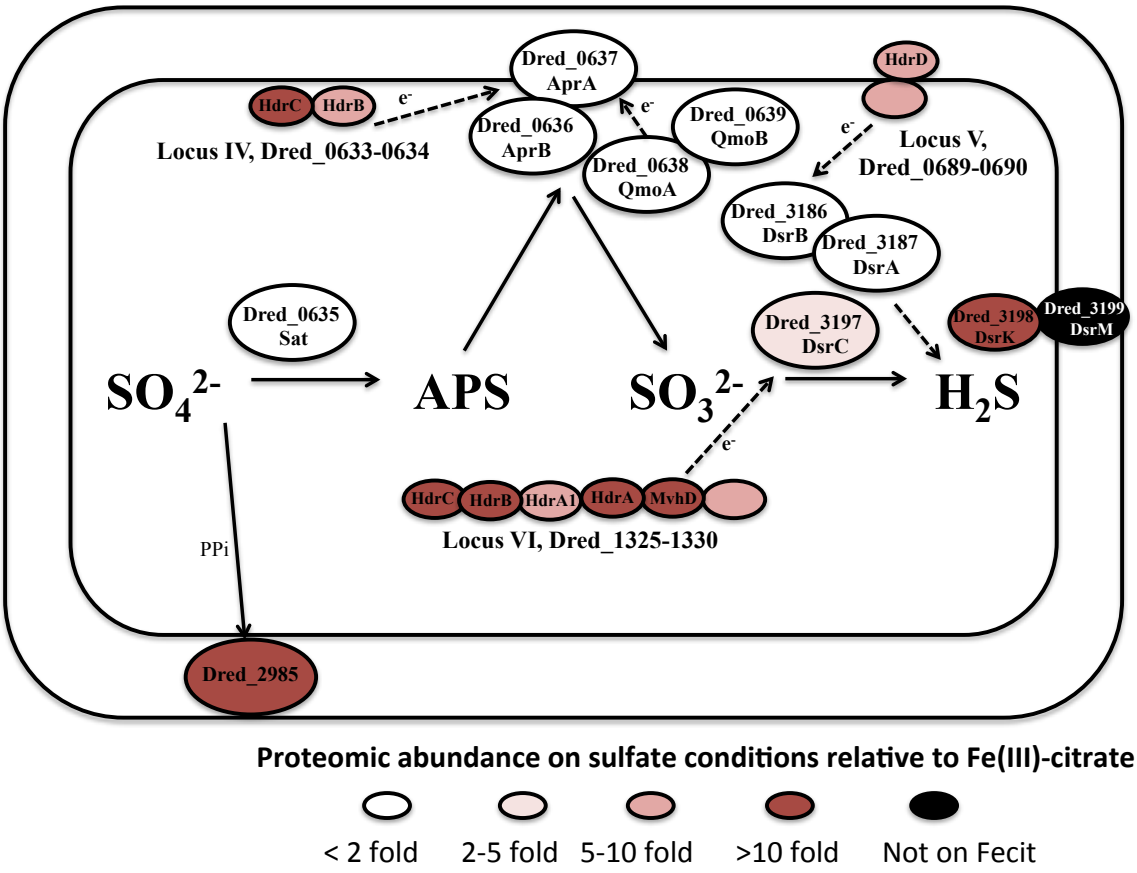

Figure 5.4: Predicted pathway of sulfate reduction in *D. reducens* based on proteomic findings. The core sulfate reduction machinery (Sat, APS reductase, sulfite reductase) does not display significant differential abundance. Instead, certain clusters of proteins encoded within *hdr*-containing loci are increased in abundance during sulfate reduction and are predicted to be involved in the process. Abundance comparisons are shown for sulfate and Fe(III)-citrate reduction conditions. All protein abundance comparisons are displayed in **Tables 5.3 and 5.4.**

The core sulfate reduction pathway involves activation of sulfate to adenosine 5'-phosphosulfate (APS) by sulfate adenyltransferase (Dred_0635), processing of the pyrophosphate formed by a pyrophosphatase (Dred_2985), reduction of APS to sulfite by APS

reductase (Dred_0636-7), and reduction of sulfite to sulfide by dissimilatory-type sulfite reductase DsrAB (Dred_3186-7, DsrB and DsrA) (Grein et al., 2013; Pereira et al., 2011). Our data reveals that in most cases, the core sulfate-reducing machinery is not differentially expressed in *D. reducens* across the cultivation conditions tested **(Table 5.3, Figure 5.4)**.

Table 5.3: Log_2 abundance comparisons of proteins putatively involved in dissimilatory sulfate reduction in *D. reducens*.

Locus tag	Protein name	Log_2 Sulf/Pyr	Log_2 Sulf/Fe(III)-citrate	Log_2 Sulf/Fe(III)-oxide	PSORTb localization
Core sulfate reduction machinery					
Dred_0635	sulfate adenyltransferase (Sat)	-0.28	0.16	-1.03	C
Dred_0636	adenylylsulfate reductase subunit beta (AprB)	-0.25	0.59	0.27	U
Dred_0637	adenylylsulfate reductase subunit alpha (AprA)	0.16	0.39	-0.23	C
Dred_2985	membrane-bound proton-translocating pyrophosphatase	0.40	3.97	1.60	CM
Dred_3186	sulfite reductase, dissimilatory-type beta subunit (DsrB)	0.42	0.99	0.36	C
Dred_3187	sulfite reductase, dissimilatory-type alpha subunit (DsrA)	0.26	0.33	0.03	C
Additional putative sulfate reduction proteins					
Dred_0638	4Fe-4S ferredoxin iron-sulfur binding domain-containing protein (QmoA)	1.07	0.77	0.21	C
Dred_0639	methyl-viologen-reducing hydrogenase, delta subunit (QmoB)	0.49	0.08	-0.04	C

Dred_3185	putative dissimilatory sulfite reductase subunit D (DsrD)	-0.02	4.03	3.35	C
Dred_3197	DsrC family protein	0.32	1.43	1.15	C
Dred_3198	hypothetical protein (DsrK)	-0.90	3.37	0.87	C
Dred_3199	nitrate reductase, gamma subunit (DsrM)	0.47	NI	-0.14	CM

Table key:

<2 fold	2-5 fold	5-10 fold	>10 fold

Note: Protein identification is based on detection of at least 2 unique peptides in a biological replicate and peptide detection in at least 50% of replicates. P-values for all ratios highlighted for abundance changes >2-fold are <0.01. NI=protein not identified. Localization is from PSORTb (Yu et al., 2010). C=cytoplasmic, CM=cytoplasmic membrane, E= extracellular, CW= cell wall, U= unknown.

Outside of the core enzymes, distinct differences are observed between the genomes of Gram-positive and Gram-negative SROs, as outlined in-depth in recent reviews (Grein et al., 2013; Pereira et al., 2011). In particular, transmembrane complexes that have been ascribed to electron transfer during sulfate reduction in model *Desulfovibrio* species, many of which contain MHC components, are not conserved in Gram-positives. One of these transmembrane complexes is QmoABC, shown to transfer electrons to the APS reductase. The genome of *D. reducens* contains predicted orthologs to QmoA (Dred_0638) and QmoB (Dred_0639), but is missing the transmembrane subunit QmoC, suggesting that other mechanisms are involved in electron transfer to APS reductase. As was observed for the core sulfate-reducing machinery, Dred_0638-9 is similarly abundant across all cultivation conditions **(Table 5.3, Figure 5.4).** Another transmembrane complex of interest is the five-subunit DsrMKJOP, described in *Desulfovibrio* to transfer electrons to the sulfite reductase. The genome of *D. reducens* encodes predicted orthologs only to two subunits and these are rather distant. Dred_3198 shares 37% sequence

identity across 81% query coverage to DsrK from *Desulfovibrio vulgaris* and Dred_3199 shares 26% identity across 74% to DsrM (http://blast.ncbi.nlm.nih.gov). Both proteins do not exhibit any discernable differential abundance on sulfate, pyruvate, and Fe(III)-oxide, but Dred_3198 is significantly lower in abundance on Fe(III)-citrate relative to sulfate (10.3-fold higher on sulfate, p-value <0.01) and Dred_3199 was not identified on Fe(III)-citrate. DsrC (Dred_3197) is a protein conserved in all SROs sequenced to date, positioned next to the Dsr complex, and found to interact with the sulfite reductase (Venceslau et al., 2014). DsrC was recently shown to form a trisulfide intermediate and to serve as a co-substrate for DsrAB (Santos et al., 2015). In *D. reducens*, DsrC is increased >2-fold on sulfate versus both Fe(III) conditions **(Table 5.3)**.

Proteins in heterodisulfide reductase-containing loci are abundant in sulfate reduction proteome

Our proteomic analysis revealed specific clusters of proteins that are abundant during sulfate reduction relative to the other cultivation conditions. Interestingly, three of these clusters fall into the *hdr*-containing loci displayed in **Figure 5.2,** specifically Dred_0633-4, Dred_0689-90, and Dred_1325-30 **(Table 5.4)**. Dred_0633-4, a predicted operon in locus IV, is significantly increased relative to Fe(III) reduction conditions but not pyruvate fermentation conditions. However, the positioning of Dred_0633 (an HdrC-type protein) and Dred_0634 (an HdrB-type protein) next to key sulfate reduction proteins including the sulfate adenyltransferase (Dred_0635), the APS reductase subunits (Dred_0636-7, AprBA), and QmoAB (Dred_0638-9) suggests an involvement in sulfate reduction. Due to their genomic localization near the AprBA, these Hdr-like proteins may be involved in electron transfer to this reductase **(Figure 5.4)**. In fact, in all sequenced *Desulfotomaculum* genomes, orthologs of these two Hdr-like proteins exist next to the sulfate adenyltransferase and APS reductase, as determined by the IMG neighborhood viewer (https://img.jgi.doe.gov).

Table 5.4: Log_2 proteomic abundance comparisons for proteins discussed from heterodisulfide reductase (*hdr*)-containing loci

Locus tag	Protein name	Log_2 Sulf/Pyr	Log_2 Sulf/Fecit	Log_2 Sulf/Feox	Localization
Locus IV: Dred_0633-4, sulfate-induced					
Dred_0633	putative heterodisulfide reductase, C subunit (HdrC)	-0.33	2.57 (<0.01)	2.62	C
Dred_0634	CoB--CoM heterodisulfide reductase (HdrB)	0.23	2.27 (<0.01)	1.02	C
Locus V: Dred_0689-90, sulfate-induced					
Dred_0689	hypothetical protein	0.23	3.76 (<0.01)	2.74	C
Dred_0690	hypothetical protein (HdrD)	0.01	2.35 (<0.01)	1.05	CM
Locus VI: Dred_1325-30, sulfate-induced					
Dred_1325	heterodisulfide reductase, C subunit (HdrC)	1.88 (<0.01)	6.02 (<0.01)	0.06	C
Dred_1326	hypothetical protein (hdrB)	1.25 (<0.01)	4.1 (<0.01)	3.81 (<0.01)	C
Dred_1327	4Fe-4S ferredoxin iron-sulfur binding domain-containing protein (HdrA1)	1.03 (<0.01)	2.98 (<0.01)	2.54 (<0.01)	C
Dred_1328	4Fe-4S ferredoxin iron-sulfur binding domain-containing protein (HdrA)	0.67 (<0.01)	4.36 (<0.01)	2.9 (<0.01)	C
Dred_1329	methyl-viologen-reducing hydrogenase, delta subunit (MvhD)	0.75 (<0.01)	4.6 (<0.01)	4.1 (<0.01)	U
Dred_1330	formate dehydrogenase	0.85 (<0.01)	3.09 (<0.01)	2.11 (<0.01)	C
Locus tag	**Protein name**	**Log_2 Fecit/pyr**	**Log_2 Fecit/Sulf**	**Log_2 Fecit/Feox**	**Localization**
Locus I: No significant differential abundance pattern					
Dred_0137/ 0143	4Fe-4S ferredoxin iron-sulfur binding domain-containing protein (HdrA)	-0.29	-0.77 (<0.01)	-0.24	U
Dred_0138	pseudogene	NI	NI	NI	
Dred_0139/	4Fe-4S ferredoxin iron-	-0.85	-0.62	0.71 (0.04)	CM

0146	sulfur binding domain-containing protein (FeS)	(0.01)			
Dred_0140/0147	4Fe-4S ferredoxin iron-sulfur binding domain-containing protein (FeS)	-0.26	-0.60 (0.01)	-0.47 (0.02)	C
Dred_0141/0148	oxidoreductase FAD/NAD(P)-binding subunit	-1.07 (<0.01)	-1.61 (<0.01)	0.09	C
Dred_0142	hypothetical protein	-0.96 (<0.01)	-1.28 (<0.01)	1.48 (<0.01)	C
Dred_0144	methyl-viologen-reducing hydrogenase, delta subunit (MvhD)	1.37	0.62	0.47	U
Dred_0145	heterodisulfide reductase subunit (HdrD)	-0.7 (0.03)	-1.61 (<0.01)	-0.43	U
Locus III: Dred_0432-3, Fe(III)-citrate-induced					
Dred_0432	hypothetical protein (FeS)	Fecit only (1 unique pep)			C
Dred_0433	CoB--CoM heterodisulfide reductase (HdrD)	1.80 (<0.01)	NI	NI	CM
Locus VI: Dred_1778-84, Fe(III)-citrate-induced					
Dred_1778	electron transfer flavoprotein subunit beta (EtfB)	0.01	-0.02	2.73 (<0.01)	C
Dred_1779	electron transfer flavoprotein subunit alpha (eEfA)	0.23	0.24	3.58 (<0.01)	U
Dred_1780	3-hydroxybutyryl-CoA dehydrogenase	1.22 (<0.01)	0.39 (0.01)	3.29 (<0.01)	C
Dred_1781	enoyl-CoA hydratase/isomerase	2.12 (<0.01)	2.12 (<0.01)	4.07 (<0.01)	C
Dred_1782	butyryl-CoA dehydrogenase	0.62 (0.02)	-0.17	1.84 (<0.01)	C
Dred_1783	hypothetical protein (HdrD)	0.98 (<0.01)	0.87 (<0.01)	1.87 (<0.01)	CM
Dred_1784	acetyl-CoA acetyltransferase	0.71 (<0.01)	0.41	3.49 (<0.01)	C

Note: Protein identification is based on detection of at least 2 unique peptides in a biological replicate (unless noted otherwise) and peptide detection in at least 50% of replicates. All significant p-values (<0.05) are shown. NI=protein not identified. Localization is from PSORTb (Yu et al., 2010). C=cytoplasmic, CM=cytoplasmic membrane, E= extracellular, CW= cell wall, U= unknown.

A significant increase in abundance is also observed for the predicted operon Dred_0689-90 on the sulfate reduction condition relative to Fe(III) reduction conditions but not relative to pyruvate conditions. Dred_0689 is annotated as a hypothetical protein and Dred_0690 is an HdrD-like protein **(Figure 5.2 and Table 5.4).** Both of these proteins have annotations that suggest involvement in lactate oxidation, described by IMG as L-lactate utilization proteins LutC and LutB respectively, which suggests an involvement in lactate-fed sulfate reduction rather than pyruvate fermentation. Furthermore, the *hdr*-containing locus is conserved across *Desulfotomaculum* species, and several species contain an adjacent L-lactate transport protein. The locus is also conserved in species of *Desulfosporosinus* and *Desulfitobacterium* (the latter of which reduces sulfite but not sulfate), suggesting that these proteins may be involved with lactate utilization and/or electron transfer to the sulfite reductase (https://img.jgi.doe.gov).

A particularly striking *hdr*-containing locus is Dred_1325-30 (locus VI in **Figure 5.2)**, where a significant increase in abundance is observed across the six proteins on sulfate relative to all other cultivation conditions (with p-values <0.05) **(Table 5.4**). For instance, compared with the Fe(III)-citrate condition, these proteins are increased >20-fold on average. The six proteins of this locus are completely conserved only in other species of *Desulfotomaculum* that are incomplete lactate oxidizers (https://img.jgi.doe.gov). Intriguingly, there is similarity between Dred_1325-30 and the FlxABCD-HdrABC cluster, recently shown in *Desulfovibrio vulgaris* Hildenborough to be essential for NADH oxidation during sulfate reduction with ethanol as electron donor and suggested to reduce DsrC through FBEB (Ramos et al., 2015). The Hdr components are completely conserved, as are parts of the Flx components. While Dred_1325-30 is missing an ortholog to FlxA (the predicted NADH dehydrogenase), Dred_1327 is a much larger protein than the HdrA from *Desulfovibrio* and contains multiple partial HdrA domains as

well as putative NADH-binding domains (MicrobesOnline, Dehal et al., 2010). This large protein may be performing the NADH-oxidizing function in the cluster, while Dred_1328 (also an HdrA-type protein) reduces ferredoxin **(Figure 5.5a)**. Therefore, it is possible that this cluster may be performing a similar function in *D. reducens*, utilizing FBEB in order to improve the energetic favorability of sulfate reduction. Another *hdr*-containing locus in *D. reducens* (Dred_0137-48) shows similarity to the Dred_1325-30 cluster and in fact encodes components of Flx missing from Dred_1325-30 **(Figure 5.5b)**. Dred_0137-48 is missing the HdrB and HdrC components of the cluster, but it is possible that this locus coordinates with Dred_1325-30, oxidizing NADH and working together to reduce ferredoxin and DsrC. The Dred_0137-48 locus is not differentially abundant across conditions in most cases (see further description below), unlike the Dred_1325-30 cluster **(Table 5.4).** Additional clusters of interest on the sulfate reduction condition (not *hdr*- containing) are displayed in **Supplementary Table 5.6.**

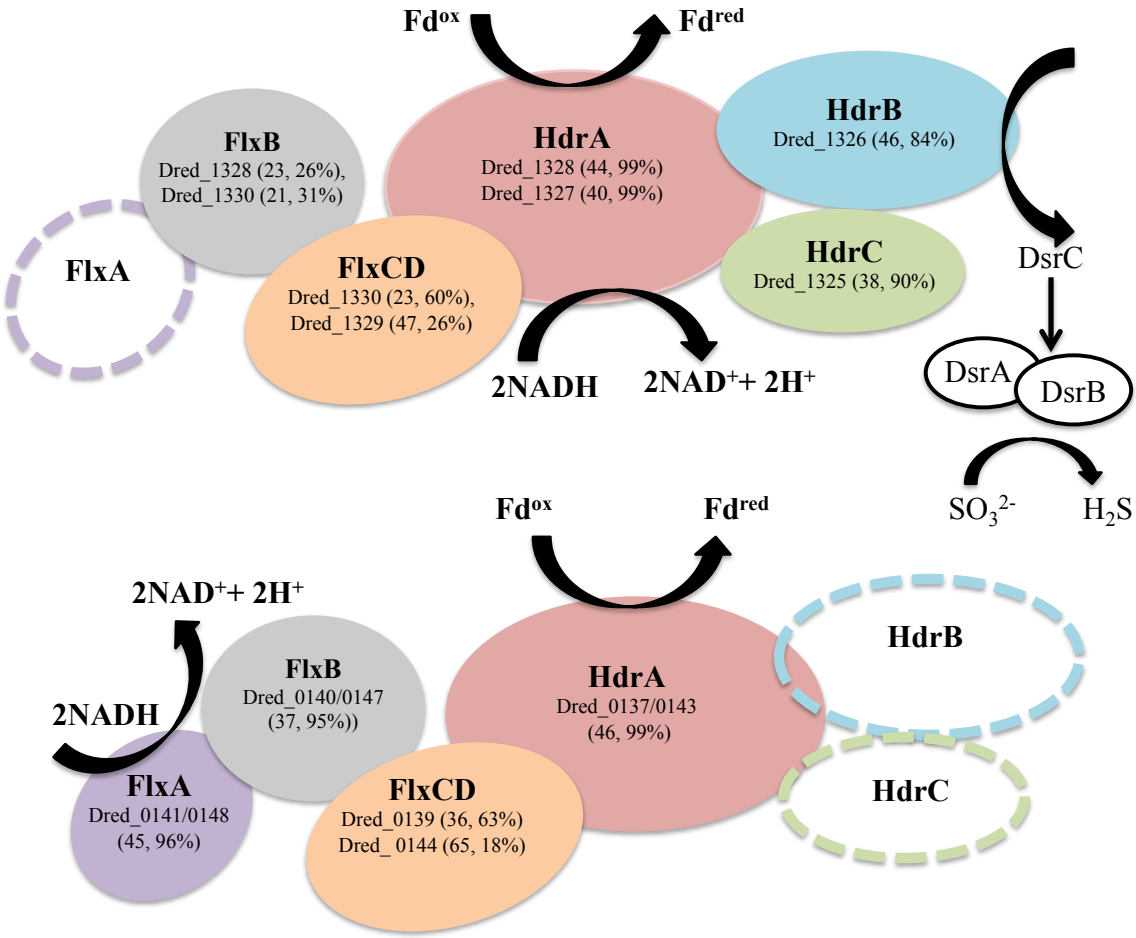

Figure 5.5: *Hdr*-containing locus VI (Dred_1325-30) is proposed to transfer electrons to DsrC.

5.5a: Dred_1325-30 is significantly increased in abundance during sulfate reduction relative to other cultivation conditions analyzed. This locus contains orthologs to proteins within the flavin-based electron bifurcation (FBEB) FlxABCD-HdrABC cluster described in *Desulfovibrio vulgaris* Hildenborough (DVU2399-2404) to be involved in electron transfer to DsrC (Ramos *et al*., 2015). Sequence similarity is displayed as percent sequence identity across percent query coverage (http://blast.ncbi.nlm.nih.gov). An open circle displays lack of an ortholog.

5.5b: *Hdr*-containing locus I (Dred_0137-148) contains similarity to several proteins within locus VI and the FlxABCD-HdrABC cluster but is missing two of the Hdr-type proteins. Dred_0141 and Dred_0148 (identical proteins) are orthologs to the FlxA protein missing from the Dred_1325-30 cluster. It is possible that locus VI (Dred_1325-30) and locus I (Dred_0137-48), both of which were identified with high numbers of unique peptides in our proteomic data, work together to carry out FBEB in order to reduce DsrC.

III. Proteome of *D. reducens* during Fe(III) reduction

All previous RNA and/or protein-based analyses of Fe(III) reduction in *D. reducens* have used soluble Fe(III) due to technical challenges associated with culturing and sample preparation

on insoluble Fe(III) (Dalla Vecchia et al., 2014a, 2014b). In this study, we have analyzed the proteomes of *D. reducens* cultivated on both soluble Fe(III)-citrate and insoluble Fe(III)-oxide, allowing for a valuable comparison of external electron acceptors.

Proteins in heterodisulfide reductase-containing loci are abundant in soluble Fe(III) reduction proteome

Three *hdr*-containing loci are highlighted in the proteome of *D. reducens* during soluble Fe(III) reduction. This includes proteins within locus VII (Dred_1777-86) locus III (Dred_0427-33), and locus I (Dred_0137-48) **(Figure 5.2).** While the electron transfer proteins (Dred_1778-9) are similarly abundant on Fe(III)-citrate, sulfate, and pyruvate, Dred_1780-4 represents the most increased cluster of three or more proteins on Fe(III)-citrate relative to pyruvate **(Table 5.4).** It is increased in abundance ~2.2-fold across the five proteins (all p-values <0.02). In addition, while the Fe(III)-citrate condition overall has nearly half of the total unique peptides observed on the sulfate and pyruvate condition, and accordingly tends to have less peptides detected for each protein, the number of unique peptides detected across Dred_1778-84 is significantly higher on Fe(III)-citrate than all other conditions. Averaged across technical triplicates and biological duplicates, the mean number of peptides/protein across the seven proteins is 42.9 on the Fe(III)-citrate condition, 17.2 on pyruvate, 20.8 on sulfate, and 8.0 on Fe(III)-oxide. Five proteins in this cluster (Dred_1782, Dred_1784, and Dred_1778-80) fall into the top twenty proteins across the Fe(III)-citrate proteome with respect to highest unique peptide counts. This result is surprising because these genes are predicted to be involved in butyrate oxidation, which is not the electron donor for any cultures analyzed in this study. It is possible that these proteins are using a different substrate than their annotation suggests, or that these enzymes are acting in the opposite direction, converting acetyl-CoA to butyrl-CoA **(Figure 5.6)**. In fact, proteins within this cluster

are similar to one of the most well described FBEB systems, the clostridial butyryl-CoA dehydrogenase/electron transferring flavoprotein (BcdA–EtfBC) complex (Buckel and Thauer, 2013; Li et al., 2008). This complex is known to catalyze the electron bifurcation from NADH to ferredoxin and crotonyl-CoA. The proteins Dred_1778-9 (electron transfer flavoproteins) and Dred_1782 (butyryl-CoA dehydrogenase) match closely to this complex, while orthologs to Dred_1780-2 and Dred_1784 catalyze the reactions leading to this FBEB. In this scheme, a protein such as the formate acetyltransferase Dred_0039 (observed on all conditions and most abundant on pyruvate) could be converting pyruvate to acetyl-CoA. Then, following FBEB, reduced ferredoxin would be available for other reductive processes in the cell. A full visual comparing the BcdA-EtfBC complex in *Clostridium kluyveri* DSM 555 with the *D. reducens* locus is displayed in **Figure 5.6** (Buckel and Thauer, 2013). *D. reducens* also contains proteins that are redundant to components of this FBEB system and these are unique to the Fe(III)-citrate condition. Also important to note, the described clostridial FBEB system lacks Hdr-like proteins. The placement of the HdrD-like protein Dred_1783 in this annotated butyrate-oxidizing cluster is unique to *D. reducens* (https://img.jgi.doe.gov).

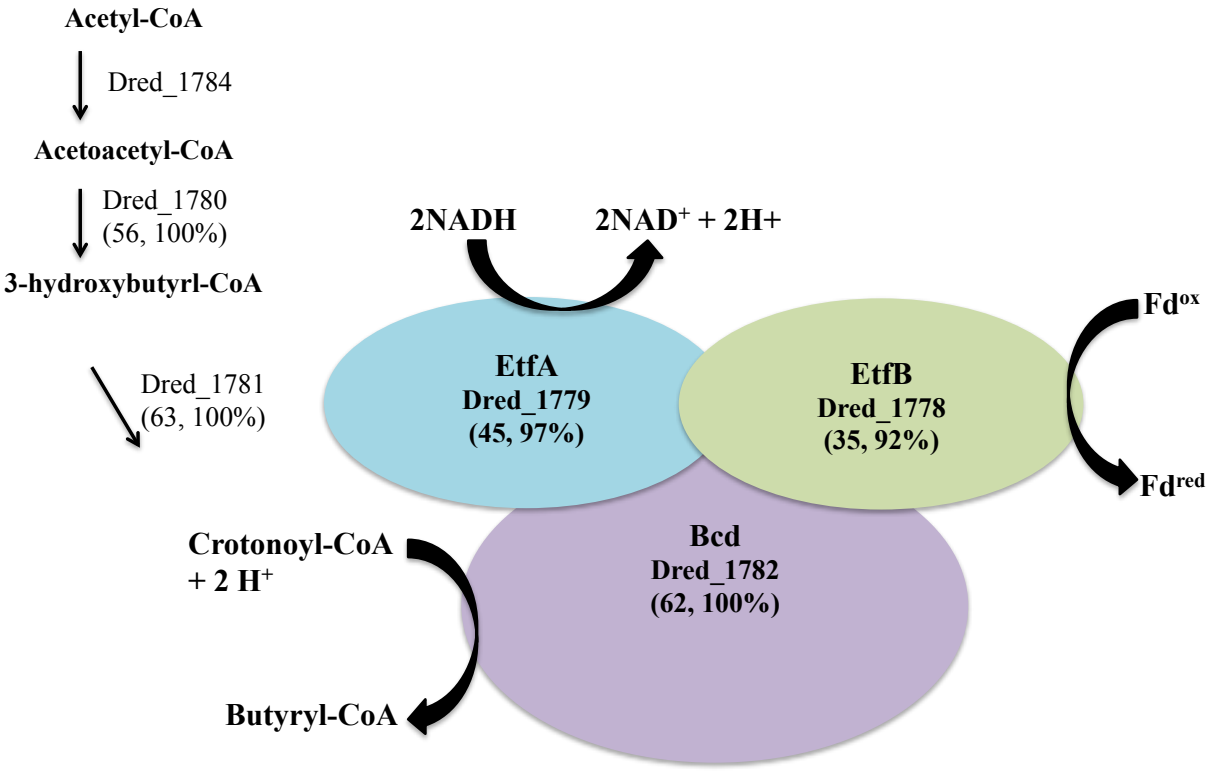

Figure 5.6: The cluster of proteins most increased on Fe(III)-citrate relative to pyruvate fermentation has similarity to a described FBEB system. A significant number of peptides and overall increased abundance was observed for proteins within *hdr*-containing locus VII (Dred_1778-84) on the Fe(III)-citrate condition. Genes within this locus are orthologs to the FBEB complex BcdA–EtfBC from *Clostridium kluyveri* DSM 555 (Li *et al*., 2008; Buckel and Thauer, 2013). Similarity between this complex (CKL_0454-8) and proteins in *D. reducens* is displayed as percent sequence identity across percent query coverage (http://blast.ncbi.nlm.nih.gov). Furthermore, redundant genes for each of the proteins involved in the FBEB step are expressed solely on the Fe(III)-citrate condition and include the electron transfer flavoproteins Dred_0573 and Dred_0572 (45, 97% and 31, 80%), and the acyl-CoA dehydrogenase domain-containing protein Dred_0402 (53, 100%). Furthermore, the enoyl-CoA hydratase/isomerase Dred_0401 is a redundant protein (60%, 100%) for the step leading to crotonoyl-CoA, also unique to the Fe(III)-citrate condition.

In the *hdr*-containing locus III (Dred_0427-33), peptides for proteins encoded between Dred_0427-31 were not identified in our study. Dred_0432-3, however, is significant on the Fe(III)-citrate condition **(Table 5.4)**. Dred_0432 was only identified on pyruvate and Fe(III)-citrate and is increased ~3.5-fold on Fe(III)-citrate (p-value <0.01). Dred_0433 is completely unique to the Fe(III)-citrate condition. The identification of Dred_0432 on Fe(III)-citrate is based

on a single unique peptide in 5/6 replicates. Dred_0433 is localized to the cytoplasmic membrane as predicted by PSORTb (Yu et al., 2010). The predicted operon is from Dred_0431-3, and Dred_0431 is a predicted permease. Dred_0432-3 encompasses the Hdr component of the locus, and interestingly, both proteins have similarity to the L-lactate utilization protein LutB, as described by IMG. As additional evidence towards a role of the proteins in Fe(III) reduction, the closest orthologs to Dred_0432-3 are all from other Gram-positive metal-reducers, specifically *Desulfosporosinus* and *Desulfitobacterium* species. In these other genera, the genes are encoded next to five permease/transport proteins (https://img.jgi.doe.gov). Dred_0432-3 is not conserved in other *Desulfotomaculum* species.

The *hdr*-containing locus Dred_0137-48 is also of interest**.** While many proteins within the locus are similar to Dred_1325-30 **(Figure 5.5)** our proteomic abundance data reveals that Dred_0137-48 is not strongly differentially abundant across conditions and that a high number of unique peptides are observed on all conditions **(Table 5.4)**. Interestingly, the Dred_0137-148 locus contains one of three redox proteins predicted as putative Fe(III) reductases in the analysis of the surfaceome of *D. reducens* (Dalla Vecchia et al., 2014a). This is the ferredoxin Dred_0143, which has an unknown localization based on PSORTb, but contains one transmembrane helix as predicted by the transmembrane helix (TMH) prediction algorithm TMHMM Server v. 2.0 (www.cbs.dtu.dk/services/TMHMM). A duplication is encoded within this locus which is only observed in two other *Desulfotomaculum* species, and Dred_0137 is identical to Dred_0143. The authors did not observe significant differential abundance of this protein between conditions tested (pyruvate fermentation and Fe(III)-citrate with lactate as electron donor), which is consistent with our findings **(Table 5.4)**. The high expression of this locus on all conditions (in contrast to the downregulation of Dred_1325-30 on Fe(III) conditions) supports the possible

involvement of Dred_0143 in Fe(III) reduction proposed by the surfaceome study (Dalla Vecchia et al., 2014a). The other two proteins identified in the surfaceome study as potential Fe(III) reductases are not supported by our proteomic data. This includes Dred_0462, a subunit of the membrane-bound, trimeric hydrogenase Dred_0461-3 **(Supplementary Table 5.3).** Dred_0462 was suggested as a putative Fe(III) reductase, although the authors observed a decrease in its abundance during Fe(III)-reduction relative to pyruvate fermentation. Similarly in our study, both Dred_0462 and Dred_0463 (the catalytic domain) are increased during pyruvate fermentation relative to Fe(III)-reduction and most abundant during sulfate-reduction (with p-values of 0.02 and 0.01 relative to pyruvate) **(Supplementary Table 5.3).** From these findings, it is most likely that this hydrogenase is utilized during sulfate reduction and/or pyruvate fermentation by *D. reducens*. Finally, the only redox-related protein that increased in abundance during Fe(III)-citrate reduction versus pyruvate fermentation in the surfaceome study was the alkyl hydroperoxide reductase Dred_1533, for which we observed no peptides for on any condition (Dalla Vecchia et al., 2014a).

Additional proteins of interest on the Fe(III) reduction condition

Dred_0701, annotated as the sole multiheme c-type cytochrome (Dred_0700-1) was identified only on the Fe(III)-oxide condition. A single peptide was identified in four out of six replicates, whereas no peptides were detected from this protein on any other condition. This is the first evidence of metal reduction-related MHC expression in *D. reducens*. This finding emphasizes the importance of testing environmentally relevant conditions like insoluble Fe(III), as previous analyses of the MHC were performed during soluble Fe(III) and U(VI) reduction. Potentially related to this finding, the protein most increased in abundance on Fe(III)-oxide relative to pyruvate is porphobilinogen deaminase (Dred_2163, HemC), a protein in the heme

biosynthesis pathway (~136.1-fold increase, p-value <0.01). This protein was identified by a single peptide in each replicate of the Fe(III)-oxide condition. Two other proteins in this pathway are also highest in abundance on the Fe(III)-oxide condition relative to all other conditions (Dred_2160 and Dred_2162, HemB and HemD respectively).

Finally, our comparative proteomic analysis provides support for the involvement of the NADH:flavin oxidoreductase (Dred_2421) in Fe(III) reduction, a protein that our group previously identified as a metal reductase based on functional screens of the *D. reducens* proteome (Otwell et al., 2015). Multiple unique peptides were observed for this protein only on Fe(III)-oxide, so therefore with stringent filtering criteria Dred_2421 is unique to the Fe(III)-oxide condition **(Supplementary Table 5.1d)**. Including data for proteins identified by a single unique peptide in at least 50% of the replicates, Dred_2421 is actually most abundant on the Fe(III)-citrate condition, increased ~1.6-fold (p-value <0.01) relative to pyruvate and ~2.3-fold (p-value <0.01) relative to the sulfate condition. Comparing the single peptide identified on all conditions, Dred_2421 is ~3 fold more abundant on Fe(III)-citrate than Fe(III)-oxide. The closest orthologs to this protein are not from *Desulfotomaculum* species, but instead from other genera of Gram-positive metal reducers, specifically *Desulfitobacterium* and *Deuslfosporosinus* species. Interestingly, in *Desulfitobacterium* species, this NADH:flavin oxidoreductase is inserted within the *hdr*-containing locus orthologous to Dred_1778-84 (https://img.jgi.doe.gov).

Conclusions

Comparative proteomic analysis of *D. reducens* cultivated on varied conditions has revealed multiple insights into the metabolism of this Gram-positive organism. Our proteomic dataset allows us to analyze predictions made by the annotated genome and form stronger hypotheses about protein function. A greater number of proteins were observed while *D.*

reducens was either reducing sulfate (with lactate as electron donor) or fermenting pyruvate compared with Fe(III)-reducing conditions. The soluble and insoluble Fe(III)-reducing proteomes, analyzed for the first time in a Gram-positive organism, were distinctive from one another, a result consistent with findings in the Gram-negative metal-reducing organisms *Geobacter sulfurreducens* and *Geobacter bemidjiensis* (Ding et al., 2008; Merkley et al., 2015). Peptides for the sole MHC annotated in the genome (Dred_0700-1) were detected only on the insoluble Fe(III) condition, and an enzyme involved in heme biosynthesis was upregulated >100-fold on Fe(III)-oxide relative to pyruvate. Certain clusters of proteins were significantly differentially abundant across cultivation conditions studied. Several of these clusters include Hdrs, and our study has suggested potential involvement of these *hdr*-containing loci in metabolic processes in *D. reducens* including sulfate and Fe(III) reduction.

While comparative expression analyses (mRNA and protein-based) are accepted methods for highlighting genes/proteins of interest, these approaches have limitations. Namely, differential expression is not necessarily directly linked with function (Price et al., 2013). For instance, our analysis of putative sulfate reduction-related proteins in *D. reducens* revealed that most of these proteins are not differentially abundant on cultivation conditions tested, which is not the result we expected. Nonetheless, comparative proteomic analysis offers a method for hypothesis generation regarding protein function and is especially useful in a poorly characterized organism such as *D. reducens*.

Acknowledgements

This chapter is modified from work published in *Frontiers in Microbiology* in February 2016. As is the open access policy of *Frontiers in Microbiology*, permission is not required for reuse of content.
Citation:
Otwell, A.E.[1], Callister, S.J.[2], Zink, E.M.[2], Smith, R.D.[2], Richardson, R.E.[3] (2016). Comparative Proteomic Analysis of *Desulfotomaculum reducens* MI-1: Insights into the Metabolic Versatility

of a Gram-positive Sulfate- and Metal-reducing Bacterium. *Front. Microbiol.* doi: 10.3389/fmicb.2016.00191.

[1]Department of Microbiology, Cornell University, USA
[2]Biological Sciences Division, Pacific Northwest National Laboratory, USA
[3]Department of Civil and Environmental Engineering, Cornell University, USA

References

Aüllo, T., Ranchou-Peyruse, A., Ollivier, B., and Magot, M. (2013). *Desulfotomaculum* spp. and related gram-positive sulfate-reducing bacteria in deep subsurface environments. *Front. Microbiol.* 4, 362. doi:10.3389/fmicb.2013.00362.

Barton, L., Tomei-Torres, F., Xu, H., and Zocco, T. (2015). *Bacteria-Metal Interactions*. , ed. D. Saffarini Cham: Springer International Publishing doi:10.1007/978-3-319-18570-5.

Bird, L. J., Bonnefoy, V., and Newman, D. K. (2011). Bioenergetic challenges of microbial iron metabolisms. *Trends Microbiol.* 19, 330–340. doi:10.1016/j.tim.2011.05.001.

Buckel, W., and Thauer, R. K. (2013). Energy conservation via electron bifurcating ferredoxin reduction and proton/Na(+) translocating ferredoxin oxidation. *Biochim. Biophys. Acta* 1827, 94–113. doi:10.1016/j.bbabio.2012.07.002.

Callister, S. J., McCue, L. A., Turse, J. E., Monroe, M. E., Auberry, K. J., Smith, R. D., et al. (2008). Comparative Bacterial Proteomics: Analysis of the Core Genome Concept. *PLoS One* 3, e1542. doi:10.1371/journal.pone.0001542.

Callister, S. J., Nicora, C. D., Zeng, X., Roh, J. H., Dominguez, M. A., Tavano, C. L., et al. (2006). Comparison of aerobic and photosynthetic *Rhodobacter sphaeroides* 2.4.1 proteomes. *J. Microbiol. Methods* 67, 424–36. doi:10.1016/j.mimet.2006.04.021.

Cardenas, E., Wu, W.-M., Leigh, M. B., Carley, J., Carroll, S., Gentry, T., et al. (2010). Significant Association between Sulfate-Reducing Bacteria and Uranium-Reducing Microbial Communities as Revealed by a Combined Massively Parallel Sequencing-Indicator Species Approach. *Appl. Environ. Microbiol.* 76, 6778–6786. doi:10.1128/AEM.01097-10.

Dalla Vecchia, E., Shao, P. P., Suvorova, E., Chiappe, D., Hamelin, R., and Bernier-Latmani, R. (2014a). Characterization of the surfaceome of the metal-reducing bacterium *Desulfotomaculum reducens*. *Front. Microbiol.* 5, 432. doi:10.3389/fmicb.2014.00432.

Dalla Vecchia, E., Suvorova, E. I., Maillard, J., and Bernier-Latmani, R. (2014b). Fe(III) reduction during pyruvate fermentation by *Desulfotomaculum reducens* strain MI-1. *Geobiology* 12, 48–61. doi:10.1111/gbi.12067.

Dehal, P. S., Joachimiak, M. P., Price, M. N., Bates, J. T., Baumohl, J. K., Chivian, D., et al. (2010). MicrobesOnline: an integrated portal for comparative and functional genomics. *Nucleic Acids Res.* 38, D396–400. doi:10.1093/nar/gkp919.

Ding, Y.-H. R., Hixson, K. K., Aklujkar, M. A., Lipton, M. S., Smith, R. D., Lovley, D. R., et al. (2008). Proteome of *Geobacter sulfurreducens* grown with Fe(III) oxide or Fe(III) citrate as the electron acceptor. *Biochim. Biophys. Acta - Proteins Proteomics* 1784, 1935–1941. doi:10.1016/j.bbapap.2008.06.011.

Grein, F., Ramos, A. R., Venceslau, S. S., and Pereira, I. A. C. (2013). Unifying concepts in anaerobic respiration: insights from dissimilatory sulfur metabolism. *Biochim. Biophys. Acta* 1827, 145–60. doi:10.1016/j.bbabio.2012.09.001.

Haouari, O., Fardeau, M.-L., Cayol, J.-L., Casiot, C., Elbaz-Poulichet, F., Hamdi, M., et al. (2008). *Desulfotomaculum hydrothermale* sp. nov., a thermophilic sulfate-reducing bacterium isolated from a terrestrial Tunisian hot spring. *Int. J. Syst. Evol. Microbiol.* 58, 2529–2535. doi:10.1099/ijs.0.65339-0.

Herrmann, G., Jayamani, E., Mai, G., and Buckel, W. (2008). Energy conservation via electron-transferring flavoprotein in anaerobic bacteria. *J. Bacteriol.* 190, 784–91. doi:10.1128/JB.01422-07.

Hori, T., Aoyagi, T., Itoh, H., Narihiro, T., Oikawa, A., Suzuki, K., et al. (2015). Isolation of microorganisms involved in reduction of crystalline iron(III) oxides in natural environments. *Front. Microbiol.* 6, 386. doi:10.3389/fmicb.2015.00386.

Junier, P., Frutschi, M., Wigginton, N. S., Schofield, E. J., Bargar, J. R., and Bernier-Latmani, R. (2009). Metal reduction by spores of *Desulfotomaculum reducens*. *Environ. Microbiol.* 11, 3007–3017. doi:10.1111/j.1462-2920.2009.02003.x.

Junier, P., Junier, T., Podell, S., Sims, D. R., Detter, J. C., Lykidis, A., et al. (2010). The genome of the Gram-positive metal- and sulfate-reducing bacterium *Desulfotomaculum reducens* strain MI-1. *Environ. Microbiol.* 12, 2738–2754. doi:10.1111/j.1462-2920.2010.02242.x.

Junier, P., Vecchia, E. D., and Bernier-Latmani, R. (2011). The Response of *Desulfotomaculum reducens* MI-1 to U(VI) Exposure: A Transcriptomic Study. *Geomicrobiol. J.* 28, 483–496. doi:10.1080/01490451.2010.512031.

Kim, S., Gupta, N., and Pevzner, P. A. (2008). Spectral probabilities and generating functions of tandem mass spectra: a strike against decoy databases. *J. Proteome Res.* 7, 3354–63. doi:10.1021/pr8001244.

Klein, M., Friedrich, M., Roger, A. J., Hugenholtz, P., Fishbain, S., Abicht, H., et al. (2001). Multiple Lateral Transfers of Dissimilatory Sulfite Reductase Genes between Major Lineages of Sulfate-Reducing Prokaryotes. *J. Bacteriol.* 183, 6028–6035. doi:10.1128/JB.183.20.6028-6035.2001.

Kuever, J., Visser, M., Loeffler, C., Boll, M., Worm, P., Sousa, D. Z., et al. (2014). Genome analysis of *Desulfotomaculum gibsoniae* strain Groll(T) a highly versatile Gram-positive sulfate-reducing bacterium. *Stand. Genomic Sci.* 9, 821–39. doi:10.4056/sigs.5209235.

Li, F., Hinderberger, J., Seedorf, H., Zhang, J., Buckel, W., and Thauer, R. K. (2008). Coupled ferredoxin and crotonyl coenzyme A (CoA) reduction with NADH catalyzed by the butyryl-CoA dehydrogenase/Etf complex from *Clostridium kluyveri*. *J. Bacteriol.* 190, 843–50. doi:10.1128/JB.01417-07.

Lipton, M. S., Paša-Tolić, L., Anderson, G. A., Anderson, D. J., Auberry, D. L., Battista, J. R., et al. (2002). Global analysis of the *Deinococcus radiodurans* proteome by using accurate mass tags. *Proc. Natl. Acad. Sci.* 99, 11049–11054. doi:10.1073/pnas.172170199.

Liu, Y., Wang, Z., Liu, J., Levar, C., Edwards, M. J., Babauta, J. T., et al. (2014). A trans-outer membrane porin-cytochrome protein complex for extracellular electron transfer by *Geobacter sulfurreducens* PCA. *Environ. Microbiol. Rep.* 6, 776–85. doi:10.1111/1758-

2229.12204.

Lovley, D. R., and Phillips, E. J. P. (1987). Rapid Assay for Microbially Reducible Ferric Iron in Aquatic Sediments. *Appl. Environ. Microbiol.* 53, 1536–1540.

Markowitz, V. M., Chen, I.-M. A., Palaniappan, K., Chu, K., Szeto, E., Pillay, M., et al. (2014). IMG 4 version of the integrated microbial genomes comparative analysis system. *Nucleic Acids Res.* 42, D560–7. doi:10.1093/nar/gkt963.

Merkley, E. D., Wrighton, K. C., Castelle, C. J., Anderson, B. J., Wilkins, M. J., Shah, V., et al. (2015). Changes in protein expression across laboratory and field experiments in *Geobacter bemidjiensis*. *J. Proteome Res.* 14, 1361–75. doi:10.1021/pr500983v.

Newsome, L., Morris, K., and Lloyd, J. R. (2014). The biogeochemistry and bioremediation of uranium and other priority radionuclides. *Chem. Geol.* 363, 164–184.

Otwell, A. E., Sherwood, R. W., Zhang, S., Nelson, O. D., Li, Z., Lin, H., et al. (2015). Identification of proteins capable of metal reduction from the proteome of the Gram-positive bacterium *Desulfotomaculum reducens* MI-1 using an NADH-based activity assay. *Environ. Microbiol.* vol. 17 (6) p. 1977-90. doi:10.1111/1462-2920.12673.

Pereira, I. A. C., Ramos, A. R., Grein, F., Marques, M. C., da Silva, S. M., and Venceslau, S. S. (2011). A comparative genomic analysis of energy metabolism in sulfate reducing bacteria and archaea. *Front. Microbiol.* 2, 69. doi:10.3389/fmicb.2011.00069.

Petrie, L., North, N. N., Dollhopf, S. L., Balkwill, D. L., and Kostka, J. E. (2003). Enumeration and Characterization of Iron(III)-Reducing Microbial Communities from Acidic Subsurface Sediments Contaminated with Uranium(VI). *Appl. Environ. Microbiol.* 69, 7467–7479. doi:10.1128/AEM.69.12.7467-7479.2003.

Polpitiya, A. D., Qian, W.-J., Jaitly, N., Petyuk, V. A., Adkins, J. N., Camp, D. G., et al. (2008). DAnTE: a statistical tool for quantitative analysis of -omics data. *Bioinformatics* 24, 1556–8. doi:10.1093/bioinformatics/btn217.

Price, M. N., Deutschbauer, A. M., Skerker, J. M., Wetmore, K. M., Ruths, T., Mar, J. S., et al. (2013). Indirect and suboptimal control of gene expression is widespread in bacteria. *Mol. Syst. Biol.* 9, 660. doi:10.1038/msb.2013.16.

Ramos, A. R., Grein, F., Oliveira, G. P., Venceslau, S. S., Keller, K. L., Wall, J. D., et al. (2015). The FlxABCD-HdrABC proteins correspond to a novel NADH dehydrogenase/heterodisulfide reductase widespread in anaerobic bacteria and involved in ethanol metabolism in *Desulfovibrio vulgaris* Hildenborough. *Environ. Microbiol.* 17, 2288–305. doi:10.1111/1462-2920.12689.

Richardson, D. J., Butt, J. N., Fredrickson, J. K., Zachara, J. M., Shi, L., Edwards, M. J., et al. (2012). The "porin-cytochrome" model for microbe-to-mineral electron transfer. *Mol. Microbiol.* 85, 201–12. doi:10.1111/j.1365-2958.2012.08088.x.

Robidart, J., Callister, S. J., Song, P., Nicora, C. D., Wheat, C. G., and Girguis, P. R. (2013). Characterizing microbial community and geochemical dynamics at hydrothermal vents using osmotically driven continuous fluid samplers. *Environ. Sci. Technol.* 47, 4399–407. doi:10.1021/es3037302.

Santos, A. A., Venceslau, S. S., Grein, F., Leavitt, W. D., Dahl, C., Johnston, D. T., et al. (2015). A protein trisulfide couples dissimilatory sulfate reduction to energy conservation. *Science*

(80-.). 350, 1541–1545. doi:10.1126/science.aad3558.

Sharma, S., Cavallaro, G., and Rosato, A. (2010). A systematic investigation of multiheme c-type cytochromes in prokaryotes. *JBIC J. Biol. Inorg. Chem.* 15, 559–571. doi:10.1007/s00775-010-0623-4.

Shi, L., Richardson, D. J., Wang, Z., Kerisit, S. N., Rosso, K. M., Zachara, J. M., et al. (2009). The roles of outer membrane cytochromes of *Shewanella* and *Geobacter* in extracellular electron transfer. *Environ. Microbiol. Rep.* 1, 220–227. doi:10.1111/j.1758-2229.2009.00035.x.

Shi, L., Rosso, K. M., Clarke, T. A., Richardson, D. J., Zachara, J. M., and Fredrickson, J. K. (2012). Molecular Underpinnings of Fe(III) Oxide Reduction by *Shewanella Oneidensis* MR-1. *Front. Microbiol.* 3. doi:10.3389/fmicb.2012.00050.

Smith, P. K., Krohn, R. I., Hermanson, G. T., Mallia, A. K., Gartner, F. H., Provenzano, M. D., et al. (1985). Measurement of protein using bicinchoninic acid. *Anal. Biochem.* 150, 76–85.

Sowell, S. M., Norbeck, A. D., Lipton, M. S., Nicora, C. D., Callister, S. J., Smith, R. D., et al. (2008). Proteomic analysis of stationary phase in the marine bacterium "*Candidatus Pelagibacter* ubique". *Appl. Environ. Microbiol.* 74, 4091–100. doi:10.1128/AEM.00599-08.

Stanley, J. R., Adkins, J. N., Slysz, G. W., Monroe, M. E., Purvine, S. O., Karpievitch, Y. V, et al. (2011). A statistical method for assessing peptide identification confidence in accurate mass and time tag proteomics. *Anal. Chem.* 83, 6135–40. doi:10.1021/ac2009806.

Strocchi, A., Furne, J. K., and Levitt, M. D. (1992). A modification of the methylene blue method to measure bacterial sulfide production in feces. *J. Microbiol. Methods* 15, 75–82. doi:10.1016/0167-7012(92)90071-B.

Suzuki, Y., Kelly, S. D., Kemner, K. M., and Banfield, J. F. (2003). Microbial Populations Stimulated for Hexavalent Uranium Reduction in Uranium Mine Sediment. *Appl. Environ. Microbiol.* 69, 1337–1346. doi:10.1128/AEM.69.3.1337-1346.2003.

Tebo, B. M., and Obraztsova, A. Y. (1998). Sulfate-reducing bacterium grows with Cr(VI), U(VI), Mn(IV), and Fe(III) as electron acceptors. *FEMS Microbiol. Lett.* 162, 193–198. doi:10.1111/j.1574-6968.1998.tb12998.x.

Venceslau, S. S., Stockdreher, Y., Dahl, C., and Pereira, I. A. C. (2014). The "bacterial heterodisulfide" DsrC is a key protein in dissimilatory sulfur metabolism. *Biochim. Biophys. Acta* 1837, 1148–64. doi:10.1016/j.bbabio.2014.03.007.

Visser, M., Parshina, S. N., Alves, J. I., Sousa, D. Z., Pereira, I. A. C., Muyzer, G., et al. (2014). Genome analyses of the carboxydotrophic sulfate-reducers *Desulfotomaculum nigrificans* and *Desulfotomaculum carboxydivorans* and reclassification of *Desulfotomaculum carboxydivorans* as a later synonym of *D. nigrificans*. *Stand. Genomic Sci.* 9. doi:10.4056/sigs.4718645.

Wall, J. D., and Krumholz, L. R. (2006). Uranium Reduction. *Annu. Rev. Microbiol.* 60, 149–166. doi:10.1146/annurev.micro.59.030804.121357.

Wang, Y., Yang, F., Gritsenko, M. A., Wang, Y., Clauss, T., Liu, T., et al. (2011). Reversed-phase chromatography with multiple fraction concatenation strategy for proteome profiling of human MCF10A cells. *Proteomics* 11, 2019–26. doi:10.1002/pmic.201000722.

Weghoff, M. C., Bertsch, J., and Müller, V. (2015). A novel mode of lactate metabolism in strictly anaerobic bacteria. *Environ. Microbiol.* 17, 670–7. doi:10.1111/1462-2920.12493.

Williamson, A. J., Morris, K., Shaw, S., Byrne, J. M., Boothman, C., and Lloyd, J. R. (2013). Microbial reduction of Fe(III) under alkaline conditions relevant to geological disposal. *Appl. Environ. Microbiol.* 79, 3320–6. doi:10.1128/AEM.03063-12.

Wiśniewski, J. R., Zougman, A., Nagaraj, N., and Mann, M. (2009). Universal sample preparation method for proteome analysis. *Nat. Methods* 6, 359–62. doi:10.1038/nmeth.1322.

Yu, N. Y., Wagner, J. R., Laird, M. R., Melli, G., Rey, S., Lo, R., et al. (2010). PSORTb 3.0: improved protein subcellular localization prediction with refined localization subcategories and predictive capabilities for all prokaryotes. *Bioinformatics* 26, 1608–15. doi:10.1093/bioinformatics/btq249.

Zverlov, V., Klein, M., Lücker, S., Friedrich, M. W., Kellermann, J., Stahl, D. A., et al. (2005). Lateral gene transfer of dissimilatory (bi)sulfite reductase revisited. *J. Bacteriol.* 187, 2203–8. doi:10.1128/JB.187.6.2203-2208.2005.

Supplementary Figures and Tables:

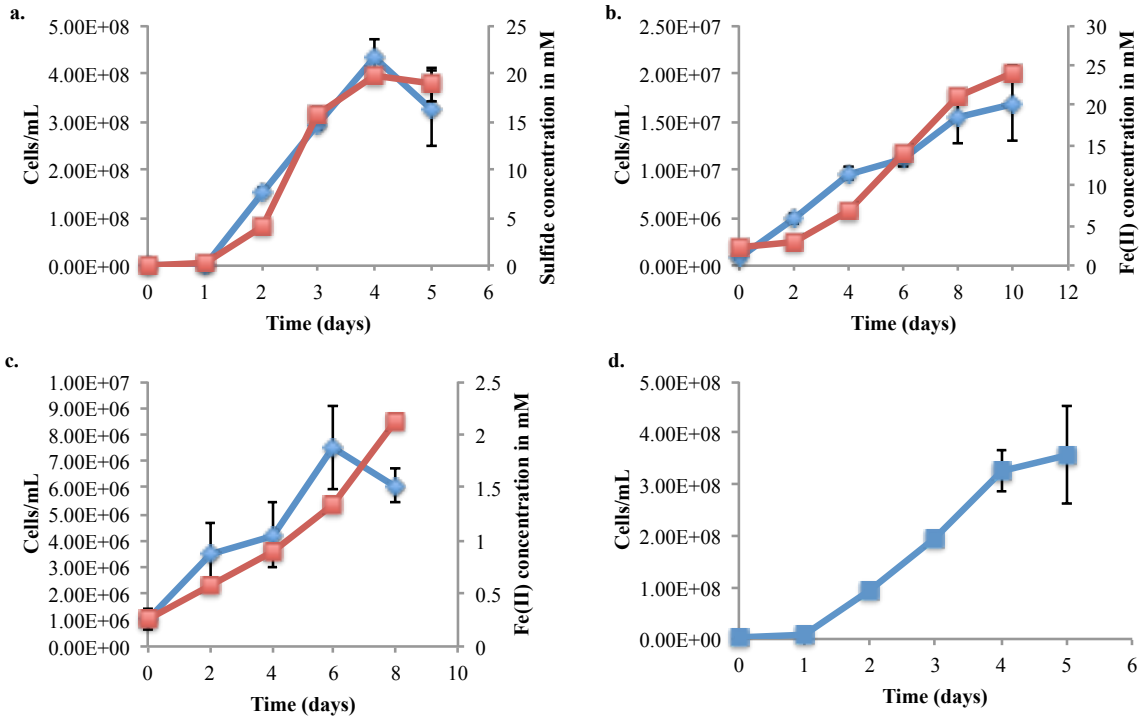

Supplementary Figure 5.1: Representative growth curves of *D. reducens*. In all graphs, microscopic counts are represented by a blue curve and displayed on the left axis. 1.a. Sulfate reduction with lactate as electron donor. 1.b. Fe(III)-citrate reduction with lactate as electron donor. 1.c. Fe(III)-oxide reduction with lactate as electron donor. 1.d. Pyruvate fermentation

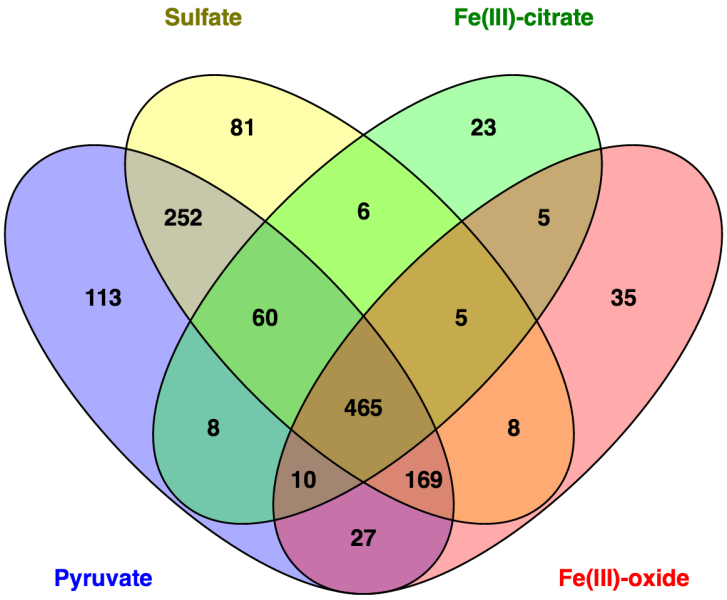

Supplementary Figure 5.2: Overlap in detected proteins between each growth condition analyzed. The Venn diagram was created using Venny 2.0 (Bardou et al., 2014) and includes all proteins confidently observed in *D. reducens* during sulfate reduction, soluble and insoluble Fe(III) reduction, and pyruvate fermentation. A core of 465 proteins was observed on all four conditions analyzed. More total proteins, as well as more unique proteins, were identified in the sulfate and pyruvate conditions compared with the Fe(III) conditions.

Supplementary Table 5.1a: Proteins observed exclusively in the pyruvate fermentation condition
Supplementary Table 5.1b: Proteins observed exclusively in the sulfate reduction condition
Supplementary Table 5.1c: Proteins observed exclusively in the Fe(III)-citrate reduction condition
Supplementary Table 5.1d: Proteins observed exclusively in the Fe(III)-oxide reduction condition
Note: Protein identification is based on detection of at least 2 unique peptides in a biological replicate and p
detection in at least 50% of replicates.
C=cytoplasmic, CM=cytoplasmic membrane, E= extracellular, CW= cell wall, U= unknown.
In Fe(III) Tables: Purple=putative oxidoreductase, Orange=porin-type protein

Supplementary Table 5.1a

Locus Tag	Description
Dred_0005	hypothetical protein
Dred_0010	pyridoxal biosynthesis lyase PdxS
Dred_0040	putative transmembrane anti-sigma factor
Dred_0059	dTMP kinase; EC_number=2.7.4.9
Dred_0122	RNA-binding S1 domain-containing protein
Dred_0125	tRNA(Ile)-lysidine synthetase
Dred_0150	hypothetical protein
Dred_0171	Baf family transcriptional activator
Dred_0178	UvrB/UvrC protein
Dred_0186	PilT domain-containing protein
Dred_0235	preprotein translocase subunit SecY
Dred_0250	anthranilate phosphoribosyltransferase
Dred_0264	putative endoribonuclease L-PSP
Dred_0343	hypothetical protein
Dred_0355	flagellar motor protein MotA
Dred_0392	oligopeptide/dipeptide ABC transporter ATPase
Dred_0393	oligopeptide/dipeptide ABC transporter ATPase
Dred_0404	glutaconate CoA-transferase; EC_number=2.8.3.12
Dred_0420	SpoOM family protein
Dred_0421	peptidase M48, Ste24p
Dred_0432	hypothetical protein
Dred_0491	deoxyuridine 5prime-triphosphate nucleotidohydrolase Dut; EC_number=3.6.1.23
Dred_0500	DNA polymerase subunit beta
Dred_0517	hypothetical protein
Dred_0536	hypothetical protein
Dred_0709	phosphate ABC transporter ATPase
Dred_0710	phosphate uptake regulator PhoU
Dred_0729	ABC transporter-like protein
Dred_0738	phosphodiesterase
Dred_0744	copper amine oxidase domain-containing protein
Dred_0761	UBA/THIF-type NAD/FAD binding protein
Dred_0783	prephenate dehydratase; EC_number=4.2.1.51
Dred_0868	type III restriction enzyme, res subunit
Dred_0952	hypothetical protein
Dred_0976	TRAG family protein
Dred_0978	hypothetical protein
Dred_1017	HAD family phosphatase
Dred_1117	hypothetical protein
Dred_1188	hypothetical protein
Dred_1200	thymidylate synthase, flavin-dependent; EC_number=2.1.1.148
Dred_1203	phage terminase GpA
Dred_1240	glutamate racemase; EC_number=5.1.1.3
Dred_1287	MarR family transcriptional regulator
Dred_1288	putative CoA-substrate-specific enzyme activase
Dred_1340	hypothetical protein
Dred_1347	hypothetical protein
Dred_1354	WD40 domain-containing protein
Dred_1358	putative radical SAM protein
Dred_1367	YheO domain-containing protein
Dred_1413	peptidoglycan-binding LysM
Dred_1445	nitrate reductase subunit gamma
Dred_1458	alpha amylase catalytic subunit
Dred_1471	citrate transporter
Dred_1491	acetyl-CoA acetyltransferase; EC_number=2.3.1.9
Dred_1517	TrkA domain-containing protein

Dred_1568	NUDIX hydrolase
Dred_1573	extracellular solute-binding protein
Dred_1586	secretion protein HlyD family protein
Dred_1607	CBS domain-containing protein
Dred_1634	phosphotransferase domain-containing protein
Dred_1641	ABC transporter, transmembrane region, type 1
Dred_1646	1A family penicillin-binding protein
Dred_1661	Holliday junction DNA helicase RuvA
Dred_1711	protein phosphatase 2C domain-containing protein
Dred_1723	ABC transporter-like protein
Dred_1755	exsB protein
Dred_1756	hypothetical protein
Dred_1791	Baf family transcriptional activator
Dred_1797	hypothetical protein
Dred_1814	ABC transporter-like protein
Dred_1840	metal dependent phosphohydrolase
Dred_1843	hypothetical protein
Dred_1852	DEAD/DEAH box helicase domain-containing protein
Dred_1875	hypothetical protein
Dred_1900	septum site-determining protein MinC
Dred_1959	hypothetical protein
Dred_1989	hypothetical protein
Dred_2006	putative serine protein kinase, PrkA
Dred_2027	methyl-accepting chemotaxis sensory transducer
Dred_2057	putative DNA-binding protein
Dred_2068	chromosome segregation protein SMC
Dred_2069	ribonuclease III; EC_number=3.1.26.3
Dred_2081	CoA-binding domain-containing protein
Dred_2097	putative manganese-dependent inorganic pyrophosphatase; EC_number=3.6.1.1
Dred_2148	lysine 2,3-aminomutase YodO family protein
Dred_2199	hypothetical protein
Dred_2286	ECF subfamily RNA polymerase sigma-24 factor
Dred_2299	hypothetical protein
Dred_2307	magnesium and cobalt transport protein CorA
Dred_2407	flagellar motor switch protein FliG
Dred_2419	hypothetical protein
Dred_2461	methyl-accepting chemotaxis sensory transducer
Dred_2471	signal-transduction protein
Dred_2493	16S ribosomal RNA methyltransferase RsmE
Dred_2499	heat-inducible transcription repressor HrcA
Dred_2595	hypothetical protein
Dred_2600	phi13 family phage major tail protein
Dred_2693	N-acetylmuramoyl-L-alanine amidase; EC_number=3.5.1.28
Dred_2709	precorrin-3B C17-methyltransferase
Dred_2751	UbiC transcription regulator-associated domain-containing protein
Dred_2756	TRAP dicarboxylate transporter subunit DctM
Dred_2758	UbiC transcription regulator-associated domain-containing protein
Dred_2760	methyl-accepting chemotaxis sensory transducer
Dred_2798	cell wall hydrolase SleB
Dred_2835	putative PAS/PAC sensor protein
Dred_2928	RND family efflux transporter MFP subunit
Dred_2950	acriflavin resistance protein
Dred_2956	carbon starvation protein CstA
Dred_3027	UDP-glucose 6-dehydrogenase; EC_number=1.1.1.22
Dred_3103	(3R)-hydroxymyristoyl-ACP dehydratase
Dred_3118	hypothetical protein
Dred_3138	O-antigen polymerase
Dred_3277	glycyl-radical activating family protein

Supplementary Table 5.1b

Locus Tag	Description
Dred_0025	ATPase
Dred_0081	Allergen V5/Tpx-1 family protein
Dred_0106	hypothetical protein
Dred_0109	aminoacyl-tRNA hydrolase; EC_number=3.1.1.29
Dred_0117	SpoIID/LytB domain-containing protein
Dred_0364	hypothetical protein
Dred_0513	helicase domain-containing protein
Dred_0515	type III restriction enzyme, res subunit
Dred_0560	phosphodiesterase
Dred_0561	regulatory protein ArsR
Dred_0586	redox-active disulfide protein 2
Dred_0662	FeoA family protein
Dred_0706	hypothetical protein
Dred_0778	3,4-dihydroxy-2-butanone 4-phosphate synthase
Dred_0890	XRE family transcriptional regulator
Dred_0916	XRE family transcriptional regulator
Dred_0991	ATPase domain-containing protein
Dred_1046	hypothetical protein
Dred_1103	anti-sigma-factor antagonist
Dred_1176	methyl-accepting chemotaxis sensory transducer
Dred_1192	helicase domain-containing protein
Dred_1531	ABC transporter-like protein
Dred_1596	dephospho-CoA kinase; EC_number=2.7.1.24
Dred_1628	CRISPR-associated Csm2 family protein
Dred_1631	hypothetical protein
Dred_1651	hydrogenase
Dred_1652	NADH dehydrogenase (quinone); EC_number=1.6.99.5
Dred_1663	hypothetical protein
Dred_1681	aspartate carbamoyltransferase; EC_number=2.1.3.2
Dred_1682	dihydroorotase, multifunctional complex type; EC_number=3.5.2.3
Dred_1683	carbamoyl-phosphate synthase, small subunit
Dred_1692	P-type HAD superfamily ATPase
Dred_1720	extracellular ligand-binding receptor
Dred_1724	ABC transporter-like protein
Dred_1740	metal-dependent hydrolase
Dred_1759	hypothetical protein
Dred_1860	UspA domain-containing protein
Dred_1884	DNA mismatch repair protein
Dred_1914	phosphotransferase domain-containing protein

Dred_1993	hypothetical protein
Dred_1995	sulfate transporter
Dred_2079	hypothetical protein
Dred_2164	glutamyl-tRNA reductase
Dred_2193	radical SAM domain-containing protein
Dred_2200	S-adenosylmethionine decarboxylase proenzyme; EC_number=4.1.1.50
Dred_2216	peptidase M24
Dred_2229	hypothetical protein
Dred_2267	molybdenum cofactor biosynthesis protein C
Dred_2316	hypothetical protein
Dred_2332	RNA methyltransferase
Dred_2350	imidazole glycerol phosphate synthase subunit HisF
Dred_2360	TrpR like protein, YerC/YecD
Dred_2363	phosphoribosylglycinamide formyltransferase
Dred_2384	protein-glutamate O-methyltransferase; EC_number=2.1.1.80
Dred_2389	type IV pilus assembly PilZ
Dred_2402	flagellar hook capping protein
Dred_2415	flagellar protein FliS
Dred_2416	hypothetical protein
Dred_2420	C_GCAxxG_C_C family protein
Dred_2425	AbrB family transcriptional regulator
Dred_2624	putative prophage repressor
Dred_2669	thioredoxin domain-containing protein
Dred_2685	hypothetical protein
Dred_2724	FeoA family protein
Dred_2772	FAD-binding molybdopterin dehydrogenase
Dred_2775	2Fe-2S iron-sulfur cluster binding domain-containing protein
Dred_2791	XRE family transcriptional regulator
Dred_2792	XRE family transcriptional regulator
Dred_2801	hypothetical protein
Dred_2804	glutamate synthase small subunit
Dred_2823	pyruvate/ketoisovalerate oxidoreductase subunit gamma
Dred_2886	ribosomal-protein-alanine acetyltransferase
Dred_2999	S-layer domain-containing protein
Dred_3070	carboxyl-terminal protease; EC_number=3.4.21.102
Dred_3160	MazG nucleotide pyrophosphohydrolase
Dred_3166	Sua5/YciO/YrdC/YwlC family protein
Dred_3215	hypothetical protein
Dred_3262	response regulator receiver protein
Dred_3273	ethanolamine utilization protein EutJ family protein
Dred_3287	hypothetical protein
Dred_3320	parB-like partition protein

Supplementary Table 5.1c

Locus Tag	Description	Localization (PSORTb)	Notes
Dred_0073	thiazole biosynthesis family protein	C	
Dred_0083	hypothetical protein	C	
Dred_0271	N-acetyl-gamma-glutamyl-phosphate reductase; EC_number=1.2.1.38	C	
Dred_0321	hypothetical protein	U	Outer membrane efflux protein
Dred_0402	acyl-CoA dehydrogenase domain-containing protein	C	See Figure 7, Dred_0401 also unique to Fe(III)-citrate (1 unique peptide)
Dred_0413	D-cysteine desulfhydrase; EC_number=4.4.1.15	C	
Dred_0416	regulatory protein IclR	C	
Dred_0433	CoB--CoM heterodisulfide reductase; EC_number=1.8.98.1	CM	In hdr Locus III, Dred_0432 also unique to Fe(III)-citrate (1 unique peptide)
Dred_0445	phosphatidylserine decarboxylase; EC_number=4.1.1.65	CM	
Dred_0572	putative electron transfer flavoprotein YdiQ	C	See Figure 7, Dred_0573 also unique to Fe(III)-citrate (1 unique peptide)
Dred_0577	dehydratase	C	
Dred_0598	MarR family transcriptional regulator	C	
Dred_0678	UDP-N-acetylglucosamine 1-carboxyvinyltransferase	C	
Dred_0740	lysine 2,3-aminomutase YodO family protein	C	
Dred_0852	hypothetical protein	C	
Dred_0963	glycosyl transferase family protein	CM	
Dred_1457	ADP-glucose type glycogen/starch synthase	C	
Dred_1578	cell wall hydrolase/autolysin	CW	
Dred_1730	FAD dependent oxidoreductase		Dred_1729 also unique to Fe(III)-citrate (1 unique peptide), Dred_1731 unique to both Fe(III) conditions
Dred_2378	MazG nucleotide pyrophosphohydrolase	C	
Dred_2480	cytidine deaminase	C	
Dred_2550	maf protein	C	
Dred_2977	hypothetical protein	C	

Supplementary Table 5.1d

Locus Tag	Description	Localization (PSORTb)	Notes
Dred_0034	transposase, IS111A/IS1328/IS1533	C	
Dred_0107	PRC-barrel domain-containing protein	C	
Dred_0162	aspartate 1-decarboxylase; EC_number=4.1.1.11	C	
Dred_0239	50S ribosomal protein L36	C	
Dred_0407	TRAP dicarboxylate transporter subunit DctP	U	
Dred_0669	stage V sporulation protein D; EC_number=2.4.1.129	CM	
Dred_0898	resolvase domain-containing protein	C	
Dred_1241	selenide, water dikinase; EC_number=2.7.9.3	CM	
Dred_1295	ethanolamine ammonia lyase large subunit	C	
Dred_1343	Hsp33 protein	C	
Dred_1502	FAD-binding molybdopterin dehydrogenase	C	
Dred_1503	2Fe-2S iron-sulfur cluster binding domain-containing protein	C	
Dred_1506	helix-turn-helix domain-containing protein	U	
Dred_1548	Nitrilase/cyanide hydratase and apolipoprotein N-acyltransferase	C	
Dred_1625	CRISPR-associated Cas1 family protein	C	
Dred_1670	preprotein translocase subunit SecF	CM	Protein export membrane protein, 6 internal helices
Dred_1714	protein kinase	CM	
Dred_1821	transposase Tn3 family protein	C	
Dred_1822	transposase Tn3 family protein	C	
Dred_1905	hypothetical protein	C	
Dred_1963	polysaccharide deacetylase	C	
Dred_2295	phosphate-binding protein	CM	
Dred_2301	extracellular solute-binding protein	U	ABC-type tungstate transport system, permease component, 1 internal helix
Dred_2319	DNA polymerase III DnaE; EC_number=2.7.7.7	C	
Dred_2334	nucleotidyl transferase	C	
Dred_2421	NADH:flavin oxidoreductase/NADH oxidase	C	Identified in Otwell *et al.* 2015, in vitro characterization as metal reductase
Dred_2465	NADPH-dependent FMN reductase	C	
Dred_2618	hypothetical protein	U	
Dred_2651	metal dependent phosphohydrolase	C	
Dred_2807	glutamine synthetase, type I; EC_number=6.3.1.2	C	
Dred_2844	FAD dependent oxidoreductase	C	Cluster Dred_2842-5 mentioned in text
Dred_2892	amidohydrolase	C	
Dred_2940	hydroxylamine reductase	C	
Dred_3145	regulatory protein DeoR	C	
Dred_3297	peptidase M23B	E	

Supplementary Table 5.2a: Proteins significantly increased in abundance during sulfate reduction compared to pyruvate fermentation

Supplementary Table 5.2b: Proteins significantly increased in abundance during Fe(III)-citrate reduction compared to pyruvate fermentation

Supplementary Table 5.2c: Proteins significantly increased in abundance during Fe(III)-oxide reduction compared to pyruvate fermentation

Note: Protein identification is based on detection of at least 2 unique peptides in a biological replicate and p
detection in at least 50% of replicates.

C=cytoplasmic, CM=cytoplasmic membrane, E= extracellular, CW= cell wall, U= unknown.

In Fe(III) Tables: Purple=putative oxidoreductase, Orange=porin-type protein

Supplementary Table 5.2a

Locus Tag	Description	Log2 Pyr/Sulf	p-value
Dred_2218	hypothetical protein	-4.53	<0.01
Dred_0025	ATPase	-3.43	<0.01
Dred_0014	D-3-phosphoglycerate dehydrogenase	-3.21	<0.01
Dred_2361	phosphoribosylamine--glycine ligase; EC_number=6.3.4.13	-3.19	<0.01
Dred_0013	class V aminotransferase	-3.11	<0.01
Dred_2771	adenine deaminase; EC_number=3.5.4.2	-3.05	<0.01
Dred_2364	phosphoribosylaminoimidazole synthetase; EC_number=6.3.3.1	-2.81	<0.01
Dred_3309	hypothetical protein	-2.56	<0.01
Dred_1655	NADH dehydrogenase (quinone); EC_number=1.6.99.5	-2.46	<0.01
Dred_2283	NifU domain-containing protein	-2.35	<0.01
Dred_2139	heavy metal transport/detoxification protein	-2.34	<0.01
Dred_3164	protein tyrosine phosphatase	-2.27	<0.01
Dred_2362	bifunctional phosphoribosylaminoimidazolecarboxamide formyltransferase/IMP cyclohydrolase; EC_number=2.1.2.3	-2.25	<0.01
Dred_3055	phosphotransferase system, phosphocarrier protein HPr	-2.21	<0.01
Dred_1129	deoxyribose-phosphate aldolase; EC_number=4.1.2.4	-2.19	<0.01
Dred_2153	hypothetical protein	-2.18	<0.01
Dred_2366	phosphoribosylformylglycinamidine synthase II; EC_number=6.3.5.3	-2.13	<0.01
Dred_0659	dinitrogenase iron-molybdenum cofactor biosynthesis protein	-2.10	<0.01
Dred_1164	hypothetical protein	-2.09	<0.01
Dred_2542	cell division topological specificity factor MinE	-2.06	<0.01
Dred_2998	S-layer domain-containing protein	-2.06	<0.01
Dred_0238	translation initiation factor IF-1	-2.00	<0.01
Dred_0561	regulatory protein ArsR	-1.97	<0.01
Dred_2385	CheD, stimulates methylation of MCP proteins	-1.96	<0.01
Dred_2578	hypothetical protein	-1.95	<0.01
Dred_2400	hypothetical protein	-1.94	<0.01
Dred_0694	anaerobic ribonucleoside-triphosphate reductase activating protein; EC_number=1.97.1.4	-1.90	<0.01
Dred_1325	heterodisulfide reductase subunit C	-1.88	<0.01
Dred_2769	basic membrane lipoprotein	-1.86	<0.01
Dred_2322	antibiotic biosynthesis monooxygenase	-1.83	<0.01
Dred_0991	ATPase domain-containing protein	-1.79	0.01
Dred_2145	multi-sensor hybrid histidine kinase	-1.78	0.04
Dred_2855	hypothetical protein	-1.78	<0.01
Dred_0994	hypothetical protein	-1.75	<0.01
Dred_2382	response regulator receiver protein	-1.72	<0.01
Dred_0763	BadM/Rrf2 family transcriptional regulator	-1.71	<0.01
Dred_0066	TatD family hydrolase	-1.69	<0.01
Dred_0657	cobyrinic acid a,c-diamide synthase	-1.66	<0.01
Dred_2222	cobyrinic acid a,c-diamide synthase	-1.65	<0.01
Dred_0593	thiamine-phosphate pyrophosphorylase; EC_number=2.5.1.3	-1.65	<0.01
Dred_2369	phosphoribosylaminoimidazole-succinocarboxamide synthase; EC_number=6.3.2.6	-1.64	<0.01
Dred_1759	hypothetical protein	-1.63	<0.01
Dred_2935	extracellular ligand-binding receptor	-1.63	<0.01
Dred_2764	molybdopterin binding domain-containing protein	-1.60	<0.01
Dred_1529	extracellular solute-binding protein	-1.60	0.04
Dred_1704	peptide deformylase; EC_number=3.5.1.88	-1.60	<0.01
Dred_2221	4Fe-4S ferredoxin iron-sulfur binding domain-containing protein	-1.60	<0.01
Dred_2634	appr-1-p processing domain-containing protein	-1.59	<0.01
Dred_0654	MOSC domain-containing protein	-1.56	<0.01
Dred_2228	4Fe-4S ferredoxin iron-sulfur binding domain-containing protein	-1.56	<0.01
Dred_0036	cold-shock DNA-binding domain-containing protein	-1.56	0.02
	4Fe-4S ferredoxin iron-sulfur		

Dred_2370	adenylosuccinate lyase	-1.50	<0.01
Dred_2697	hypothetical protein	-1.49	<0.01
Dred_1069	NusB antitermination factor	-1.46	<0.01
Dred_0546	redox-active disulfide protein 2	-1.45	<0.01
Dred_2316	hypothetical protein	-1.45	0.03
Dred_2553	hypothetical protein	-1.45	<0.01
Dred_2365	amidophosphoribosyltransferase	-1.43	<0.01
Dred_2439	response regulator receiver modulated CheB methylesterase; EC_number=3.1.1.61	-1.41	0.01
Dred_1802	hypothetical protein	-1.39	<0.01
Dred_2491	histidine triad (HIT) protein	-1.38	<0.01
Dred_2273	aldehyde ferredoxin oxidoreductase; EC_number=1.2.7.5	-1.38	<0.01
Dred_2482	putative metalloprotease	-1.35	<0.01
Dred_2384	protein-glutamate O-methyltransferase; EC_number=2.1.1.80	-1.33	<0.01
Dred_1273	hypothetical protein	-1.32	0.01
Dred_3255	anthranilate phosphoribosyltransferase	-1.31	<0.01
Dred_1740	metal-dependent hydrolase	-1.30	0.04
Dred_0653	NifU domain-containing protein	-1.30	<0.01
Dred_2332	RNA methyltransferase	-1.29	<0.01
Dred_2071	acyl carrier protein	-1.26	0.01
Dred_1326	hypothetical protein	-1.25	<0.01
Dred_2368	phosphoribosylformylglycinamidine synthase PurS	-1.24	<0.01
Dred_3178	response regulator receiver protein	-1.24	0.01
Dred_0764	class V aminotransferase	-1.22	<0.01
Dred_0560	phosphodiesterase	-1.22	0.03
Dred_2351	1-(5-phosphoribosyl)-5-[(5-phosphoribosylamino)methylideneamino] imidazole-4-carboxamide isomerase; EC_number=5.3.1.16	-1.22	0.01
Dred_1629	CRISPR-associated RAMP Csm3 family protein	-1.20	0.01
Dred_0236	type I methionine aminopeptidase	-1.20	<0.01
Dred_0298	hypothetical protein	-1.19	<0.01
Dred_2883	amino acid-binding ACT domain-containing protein	-1.18	<0.01
Dred_0775	Holliday junction resolvase YqgF	-1.18	0.01
Dred_3153	F0F1 ATP synthase subunit delta	-1.16	0.01
Dred_1166	homoserine kinase	-1.15	<0.01
Dred_1689	orotate phosphoribosyltransferase; EC_number=2.4.2.10	-1.14	<0.01
Dred_0459	hypothetical protein	-1.13	0.02
Dred_2151	biotin synthase; EC_number=2.8.1.6	-1.13	<0.01
Dred_3322	methyltransferase GidB	-1.12	<0.01
Dred_2460	hypothetical protein	-1.12	0.02
Dred_0203	50S ribosomal protein L11	-1.11	<0.01
Dred_2383	MCP methylation inhibitor CheC	-1.09	0.02
Dred_0638	4Fe-4S ferredoxin iron-sulfur binding domain-containing protein	-1.07	<0.01
Dred_2157	AsnC family transcriptional regulator	-1.06	<0.01
Dred_1591	peptide deformylase; EC_number=3.5.1.88	-1.06	0.01
Dred_3231	OsmC family protein	-1.06	<0.01
Dred_2271	hypothetical protein	-1.05	<0.01
Dred_1687	orotidine 5prime-phosphate decarboxylase; EC_number=4.1.1.23	-1.03	<0.01
Dred_3245	cold-shock DNA-binding domain-containing protein	-1.03	<0.01
Dred_1327	4Fe-4S ferredoxin iron-sulfur binding domain-containing protein	-1.03	<0.01
Dred_0128	hypothetical protein	-1.03	<0.01
Dred_1520	GCN5-like N-acetyltransferase	-1.02	<0.01
Dred_1742	hypothetical protein	-1.02	<0.01
Dred_0367	electron transfer flavoprotein subunit beta	-1.01	<0.01
Dred_0098	SpoVG family protein	-1.01	0.02
Dred_3321	cobyrinic acid a,c-diamide synthase	-1.00	0.01
Dred_0205	50S ribosomal protein L10	-1.00	0.02
Dred_0115	histone family protein DNA-binding protein	-1.00	0.01
Dred_3003	short-chain dehydrogenase/reductase SDR	-1.00	0.02
Dred_1344	stress responsive alpha-beta barrel domain-containing protein	-0.99	<0.01

Supplementary Table 5.2b

Locus Tag	Description	Log2 Pyr/Fecit	p-value	Localization (PSORTb)	Notes
Dred_1817	hypothetical protein	-3.18	<0.01	C	
Dred_0678	UDP-N-acetylglucosamine 1-carboxyvinyltransferase	-3.04	<0.01	C	
Dred_1919	phosphodiesterase	-2.68	<0.01	C	
Dred_2764	molybdopterin binding domain-containing protein	-2.56	<0.01	C	
Dred_1816	beta-lactamase domain-containing protein	-2.22	<0.01	C	
Dred_0443	alpha-glucan phosphorylase; EC_number=2.4.1.1	-2.15	<0.01	U	
Dred_1781	enoyl-CoA hydratase/isomerase	-2.12	<0.01	C	In hdr-loci VII
Dred_0383	PAS/PAC sensor-containing diguanylate cyclase	-2.06	<0.01	CM	
Dred_0528	XRE family transcriptional regulator	-2.06	<0.01	CM	
Dred_0522	ATPase central domain-containing protein	-2.03	<0.01	CM	
Dred_3057	excinuclease ABC subunit C	-2.03	0.01	C	
Dred_2252	helicase domain-containing protein	-1.83	<0.01	C	
Dred_2536	ribonuclease	-1.64	<0.01	C	
Dred_1186	hypothetical protein	-1.63	<0.01	C	
Dred_2400	hypothetical protein	-1.51	0.03	E	Flagellar assembly protein
Dred_3175	putative transaldolase; EC_number=2.2.1.2	-1.46	<0.01	C	
Dred_2507	hypothetical protein	-1.45	<0.01	U	
Dred_2277	iron-containing alcohol dehydrogenase	-1.40	0.02	C	
Dred_2017	TatD-related deoxyribonuclease	-1.35	<0.01	C	
Dred_0381	pyruvate kinase	-1.33	0.01	C	
Dred_0041	phosphoribulokinase/uridine kinase	-1.32	<0.01	C	
Dred_0254	tryptophan synthase subunit alpha; EC_number=4.2.1.20	-1.29	0.01	C	
Dred_1780	3-hydroxybutyryl-CoA dehydrogenase; EC_number=1.1.1.157	-1.22	<0.01	C	In hdr-loci VII
Dred_2145	multi-sensor hybrid histidine kinase	-1.21	0.01	CM	
Dred_2273	aldehyde ferredoxin oxidoreductase; EC_number=1.2.7.5	-1.20	<0.01	C	
Dred_0009	metal dependent phosphohydrolase	-1.18	0.02	C	
Dred_3222	ybaK/ebsC protein	-1.17	0.03	C	
Dred_2883	amino acid-binding ACT domain-containing protein	-1.08	<0.01	C	
Dred_0136	phosphopyruvate hydratase; EC_number=4.2.1.11	-1.03	<0.01	C	

Supplementary Table 5.2c

Locus Tag	Description	Log2 Pyr/Feox	p-value	Localization (PSORTb)	Notes
Dred_1424	hypothetical protein	-6.51	<0.01	C	
Dred_2188	GntR domain-containing protein	-4.60	<0.01	C	
Dred_1398	phosphomannomutase; EC_number=5.4.2.8	-4.60	<0.01	C	
Dred_0751	ribosome small subunit-dependent GTPase A	-4.57	<0.01	C	
Dred_0315	xanthine dehydrogenase accessory factor	-4.42	0.02	U	
Dred_2518	RNP-1-like RNA-binding protein	-3.85	<0.01	U	
Dred_3113	WecB/TagA/CpsF family glycosyl transferase; EC_number=2.4.1.187	-3.70	<0.01	U	
Dred_0001	chromosomal replication initiation protein	-3.41	<0.01	C	
Dred_1278	2-hydroxyglutaryl-CoA dehydratase, D-component	-3.31	<0.01	C	
Dred_1160	GTP-binding protein EngA	-3.31	0.03	CM	
Dred_0381	pyruvate kinase	-3.24	<0.01	C	
Dred_2001	two component sigma-54 specific Fis family transcriptional regulator	-3.22	0.01	C	
Dred_0423	hydroxylamine reductase	-3.19	<0.01	C	
Dred_2458	hypothetical protein	-2.97	<0.01	C	
Dred_2845	glycerol kinase	-2.96	<0.01	C	Cluster Dred_2842-5 mentioned in text
Dred_0528	XRE family transcriptional regulator	-2.94	<0.01	CM	
Dred_0179	ATP:guanido phosphotransferase	-2.79	0.04	C	
Dred_0865	restriction endonuclease R.SthI	-2.67	<0.01	C	
Dred_2071	acyl carrier protein	-2.49	<0.01	C	
Dred_0009	metal dependent phosphohydrolase	-2.43	<0.01	C	
Dred_0269	hypothetical protein	-2.18	<0.01	C	predicted oxidoreductase activity
Dred_2048	HSR1-like GTP-binding protein	-2.18	<0.01	C	
Dred_0007	DNA gyrase subunit A	-2.06	0.01	C	
Dred_2618	hypothetical protein	-2.01	<0.01	U	
Dred_0398	peptide chain release factor 3	-1.92	<0.01	C	
Dred_1525	nitrogen-specific signal transduction histidine kinase NtrB	-1.91	0.01	CM	
Dred_0613	YheO domain-containing protein	-1.86	0.01	C	
Dred_1325	heterodisulfide reductase subunit C	-1.82	0.02	C	
Dred_0727	extracellular solute-binding protein	-1.79	0.01	U	
Dred_0239	50S ribosomal protein L36	-1.77	<0.01	C	
Dred_0034	transposase, IS111A/IS1328/IS1533	-1.71	0.01	C	
Dred_0385	methyl-accepting chemotaxis sensory transducer	-1.65	0.03	CM	
Dred_2043	NADH dehydrogenase subunit D; EC_number=1.6.5.3	-1.64	0.01	C	Nuo subunit
Dred_2348	ATP-dependent DNA helicase PcrA	-1.59	<0.01	C	
Dred_1423	von Willebrand factor, type A	-1.57	<0.01	U	
Dred_2346	NAD-dependent DNA ligase; EC_number=6.5.1.2	-1.51	0.01	C	
Dred_3026	NAD-dependent epimerase/dehydratase	-1.44	0.01	C	
Dred_2570	SMC domain-containing protein	-1.42	<0.01	C	
Dred_1239	superoxide dismutase; EC_number=1.15.1.1	-1.39	<0.01	E	
Dred_0670	UDP-N-acetylmuramyl-tripeptide synthetase	-1.38	<0.01	C	
Dred_0098	SpoVG family protein	-1.29	0.04	C	
Dred_0612	hypothetical protein	-1.26	<0.01	U	
Dred_2488	hypothetical protein	-1.23	0.01	U	Outer membrane efflux protein, 2 internal helices
Dred_2063	S-adenosyl-L-homocysteine hydrolase; EC_number=3.3.1.1	-1.23	<0.01	C	
Dred_1908	phosphoglycerate mutase	-1.22	<0.01	C	
Dred_3002	UDP-glucose 4-epimerase	-1.16	0.01	C	
Dred_1242	SirA family protein	-1.13	0.01	C	
Dred_2273	aldehyde ferredoxin oxidoreductase; EC_number=1.2.7.5	-1.10	<0.01	C	
Dred_2473	glycyl-tRNA synthetase subunit alpha; EC_number=6.1.1.14	-1.10	<0.01	C	
Dred_3033	polysaccharide biosynthesis protein CapD	-1.09	0.02	C	
Dred_0203	50S ribosomal protein L11	-1.03	<0.01	C	
Dred_2459	hypothetical protein	-1.03	<0.01	C	
Dred_2878	putative molybdopterin biosynthesis protein MoeA/LysR substrate binding-domain-containing protein	-1.01	<0.01	C	
Dred_1130	diaminopimelate decarboxylase	-1.01	0.03	C	

Supplementary Table 5.3: Log_2 protein abundance comparisons for clusters of interest for involvement in lactate and/or pyruvate utilization.
Note: Protein identification is based on detection of at least 2 unique peptides in a biological replicate and peptide detection in at least 50% of replicates. NI=protein not identified. NA= not applicable.

Locus Tag	Description	Log2 Pyr/sulf	P-value	Log2 Pyr/fecit	P-value	Log2 Pyr/feox	P-value
Dred_0367	electron transfer flavoprotein subunit beta	-1.01	<0.01	-0.71	0.03	0.20	0.52
Dred_0368	electron transfer flavoprotein subunit alpha	-0.49	0.08	0.72	0.01	0.97	0.02
Dred_0369	FAD linked oxidase domain-containing protein	-0.47	0.03	-0.54	0.03	-0.64	<0.01
Dred_0047	pyruvate flavodoxin/ferredoxin oxidoreductase domain-containing protein	-0.06	0.76	0.54	<0.01	0.10	0.57
Dred_0048	thiamine pyrophosphate binding domain-containing protein	0.54	0.07	1.77	<0.01	1.51	0.03
Dred_0049	pyruvate ferredoxin/flavodoxin oxidoreductase	-0.06	0.79	-0.19	0.40	1.96	<0.01
Dred_2750	formate C-acetyltransferase; EC_number=2.3.1.54	1.64	<0.01	2.70	<0.01	-0.11	0.59
Dred_2751	UbiC transcription regulator-associated domain-containing protein	Pyruvate only	NA	NI	NA	NI	NA
Dred_2752	glycyl-radical activating family protein	0.98	0.12	NI	NA	2.41	<0.01
Dred_2753	formate C-acetyltransferase	NI	NA	NI	NA	NI	NA
Dred_1893	pyruvate dehydrogenase (pseudogene)	NI	NA	NI	NA	NI	NA

Supplementary Table 5.4: Log_2 protein abundance comparisons for the six hydrogenases annotated in the genome of *D. reducens.*

Note: Protein identification is based on detection of at least 2 unique peptides in a biological replicate and peptide detection in at least 50% of replicates.

NI=protein not identified. NA= not applicable.
C=cytoplasmic, CM=cytoplasmic membrane, E= extracellular, CW= cell wall, U= unknown (Junier et al., 2010).

Locus tag	Protein name	Log 2 Pyr/Sulf	P-value	Log2 Pyr/Fe(III)-citrate	P-value	Log2 Pyr/Fe(III)-oxide	P-value	PSORTb localization	Notes
Dred_1440	hydrogenase large subunit	NI	NA	NI	NA	NI	NA	C	
Dred_1794	hydrogenase large subunit	3.02	<0.01	3.05	<0.01	2.45	<0.01	C	Likely involved in pyruvate-ferredoxin oxidoreductase pathway
Dred_0461	putative hydrogenase cytochrome b subunit	NI	NA	NI	NA	NI	NA	CM	
Dred_0462	4Fe-4S ferredoxin iron-sulfur binding domain-containing protein	-0.84	0.02	NI	NA	0.40	0.22	CM	
Dred_0463	hydrogenases, Fe-only	-0.75	0.01	3.68	<0.01	1.44	<0.01	C	
Dred_1651	hydrogenases, Fe-only	sulfate only	NA	NI	NA	NI	NA	C	
Dred_1652	NADH dehydrogenase (quinone)	sulfate only	NA	NI	NA	NI	NA	C	Similarity to NuoEFG subunits
Dred_1653	NADH dehydrogenase (ubiquinone), 24 kDa subunit	NI	NA	NI	NA	NI	NA	C	
Dred_1654	hydrogenases, Fe-only	-0.30	0.20	1.39	<0.01	2.40	<0.01	C	
Dred_1655	NADH dehydrogenase (quinone)	-2.46	<0.01	-0.41	0.34	-0.14	0.74	C	Similarity to NuoEFG subunits
Dred_1656	NADH dehydrogenase (ubiquinone), 24 kDa subunit	-0.77	0.09	0.92	0.01	NI	NA	C	
Dred_3290	hydrogenases, Fe-only	NI	NA	NI	NA	NI	NA	C	
Dred_3291	NADH dehydrogenase (quinone)	NI	NA	NI	NA	NI	NA	C	
Dred_3292	NADH dehydrogenase (ubiquinone), 24 kDa subunit	NI	NA	NI	NA	NI	NA	C	

Supplementary Table 5.5: Log_2 protein abundance comparisons for putative respiration-related proteins in *D. reducens.*

Note: Protein identification is based on detection of at least 2 unique peptides in a biological replicate and peptide detection in at least 50% of replicates.

NI=protein not identified. NA= not applicable.

Locus tag	Protein name	Log 2 Pyr/Sulf	P-value	Log2 Pyr/Fe(III)-citrate	P-value	Log2 Pyr/Fe(III)-oxide	P-value
Dred_2036	NuoN	NI	NA	NI	NA	NI	NA
Dred_2037	NuoM	NI	NA	NI	NA	NI	NA
Dred_2038	NuoL	NI	NA	NI	NA	NI	NA
Dred_2039	NuoK	NI	NA	NI	NA	NI	NA
Dred_2040	NuoJ	NI	NA	NI	NA	NI	NA
Dred_2041	NuoI	0.84	0.26	NI	NA	NI	NA
Dred_2042	NuoH	NI	NA	NI	NA	NI	NA
Dred_2043	NuoD	-0.07	0.80	NI	NA	-1.64	0.01
Dred_2044	NuoC	1.46	<0.01	NI	NA	NI	NA
Dred_2045	NuoB	-0.07	0.82	NI	NA	NI	NA
Dred_2046	NuoA	NI	NA	NI	NA	NA	NA
Dred_3149	subunit epsilon	-0.30	0.22	2.82	<0.01	1.78	<0.01
Dred_3150	subunit beta	-0.38	0.05	1.15	<0.01	0.21	0.24
Dred_3151	subunit gamma	-0.20	0.52	1.82	<0.01	-0.40	0.16
Dred_3152	subunit alpha	-0.37	0.10	1.03	<0.01	0.25	0.21
Dred_3153	subunit delta	-1.16	0.01	NI	NA	1.26	0.03
Dred_3154	subunit b	-0.27	0.38	5.11	<0.01	0.17	0.70
Dred_3155	subunit c	NI	NA	NI	NA	NI	NA
Dred_3156	subunit a	NI	NA	NI	NA	NI	NA

Supplementary Table 5.6: Log_2 protein abundance comparisons for two additional clusters of proteins that are significantly increased during sulfate reduction relative to all other conditions.

Note: Protein identification is based on detection of at least 2 unique peptides in a biological replicate and peptide detection in at least 50% of replicates.

NI=protein not identified. NA= not applicable.

The first cluster (Dred_2361-70) is predicted to be involved in purine metabolism.

The second cluster contains chemotaxis-related proteins, suggesting that chemotaxis is turned on in *D. reducens* especially during sulfate reduction.

Locus Tag	Description	Log2 Sulf/pyr	P-value	Log2 Sulf/fecit	P-value	Log2 Sulf/feox	P-value
Dred_2361	phosphoribosylamine--glycine ligase bifunctional	3.19	<0.01	3.25	<0.01	3.72	0.07
Dred_2362	phosphoribosylaminoimidazolecarboxamide formyltransferase/IMP cyclohydrolase	2.25	<0.01	1.68	<0.01	1.67	0.01
Dred_2363	phosphoribosylglycinamide formyltransferase	sulfate only	NA	NI	NA	NI	NA
Dred_2364	phosphoribosylaminoimidazole synthetase	2.81	<0.01	NI	NA	NI	NA
Dred_2365	amidophosphoribosyltransferase	1.43	<0.01	NI	NA	NI	NA
Dred_2366	phosphoribosylformylglycinamidine synthase II	2.13	<0.01	NI	NA	0.60	0.17
Dred_2367	phosphoribosylformylglycinamidine synthase I	0.78	0.04	NI	NA	NI	NA
Dred_2368	phosphoribosylformylglycinamidine synthase PurS	1.24	<0.01	NI	NA	NI	NA
Dred_2369	phosphoribosylaminoimidazole-succinocarboxamide synthase	1.64	<0.01	NI	NA	NI	NA
Dred_2370	adenylosuccinate lyase	1.50	<0.01	2.56	<0.01	1.21	0.09
Dred_1176	methyl-accepting chemotaxis sensory transducer	sulfate only	NA	NI	NA	NI	NA
Dred_2382	response regulator receiver protein	1.72	<0.01	NI	NA	NI	NA
Dred_2383	MCP methylation inhibitor CheC	1.09	0.02	1.47	<0.01	1.15	<0.01
Dred_2384	protein-glutamate O-methyltransferase; EC_number=2.1.1.80	1.33	<0.01	NI	NA	NI	NA
Dred_2385	CheD, stimulates methylation of MCP proteins	1.96	<0.01	NI	NA	NI	NA
Dred_2439	response regulator receiver modulated CheB methylesterase; EC_number=3.1.1.61	1.41	0.01	0.66	0.06	NI	NA
Dred_2441	putative CheW protein	0.79	<0.01	1.92	<0.01	2.26	<0.01

Chapter 6

Proteomic analysis of an Fe(III)-reducing co-culture established between *Desulfotomaculum reducens* MI-1 and *Geobacter sulfurreducens* PCA

Summary:

Fe(III)-reducing co-cultures were established between the Gram-positive sulfate-reducing, metal-reducing and fermentative bacterium *Desulfotomaculum reducens* MI-1 and the Gram-negative model metal-reducing bacterium *Geobacter sulfurreducens* PCA. Co-cultures were fed pyruvate, a fermentable substrate for *D. reducens* which is also used as an electron donor for Fe(III) reduction. *G. sulfurreducens* does not utilize pyruvate but can use products of pyruvate fermentation (acetate and H_2) as electron donors for Fe(III) reduction. Both organisms in the co-culture appear to contribute to Fe(III) reduction, and enhanced rates of Fe(III) reduction were observed relative to pure culture cultivation with both soluble and insoluble Fe(III). Global comparative proteomic analysis was performed on soluble Fe(III)-citrate-reducing cultures in order to gain insight into changes associated with co-culture versus pure culture growth. Proteins previously associated with Fe(III) reduction in *G. sulfurreducens,* including c-type cytochromes and type IV pili-related proteins, showed a significant increase in abundance during co-culture growth compared with pure culture growth. *D. reducens* ribosomal proteins were significantly more abundant during co-culture growth, likely a reflection of faster growth rates during cultivation with *G. sulfurreducens*. At the same time, widespread decreases in *D. reducens* central metabolism-related proteins were observed in the co-culture. In addition to shotgun proteomic methods, we developed quantitative targeted assays (Multiple Reaction Monitoring – MRM) for enzyme-specific peptides, including metal reductases. The assays were validated in the co-culture and comparisons of protein abundances from the MRM and shotgun methods show strong positive correlations.

Introduction

Microorganisms capable of metal reduction are major drivers of nutrient cycling in anaerobic environments (Bird et al., 2011; Hori et al., 2015; Lovley, 1993). These organisms are also of interest for application in heavy metal and radionuclide remediation as well as microbial fuel cell development (Lovley, 2012; Lovley et al., 2011; Newsome et al., 2014; Wall and Krumholz, 2006). Studies on *Geobacter* species have been instrumental in developing an understanding of microbial metal reduction, from the initial discovery of this type of metabolism to elucidation of proteins involved in extracellular electron transfer (Leang et al., 2003; Lovley and Phillips, 1988; Reguera et al., 2005; Santos et al., 2015). One feature of *Geobacter* genomes, which is shared with other characterized Gram-negative metal-reducing bacteria, is a high number of predicted multiheme c-type cytochromes (MHCs) (Sharma et al., 2010a; Shi et al., 2007). *Geobacter sulfurreducens* PCA serves as model organism for the genus, and a number of MHCs have been identified and characterized for their role in Fe(III) reduction (Coppi et al., 2001; Leang et al., 2003; Lloyd et al., 2003; Qian et al., 2011). Additionally, the type IV pili of *G. sulfurreducens* has been shown to be involved in extracellular electron transfer, serving as biological 'nanowires' (Cologgi et al., 2011; Reguera et al., 2005; Vargas et al., 2013).

Along with *Geobacter* species, a diversity of microorganisms are capable of reducing metals (Barton et al., 2015; Petrie et al., 2003; Weber et al., 2006; Williamson et al., 2013). In addition to Proteobacteria like *Shewanella* species and *Anaeromyxobacter dehalogenans*, multiple Firmicutes have been shown to reduce metals and radionuclides including Fe(III), Mn(IV), Cr(VI), and U(VI) (Kim et al., 2012; Suzuki et al., 2004; Tebo and Obraztsova, 1998; Wrighton et al., 2011). However, proteins involved in metal reduction by Gram-positive bacteria are poorly characterized. Some species, such as *Thermincola potens*, encode an abundance of predicted MHCs, and there is evidence that these MHCs are involved in the reduction of Fe(III)

(Carlson et al., 2012). However, the presence of multiple MHCs is uncommon in the genomes of sequenced Gram-positive bacteria (Sharma et al., 2010b). *Desulfotomaculum reducens* MI-1 is a gram-positive bacterium that is capable of both dissimilatory sulfate and metal reduction (Tebo and Obraztsova, 1998). This Firmicute has only one annotated MHC, while another Fe(III)-reducing organism in the genus (*Desulfotomaculum hydrothermale*) reportedly has none (Amin et al., 2013; Junier et al., 2010). Multiple studies have focused on metabolic processes in *D. reducens*, including Fe(III) reduction (Dalla Vecchia et al., 2014a, 2014b; Otwell et al., 2015). While pathways of electron transfer to Fe(III) in *D. reducens* are only partly elucidated, there is evidence that the organism utilizes a soluble electron shuttle (likely riboflavin) to reduce insoluble Fe(III) when cultivated with pyruvate, a fermentable substrate (Dalla Vecchia et al., 2014b). While grown with the non-fermentable electron donor lactate, however, direct contact with Fe(III) oxide particles is required for reduction (Dalla Vecchia et al., 2014a). Furthermore, comparative proteomic analysis of *D. reducens* cultivated on four different conditions, including soluble and insoluble Fe(III), was recently performed (Otwell et al., 2016). From this study, there is evidence that the MHC is involved in insoluble Fe(III)-oxide reduction (but not soluble Fe(III)-citrate reduction) when lactate is the electron donor.

In environmental settings, Fe(III) reduction is inevitably carried out by multiple populations of microorganisms, but nearly all studies focusing on pathways of microbial metal reduction have been performed in pure culture. Methods available for analyzing microbial consortia are expanding and understanding of microbial communities is rapidly growing. Multiple studies have cultivated *Geobacter* in co-culture with various other species (Kaden et al., 2002; Kato et al., 2012; Rotaru et al., 2012, 2014a, 2014b; Shrestha et al., 2013a; Smith et al., 2015; Summers et al., 2010). A range of mechanisms for interspecies electron transfer (IET) has

been documented in these studies, including through a soluble electron shuttle (Kaden et al., 2002; Smith et al., 2015), through metabolic end-products such as hydrogen or formate (Rotaru et al., 2012), and through conductive minerals (Kato et al., 2012). Furthermore, direct interspecies electron transfer (DIET) has been identified in several studies, with *Geobacter metallireducens* donating electrons to either *G. sulfurreducens* or to a methanogen (Rotaru et al., 2014a, 2014b; Shrestha et al., 2013a; Summers et al., 2010). The type IV pili have been shown to be essential for DIET. Knocking out the gene for the structural pilin subunit PilA from *G. metallireducens* (in co-culture as the electron-donating organism) or *G. sulfurreducens* (in co-culture as the electron-accepting organism) prevented co-culture growth (Rotaru et al., 2014a, 2014b; Summers et al., 2010). MHCs also have been shown to be important, namely OmcS, the MHC localized to the pili of *Geobacter* (Leang et al., 2010; Shrestha et al., 2013b; Summers et al., 2010). None of these studies, however, have been performed on Fe(III)-reducing cultures.

In this study, we created Fe(III)-reducing co-cultures consisting of phylogenetically distinct Fe(III)-reducing bacteria that are sequenced representatives of environmentally abundant genera, specifically *D. reducens* and *G. sulfurreducens*. These and related genera have been found to co-occur at metal reduction sites of interest, such as U(VI) bioremediation study sites in Oak Ridge, TN and Rifle, CO (Cardenas et al., 2010; Chandler et al., 2006; Zhang et al., 2015). Co-cultures were fed pyruvate, and *G. sulfurreducens,* which does not utilize pyruvate, must rely upon *D. reducens* for production of electron donor (i.e. acetate, H_2). This is reminiscent of trophic interactions likely occurring in the environment, where fermenters and incomplete oxidizers provide fermentation acids (most importantly acetate) as well as H_2 for use by Fe(III)-reducers like *Geobacter* (Lovley et al., 2004). Following phenotypic analysis of *D*. reducens-G. *sulfurreducens* co-cultures, comparative proteomic analyses were performed in order to gain

further biological insight into the consortium. We also implemented targeted quantification of biomarker peptides using assays created for *D. reducens* and *G. sulfurreducens*. This work provides the first proteomic-based analysis of an Fe(III)-reducing co-culture and gives insight into these populations' responses to growth in mixed culture.

Materials and Methods

Cultivation conditions

Desulfotomaculum reducens MI-1 was purchased from the ATCC (American Type Culture Collection) and *Geobacter sulfurreducens* PCA was purchased from the DSMZ (Deutsche Sammlung von Mikroorganismen und Zellkulturen). In order to establish a co-culture with these organisms, a modified Widdel-based medium was created consisting per liter of 0.3g KH_2PO_4, 0.5g NH_4Cl, 1g NaCl, 0.4g $MgCl_2x6H_2O$, 0.1g $CaCl_2x2H_2O$, 0.1g KCl, 2.5g $NaHCO_3$, and trace metals (Klemps et al., 1985). 30 mM Fe(III)-citrate or 50 mM Fe(III)-oxide was added as electron acceptor. Media was bubbled with 80/20 N_2/CO_2. Vitamins were added following autoclaving along with either 20 mM pyruvate or acetate as electron donor. Experiments were performed in 160 mL serum bottles (100mL culture with 60 mL headspace) or the same culture volume to headspace ratio in 1 L bottles (the larger culture volumes were used for preparation of cells for proteomic analyses). Since *G. sulfurreducens* is capable of faster rates of Fe(III) reduction than *D. reducens*, in order to create conditions where both bacteria contribute to Fe(III)-reduction, we developed a co-culture system where *G. sulfurreducens* relies on *D. reducens* for production of electron donor. Lactate was considered as a non-fermentable substrate, but lactate oxidation by *G. sulfurreducens* has been demonstrated (Call and Logan, 2011). Butyrate was also considered as a reported electron donor for *D. reducens*, but we failed to produce growth rates and Fe(III) reduction rates comparable to those observed with lactate or

pyruvate as electron donor (Dalla Vecchia et al., 2014b; Otwell et al., 2016; Tebo and Obraztsova, 1998). Therefore, pyruvate was selected as a substrate shown to support fermentative growth as well as Fe(III) reduction by *D. reducens* (with acetate, CO_2 and H_2 as products during fermentation) that is not utilized by *G. sulfurreducens* (Dalla Vecchia et al., 2014b). In previous studies published on *D. reducens*, 0.5 g/L of yeast extract has been added due to the reported fastidious nature of the organism (Junier et al., 2010). As yeast extract can serve as an undefined electron source, studies were done in order to minimize the concentration of yeast extract added to the cultures. Addition of $1/10^{th}$ of the regular amount of yeast extract (0.05 g/L) did not significantly impact Fe(III) reduction rates or growth by *D. reducens*, and so this concentration was used for all studies **(Supplementary Figure 6.1)**. Minimal growth and Fe(III) reduction by *G. sulfurreducens* on these conditions (Fe(III), pyruvate, and 0.05 g/L yeast extract) was confirmed **(Supplementary Figure 1)**. *D. reducens* pure cultures were cultivated on the same Fe(III)-reducing culture conditions as the co-culture (20 mM pyruvate, 0.05 g/L yeast extract), while *G. sulfurreducens* pure cultures contained 20 mM acetate, 7.5 mmol/L hydrogen gas, and 0.05 g/L yeast extract. Duplicate cultures were harvested at two timepoints for the co-cultures and *D. reducens* pure cultures (details below), including a mid-late exponential phase timepoint. *G. sulfurreducens* duplicates were harvested at mid-late exponential phase. Pellets were stored at -80°C until proteins were extracted for proteomic analysis.

Analytical techniques

Cultures were monitored by cell counts (acridine orange was used for staining) and the ferrozine assay to measure accumulation of Fe(II) (Lovley and Phillips, 1987). Hydrogen was quantified using a gas chromatography (GC) instrument equipped with a thermal conductivity detector (TCD) as previously described (Rowe et al., 2012; Smatlak et al., 1996). For

quantification of pyruvate and acetate, a high-performance liquid chromatography (HPLC) system (Waters 600E system controller, Waters 717 Plus autosampler, Waters 410 refractive index detector (Waters Corp, Milford, MA, USA)) was employed. An Aminex HPX-87H (300mm x 7.8mm) (Bio-Rad) column was used with the following running conditions: column temperature: 60° C, flow rate: 0.6mL/min, mobile phase: 5 mM H_2SO_4 (diluted with milliQ H_2O from high purity 99.999% H_2SO_4 (Sigma-Adrich). Data was analyzed with a PeakSimple Chromatography Data System SRI Model 302 and PeakSimple software v4.44 (Schemback, Germany). Phase analysis of the microbially-formed precipitate was performed using powder X-ray diffraction using a Scintag XDS2000 diffractometer (ThermoARL, USA) with a CuKα radiation operating at 40kV and 40mA with a scan rate of 3 degrees/minute. The powder x-ray diffraction was performed on a wet slurry of the precipitate, spread onto a zero-background quartz sample holder.

Shotgun proteomic data generation

Proteins were extracted from harvested cells and digested according to previously established protocols (Otwell et al., 2016). From each digest, 100 μg of peptides from biological replicates were pooled then separated using C18 reverse phase high pH fractionation according to previously published protocols (Wang et al., 2011 reversed phase). Ninety-six fractions were collected from each pooled sample, dried overnight in a SpeedVac, and suspended in 100 ml of 50% methanol. Fractions were combined resulting in 12 fractions for the co-culture, 12 fractions for *D. reducens*, and 12 fractions for *G. sulfurreducens*. The combined fractions were concentrated to dryness then suspended in nanopure water to achieve a final concentration of 0.1 mg/ml. Additionally, peptides from the unfractionated samples were transferred to MicroSolv ALS vials and diluted with nanopure water to a final concentration of 0.1 μg/μL.

Mass spectra for fractionated and unfractionated peptide samples were generated using an Agilent LC system (Agilent Technologies, Santa Clara, CA) coupled to a hybrid ion trap Orbitrap Velos mass spectrometer (Thermo Scientific, San Jose, CA) equipped with an ion funnel and electrospray ionization (ESI) interface. Seven mg from each peptide sample (36 peptide fractionated samples and 30 unfractionated samples) was injected to the instrument. All peptide samples were randomized and blocked prior measurements made by the mass spectrometer. Conditions for peptide separation and HPLC operating conditions have been previously published (Robidart et al., 2013; Sowell et al., 2008). Orbitrap spectra were collected from 400 to 2,000 m/z at a resolution of 100k followed by data-dependent ion trap tandem mass (MS/MS) spectra generation of the six most abundant ions using 35% collision energy (CID). Additional mass spectrometer operating conditions have been previously described (Robidart et al., 2013; Sowell et al., 2008).

Peptide sequences were assigned to tandem mass spectra using the MSGF search algorithm (Kim et al., 2008 spectral probabilities) and the translated *Desulfotomaculum reducens* MI-1 and *Geobacter sulfurreducens* PCA RefSeq annotated genome sequences downloaded from the U.S. Department of Energy's Joint Genome Institute's (JGI) IMG (Markowitz et al., 2014 img 4 version) and the National Institutes of Health (NCBI) National Center for Biotechnology Information (https://www.ncbi.nlm.nih.gov/), respectively. From measured peptides, an empirical peptide database was generated for use as a library to match high-resolution parent ion spectra (i.e. AMT tag approach, (Lipton et al., 2002) generated by the Orbitrap Velos instrument from the unfractionated samples. These unfractionated peptide samples were used to obtain label-free abundance measurements for use in relative quantification comparisons. The area under each peptide peak, constructed from ion intensities (ion current) measured across

instrument scans, was used to represent the arbitrary abundances of peptides (Lipton et al., 2002; Sowell et al., 2008). The dataset of peptides along with their label free abundances were filtered to achieve a false discovery rate of ≤ 5% according to established protocols (Stanley et al., 2011). Abundances of peptides were $\log_2$ transformed, and those abundances associated for each organism within the co-culture were separated and normalized to a common central tendency (mean) (Callister et al., 2006) to account for systematic differences in biomass when comparing each co-culture organism to their pure culture growth condition (**Supplementary Figure 6.2**). Protein abundances were estimated by taking the mean of peptides identifying a given protein and only unique peptides (peptides identifying a single protein) were used unless noted. A protein was considered present within a growth condition if identified by 2 or more unique peptides. Logarithmic transformation and normalization were carried out using the InfernoRDN (previously known as DAnTE, (Polpitiya et al., 2008)) proteomics analysis software tool.

Multiple reaction monitoring (MRM) mass spectrometry for targeted quantitation of peptide biomarkers

I. Selection of proteotypic peptides

Known metal reductases were identified based on literature in order to select biomarkers for which to design synthetic isotopically-labeled peptides. Peptides were mainly selected from peptides previously detected in shotgun proteomic data generated by our group on cultures of *D. reducens* and *G. sulfurreducens*. Established selection criteria for biomarker peptide sequences were followed, including length ranges, correct tryptic cleave site, and avoidance of problematic peptides (for instance peptides containing methionine residues that easily undergo oxidation during processing were typically excluded) (Lange et al., 2008). Grade 3 (maximum assurance) isotopically-labeled synthetic peptides were ordered from Pierce (Thermo Fischer Scientific).

II. Assay development using stable isotope-labeled synthetic peptides

The stable isotope-labeled synthetic peptides were diluted to 25 ng/ml (assuming 50% of manufacturer's stated yield) with 20% methanol/0.2% glacial acetic acid in Milli-Q water and infused at 5-10 ml/min into a AB/Sciex 4000 Q Trap mass spectrometer fitted with the TurboIonspray source. All MS and MS/MS spectra were acquired in positive ion mode. Product ion (CID) MS/MS ions were selected for each peptide by comparison of acquired spectra with theoretical, *in silico*, fragment ions obtained by use of the online UCSF Protein Prospector MS-Product module. Three of the most intense y-product and/or b-product ions were chosen, when possible, for each peptide with Q3 m/z values larger than the parent ion m/z (Q1). Relevant instrument MRM parameters for each Q1/Q3 transition ion pair were optimized using parameter ramping following the instrument manufacturer's recommended protocol. In cases where a peptide was detectable in multiple charge states, the charge state m/z yielding the best combination of parent ion intensity and product ion selection were used for generation of the MRM acquisition table. Further validation and optimization was done by pooling 1-5ml of each 25 ng/ml peptide dilution (which was dried in a Speed-Vap and reconstituted in 0.1% formic acid). The reconstituted synthetic peptide pool was analyzed by tandem MRM-triggered IDA analysis on the 4000 Q Trap fitted with a Microionspray II (nanospray) source. Prior to MRM analysis of samples, a mixture of synthetic peptides was spiked into samples as internal standards. The final internal standard peptide pool was made by diluting the synthetic peptides so that the intensity of the highest transition ion pair peak fell within an order of magnitude of 2e4 counts. Four of the synthetic peptides were found to be of low quality and were deemed unsuitable for use as internal standards. The unlabeled, native peptides they corresponded to were assigned a single transition ion pair from the nearest neighboring (based on HPLC elution time) synthetic peptide for internal standard purposes.

III. Validation of unlabeled, native peptide MRM transition pairs

Transition ion pairs (Q1 m/z and Q3 y-ion m/z) for MRM detection of native peptides from cell culture trypsin digests were obtained by compensating for the increase in molecular weight due to stable isotopes in the corresponding synthetic peptide. For validation of the *D. reducens* culture-specific peptides, equal amounts of the *D. reducens* cell culture digests were pooled, dried and reconstituted in 0.1% formic acid. The equivalent of 1 mg (based on the concentration of each trypsin-digested peptide pool) was injected for tandem MRM-triggered IDA analysis on the 4000 Q Trap system fitted with the Microionspray source using the highest intensity transition ion pair for each peptide as the trigger for IDA (MS/MS) acquisition. The *G. sulfurreducens* culture-specific peptide transitions were validated in a similar fashion using a pool of the *G. sulfurreducens* cell culture digests. Final validation of all native, unlabeled peptide MRM transitions was done in the same way by pooling equal amounts of co-culture cell culture digests, drying, reconstitution and injection of the equivalent of 1 mg for tandem MRM-triggered IDA analysis as before. Retention times for each peptide and any false positives were obtained by manual inspection of acquired CID (MS/MS) spectra.

IV. Final MRM assays

10 ml of each cell culture digest, equivalent to 18mg, was dried and reconstituted in 90ml of the heavy, synthetic peptide internal standard pool. 5ml, equivalent to 1 mg, was injected for MRM data acquisition. A 60 minute gradient was used following 10 minute trapping and a single MRM method was used for all transitions (25ms dwell time for each transition pair and 3.24sec cycle time). The raw MRM data was acquired using Analyst version 1.6.1 (AB/Sciex) and processed using MultiQuant version 2.1.1 (AB/Sciex).

Results

I. Phenotypic characterization of *D. reducens*-G. *sulfurreducens* co-cultures

In this study, we established pyruvate-fed Fe(III)-reducing co-cultures between *D. reducens* and *G. sulfurreducens*. In this scheme, *G. sulfurreducens* relies upon *D. reducens* for production of electron donor, and both organisms are capable of reducing Fe(III) (**Figure 6.1)**. The co-culture displayed enhanced rates of Fe(III)-reduction compared with pure culture controls. This phenotype was observed in studies performed on both soluble Fe(III)-citrate as well as insoluble Fe(III)-oxide (**Figure 6.2)**.

Figure 6.1: An Fe(III)-reducing co-culture was established between *Desulfotomaculum reducens* MI-1 and *Geobacter sulfurreducens* PCA. Pyruvate was fed as electron donor, which is only used by *D. reducens*. Acetate and H_2 are produced during pyruvate fermentation by *D. reducens*, and pyruvate is also used as an electron donor for Fe(III) reduction. *G. sulfurreducens* can utilize products of pyruvate fermentation (acetate, H_2) as electron donors, and t$_h$erefore must rely on *D. reducens* in order to grow and reduce Fe(III) in the co-culture.

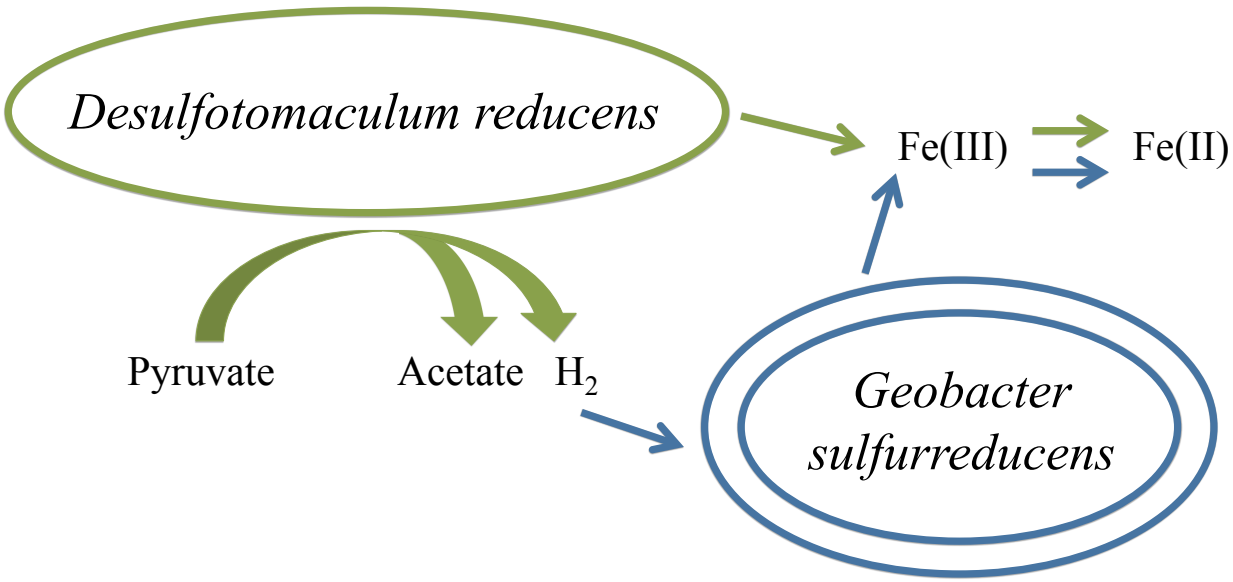

Figure 6.2a: The *G. sulfurreducens-D. reducens* co-culture displays enhanced rates of soluble Fe(III)-citrate compared with either organism in pure culture. Cultures were inoculated with 20 mM Fe(III)-citrate. **2b: The *G. sulfurreducens-D. reducens* co-culture displays enhanced rates of insoluble Fe(III)-oxide compared with either organism in pure culture.** Cultures were inoculated with 50 mM Fe(III)-oxide. By the final co-culture timepoint, a thick biofilm had formed that could not be disturbed with heavy shaking, which accounts for variable Fe(II) concentrations.

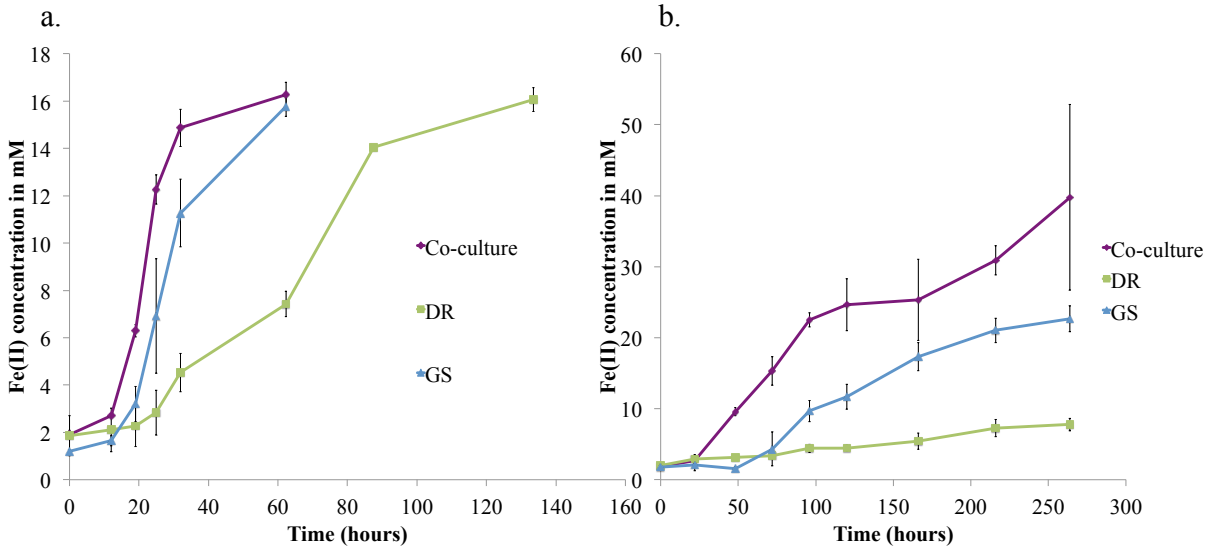

The use of a substrate (pyruvate) as electron donor that is fermentable by *D. reducens* calls into question whether *D. reducens* is actually reducing Fe(III) in the co-culture or simply fermenting. Evidence suggests that *D. reducens* is contributing to Fe(III) reduction, as a distinct black precipitate is formed during co-culture growth that is also formed during *D. reducens* pure culture growth. This precipitate is not formed during Fe(III)-citrate reduction by *G. sulfurreducens* in pure culture (**Figure 6.3a).** The precipitate forms when ~50% of the Fe(III)-citrate has been reduced in both the co-culture and *D. reducens* pure culture. Microscopy clearly showed that *G. sulfurreducens* cells localize with the *D. reducens*-formed precipitate (**Figure 6.3b).** Co-localization of both *G. sulfurreducens* and *D. reducens* on the precipitate is observed later in the growth curve (reduction of >75% of Fe(III)-citrate) **(Figure 6.3c)**. Powder X-ray

diffraction (pXRD) was used to analyze the crystalline phase of the precipitate, which indicated the formation of vivianite, an Fe(II)-phosphate-hydrate with the formula $Fe_3(PO_4)_2*8H_2O$ **(Supplementary Figure 6.3)**. As *D. reducens* produces the Fe(II)-precipitate in pure culture while reducing Fe(III), and the precipitate is also formed during co-culture growth, the most likely conclusion is that *D. reducens* is contributing to Fe(III) reduction in the co-culture. One final phenotype worth noting occurs during Fe(III)-oxide reduction. In *D. reducens*-*G. sulfurreducens* co-cultures, enhanced biofilm formation is observed compared to pure culture growth **(Supplementary Figure 6.4)**. A biofilm begins to form on the bottle (inverted during growth) of co-cultures within 1-2 days, which grows thick throughout the incubation period. *G. sulfurreducens* pure cultures eventually form a biofilm, but much later in the growth phase as determined by concentration of Fe(III) reduced. Biofilm formation is not observed in *D. reducens* pure cultures.

Figure 6.3: A dark-colored precipitate is formed during Fe(III) reduction in the co-culture that phenotypically resembles a precipitate formed in the *D. reducens* pure culture. In **a,** fully reduced 30 mM Fe(III)-citrate cultures are pictured. The *G. sulfurreducens* pure culture does not form the precipitate, while *D. reducens* and the co-culture does. **b.** Formation of the precipitate is observed when ~50% of the Fe(III)-citrate has been reduced, and *G. sulfurreducens* cells localize with the precipitate. This image was taken at the 60-hour timepoint in the co-culture harvested for proteomic analysis. Acridine orange stain, 1000X magnification. **c.** Later in the growth phase (>75% of the Fe(III)-citrate has been reduced), *G. sulfurreducens* and *D. reducens* cells (longer cells) co-localize with the precipitate. This image was captured at the 72-hour timepoint in the co-culture harvested for proteomic analysis. Acridine orange stain, 1000X magnification.

a.

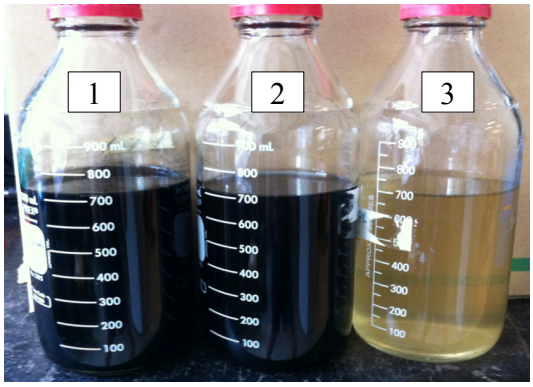

1) Co-culture, 2) ***Desulfotomaculum reducens*** **pure,**
3) *Geobacter sulfurreducens* pure

b.

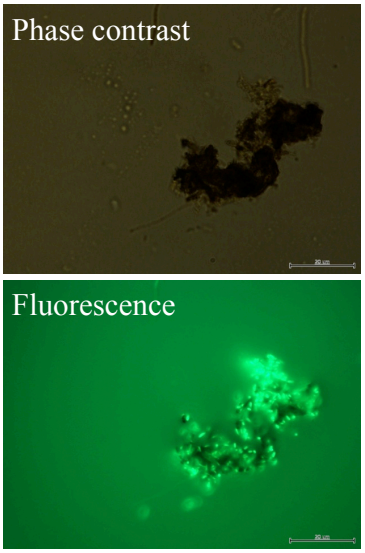

c.

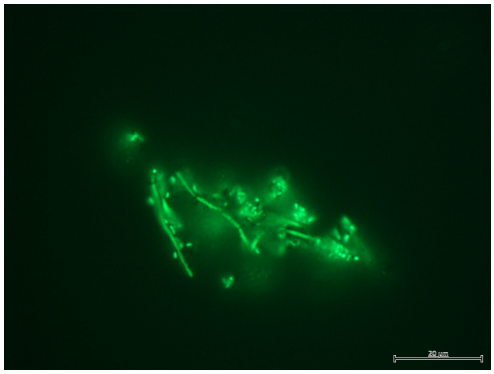

Concentrations of pyruvate, acetate, and hydrogen were also monitored in Fe(III)-citrate-reducing co-cultures. Increased rates of pyruvate oxidation by *D. reducens* were observed in co-cultures compared to pure culture controls and both *D. reducens* and *G. sulfurreducens* grow faster in co-culture (**Figure 6.4**). The faster pyruvate-degradation rates were observed from the beginning of growth, before discernible levels of acetate or hydrogen have accumulated in the *D. reducens* pure culture. For instance, after 48-hours of cultivation, the pyruvate concentration is ~19.5 mM in the co-culture compared with ~24.1 in the *D. reducens* pure culture. At the same time, acetate and hydrogen concentrations are below detection in the co-culture and *D. reducens* pure culture **(Figure 6.4).** This suggests that the enhanced pyruvate oxidation phenotype observed during co-culture growth is not simply a result of inhibitory waste products (acetate and

hydrogen) building up in the pure culture. It is notable that in both *D. reducens* pure cultures and co-cultures, hydrogen levels do not start to accumulate until a large proportion of the Fe(III) has been reduced (when nearly no Fe(III) is left in the co-culture and when >50% of the Fe(III) has been reduced in the *D. reducens* pure culture, **Figure 6.4**). This suggests that while growing in pure culture, *D. reducens* shuttles electrons to the reduction of Fe(III) rather than to the production of hydrogen, at least initially. In co-cultures, hydrogen is either being used directly by *G. sulfurreducens* to reduce Fe(III) or is not being produced as *D. reducens* contributes to Fe(III) reduction. In *G. sulfurreducens* pure cultures, ~4 mM acetate and ~4.4 mmol/L hydrogen was utilized respectively (**Supplementary Figure 6.5)**.

Our studies suggest that there is an inherent advantage of co-culture growth for *D. reducens* and *G. sulfurreducens* while reducing soluble Fe(III)-citrate and insoluble Fe(III)-oxide on the cultivation conditions tested. In order to gain further biological insights into this co-culture, we performed both global and targeted proteomic analyses on Fe(III)-citrate reducing co-cultures. Issues with protein extraction from *G. sulfurreducens* insoluble Fe(III) cultures prevented proteomic analysis on the Fe(III)-oxide condition. Fe(III) reduction curves for cultures analyzed are displayed in **Figure 6.4,** and harvesting timepoints are highlighted. Growth curves for *D. reducens*-*G. sulfurreducens* co-cultures and pure cultures based on fluorescent microscopy are also displayed.

Figure 6.4: Phenotypic comparisons between *D. reducens*-*G. sulfurreducens* co-cultures and pure cultures. Concentrations of substrates and products were monitored including pyruvate, acetate, hydrogen, and Fe(II). Cell growth was also monitored with fluorescent microscopy. The co-culture displays faster rates of pyruvate oxidation and Fe(II) reduction. Growth rates are also faster during co-culture growth. Stars represent harvesting timepoints. Cultures were inoculated with 30 mM Fe(III)-citrate and 20 mM pyruvate (or 20 mM acetate for *G. sulfurreducens* pure cultures). *G. sulfurreducens* duplicates are displayed separately due to inconsistent lag phases. Note: after the 48-hour co-culture timepoint, *G. sulfurreducens* were nearly completely localized to Fe(II)-precipitates, causing difficulties acquiring accurate microscopic counts.

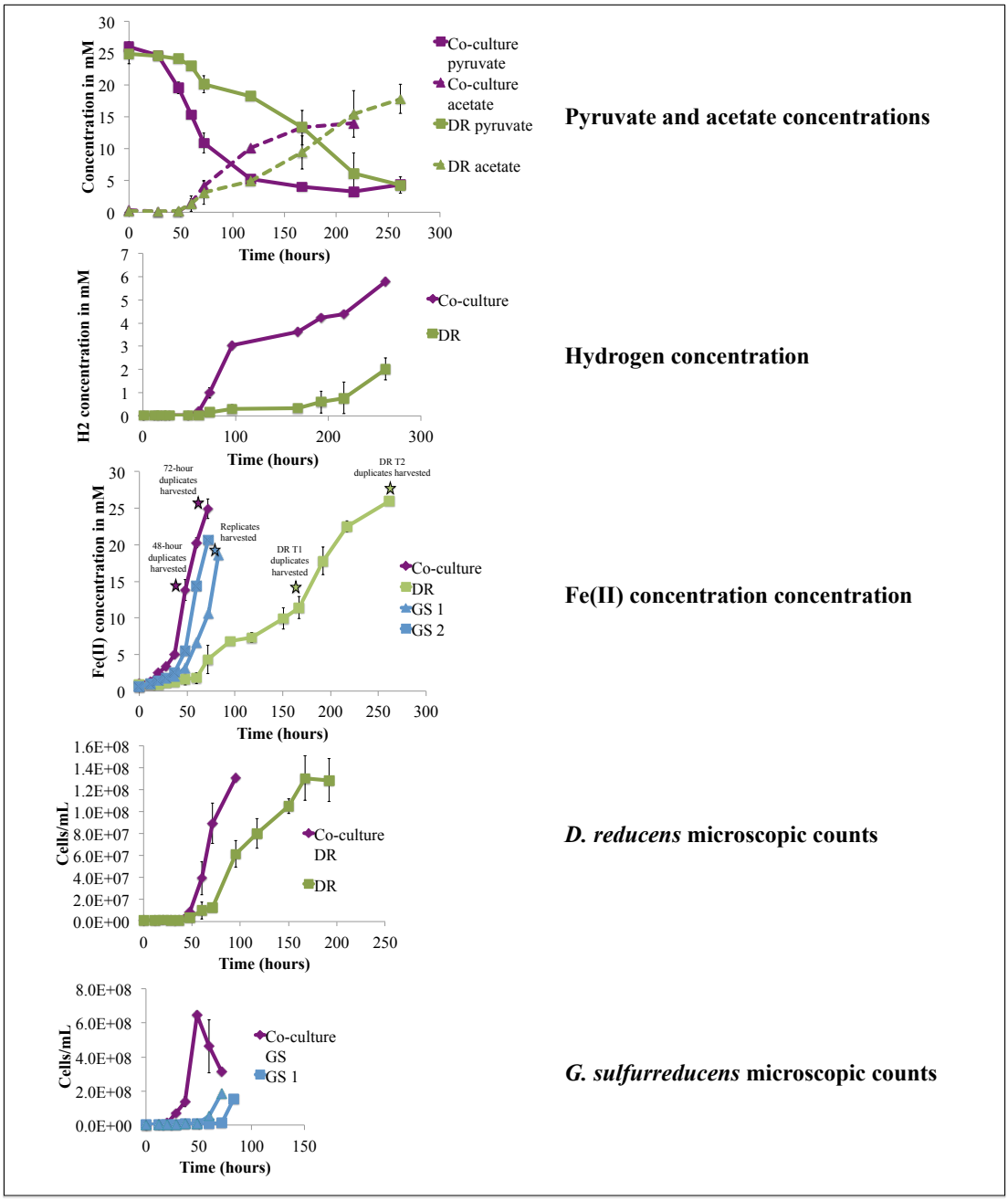

II. Proteomic analyses of co-cultures

A. Global comparative proteomic analysis of co-cultures versus pure cultures

The total number of proteins confidently identified varied across cultures/timepoints and is displayed in **Table 6.1**, along with other global analyses of the proteomic data. Proteomes of replicates for each condition (biological duplicates and technical triplicates) clustered tightly, forming distinctive groups for each culture/timepoint. A visual representation of this clustering is displayed in the heat map in **Supplementary Figure 6.6.**

Table 6.1a: Global analyses of comparative proteomic data generated

Condition	Proteins identified	Average # distinct peptides detected per protein	Average log_2 peptide ion intensity
DR T1	617	11.0 (SD 12.6)	22.6 (SD 1.7)
DR T2	471	9.9 (SD 13.4)	22.3 (SD 1.9)
CoC T1 (DR)	605	7.7 (SD 9.2)	22.9 (SD 1.4)
CoC T2 (DR)	395	8.9 (SD 12.1)	22.7 (SD 1.5)
GS	1250	9.9 (SD 13.6)	22.8 (SD 1.4)
CoC T1 (GS)	973	8.8 (SD 12.6)	22.8 (SD 1.5)
CoC T2 (GS)	585	10.8 (SD 15.1)	22.7 (SD 1.5)

Note: Protein identification based on at least 2 unique peptides observed in a biological replicate and detection in at least 50% of replicates

Co-cultures and pure cultures most similar in their growth phase were compared in order to reduce proteomic differential abundance resulting from growth phase differences. For *G. sulfurreducens*, the cultures harvested at 48-hours were compared with the *G. sulfurreducens* co-culture proteome because by the 72-hour timepoint, most of the Fe(III) was reduced and *G. sulfurreducens* cells were no longer growing exponentially **(Figure 6.4)**. For comparative proteomic analysis of *D. reducens* proteins, the pure culture harvested at 262 hours (DR T2) was disregarded because although Fe(II) levels match closely with the 72-hour co-culture, the

organism was no longer in exponential phase. This matches with other findings, where *D. reducens* cells continue to reduce Fe(III) after they are no longer growing (Dalla Vecchia et al., 2014b; Otwell et al., 2016). For the *D. reducens* co-culture proteome, at the 72-hour timepoint *D. reducens* is still in exponential growth with >10mM pyruvate left to oxidize **(Figure 6.4)**. However, surprisingly, far fewer proteins were found in samples from the 72-hour co-culture timepoint than in samples from the 48-hour timepoint **(Table 6.1b)**. It is possible that the Fe(II) precipitates present at the 72-hour timepoint (**Figure 6.3c**) could be interfering with protein extraction and mass spectrometry techniques, leading to identification of fewer proteins. Another possible explanation is that the proteome of *D. reducens* while in c-culture with *G. sulfurreducens* is truly simpler at this timepoint (further description below). Other parameters used for comparing conditions (including average $\log_2$ fold change of average ion intensities, **Table 6.1b**) also support that the 48-hour co-culture proteome matches more closely with the pure culture proteome (DR T1). Therefore, the *D. reducens* co-culture proteome at 48-hours was compared with the pure culture proteome, but the 72-hour timepoint was also considered in comparative proteomic analyses described below. Based on these comparisons, significant proteins in co-culture proteomes or pure culture proteomes are displayed in Supplementary Tables. This includes *G. sulfurreducens* proteins significantly increased (>2-fold, $p<0.05$) or decreased in the co-culture proteome relative to the pure culture (**Supplementary Table 6.1a)**, *G. sulfurreducens* proteins exclusively identified in either the co-culture (**Supplementary Table 6.1b)** or pure culture **(Supplementary Table 6.1c)**, *D. reducens* proteins significantly increased (>2-fold, $p<0.05$) or decreased in the co-culture proteome relative to the pure culture **(Supplementary Table 6.2a)**, and *D. reducens* proteins exclusively identified in either the co-culture **(Supplementary Table 6.2b)** or pure culture **(Supplementary Table 6.2c**).

Table 6.1b: Global comparisons of proteomic data between conditions

Proteomic comparison	Proteins shared between conditions compared	Average log_2 fold change of average ion intensities between shared proteins	Proteins significantly increased	Proteins significantly decreased	Proteins exclusive to either condition compared
D. reducens **proteomic comparisons**					
DR T1 vs DR T2	422	0.59	133	36	190, 45
CoC T1 vs CoC T2	375	0.60	97	9	227, 18
CoC T1 vs DR T1	480	0.2	134	105	124, 136
CoC T2 vs DR T1	358	-0.48	50	136	37, 258
G. sulfurreducens **proteomic comparisons**					
CoC T1 vs CoC T2	541	0.3	111	34	431, 43
CoC T1 vs GS	923	-0.36	47	155	47, 324
CoC T2 vs GS	563	-0.69	23	183	22, 687

Note: Protein identification based on at least 2 unique peptides observed in a biological replicate and detection in at least 50% of replicates
Significance defined as >2-fold increase (p <0.05)

B. G. sulfurreducens proteomes in co-culture compared to pure culture: MHCs and pili-related proteins show significant enrichment

In comparing the *G. sulfurreducens* co-culture proteome with that of the pure culture, fewer total proteins were confidently identified (973 versus 1250), fewer proteins were significantly increased (47 versus 155), and fewer proteins were exclusively identified in the co-culture proteome compared to the pure culture proteome (324 versus 47) **(Table 6.1).** Furthermore, housekeeping genes are decreased in the *G. sulfurreducens* co-culture relative to the pure culture. The subunits of RNA polymerase are decreased ~1.5 fold in the co-culture, with an average p <0.01. RpoD (GSU3089) is decreased 1.6 fold in the co-culture proteome relative to the pure

culture (p <0.01). Ribosomal proteins are consistently decreased in the co-culture proteome (1.2 fold on average relative to the pure culture), and seven of these proteins are included in the significantly decreased list **(Supplementary Table 6.1a).**

Given these global comparisons, where *G. sulfurreducens* proteins in the co-culture exhibit global decreases relative to the pure culture, it is intriguing that multiple c-type cytochromes and type IV pili-related proteins are significantly increased in abundance in the co-culture. A complete list of c-type cytochromes and type IV pili-related proteins increased in the co-culture (all p-values <0.05) is displayed in **Table 6.2**. Previous studies focused on metal reduction by *G. sulfurreducens* have identified many of the proteins in this table. The MHC most highly increased in abundance is PccJ (GSU2494), a periplasmic protein with 16 heme-binding sites. PccJ was increased in abundance in the co-culture ~31-fold (p <0.01) relative to the pure culture. This protein has been associated with extracellular electron transfer multiple times in the literature, including in an analysis of Fe(III) oxide reduction, an analysis of electron transfer to electrodes, and an analysis of the genome of *G. sulfurreducens* KN400, a strain with enhanced extracellular electron transfer and electricity production (Aklujkar et al., 2013; Butler et al., 2012; Holmes et al., 2006). Two proteins encoded in the same predicted operon (GSU2495-6) are also increased in abundance in the co-culture. GSU2495 is a MHC, while GSU2496 is a hypothetical protein **(Table 6.2a**). Another MHC significantly increased in the co-culture proteome relative to the pure culture is OmcC (GSU2731), an outer membrane protein with 12 heme groups (2.2-fold increase, p <0.01, **Table 6.2a**). This protein is encoded in a parallel gene cluster to the well-characterized Fe(III) reductase OmcB (GSU2737). Both gene clusters also include a putative transcription factor, a porin-like outer membrane protein and a periplasmic MHC. Recent studies show that OmcB and OmcC (along with their respective clusters) share

overlapping roles in Fe(III) reduction by *G. sulfurreducens* (Liu et al., 2014, 2015). In the *G. sulfurreducens* pure culture proteome, where more total proteins were identified and over three times as many proteins were significantly increased, only two c-type cytochromes are significantly increased in abundance (GSU0594 and GSU2513). Proteomic information for all c-type cytochromes identified in this study is in **Supplementary Table 6.3.** This includes multiple characterized MHCs predicted to be involved in extracellular electron transfer in *G. sulfurreducens* (including PpcA, OmcB, OmcS, and OmcZ), which were found to not be differentially abundant between pure culture and co-culture conditions based on shotgun proteomic analysis.

Table 6.2a: *G. sulfurreducens* c-type cytochromes increased in abundance in the co-culture proteome relative to the pure culture or identified exclusively during co-culture growth

Locus Tag	Protein name	Co/Pure (log_2)	P-value	Number of distinct peptides detected in Co	Number of distinct peptides detected in Pure	Localization
GSU0357	cytochrome c nitrite reductase	0.69	<0.01	17	14	periplasmic
GSU0466	cytochrome c peroxidase (MacA)	0.97	<0.01	20	14	periplasmic
GSU0746	cytochrome p460, 1 heme-binding site	1.74	<0.01	2	1	non-cytoplasmic, unknown
GSU1024	cytochrome c (PpcD)	1.68	0.02	1	1	non-cytoplasmic, unknown
GSU1996	cytochrome c	1.61	<0.01	16	9	periplasmic
GSU2201	cytochrome c (PpcF)	0.69	0.02	14	9	non-cytoplasmic, unknown
GSU2494	cytochrome c (PpcJ)	4.95	<0.01	2	1	periplasmic
GSU2495	cytochrome c	0.88	0.03	3	3	periplasmic or extracellular
GSU2731	lipoprotein cytochrome c (OmcC)	1.13	<0.01	29	16	non-cytoplasmic, unknown
GSU2743	cytochrome c,	1.00	<0.01	6	4	non-

	1 heme-binding site					cytoplasmic, unknown
GSU2801	cytochrome c	0.76	<0.01	13	14	non-cytoplasmic, unknown
GSU2882	cytochrome c (OmcG)	2.61	0.01	2	1	Extracellular
GSU2887	lipoprotein cytochrome c	1.14	<0.01	1	2	Extracellular
GSU2937	cytochrome c	0.92	0.01	6	7	periplasmic
GSU3137	cytochrome c	1.50	<0.01	3	1	periplasmic
GSU1284	cytochrome c, 1 heme-binding site	NA	NA	2	NA	non-cytoplasmic, unknown
GSU1334	cytochrome c	NA	NA	1	NA	non-cytoplasmic, unknown
GSU1648	cytochrome c (MacC)	NA	NA	1	NA	periplasmic
GSU1740	cytochrome c, 1 heme-binding site	NA	NA	2	NA	non-cytoplasmic, unknown
GSU1760	cytochrome c (PpcE)	NA	NA	1	NA	non-cytoplasmic, unknown
GSU2299	cytochrome c	NA	NA	25	NA	periplasmic
GSU3428	cytochrome c, 1 heme-binding site	NA	NA	2	NA	periplasmic

Note: Number of distinct peptides refers to the highest number of distinct peptides detected per protein in a particular replicate
NA=not applicable
Localization based on PSORTb, reference: Yu, N. Y., Wagner, J. R., Laird, M. R., Melli, G., Rey, S., Lo, R., et al. (2010). PSORTb 3.0: improved protein subcellular localization prediction with refined localization subcategories and predictive capabilities for all prokaryotes. Bioinformatics 26, 1608–15. doi:10.1093/bioinformatics/btq249.

The core structural protein of the type IV pilus (PilA, GSU1496) was increased 6.2-fold (p<0.01) in the co-culture proteome compared to the pure culture proteome (**Table 6.2b)**. GSU1497, a hypothetical protein that has been predicted to encode for a head domain missing from PilA but found in most type IV pilins, is also increased ~2.4-fold (p<0.01) in the co-culture proteome (Bonanni et al., 2013). Furthermore, four putative pili biogenesis-related proteins were identified in this study, including PilQ, PilM, PilW, and PilY (GSU2028, GSU2032, GSU2035, and GSU2038 respectively). All of these proteins were increased in abundance in the co-culture

proteome compared with the pure culture proteome, three of which were significantly increased **(Table 6.2b)**.

Table 6.2b: *G. sulfurreducens* type IV pili-related proteins increased in abundance in the co-culture proteome relative to pure culture

Locus Tag	Protein name	Co/Pure (log_2)	p-value	Number of distinct peptides detected in Co	Number of distinct peptides detected in Pure
GSU1496	hypothetical protein (PilA)	2.64	<0.01	3	2
GSU1497	hypothetical protein	1.26	<0.01	10	3
GSU2028	type IV pilus secretin lipoprotein PilQ	1.21	<0.01	6	5
GSU2032	type IV pilus biogenesis ATPase PilM	0.54	0.43	1	2
GSU2035	type IV pilus minor pilin PilW	1.06	<0.01	4	2
GSU2038	type IV pilus assembly protein PilY	1.80	<0.01	23	10

Note: Number of distinct peptides refers to the highest number of distinct peptides detected per protein in a particular replicate

The predicted operon containing OmpJ (GSU3304-6), a putative porin, is also increased in abundance in the co-culture proteome. OmpJ (GSU3304) is one of the most abundant outer membrane proteins in *G. sulfurreducens*, and an OmpJ-deficient mutant is not capable of reducing metals including soluble and insoluble Fe(III) (Afkar et al., 2005). OmpJ is increased although not significantly in the co-culture (~1.6-fold, p=0.23), while the rest of the predicted operon (GSU 3305-6, both hypothetical proteins) is increased with significant p-values (~3.9-fold increase, p <0.01 and 1.5-fold increase, p <0.01 respectively).

C. *D. reducens proteomes in co-culture compared to pure culture: faster growth rates but decreased abundance of central metabolism proteins*

Ribosomal proteins are significantly increased in the *D. reducens* co-culture proteome (48-hour) compared with the pure culture, on average 4.5-fold *(p*=0.03). 41 of these ribosomal proteins are significantly increased proteins **(Supplementary Table 6.2a)** and comprise >30% of this table. In the 72-hour co-culture timepoint, where far fewer proteins were identified and overall $\log_2$ abundance comparisons are decreased relative to the pure culture (**Table 6.1**), ribosomal proteins are increased 2.7 fold *(p*=0.03). In fact, ~60% of the proteins significantly increased in the 72-hour co-culture proteome relative to the pure culture are ribosomal proteins. This is consistent with the enhanced growth rates observed for *D. reducens* cells when grown in co-culture with *G. sulfurreducens* **(Figure 6.4)**.

Given the increase in *D. reducens* ribosomal protein abundance in the co-culture, a surprising finding is that central metabolic pathways are significantly enriched in the pure culture proteome relative to the co-culture. Enrichment analysis of significant pure culture proteins relative to the 48-hour co-culture (including proteins increased >2-fold, $p < 0.05$ or exclusively identified, **Supplementary Tables 6.2a and 6.2c**) reveals enrichment of proteins putatively involved in central metabolic pathways. This includes the pentose phosphate pathway (*p*=0.01 for enrichment analysis), glycolysis and gluconeogenesis *(p*=0.02 for enrichment analysis), and metabolism of several amino acids (Database for Annotation, Visualization and Integrated Discovery (DAVID), Huang et al., 2009a, 2009b). An even greater enrichment in pathways related to central metabolism is observed when comparing the pure culture proteome with the 72-hour co-culture proteome. The pentose phosphate pathway ($p < 0.01$), glycolysis and gluconeogenesis (*p*=0.03), and multiple amino acid metabolism pathways are still enriched, along with fatty acid biosynthesis (*p*=0.04) and C5 branched dibasic acid metabolism (*p*=0.055) (Database for Annotation, Visualization and Integrated Discovery (DAVID), Huang et al., 2009a,

2009b). **Supplementary Figure 6.7** displays an example of this enrichment, highlighting proteins annotated in the glycolysis/gluconeogenesis pathway that were significantly upregulated in the *D. reducens* pure culture proteome relative to the co-culture (48 and 72-hour timepoints) (KEGG pathway, Kanehisa and Goto, 2000; Kanehisa et al., 2014).

Our group previously analyzed the proteomes of *D. reducens* during cultivation on four different growth conditions (sulfate reduction, Fe(III)-citrate reduction, Fe(III)-oxide reduction, and pyruvate fermentation) (Otwell et al., 2016). Comparison of *D. reducens* proteins exclusive to co-culture growth (**Supplementary Table 6.2b)** with these previous datasets reveals that five proteins are completely unique to co-culture cultivation **(Supplementary Table 6.4)**. All of these proteins were identified with high confidence in the co-culture 48-hour proteome (2 to 10 distinct peptides detected) and no peptides were detected in the previous dataset. Three of these proteins are putatively involved in the same pathway, synthesizing anthranilate through chorismate by use of the shikimate pathway. This pathway leads to synthesis of tryptophan, as well as various secondary metabolites (KEGG pathway, Kanehisa and Goto, 2000; Kanehisa et al., 2014). Another *D. reducens* protein exclusively identified during co-culture growth with *G. sulfurreducens* is a hypothetical protein described as a putative ABC transporter, specifically a transporter of metallic cation, iron-siderophore and vitamin B12 molecules. Proteomic information for these proteins is provided in **Supplementary Table 6.4.**

D. Multiple reaction monitoring (MRM) for targeted quantification of peptide biomarkers

Targeted peptide quantification through multiple reaction monitoring (MRM) is a valuable technique that has mainly been utilized for quantifying clinical biomarkers in human patients (Arsène-Ploetze et al., 2015). While it has been applied to dechlorination research, the method has not been implemented in the study of most environmental processes, including metal

reduction (Arsène-Ploetze et al., 2015; Rowe et al., 2012, 2015; Werner et al., 2009). A variety of peptide biomarkers for *D. reducens* and *G. sulfurreducens* were selected for quantification. This includes MHCs (including OmcB, OmcS, OmcZ) from *G. sulfurreducens* as well as citrate synthase. Expression levels of OmcB have been shown to correlate with rates of Fe(III) reduction in *G. sulfurreducens*, while citrate synthase has been previously recognized as a biomarker of the metabolic rate of *G. sulfurreducens* (Chin et al., 2004; Holmes et al., 2005; Wilkins et al., 2011). While *D. reducens* is a much less characterized organism, we created peptide biomarkers for metal reductases previously identified by our group in functional-based studies (Otwell et al., 2015). Proteins involved in riboflavin biosynthesis were also targeted based on prior evidence for a flavin-based soluble electron shuttle during Fe(III) reduction while fermenting pyruvate (Dalla Vecchia et al., 2014b). The complete list of proteotypic peptides designed and synthesized as biomarkers in *D. reducens* and *G. sulfurreducens* is displayed in **Supplementary Table 6.5.** Several of these peptides were not monitored in the final co-culture experiment due to a lack of detection during the validation stage in pure culture. **Table 6.3** displays relative biomarker peptide levels detected in co-cultures, *G. sulfurreducens* pure cultures, and *D. reducens* pure cultures derived from MRM analysis. Values are MRM peak areas normalized to the peak area of the corresponding isotopically-heavy synthetic peptide (which serves as an internal standard). Overall, protein abundance ratios based on MRM reflect abundance ratios derived from AMT tag-based comparative proteomic analysis **(Table 6.3 and Supplementary Figure 6.8).**

Table 6.3: Comparison of protein abundance ratios based on multiple reaction monitoring (MRM) and accurate mass and time (AMT) tag-based proteomics 6.3a. Comparison of *G. sulfurreducens* biomarkers. 6.3b. Comparison of *D. reducens* biomarkers.

			Log$_2$ Co48/GS			Log$_2$ Co48/Co72		
Protein name	**Locus tag**	**Peptide sequence**	**MRM**	**MRM Avg**	**AMT tag**	**MRM**	**MRM Avg**	**AMT tag**
OmcB	GSU 2737	ATNGAAGPVV NWDPNNNR	0.56	0.92	0.35	2.91	3.82	1.34
OmcB	GSU 2737	AITDADGILGF VNSHYLAAGG QLFGK	0.74			3.37		
OmcB	GSU 2737	DVMGAAFNAN LLIHDPGGYAH NR	1.46			5.19		
OmcS	GSU 2504	FNLAYEFTTIA DASGNSIYGTD PNTSSLQGR	1.66	1.29	0.10	3.62	3.77	Co48 only
OmcS	GSU 2504	FVDGSIATTGL PIK	0.93			3.91		
OmcZ	GSU 2076	IIASATLATGK	-1.13	-0.07	0.21	2.51	3.92	Co48 only
OmcZ	GSU 2076	VSVPALVEGV YELR	0.54			5.16		
OmcZ	GSU 2076	VVATSPDFATN GYVTVK	0.37			4.08		
citrate synthase	GSU 1106	TPGLKDDPLFK	0.04	-0.23	-0.20	1.21	0.68	0.00
citrate synthase	GSU 1106	IPVIAAFIYNLK	-0.51			0.16		

			Log$_2$ Co72/DRT1			Log$_2$ Co48/DRT1			Log$_2$ Co48/Co72		
Protein name	**Locus tag**	**Peptide sequence**	**MRM**	**MRM Avg**	**AMT tag**	**MRM**	**MRM Avg**	**AMT tag**	**MRM**	**MRM Avg**	**AMT tag**
dihydroorotate dehydrogenase 1B	Dred_1686	AVEGAGADGLSV INTLLGMAIDVR	-0.78	-0.78	-0.23	-0.99	-0.99	-0.60	-0.22	-0.22	-0.37
riboflavin synthase a	Dred_2092	DLRPGSQVNLER	-1.20	-0.48	DR only	-1.09	-0.59	DR only	0.12	-0.11	DR only
riboflavin synthase a	Dred_2092	LGGHMVSGHVD GVGTIAGK	0.25			-0.09			-0.34		
riboflavin synthase b	Dred_2090	VFEGHLLGQELK	-2.04	-1.50	-1.86	-1.78	-1.69	-2.24	0.25	-0.19	-0.39
riboflavin synthase b	Dred_2090	ISLDSNLPVIFGVL TVDTIEQAIER	-0.97			-1.60			-0.63		
Sat	Dred_0635	GELPPLEFGR	0.72	-0.44	0.13	0.76	-0.77	-0.53	0.03	-0.33	-0.65
Sat	Dred_0635	YAGYYAHPAETR	-1.25			-1.79			-0.54		
Sat	Dred_0635	ATFFTDDADHPGVQK	-0.80			-1.28			-0.48		
pyruvate ferredoxin/flavodoxin	Dred_0049	EALYIPNFGVEQR	-1.81	-1.16	-1.25	-1.86	-0.86	-1.37	-0.05	0.30	-0.13

oxidoreductase											
pyruvate ferredoxin/flavodoxin oxidoreductase	Dred_0049	VLAIPALEISK	-0.51			0.15			0.66		

Note: blue shading highlights side-by-side comparisons of ratios derived from MRM and AMT tag-based proteomic techniques. This data is represented visually in **Supplementary Figure 6.8.**

Discussion

In this study, we established an Fe(III)-reducing co-culture between *D. reducens* and *G. sulfurreducens*. The culture was grown with pyruvate as electron donor, which *D. reducens* potentially oxidizes to acetate and hydrogen, both of which can be used as electron donor by *G. sulfurreducens* **(Figure 6.1)**. Although pyruvate is a fermentable substrate by *D. reducens*, evidence suggests that this Gram-positive organism is contributing to Fe(III) reduction in the co-culture. We observed enhanced rates of Fe(III)-reduction when cultivated with both soluble and insoluble Fe(III). Growth rates were higher in the co-culture, and pyruvate was oxidized at faster rates. These findings together suggest that the organisms form a mutually beneficial association while reducing Fe(III).

In the *D. reducens* co-culture proteome, ribosomal proteins were significantly increased in abundance, likely a reflection of faster growth rates than during pure culture growth **(Figure 6.4)**. Based on the increase in ribosomal protein abundance and growth rate, it seems most likely that proteins involved in central metabolic pathways (i.e. carbon metabolism) would also be increased in order to support cell growth. However, overall fewer proteins were identified in the *D. reducens* co-culture proteome (48-hour) and multiple central metabolic pathways were enriched in the pure culture proteome relative to the co-culture. These global proteomic trends suggest that *D. reducens* is living and replicating more efficiently while in co-culture with *G. sulfurreducens* and is likely deriving some benefit from this association. The trend is even more

pronounced in the 72-hour co-culture proteome, possibly suggesting that *D. reducens* has continued to adjust to inhabitance with *G. sulfurreducens* by further downregulating basic metabolic proteins. The far fewer proteins detected for the 72-hour timepoint could also be a reflection of this **(Table 6.1)**. The mechanism by which *D. reducens* is benefiting during co-culture growth with *G. sulfurreducens* is unknown at this time.

One possible explanation for faster rates of Fe(III) reduction during co-culture growth could be the excretion of a soluble metabolite by one of the organisms. Multiple studies have documented soluble molecules enhancing rates of Fe(III) reduction, including flavins, quinones, and antibiotics (Hernandez et al., 2004; Lovley et al., 1998; Marsili et al., 2008). Proteomic data provides a preliminary suggestion of production of a secondary metabolite by *D. reducens* during co-culture growth. By comparing *D. reducens* proteins exclusively identified during co-culture growth (**Supplementary Table 6.2b)** with comparative proteomic datasets generated for *D. reducens* cultivated on various conditions, (33 replicate samples in total) five proteins were found to be completely unique to co-culture growth (Otwell et al., 2016). Three out of five of these proteins are putatively involved in synthesis of anthranilate through chorismate by use of the shikimate pathway. Other proteins in this pathway are also significantly increased during co-culture growth **(Supplementary Table 6.4)**. Anthranilate has been shown to be a precursor of *Pseudomonas* quinolone signal (PQS), a key molecule involved in quorum sensing in *Pseudomonas aeruginosa* (McGrath et al., 2004; McKnight et al., 2000). PQS has also been shown to interact with Fe(III), as an Fe(III)-chelator as well as a facilitator of siderophore-mediated iron uptake (Bredenbruch et al., 2006; Diggle et al., 2007). It is possible that a metabolite, not necessarily PQS but perhaps a molecular similar in structure, is synthesized by *D. reducens* while in co-culture with *G. sulfurreducens*. These three proteins could also potentially

be involved in tryptophan biosynthesis (KEGG pathway, Kanehisa and Goto, 2000; Kanehisa et al., 2014). However, synthesis of other amino acids is not increased during co-culture growth, and given the global patterns of decreased basic metabolic proteins in the *D. reducens* co-culture proteome, this is unlikely. Another *D. reducens* protein exclusive to co-culture growth was Dred_2840, a predicted transporter of metallic cation, iron-siderophore and vitamin B12 molecules. This transporter was identified by multiple unique peptides in all replicates of both co-culture timepoints, but no peptides for it were detected in the previous dataset (Otwell et al., 2016). This protein could potentially transport a molecule produced by *D. reducens* during co-culture growth. Future investigations are warranted in order to better elucidate microbial interactions in this Fe(III)-reducing co-culture and investigate potential excretion of secondary metabolites.

In the *G. sulfurreducens* co-culture proteome, multiple proteins putatively involved in extracellular electron transfer based on previous studies were significantly increased in abundance relative to the pure culture proteome. This finding could relate to the enhanced rates of Fe(III) reduction observed during co-culture growth. While we do not have direct support for a particular mechanism of interspecies electron transfer in *D. reducens*-*G. sulfurreducens* co-cultures, comparative proteomic analysis of *G. sulfurreducens* proteins leads to an intriguing suggestion of DIET. Previous studies analyzing DIET in co-cultures involving species of *Geobacter* have found that the type IV pili are essential. Co-culture growth in DIET cultures was prevented by deleting PilA from either *G. metallireducens* (the electron-donating organism in the study) or *G. sulfurreducens* (the electron-accepting organism in the study) (Rotaru et al., 2014a, 2014b; Shrestha et al., 2013b; Summers et al., 2010). In *D. reducens*-*G. sulfurreducens* co-cultures, PilA (GSU1496) was increased 6.2-fold (p <0.01) and GSU1497 was increased 2.4-fold

(p <0.01) relative to the pure culture. Furthermore, four proteins were identified from a predicted operon involved in type IV pilus biogenesis, which were increased on average 2.3-fold **(Table 6.2b)**. The increased abundance of type IV pili-related proteins could also relate to the enhanced biofilm phenotype observed during Fe(III)-oxide reduction in co-cultures, as the pili have also been shown to be involved in biofilm formation in *Geobacter* (Reguera et al., 2006).

The MHC OmcS (which is localized to the pili) is also predicted to be involved in DIET (Shrestha et al., 2013b; Summers et al., 2010). Shotgun proteomic analysis in the current study revealed that multiple MHCs are significantly increased in abundance during *D. reducens*-*G. sulfurreducens* co-culture growth relative to pure culture grown **(Table 6.2a)**, but OmcS was not differentially abundant **(Supplementary Table 6.3)**. However, MRM assays, targeting specific peptides from OmcS, showed a significant increase of OmcS on the 48-hour co-culture condition (2.5-fold increase on average, **Table 6.3**). Due to this discrepancy, manual analysis of raw peptide data from AMT tag-based shotgun proteomics was performed. Eleven distinct peptides were identified for OmcS in the co-culture, versus five in the pure culture. When the ion intensities of the same peptides are compared against each other ($\log_2$ co-culture versus $\log_2$ pure culture), the AMT tag data supports the MRM data. For each of the five OmcS peptides common to both conditions, average ion intensity is significantly increased in the co-culture (2.2, 3.9, 5.0, 2.4, and 3.8-fold respectively) **(Supplementary Table 6.6)**. The sole MRM biomarker peptide detected by AMT tag in both the co-culture and pure culture proteomes (FVDGSIATTGLPIK) is 2.2-fold increased in the co-culture, quite similar to the 1.9-fold increase based on MRM assays **(Supplementary Table 6.6, Table 6.3)**. Taken together, our data supports that OmcS is significantly increased during co-culture growth of *G. sulfurreducens* relative to pure culture growth. It also highlights a disadvantage of global proteomic datasets, where variance in peptide

ion efficiency can obscure results. It also points to the advantage of employing parallel proteomic techniques, as well as a benefit of quantifying specific, validated peptides with the MRM technique.

Previous studies analyzing DIET also found decreased expression of proteins involved in hydrogen utilization in co-cultures of *G. metallireducens* and *G. sulfurreducens* relative to non-DIET cultures. This included the sole hydrogenase involved in the uptake of hydrogen in *G. sulfurreducens* (Hyb, GSU0782-6) as well as a predicted operon necessary for expression of this hydrogenase (GSU0305-9) (Shrestha et al., 2013b). In our comparative proteomic analysis, Hyb does not show a significant pattern of relative abundance. However, proteins encoded between GSU0305-9 show decreased abundance during co-culture growth relative to pure culture growth. Proteins are 2.2-fold (p <0.01), 2.1-fold (p <0.01), 1.3-fold (p=0.3), 2.4-fold (p <0.01), and 1.6-fold (p <0.01) decreased in the *G. sulfurreducens* co-culture respectively. This finding further supports the possibility of DIET from *D. reducens* to *G. sulfurreducens* during co-culture growth. Instead of producing hydrogen, *D. reducens* could potentially be transferring electrons directly to *G. sulfurreducens*. Future investigations, including genetic studies, are necessary in order to test whether DIET is occurring in *D. reducens*-G. *sulfurreducens* co-cultures.

Acknowledgements:

Authors that contributed to this work include:

Anne E. Otwell[1], Stephen J. Callister[2], Robert W. Sherwood[3], Sheng Zhang[3], Ruth E. Richardson[4]

[1]Cornell University, Department of Microbiology, Ithaca, NY, USA
[2]Pacific Northwest National Laboratory, Biological Sciences Division, Richland, WA, USA
[3]Cornell University, Proteomics and Mass Spectrometry Facility, Ithaca, NY, USA
[4]Cornell University, Department of Civil and Environmental Engineering, Ithaca, NY USA

We would like to thank Abby Goldman and the Lara Estroff Lab of Cornell University for analyzing Fe(II) precipitates with XRD, Mytien Nguyen and the Lars Angenent Lab of Cornell

University for assistance with HPLC, and Alex Hernsdorf formerly of Cornell University for assistance with development of MRM peptide biomarkers.

References:

Afkar, E., Reguera, G., Schiffer, M., and Lovley, D. R. (2005). A novel Geobacteraceae-specific outer membrane protein J (OmpJ) is essential for electron transport to Fe(III) and Mn(IV) oxides in Geobacter sulfurreducens. *BMC Microbiol.* 5, 41. doi:10.1186/1471-2180-5-41.

Aklujkar, M., Coppi, M. V., Leang, C., Kim, B. C., Chavan, M. A., Perpetua, L. A., et al. (2013). Proteins involved in electron transfer to Fe(III) and Mn(IV) oxides by Geobacter sulfurreducens and Geobacter uraniireducens. *Microbiology* 159, 515–535. doi:10.1099/mic.0.064089-0.

Amin, O., Fardeau, M.-L., Valette, O., Hirschler-Réa, A., Barbe, V., Médigue, C., et al. (2013). Genome Sequence of the Sulfate-Reducing Bacterium Desulfotomaculum hydrothermale Lam5T. *Genome Announc.* 1. doi:10.1128/genomeA.00114-12.

Arsène-Ploetze, F., Bertin, P. N., and Carapito, C. (2015). Proteomic tools to decipher microbial community structure and functioning. *Environ. Sci. Pollut. Res. Int.* 22, 13599–612. doi:10.1007/s11356-014-3898-0.

Barton, L., Tomei-Torres, F., Xu, H., and Zocco, T. (2015). *Bacteria-Metal Interactions*. , ed. D. Saffarini Cham: Springer International Publishing doi:10.1007/978-3-319-18570-5.

Bird, L. J., Bonnefoy, V., and Newman, D. K. (2011). Bioenergetic challenges of microbial iron metabolisms. *Trends Microbiol.* 19, 330–340. doi:10.1016/j.tim.2011.05.001.

Bonanni, P. S., Massazza, D., and Busalmen, J. P. (2013). Stepping stones in the electron transport from cells to electrodes in Geobacter sulfurreducens biofilms. *Phys. Chem. Chem. Phys.* 15, 10300–6. doi:10.1039/c3cp50411e.

Bredenbruch, F., Geffers, R., Nimtz, M., Buer, J., and Häussler, S. (2006). The Pseudomonas aeruginosa quinolone signal (PQS) has an iron-chelating activity. *Environ. Microbiol.* 8, 1318–1329. doi:10.1111/j.1462-2920.2006.01025.x.

Butler, J. E., Young, N. D., Aklujkar, M., and Lovley, D. R. (2012). Comparative genomic analysis of Geobacter sulfurreducens KN400, a strain with enhanced capacity for extracellular electron transfer and electricity production. *BMC Genomics* 13, 471. doi:10.1186/1471-2164-13-471.

Call, D. F., and Logan, B. E. (2011). Lactate oxidation coupled to iron or electrode reduction by Geobacter sulfurreducens PCA. *Appl. Environ. Microbiol.* 77, 8791–4. doi:10.1128/AEM.06434-11.

Callister, S. J., Barry, R. C., Adkins, J. N., Johnson, E. T., Qian, W.-J., Webb-Robertson, B.-J. M., et al. (2006). Normalization approaches for removing systematic biases associated with mass spectrometry and label-free proteomics. *J. Proteome Res.* 5, 277–86. doi:10.1021/pr050300l.

Cardenas, E., Wu, W.-M., Leigh, M. B., Carley, J., Carroll, S., Gentry, T., et al. (2010). Significant association between sulfate-reducing bacteria and uranium-reducing microbial

communities as revealed by a combined massively parallel sequencing-indicator species approach. *Appl. Environ. Microbiol.* 76, 6778–6786. doi:10.1128/AEM.01097-10.

Carlson, H. K., Iavarone, A. T., Gorur, A., Yeo, B. S., Tran, R., Melnyk, R. A., et al. (2012). Surface multiheme c-type cytochromes from Thermincola potens and implications for respiratory metal reduction by Gram-positive bacteria. *Proc. Natl. Acad. Sci.* doi:10.1073/pnas.1112905109.

Chandler, D. P., Jarrell, A. E., Roden, E. R., Golova, J., Chernov, B., Schipma, M. J., et al. (2006). Suspension array analysis of 16S rRNA from Fe- and SO(4)2- reducing bacteria in uranium-contaminated sediments undergoing bioremediation. *Appl. Environ. Microbiol.* 72, 4672–87. doi:10.1128/AEM.02858-05.

Chin, K.-J., Esteve-Núñez, A., Leang, C., and Lovley, D. R. (2004). Direct correlation between rates of anaerobic respiration and levels of mRNA for key respiratory genes in Geobacter sulfurreducens. *Appl. Environ. Microbiol.* 70, 5183–9. doi:10.1128/AEM.70.9.5183-5189.2004.

Cologgi, D. L., Lampa-Pastirk, S., Speers, A. M., Kelly, S. D., and Reguera, G. (2011). Extracellular reduction of uranium via Geobacter conductive pili as a protective cellular mechanism. *Proc. Natl. Acad. Sci.* doi:10.1073/pnas.1108616108.

Coppi, M. V, Leang, C., Sandler, S. J., and Lovley, D. R. (2001). Development of a genetic system for Geobacter sulfurreducens. *Appl. Environ. Microbiol.* 67, 3180–7. doi:10.1128/AEM.67.7.3180-3187.2001.

Dalla Vecchia, E., Shao, P. P., Suvorova, E., Chiappe, D., Hamelin, R., and Bernier-Latmani, R. (2014a). Characterization of the surfaceome of the metal-reducing bacterium Desulfotomaculum reducens. *Front. Microbiol.* 5, 432. doi:10.3389/fmicb.2014.00432.

Dalla Vecchia, E., Suvorova, E. I., Maillard, J., and Bernier-Latmani, R. (2014b). Fe(III) reduction during pyruvate fermentation by Desulfotomaculum reducens strain MI-1. *Geobiology* 12, 48–61. doi:10.1111/gbi.12067.

Diggle, S. P., Matthijs, S., Wright, V. J., Fletcher, M. P., Chhabra, S. R., Lamont, I. L., et al. (2007). The Pseudomonas aeruginosa 4-quinolone signal molecules HHQ and PQS play multifunctional roles in quorum sensing and iron entrapment. *Chem. Biol.* 14, 87–96. doi:10.1016/j.chembiol.2006.11.014.

Hernandez, M. E., Kappler, A., and Newman, D. K. (2004). Phenazines and Other Redox-Active Antibiotics Promote Microbial Mineral Reduction. *Appl. Environ. Microbiol.* 70, 921–928. doi:10.1128/AEM.70.2.921-928.2004.

Holmes, D. E., Chaudhuri, S. K., Nevin, K. P., Mehta, T., Methé, B. A., Liu, A., et al. (2006). Microarray and genetic analysis of electron transfer to electrodes in Geobacter sulfurreducens. *Environ. Microbiol.* 8, 1805–15. doi:10.1111/j.1462-2920.2006.01065.x.

Holmes, D. E., Nevin, K. P., O'Neil, R. A., Ward, J. E., Adams, L. A., Woodard, T. L., et al. (2005). Potential for quantifying expression of the Geobacteraceae citrate synthase gene to assess the activity of Geobacteraceae in the subsurface and on current-harvesting electrodes. *Appl. Environ. Microbiol.* 71, 6870–7. doi:10.1128/AEM.71.11.6870-6877.2005.

Hori, T., Aoyagi, T., Itoh, H., Narihiro, T., Oikawa, A., Suzuki, K., et al. (2015). Isolation of microorganisms involved in reduction of crystalline iron(III) oxides in natural environments.

Front. Microbiol. 6, 386. doi:10.3389/fmicb.2015.00386.

Huang, D. W., Sherman, B. T., and Lempicki, R. A. (2009a). Bioinformatics enrichment tools: paths toward the comprehensive functional analysis of large gene lists. *Nucleic Acids Res.* 37, 1–13. doi:10.1093/nar/gkn923.

Huang, D. W., Sherman, B. T., and Lempicki, R. A. (2009b). Systematic and integrative analysis of large gene lists using DAVID bioinformatics resources. *Nat. Protoc.* 4, 44–57. doi:10.1038/nprot.2008.211.

Junier, P., Junier, T., Podell, S., Sims, D. R., Detter, J. C., Lykidis, A., et al. (2010). The genome of the Gram-positive metal- and sulfate-reducing bacterium Desulfotomaculum reducens strain MI-1. *Environ. Microbiol.* 12, 2738–2754. doi:10.1111/j.1462-2920.2010.02242.x.

Kaden, J., S Galushko, A., and Schink, B. (2002). Cysteine-mediated electron transfer in syntrophic acetate oxidation by cocultures of Geobacter sulfurreducens and Wolinella succinogenes. *Arch. Microbiol.* 178, 53–8. doi:10.1007/s00203-002-0425-3.

Kanehisa, M., and Goto, S. (2000). KEGG: kyoto encyclopedia of genes and genomes. *Nucleic Acids Res.* 28, 27–30. Available at: http://www.pubmedcentral.nih.gov/articlerender.fcgi?artid=102409&tool=pmcentrez&rendertype=abstract [Accessed July 10, 2014].

Kanehisa, M., Goto, S., Sato, Y., Kawashima, M., Furumichi, M., and Tanabe, M. (2014). Data, information, knowledge and principle: back to metabolism in KEGG. *Nucleic Acids Res.* 42, D199–205. doi:10.1093/nar/gkt1076.

Kato, S., Hashimoto, K., and Watanabe, K. (2012). Microbial interspecies electron transfer via electric currents through conductive minerals. *Proc. Natl. Acad. Sci. U. S. A.* 109, 10042–6. doi:10.1073/pnas.1117592109.

Kim, S., Gupta, N., and Pevzner, P. A. (2008). Spectral probabilities and generating functions of tandem mass spectra: a strike against decoy databases. *J. Proteome Res.* 7, 3354–63. doi:10.1021/pr8001244.

Kim, S.-H., Harzman, C., Davis, J. K., Hutcheson, R., Broderick, J. B., Marsh, T. L., et al. (2012). Genome sequence of Desulfitobacterium hafniense DCB-2, a Gram-positive anaerobe capable of dehalogenation and metal reduction. *BMC Microbiol.* 12, 21. doi:10.1186/1471-2180-12-21.

Klemps, R., Cypionka, H., Widdel, F., and Pfennig, N. (1985). Growth with hydrogen, and further physiological characteristics of Desulfotomaculum species. *Arch. Microbiol.* 143, 203–208. doi:10.1007/BF00411048.

Lange, V., Picotti, P., Domon, B., and Aebersold, R. (2008). Selected reaction monitoring for quantitative proteomics: a tutorial. *Mol. Syst. Biol.* 4, 222. doi:10.1038/msb.2008.61.

Leang, C., Coppi, M. V., and Lovley, D. R. (2003). OmcB, a c-Type Polyheme Cytochrome, Involved in Fe(III) Reduction in Geobacter sulfurreducens. *J. Bacteriol.* 185, 2096–2103. doi:10.1128/JB.185.7.2096-2103.2003.

Leang, C., Qian, X., Mester, T., and Lovley, D. R. (2010). Alignment of the c-Type Cytochrome OmcS along Pili of Geobacter sulfurreducens. *Appl. Environ. Microbiol.* 76, 4080–4084. doi:10.1128/AEM.00023-10.

Lipton, M. S., Paša-Tolić, L., Anderson, G. A., Anderson, D. J., Auberry, D. L., Battista, J. R., et al. (2002). Global analysis of the Deinococcus radiodurans proteome by using accurate mass tags. *Proc. Natl. Acad. Sci.* 99, 11049–11054. doi:10.1073/pnas.172170199.

Liu, Y., Fredrickson, J. K., Zachara, J. M., and Shi, L. (2015). Direct involvement of ombB, omaB, and omcB genes in extracellular reduction of Fe(III) by Geobacter sulfurreducens PCA. *Front. Microbiol.* 6, 1075. doi:10.3389/fmicb.2015.01075.

Liu, Y., Wang, Z., Liu, J., Levar, C., Edwards, M. J., Babauta, J. T., et al. (2014). A trans-outer membrane porin-cytochrome protein complex for extracellular electron transfer by Geobacter sulfurreducens PCA. *Environ. Microbiol. Rep.* 6, 776–85. doi:10.1111/1758-2229.12204.

Lloyd, J. R., Leang, C., Hodges Myerson, A. L., Coppi, M. V, Cuifo, S., Methe, B., et al. (2003). Biochemical and genetic characterization of PpcA, a periplasmic c-type cytochrome in Geobacter sulfurreducens. *Biochem. J.* 369, 153–161. doi:10.1042/BJ20020597.

Lovley, D. R. (1993). Dissimilatory metal reduction. *Annu. Rev. Microbiol.* 47, 263–290. doi:10.1146/annurev.mi.47.100193.001403.

Lovley, D. R. (2012). Electromicrobiology. *Annu. Rev. Microbiol.* 66, 391–409. doi:10.1146/annurev-micro-092611-150104.

Lovley, D. R., Fraga, J. L., Blunt-Harris, E. L., Hayes, L. A., Phillips, E. J. P., and Coates, J. D. (1998). Humic Substances as a Mediator for Microbially Catalyzed Metal Reduction. *Acta Hydrochim. Hydrobiol.* 26, 152–157. doi:10.1002/(SICI)1521-401X(199805)26:3<152::AID-AHEH152>3.0.CO;2-D.

Lovley, D. R., Holmes, D. E., and Nevin, K. P. (2004). "Dissimilatory Fe(III) and Mn(IV) Reduction," in (Academic Press), 219–286. Available at: http://www.sciencedirect.com/science/article/pii/S0065291104490055.

Lovley, D. R., and Phillips, E. J. P. (1987). Rapid Assay for Microbially Reducible Ferric Iron in Aquatic Sediments. *Appl. Environ. Microbiol.* 53, 1536–1540. Available at: http://aem.asm.org/content/53/7/1536.

Lovley, D. R., and Phillips, E. J. P. (1988). Novel Mode of Microbial Energy Metabolism: Organic Carbon Oxidation Coupled to Dissimilatory Reduction of Iron or Manganese. *Appl. Environ. Microbiol.* 54, 1472–1480. Available at: http://www.ncbi.nlm.nih.gov/pmc/articles/PMC202682/.

Lovley, D. R., Ueki, T., Zhang, T., Malvankar, N. S., Shrestha, P. M., Flanagan, K. A., et al. (2011). Geobacter: the microbe electric's physiology, ecology, and practical applications. *Adv. Microb. Physiol.* 59, 1–100. doi:10.1016/B978-0-12-387661-4.00004-5.

Markowitz, V. M., Chen, I.-M. A., Palaniappan, K., Chu, K., Szeto, E., Pillay, M., et al. (2014). IMG 4 version of the integrated microbial genomes comparative analysis system. *Nucleic Acids Res.* 42, D560–7. doi:10.1093/nar/gkt963.

Marsili, E., Baron, D. B., Shikhare, I. D., Coursolle, D., Gralnick, J. A., and Bond, D. R. (2008). Shewanella secretes flavins that mediate extracellular electron transfer. *Proc. Natl. Acad. Sci.* 105, 3968–3973. doi:10.1073/pnas.0710525105.

McGrath, S., Wade, D. S., and Pesci, E. C. (2004). Dueling quorum sensing systems in Pseudomonas aeruginosa control the production of the Pseudomonas quinolone signal

(PQS). *FEMS Microbiol. Lett.* 230, 27–34. doi:10.1016/S0378-1097(03)00849-8.

McKnight, S. L., Iglewski, B. H., and Pesci, E. C. (2000). The Pseudomonas quinolone signal regulates rhl quorum sensing in Pseudomonas aeruginosa. *J. Bacteriol.* 182, 2702–2708. doi:10.1128/JB.182.10.2702-2708.2000.

Newsome, L., Morris, K., and Lloyd, J. R. (2014). The biogeochemistry and bioremediation of uranium and other priority radionuclides. *Chem. Geol.* 363, 164–184. Available at: http://www.sciencedirect.com/science/article/pii/S0009254113004907 [Accessed December 3, 2013].

Otwell, A. E., Callister, S. J., Zink, E. M., Smith, R. D., and Richardson, R. E. (2016). Comparative Proteomic Analysis of Desulfotomaculum reducens MI-1: Insights into the Metabolic Versatility of a Gram-positive Sulfate and Metal-reducing Bacterium. *Front. Microbiol.* 7. doi:10.3389/fmicb.2016.00191.

Otwell, A. E., Sherwood, R. W., Zhang, S., Nelson, O. D., Li, Z., Lin, H., et al. (2015). Identification of proteins capable of metal reduction from the proteome of the Gram-positive bacterium Desulfotomaculum reducens MI-1 using an NADH-based activity assay. *Environ. Microbiol.* 17, 1977–1990. doi:10.1111/1462-2920.12673.

Petrie, L., North, N. N., Dollhopf, S. L., Balkwill, D. L., and Kostka, J. E. (2003). Enumeration and Characterization of Iron(III)-Reducing Microbial Communities from Acidic Subsurface Sediments Contaminated with Uranium(VI). *Appl. Environ. Microbiol.* 69, 7467–7479. doi:10.1128/AEM.69.12.7467-7479.2003.

Polpitiya, A. D., Qian, W.-J., Jaitly, N., Petyuk, V. A., Adkins, J. N., Camp, D. G., et al. (2008). DAnTE: a statistical tool for quantitative analysis of -omics data. *Bioinformatics* 24, 1556–8. doi:10.1093/bioinformatics/btn217.

Qian, X., Mester, T., Morgado, L., Arakawa, T., Sharma, M. L., Inoue, K., et al. (2011). Biochemical characterization of purified OmcS, a c-type cytochrome required for insoluble Fe(III) reduction in Geobacter sulfurreducens. *Biochim. Biophys. Acta - Bioenerg.* 1807, 404–412. doi:10.1016/j.bbabio.2011.01.003.

Reguera, G., McCarthy, K. D., Mehta, T., Nicoll, J. S., Tuominen, M. T., and Lovley, D. R. (2005). Extracellular electron transfer via microbial nanowires. *Nature* 435, 1098–1101. doi:10.1038/nature03661.

Reguera, G., Pollina, R.B., Nicoll, J.S., Lovley, D.R. (2006). Possible Nonconductive Role of Geobacter sulfurreducens Pilus Nanowires in Biofilm Formation. *J. Bacteriol.* March 2007 vol. 189 no. 5 2125-2127.

Robidart, J., Callister, S. J., Song, P., Nicora, C. D., Wheat, C. G., and Girguis, P. R. (2013). Characterizing microbial community and geochemical dynamics at hydrothermal vents using osmotically driven continuous fluid samplers. *Environ. Sci. Technol.* 47, 4399–407. doi:10.1021/es3037302.

Rotaru, A.-E., Shrestha, P. M., Liu, F., Markovaite, B., Chen, S., Nevin, K. P., et al. (2014a). Direct interspecies electron transfer between Geobacter metallireducens and Methanosarcina barkeri. *Appl. Environ. Microbiol.* 80, 4599–605. doi:10.1128/AEM.00895-14.

Rotaru, A.-E., Shrestha, P. M., Liu, F., Shrestha, M., Shrestha, D., Embree, M., et al. (2014b). A

new model for electron flow during anaerobic digestion: direct interspecies electron transfer to Methanosaeta for the reduction of carbon dioxide to methane. *Energy Environ. Sci.* 7, 408–415. doi:10.1039/C3EE42189A.

Rotaru, A.-E., Shrestha, P. M., Liu, F., Ueki, T., Nevin, K., Summers, Z. M., et al. (2012). Interspecies electron transfer via hydrogen and formate rather than direct electrical connections in cocultures of Pelobacter carbinolicus and Geobacter sulfurreducens. *Appl. Environ. Microbiol.* 78, 7645–51. doi:10.1128/AEM.01946-12.

Rowe, A. R., Heavner, G. L., Mansfeldt, C. B., Werner, J. J., and Richardson, R. E. (2012). Relating chloroethene respiration rates in Dehalococcoides to protein and mRNA biomarkers. *Environ. Sci. Technol.* 46, 9388–97. doi:10.1021/es300996c.

Rowe, A. R., Mansfeldt, C. B., Heavner, G. L., and Richardson, R. E. (2015). Relating mRNA and protein biomarker levels in a Dehalococcoides and Methanospirillum-containing community. *Appl. Microbiol. Biotechnol.* 99, 2313–27. doi:10.1007/s00253-014-6220-7.

Santos, T. C., Silva, M. A., Morgado, L., Dantas, J. M., and Salgueiro, C. A. (2015). Diving into the redox properties of Geobacter sulfurreducens cytochromes: a model for extracellular electron transfer. *Dalton Trans.* 44, 9335–44. doi:10.1039/c5dt00556f.

Sharma, S., Cavallaro, G., and Rosato, A. (2010a). A systematic investigation of multiheme c-type cytochromes in prokaryotes. *JBIC J. Biol. Inorg. Chem.* 15, 559–571. doi:10.1007/s00775-010-0623-4.

Sharma, S., Cavallaro, G., and Rosato, A. (2010b). A systematic investigation of multiheme c-type cytochromes in prokaryotes. *J. Biol. Inorg. Chem. JBIC a Publ. Soc. Biol. Inorg. Chem.* 15, 559–571. doi:10.1007/s00775-010-0623-4.

Shi, L., Squier, T. C., Zachara, J. M., and Fredrickson, J. K. (2007). Respiration of metal (hydr)oxides by Shewanella and Geobacter: a key role for multihaem c-type cytochromes. *Mol. Microbiol.* 65, 12–20. doi:10.1111/j.1365-2958.2007.05783.x.

Shrestha, P. M., Rotaru, A.-E., Aklujkar, M., Liu, F., Shrestha, M., Summers, Z. M., et al. (2013a). Syntrophic growth with direct interspecies electron transfer as the primary mechanism for energy exchange. *Environ. Microbiol. Rep.* 5, 904–10. doi:10.1111/1758-2229.12093.

Shrestha, P. M., Rotaru, A.-E., Summers, Z. M., Shrestha, M., Liu, F., and Lovley, D. R. (2013b). Transcriptomic and genetic analysis of direct interspecies electron transfer. *Appl. Environ. Microbiol.* 79, 2397–404. doi:10.1128/AEM.03837-12.

Smatlak, C. R., Gossett, J. M., and Zinder, S. H. (1996). Comparative Kinetics of Hydrogen Utilization for Reductive Dechlorination of Tetrachloroethene and Methanogenesis in an Anaerobic Enrichment Culture. *Environ. Sci. Technol.* 30, 2850–2858. doi:10.1021/es9602455.

Smith, J. A., Nevin, K. P., and Lovley, D. R. (2015). Syntrophic growth via quinone-mediated interspecies electron transfer. *Front. Microbiol.* 6, 121. doi:10.3389/fmicb.2015.00121.

Sowell, S. M., Norbeck, A. D., Lipton, M. S., Nicora, C. D., Callister, S. J., Smith, R. D., et al. (2008). Proteomic analysis of stationary phase in the marine bacterium "Candidatus Pelagibacter ubique". *Appl. Environ. Microbiol.* 74, 4091–100. doi:10.1128/AEM.00599-08.

Stanley, J. R., Adkins, J. N., Slysz, G. W., Monroe, M. E., Purvine, S. O., Karpievitch, Y. V, et

al. (2011). A statistical method for assessing peptide identification confidence in accurate mass and time tag proteomics. *Anal. Chem.* 83, 6135–40. doi:10.1021/ac2009806.

Summers, Z. M., Fogarty, H. E., Leang, C., Franks, A. E., Malvankar, N. S., and Lovley, D. R. (2010). Direct exchange of electrons within aggregates of an evolved syntrophic coculture of anaerobic bacteria. *Science* 330, 1413–5. doi:10.1126/science.1196526.

Suzuki, Y., Kelly, S. D., Kemner, K. M., and Banfield, J. F. (2004). Enzymatic U(VI) reduction by Desulfosporosinus species. *Radiochim. Acta* 92, 11–16. doi:10.1524/ract.92.1.11.25404.

Tebo, B. M., and Obraztsova, A. Y. (1998). Sulfate-reducing bacterium grows with Cr(VI), U(VI), Mn(IV), and Fe(III) as electron acceptors. *FEMS Microbiol. Lett.* 162, 193–198. doi:10.1111/j.1574-6968.1998.tb12998.x.

Vargas, M., Malvankar, N. S., Tremblay, P.-L., Leang, C., Smith, J. A., Patel, P., et al. (2013). Aromatic Amino Acids Required for Pili Conductivity and Long-Range Extracellular Electron Transport in Geobacter sulfurreducens. *MBio* 4. doi:10.1128/mBio.00105-13.

Wall, J. D., and Krumholz, L. R. (2006). Uranium reduction. *Annu. Rev. Microbiol.* 60, 149–166. doi:10.1146/annurev.micro.59.030804.121357.

Wang, Y., Yang, F., Gritsenko, M. A., Wang, Y., Clauss, T., Liu, T., et al. (2011). Reversed-phase chromatography with multiple fraction concatenation strategy for proteome profiling of human MCF10A cells. *Proteomics* 11, 2019–26. doi:10.1002/pmic.201000722.

Weber, K. A., Achenbach, L. A., and Coates, J. D. (2006). Microorganisms pumping iron: anaerobic microbial iron oxidation and reduction. *Nat. Rev. Microbiol.* 4, 752–64. doi:10.1038/nrmicro1490.

Werner, J. J., Ptak, A. C., Rahm, B. G., Zhang, S., and Richardson, R. E. (2009). Absolute quantification of Dehalococcoides proteins: enzyme bioindicators of chlorinated ethene dehalorespiration. *Environ. Microbiol.* 11, 2687–2697. doi:10.1111/j.1462-2920.2009.01996.x.

Wilkins, M. J., Callister, S. J., Miletto, M., Williams, K. H., Nicora, C. D., Lovley, D. R., et al. (2011). Development of a biomarker for Geobacter activity and strain composition; Proteogenomic analysis of the citrate synthase protein during bioremediation of U(VI). *Microb. Biotechnol.* 4, 55–63. doi:10.1111/j.1751-7915.2010.00194.x.

Williamson, A. J., Morris, K., Shaw, S., Byrne, J. M., Boothman, C., and Lloyd, J. R. (2013). Microbial reduction of Fe(III) under alkaline conditions relevant to geological disposal. *Appl. Environ. Microbiol.* 79, 3320–6. doi:10.1128/AEM.03063-12.

Wrighton, K. C., Thrash, J. C., Melnyk, R. A., Bigi, J. P., Byrne-Bailey, K. G., Remis, J. P., et al. (2011). Evidence for direct electron transfer by a gram-positive bacterium isolated from a microbial fuel cell. *Appl. Environ. Microbiol.* 77, 7633–9. doi:10.1128/AEM.05365-11.

Zhang, P., Wu, W.-M., Van Nostrand, J. D., Deng, Y., He, Z., Gihring, T., et al. (2015). Dynamic Succession of Groundwater Functional Microbial Communities in Response to Emulsified Vegetable Oil Amendment during Sustained In Situ U(VI) Reduction. *Appl. Environ. Microbiol.* 81, 4164–72. doi:10.1128/AEM.00043-15.

Supplementary Figures and Tables

Supplementary Figure 6.1: Concentration of yeast extract in culture medium was reduced 10X from previously reported *D. reducens* cultivation conditions. Reducing yeast extract (YE) concentration from 0.3 g/L to 0.05 g/L did not significantly impact growth or Fe(III) reduction by *D. reducens*. Accordingly, 0.05 g/L concentration of yeast extract was selected for co-culture medium. Lack of significant growth or Fe(III) reduction by *G. sulfurreducens* on cultivation conditions selected for co-culture growth was confirmed.

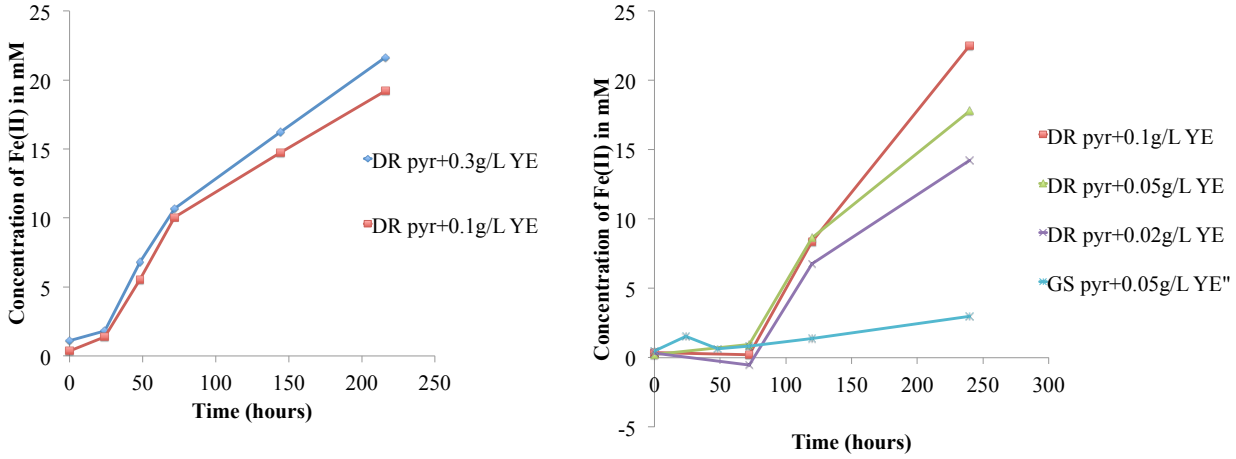

Supplementary Figure 6.2: Normalization of peptide ion intensity was performed in order to account for systematic differences in biomass when comparing each co-culture organism to their pure culture growth condition. Abundances of peptides were $\log_2$ transformed and normalized to a common central tendency (mean). Average peptide ion intensity data prior to normalization is displayed in **a**, while **b** shows data following normalization. Red color refers to average peptide ion intensity for replicates of *D. reducens* co-culture proteomes, green refers to *G. sulfurreducens* co-culture proteomes, blue refers to *D. reducens* pure culture proteomes, and purple refers to the *G. sulfurreducens* pure cultures proteome.

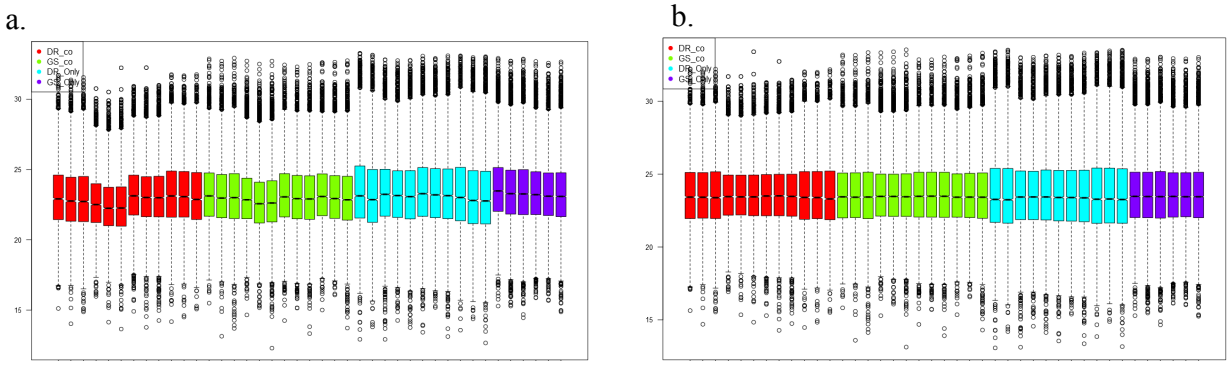

Supplementary Figure 6.3: Powder X-ray diffraction identifies the precipitate formed during *D. reducens* pure culture growth (top) and *G. sulfurreducens-D. reducens* co-culture growth (middle) to be vivianite, a crystalline Fe(II)-phosphate-hydrate, ($Fe_3(PO_4)_2 \cdot 8H_2O$). The reference PDF pattern (#01-079-1928) is shown in the bottom panel.

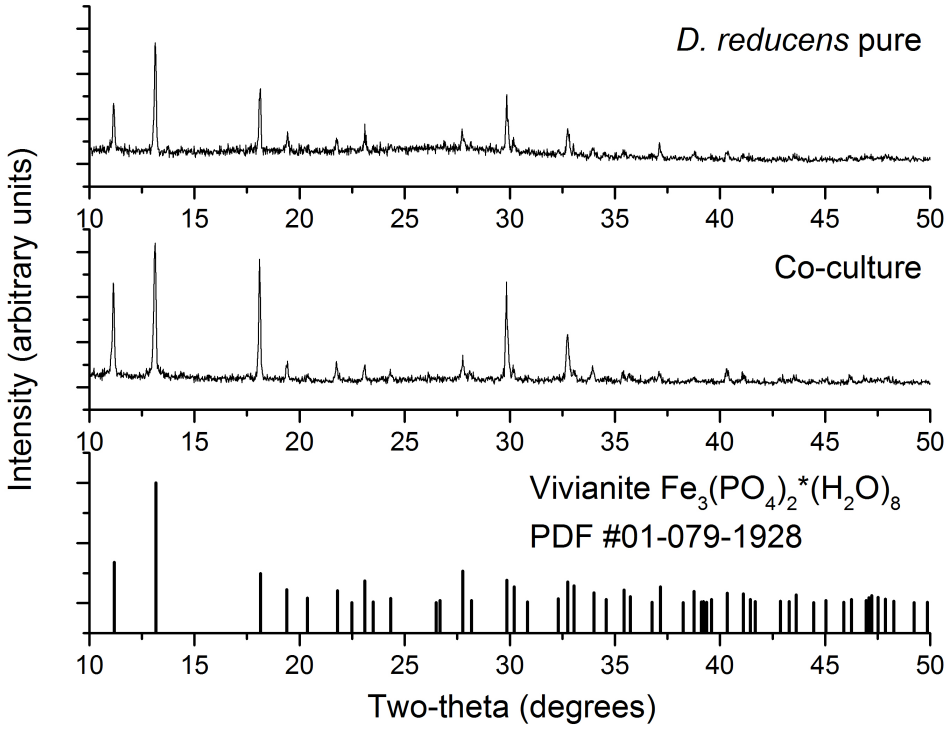

Supplementary Figure 6.4: Enhanced biofilm phenotype is observed in the *D. reducens*-*G. sulfurreducens* co-culture. In the co-culture, biofilm formation is observed after 1-2 days of growth on Fe(III)-oxide (~5 mM Fe(II) produced). In *G. sulfurreducens* pure cultures, a biofilm is observed much later in the growth phase, when >20 mM Fe(II) is produced. Biofilm formation is not observed for *D. reducens* cells reducing Fe(III)-oxide in pure culture. **Figure 6.2b** displays a representative Fe(III) reduction growth curve for the Fe(III)-oxide cultivation condition.

1. **Co-culture**
2. ***Desulfotomaculum reducens* pure**
3. ***Geobacter sulfurreducens* pure**

Supplementary Figure 6.5: Utilization of acetate and hydrogen by *G. sulfurreducens* pure cultures. Cultures were given 20 mM acetate and 7.5 mM hydrogen. Disappearance of each potential electron donor for *G. sulfurreducens* is displayed throughout the growth phase.

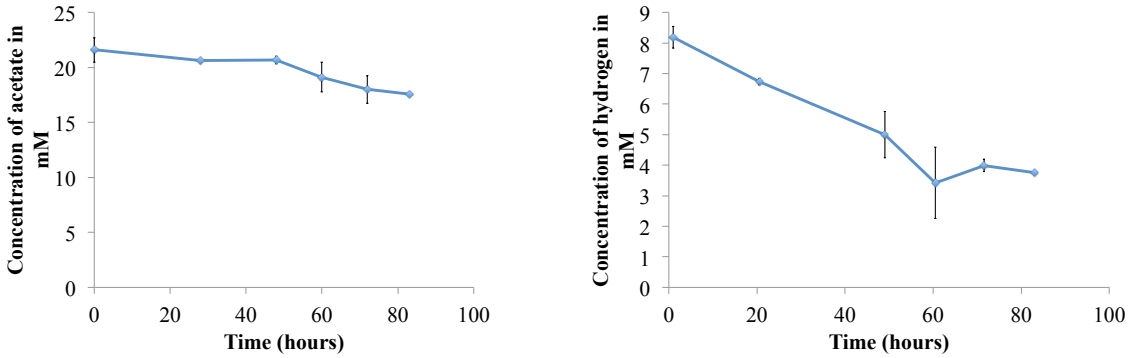

Supplementary Figure 6.6: Heat maps of a) *G. sulfurreducens* proteins identified in co-culture and pure culture proteomes and b) *D. reducens* proteins identified in co-culture and pure culture proteomes. All biological duplicates and technical triplicates cluster tightly together. The heatmap command in R was used in order to represent relatedness of the proteomes of *D. reducens* analyzed based on hierarchical clustering (R Core Team (2012). R: A language and environment for statistical computing. R Foundation for Statistical Computing, Vienna, Austria ISBN 3-900051-07-0, URL http://www.R-project.org/). Data input for each replicate consisted of the average ion intensity for all proteins observed, and data for all detected peptides was included.

a.

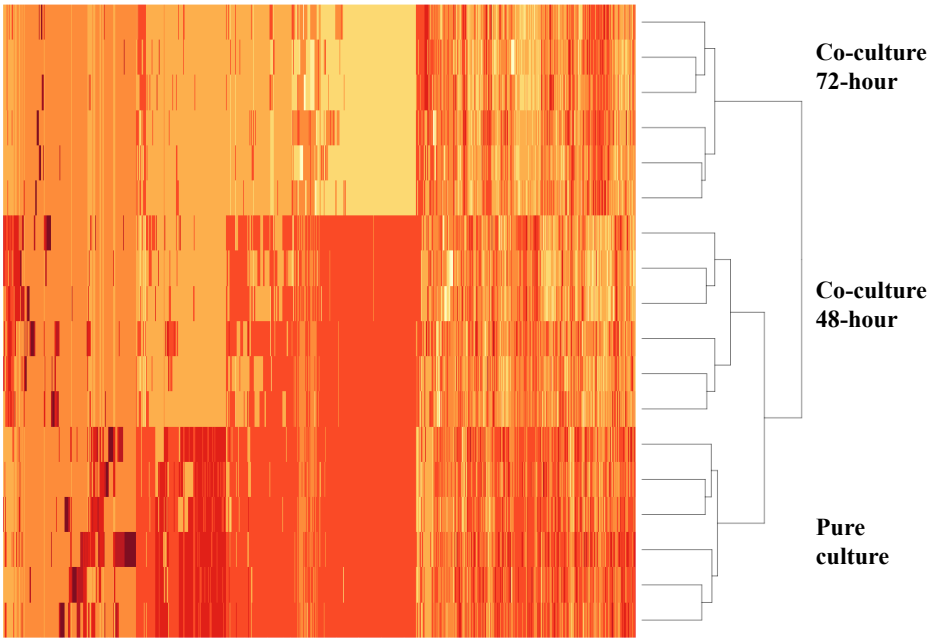

b.

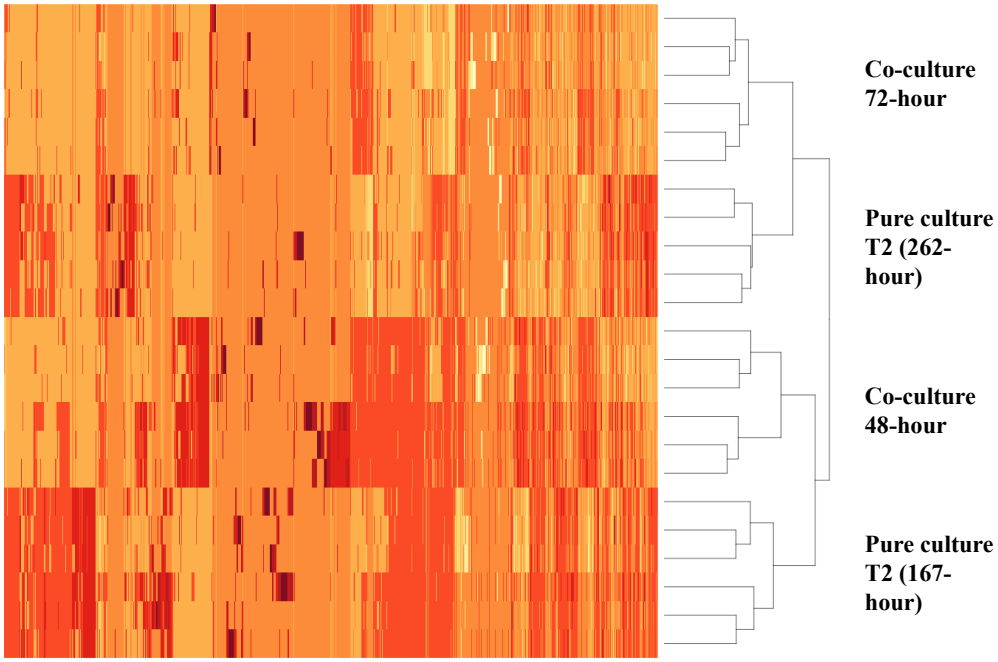
Co-culture 72-hour
Pure culture T2 (262-hour)
Co-culture 48-hour
Pure culture T2 (167-hour)

Supplementary Figure 6.7: *D. reducens* proteins putatively involved in central metabolic pathways, including glycolysis/gluconeogenesis, are enriched in the pure culture proteome relative to the co-culture proteome.
Enrichment analysis (DAVID, Huang et al., 2009a, 2009b) revealed significant enrichment of *D. reducens* proteins involved in central metabolic pathways during pure culture growth relative to co-culture growth. *D. reducens* proteins putatively involved in glycolysis/gluconeogensis that were significantly increased proteins during pure culture growth (including those increased >2-fold, p <0.01 and those exclusively identified) are displayed with stars. The pathway is from KEGG (Kanehisa and Goto, 2000; Kanehisa et al., 2014)
Blue=enriched in pure culture relative to both co-culture timepoints.
Purple=enriched in pure culture relative to co-culture 72-hour timepoint only.
References:
Huang, D. W., Sherman, B. T., and Lempicki, R. A. (2009a). Bioinformatics enrichment tools: paths toward the comprehensive functional analysis of large gene lists. Nucleic Acids Res. 37, 1–13. doi:10.1093/nar/gkn923.
Huang, D. W., Sherman, B. T., and Lempicki, R. A. (2009b). Systematic and integrative analysis of large gene lists using DAVID bioinformatics resources. Nat. Protoc. 4, 44–57. doi:10.1038/nprot.2008.211.
Kanehisa, M., and Goto, S. (2000). KEGG: kyoto encyclopedia of genes and genomes. *Nucleic Acids Res.* 28, 27–30.
Kanehisa, M., Goto, S., Sato, Y., Kawashima, M., Furumichi, M., and Tanabe, M. (2014). Data, information, knowledge and principle: back to metabolism in KEGG. *Nucleic Acids Res.* 42, D199–205. doi:10.1093/nar/gkt1076.

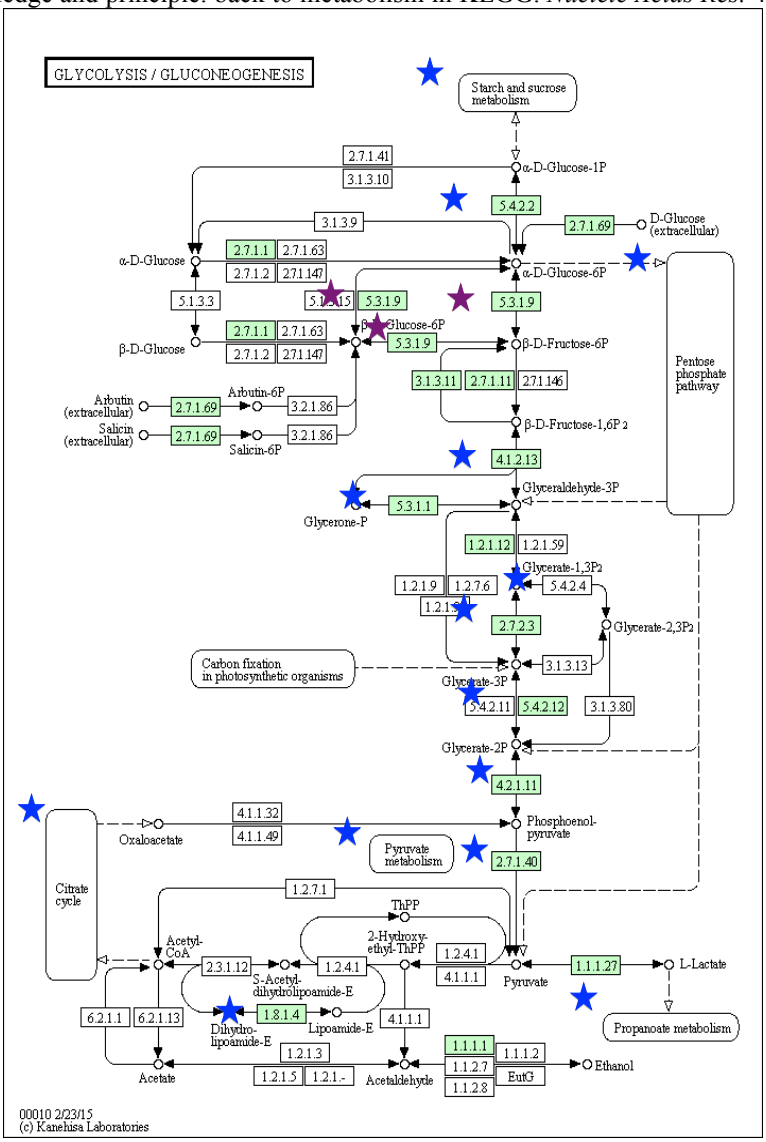

Supplementary Figure 6.8: Comparison of proteomic ratios of biomarkers derived from Multiple Reaction Monitoring (MRM) versus AMT tag proteomic analysis. A positive correlation is observed between the two methods of proteomic analysis. Data plotted in this figure is displayed in **Table 6.3**.

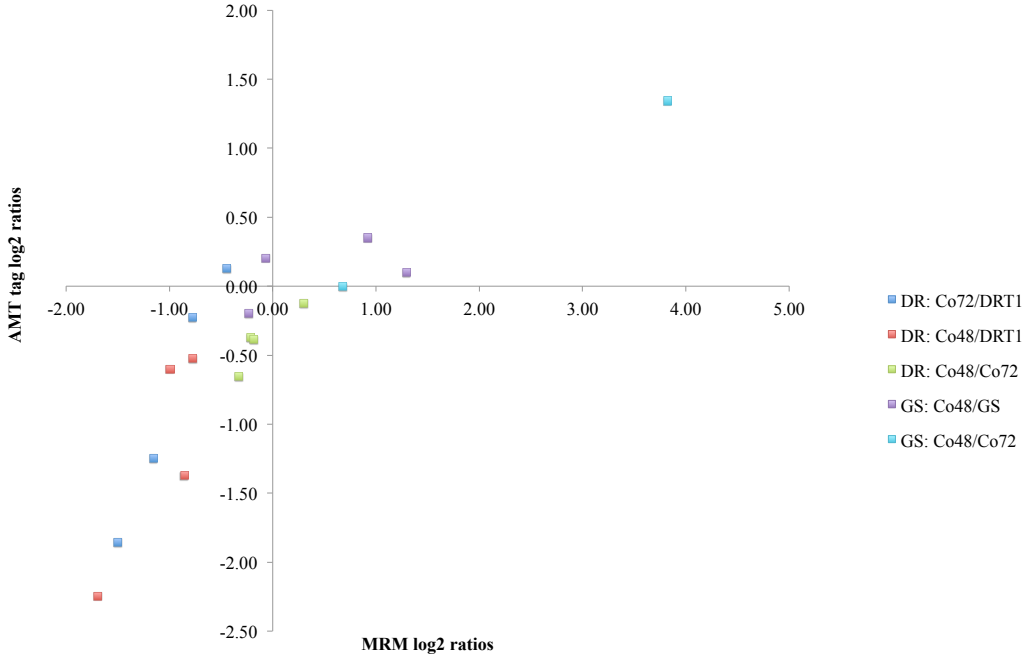

Supplementary Table 6.1a: *G. sulfurreducens* proteins significantly increased and decreased during co-culture growth relative to pure culture growth

Locus Tag	Description	CoC/Pure (log2)	p-value
GSU3402	hypothetical protein	3.21	<0.01
GSU0489	competence ATPase ComM	2.69	<0.01
GSU1496	hypothetical protein	2.64	<0.01
GSU3378	glutamate--ammonia ligase adenylyltransferase	2.48	0.02
GSU1213	hypothetical protein	2.47	<0.01
GSU1710	integrase family protein	2.45	<0.01
GSU1398	SCO family protein	2.44	<0.01
GSU2360	maltooligosyl trehalose synthase	2.09	0.03
GSU3305	hypothetical protein	1.97	<0.01
GSU1283	NosL family protein	1.81	<0.01
GSU2038	type IV pilus assembly protein PilY	1.80	<0.01
GSU2936	hypothetical protein	1.77	<0.01
GSU0184	HAD superfamily hydrolase	1.77	0.02
GSU3151	hypothetical protein	1.70	<0.01
GSU1408	MRP-like NifH superfamily NTPase	1.69	<0.01
GSU1996	cytochrome c	1.61	<0.01
GSU2850	50S ribosomal protein L16	1.51	<0.01
GSU2200	hypothetical protein	1.44	<0.01
GSU1337	lipoprotein	1.42	<0.01
GSU3130	lipoprotein	1.41	<0.01
GSU1394	laccase family multicopper oxidase	1.39	<0.01
GSU3612	30S ribosomal protein S12	1.38	0.01
GSU1735	branched-chain amino acid ABC transporter substrate-binding protein	1.38	<0.01
GSU2055	TRAP proton/solute symporter, periplasmic substrate-binding protein	1.35	<0.01
GSU1876	hypothetical protein	1.28	<0.01
GSU1497	hypothetical protein	1.26	<0.01
GSU0800	amino acid ABC transporter substrate-binding protein	1.21	<0.01
GSU2028	type IV pilus secretin lipoprotein PilQ	1.21	<0.01
GSU2496	hypothetical protein	1.17	<0.01
GSU1178	succinate dehydrogenase/fumarate reductase iron-sulfur subunit	1.15	<0.01
GSU2493	NHL repeat domain-containing protein	1.14	<0.01
GSU2731	lipoprotein cytochrome c	1.13	<0.01
GSU3606	response receiver CheY associated with MCPs of classes 40H and 40+24H	1.13	0.05
GSU0454	1,4-dihydroxy-6-naphthoate synthase	1.10	<0.01
GSU1734	branched-chain amino acid ABC transporter substrate-binding protein	1.10	<0.01
GSU3406	polar amino acid/opine ABC transportersubstrate-binding protein	1.09	<0.01
GSU2853	30S ribosomal protein S19	1.07	0.01
GSU2551	LysM domain-containing protein	1.07	<0.01
GSU2035	type IV pilus minor pilin PilW	1.06	<0.01
GSU0317	hypothetical protein	1.05	<0.01
GSU1239	glutamate synthase	1.05	0.04
GSU3298	transcriptional regulator	1.02	<0.01

GSU2742	hypothetical protein	1.02	<0.01
GSU1002	amidohydrolase	1.01	<0.01
GSU2743	cytochrome c, 1 heme-binding site	1.00	<0.01
GSU3280	thioredoxin-like protein disulfide reductase	1.00	<0.01
GSU2713	hypothetical protein	1.00	<0.01
GSU1220	response regulator, GspIIEN domain-containing	-1.00	0.01
GSU1698	hypothetical protein GSU1698	-1.00	<0.01
GSU0270	glucosamine--fructose-6-phosphate aminotransferase	-1.00	<0.01
GSU1198	D-3-phosphoglycerate dehydrogenase	-1.00	<0.01
GSU2089	rod shape-determining protein MreB	-1.00	<0.01
GSU2086	hypothetical protein GSU2086	-1.00	<0.01
GSU0146	twitching motility pilus retraction protein	-1.01	0.03
GSU0465	elongation factor P	-1.01	<0.01
GSU0074	isoprenoid biosynthesis protein	-1.01	0.01
GSU1594	zinc-dependent peptidase	-1.03	0.01
GSU2075	subtilase family serine protease	-1.03	0.02
GSU2433	ATP-dependent protease	-1.03	<0.01
GSU2875	30S ribosomal protein S9	-1.04	<0.01
GSU1705	3-methyl-2-oxobutanoate hydroxymethyltransferase	-1.04	<0.01
GSU0486	threonine dehydratase	-1.05	<0.01
GSU0306	hydrogenase maturation protein HypF	-1.05	0.01
GSU3069	undecaprenyldiphospho-muramoylpentapeptide beta-N-acetylglucosaminyltransferase	-1.05	<0.01
GSU1812	arginyl-tRNA ligase	-1.06	<0.01
GSU1866	PhoH-related ATPase	-1.07	<0.01
GSU2718	bidirectional NAD-reducing hydrogenase, large subunit	-1.07	<0.01
GSU1626	GntR family transcriptional regulator	-1.07	<0.01
GSU1802	ATP-binding protein YjeF	-1.08	<0.01
GSU2602	integration host factor subunit beta	-1.09	<0.01
GSU0332	multifunctional aminopeptidase A	-1.09	<0.01
GSU2012	nitrogen fixation iron-sulfur cluster assembly protein NifU	-1.09	<0.01
GSU1120	response receiver	-1.10	0.01
GSU0666	30S ribosomal protein S18	-1.10	<0.01
GSU1243	phosphopantetheine adenylyltransferase	-1.10	<0.01
GSU1681	BioD and DRTGG domain-containing protein	-1.11	<0.01
GSU3266	ATP-dependent DNA helicase, PcrA/UvrD/Rep family	-1.11	<0.01
GSU2243	UDP-N-acetylglucosamine 2-epimerase	-1.12	0.01
GSU2835	methionine aminopeptidase	-1.12	<0.01
GSU0384	ferritin-like domain-containing protein	-1.12	<0.01
GSU0933	uracil phosphoribosyltransferase	-1.13	0.01
GSU0305	hydrogenase nickel incorporation protein HypB	-1.13	<0.01
GSU0129	polypeptide formylmethionine deformylase	-1.13	<0.01
GSU2082	nucleoside diphosphate-sugar dehydratase	-1.13	<0.01
GSU0990	hypothetical protein GSU0990	-1.14	<0.01
GSU0535	cysteine synthase A	-1.15	<0.01
GSU1999	RNA-binding protein Hfq	-1.15	0.04
GSU2847	50S ribosomal protein L14	-1.15	<0.01

GSU3003	hypothetical protein GSU3003	-1.15	<0.01
GSU0651	nitrilase/amidohydrolase superfamily protein, class 8	-1.15	<0.01
GSU0151	acetylornithine aminotransferase	-1.16	<0.01
GSU1629	glyceraldehyde-3-phosphate dehydrogenase, type I	-1.16	<0.01
GSU3519	cold shock DNA/RNA-binding protein	-1.16	0.05
GSU0150	acetylglutamate kinase	-1.16	<0.01
GSU2565	sensor histidine kinase	-1.16	<0.01
GSU3374	ribulose-phosphate 3-epimerase	-1.16	<0.01
GSU1934	pantothenate kinase	-1.16	<0.01
GSU1859	2-oxoacid:ferredoxin oxidoreductase subunit gamma	-1.17	<0.01
GSU3007	adenosylcobalamin-5\'-phosphate phosphatase	-1.17	0.01
GSU1376	hypothetical protein GSU1376	-1.18	<0.01
GSU0133	hypothetical protein GSU0133	-1.18	<0.01
GSU3066	D-alanine--D-alanine ligase	-1.18	<0.01
GSU3447	peroxiredoxin, 1-Cys subfamily	-1.19	0.01
GSU0033	molecular chaperone DnaK	-1.20	<0.01
GSU0090	heterodisulfide oxidoreductase, FAD-binding and iron-sulfur cluster-binding subunit A	-1.21	0.01
GSU0945	cystathionine gamma-synthase/beta-lyase	-1.21	0.01
GSU1801	hypothetical protein GSU1801	-1.22	<0.01
GSU1090	response receiver	-1.22	<0.01
GSU2002	FAD-dependent pyridine nucleotide-disulfide oxidoreductase family protein	-1.22	<0.01
GSU0977	hypothetical protein GSU0977	-1.22	<0.01
GSU3408	L-threonine aldolase	-1.22	<0.01
GSU1048	SEC-C motif domain-containing protein	-1.23	0.02
GSU0914	ATP-dependent RNA helicase RhlE	-1.23	0.03
GSU3209	hypothetical protein GSU3209	-1.23	<0.01
GSU1804	pyridoxine 5\'-phosphate synthase	-1.24	<0.01
GSU0159	dihydrodipicolinate synthase	-1.25	<0.01
GSU1896	3-deoxy-manno-octulosonate cytidylyltransferase	-1.26	<0.01
GSU0229	long-chain-fatty-acid--CoA ligase	-1.26	<0.01
GSU3213	GTPase CgtA	-1.27	0.01
GSU2536	dienelactone hydrolase family protein	-1.27	0.01
GSU1915	1-deoxy-D-xylulose 5-phosphate reductoisomerase	-1.28	<0.01
GSU0308	hydrogenase expression/formation protein HypD	-1.28	<0.01
GSU0453	futalosine hydrolase	-1.29	0.01
GSU0032	heat shock protein GrpE	-1.31	0.01
GSU2106	PglZ domain-containing protein	-1.32	<0.01
GSU1885	HPr kinase/phosphorylase	-1.32	0.05
GSU1755	dihydroorotate dehydrogenase 1B	-1.32	<0.01
GSU0197	short-chain dehydrogenase	-1.32	<0.01
GSU1589	ribosome-binding factor A	-1.33	<0.01
GSU2888	anaerobic magnesium-protoporphyrin IX monomethyl ester oxidative cyclase-like protein	-1.34	<0.01
GSU0094	DNA polymerase III subunits gamma and tau	-1.34	0.06
GSU1531	phosphoribosyl-AMP cyclohydrolase	-1.35	<0.01
GSU1119	response receiver histidine kinase	-1.35	<0.01
GSU3100	bifunctional histidinal dehydrogenase/ histidinol dehydrogenase	-1.36	0.01
GSU2264	UDP-N-acetylglucosamine acyltransferase	-1.37	<0.01
GSU1371	NADPH-dependent enal/enone/nitroreductase, Oye family	-1.37	<0.01
GSU1436	hypothetical protein GSU1436	-1.37	<0.01

GSU1328	hypothetical protein GSU1328	-1.38	<0.01
GSU1818	cofactor-independent phosphoglycerate mutase	-1.38	<0.01
GSU2854	50S ribosomal protein L2	-1.38	<0.01
GSU3158	cysteine synthase B	-1.38	<0.01
GSU1691	6,7-dimethyl-8-ribityllumazine synthase	-1.39	<0.01
GSU1467	2-oxoglutarate:ferredoxin oxidoreductase, ferredoxin subunit	-1.39	<0.01
GSU3339	co-chaperonin GroES	-1.39	<0.01
GSU2306	5-carboxyamino-1-(5-phosphoribosyl)imidazole carboxymutase	-1.40	<0.01
GSU2087	phosphoheptose isomerase	-1.40	<0.01
GSU0442	dehypoxanthinylfutalosine cyclase	-1.40	<0.01
GSU2237	DNA-directed RNA polymerase subunit omega	-1.40	0.02
GSU0658	ATP-dependent chaperone ClpB	-1.42	<0.01
GSU0777	periplasmically oriented, membrane-bound formate dehydrogenase, major subunit, selenocysteine-containing	-1.43	<0.01
GSU3465	tRNA modification GTPase TrmE	-1.43	0.03
GSU2427	hypothetical protein GSU2427	-1.43	0.01
GSU3411	ATP-dependent DNA helicase PcrA	-1.43	<0.01
GSU2011	nitrogen fixation iron-sulfur cluster assembly cysteine desulfurase NifS	-1.44	<0.01
GSU0890	NAD-dependent DNA ligase	-1.46	<0.01
GSU3147	molybdopterin nucleotidyltransferase and molybdopterin-guanine dinucleotide biosynthesis protein MobB	-1.47	0.04
GSU2436	pyruvate dehydrogenase E1 component subunit beta	-1.48	0.02
GSU3138	response receiver histidine kinase	-1.48	<0.01
GSU2465	metal-dependent hydrolase	-1.48	<0.01
GSU1883	phosphotransferase system, mannose-type, protein IIA	-1.50	<0.01
GSU1585	hypothetical protein GSU1585	-1.50	<0.01
GSU2992	cobalt-precorrin-3 C17-methyltransferase and adenosylcobyric acid synthase	-1.51	<0.01
GSU1884	glmZ(sRNA)-inactivating NTPase	-1.52	<0.01
GSU0547	DNA mismatch repair ATPase MutS-2	-1.55	<0.01
GSU3157	alpha/beta fold family hydrolase	-1.56	<0.01
GSU1156	asparaginyl-tRNA ligase	-1.57	<0.01
GSU1891	response receiver-modulated cyclic diguanylate phosphodiesterase	-1.58	0.01
GSU2923	glutamate racemase	-1.58	<0.01
GSU2198	(dimethylallyl)adenosine tRNA methylthiotransferase	-1.58	0.01
GSU2683	2-dehydropantoate 2-reductase	-1.59	<0.01
GSU2309	metal-dependent hydrolase	-1.60	<0.01
GSU3162	L-allo-threonine aldolase, stereospecific	-1.61	0.03
GSU2844	30S ribosomal protein S14	-1.62	0.01
GSU2848	30S ribosomal protein S17	-1.64	<0.01
GSU0012	protoporphyrinogen oxidase	-1.65	<0.01
GSU0006	NAD(P)H-dependent glycerol-3-phosphate dehydrogenase	-1.66	<0.01
GSU3145	molybdopterin sulfurtransferase	-1.67	<0.01
GSU2839	50S ribosomal protein L30	-1.71	<0.01
GSU3456	polypeptide formylmethionine deformylase	-1.74	<0.01
GSU0084	hypothetical protein GSU0084	-1.74	0.03
GSU1116	GAF domain-containing protein	-1.76	<0.01
GSU1583	dethiobiotin synthetase	-1.77	<0.01
GSU2246	bifunctional UDP-N-acetylglucosamine 4,6-dehydratase/UDP-2-acetamido-2,6-dideoxy-alpha-D-xylo-4-hexulose 5-epimerase	-1.77	<0.01

GSU3085	dimetal-binding protein YqfO	-1.78	<0.01
GSU2014	hypothetical protein GSU2014	-1.78	0.02
GSU0106	chromosome partitioning ATPase Soj	-1.83	<0.01
GSU2093	ABC transporter ATP-binding protein	-1.87	<0.01
GSU1263	RNA-binding protein YhbY	-1.89	0.01
GSU1128	acyl-CoA thioesterase	-1.90	0.01
GSU1741	pppGpp 5\'-phosphohydrolase and exopolyphosphatase	-1.93	0.01
GSU0934	hypothetical protein GSU0934	-2.06	<0.01
GSU0534	helix-turn-helix iron-sulfur cluster-binding transcriptional regulator IscR	-2.20	<0.01
GSU3383	aspartyl/glutamyl-tRNA amidotransferase subunit C	-2.22	<0.01
GSU1209	hypothetical protein GSU1209	-2.35	<0.01
GSU0088	heterodisulfide oxidoreductase, iron-sulfur cluster-binding subunit D	-2.38	0.03
GSU0095	YbaB/EbfC family DNA-binding protein	-2.90	<0.01
GSU0594	cytochrome c	-2.94	<0.01
GSU1320	sigma-54-dependent transcriptional response regulator	-2.94	<0.01
GSU1174	nucleoside triphosphate pyrophosphohydrolase	-3.07	<0.01
GSU3174	type VI secretion system needle tube protein TssD	-3.34	<0.01
GSU1183	O-acetyl-L-homoserine sulfhydrylase	-3.37	<0.01
GSU1346	sulfate ABC transporter substrate-binding protein	-3.47	<0.01

Supplementary Table 6.1b: *G. sulfurreducens* proteins exclusively detected during co-culture growth compared with pure culture growth

Note: Number of distinct peptides refers to the highest number of distinct peptides detected per protein in a particular replicate

Locus Tag	Description	Number of distinct peptides
GSU0013	MarR family winged helix-turn-helix transcriptional regulator	2
GSU0182	lipoprotein	3
GSU0329	type II secretion system lipoprotein GspD	5
GSU0526	O-acetyl-ADP-ribose deacetylase	2
GSU0571	dihydrofolate reductase	2
GSU0693	sensor histidine kinase, PAS, PAS and PAS domain-containing	2
GSU0737	antitoxin	3
GSU0746	cytochrome p460, 1 heme-binding site	2
GSU0753	lipoprotein	2
GSU0786	periplasmically oriented, membrane-bound	4
GSU0910	aldehyde:ferredoxin oxidoreductase, tungsten-containing	7
GSU1013	peptidoglycan-binding lipoprotein, OmpA family	2
GSU1138	2',3'-cyclic-nucleotide 2'-phosphodiesterase	2
GSU1160	hypothetical protein	2
GSU1176	succinate dehydrogenase/fumarate reductase, cytochrome b558 subunit	2
GSU1236	glutamine amidotransferase	2
GSU1258	NosL family protein	3
GSU1284	cytochrome c, 1 heme-binding site	2
GSU1359	helicase	2
GSU1409	NifU-like domain-containing protein	2
GSU1415	response regulator	2
GSU1694	HAD superfamily hydrolase	2
GSU1740	cytochrome c, 1 heme-binding site	2
GSU1924	IPT/TIG domain-containing protein	3
GSU1948	hypothetical protein	3
GSU2005	branched-chain amino acid ABC transporter substrate-binding protein	21
GSU2026	shikimate kinase	2
GSU2104	lipoprotein	4
GSU2268	outer membrane protein assembly complex protein YaeT	2
GSU2299	cytochrome c	25
GSU2395	hypothetical protein	7
GSU2494	cytochrome c	2
GSU2506	sigma-54-dependent sensor transcriptional response regulator	2
GSU2516	hypothetical protein	3
GSU2618	preprotein translocase subunit YajC	2
GSU2657	multicopper oxidase, manganese oxidase family	2
GSU2730	hypothetical protein	2
GSU2773	hypothetical protein	2
GSU2786	cysteine desulfurase	3
GSU2829	deoxyribodipyrimidine photo-lyase	2
GSU2882	cytochrome c	2
GSU2979	2-amino-4-hydroxy-6-hydroxymethyldihydropteridine pyrophosphokinase	2
GSU3137	cytochrome c	3
GSU3291	membrane-bound proton-translocating pyrophosphatase	2
GSU3361	transglutaminase domain-containing protein	5
GSU3428	cytochrome c, 1 heme-binding site	2
GSU3444	trifunctional NADH dehydrogenase I subunit B/C/D	2

Supplementary Table 6.1c: *G. sulfurreducens* proteins exclusively detected during pure culture growth compared with co-culture growth

Note: Number of distinct peptides refers to the highest number of distinct peptides detected per protein in a particular replicate

Locus Tag	Description	Number of distinct peptides
GSU0000.1	chromosomal replication initiation protein	2
GSU0005	hypothetical protein	2
GSU0008	response receiver sensor histidine kinase, PAS domain-containing	4
GSU0017	transcription-repair coupling factor	12
GSU0022	twin arginine translocase protein A	2
GSU0025	biopolymer transport TolB-like protein	5
GSU0031	heat-inducible transcription repressor HrcA	2
GSU0051	CRISPR-associated helicase Cas3	2
GSU0075	SDR_a2 family oxidoreductase	3
GSU0082	23S rRNA synthase	4
GSU0092	heterodisulfide oxidoreductase, iron-sulfur cluster-binding subunit C	2
GSU0104	response regulator	3
GSU0107	ParB-like nuclease domain-containing protein	3
GSU0115	4-hydroxythreonine-4-phosphate dehydrogenase	3
GSU0125	hypothetical protein	3
GSU0127	tRNA 2-thiocytidine biosynthesis protein TtcA	2
GSU0141	hypothetical protein	7
GSU0168	Fic family protein	2
GSU0177	acetyltransferase	4
GSU0195	flavin and coenzyme A sequestration protein dodecin	2
GSU0201	aerobic-type carbon monoxide dehydrogenase, large subunit-like protein	3
GSU0205	TetR family transcriptional regulator	2
GSU0227	DNA methyltransferase	2
GSU0231	hypothetical protein	2
GSU0237	dehydratase, NodN/MaoC domain-containing	3
GSU0240	malonyl-CoA--acyl carrier protein transacylase	3
GSU0244	radical SAM domain-containing iron-sulfur cluster-binding oxidoreductase	3
GSU0273	radical SAM domain-containing iron-sulfur cluster-binding oxidoreductase	2
GSU0283	sensor histidine kinase	4
GSU0285	DNA repair protein RadA	5
GSU0286	HEAT-like repeat-containing protein	3
GSU0288	HEAT-like repeat-containing protein	2
GSU0310	phospholipase, patatin family	7
GSU0312	PilZ domain-containing protein	3
GSU0355	hypothetical protein	2
GSU0372	sigma-54-dependent transcriptional response regulator	3
GSU0403	response receiver CheY associated with MCPs of classes 40H and 40+24H	2
GSU0450	PEP synthetase regulatory protein	3
GSU0459	3-oxoacyl-(ACP) synthase-like protein	3
GSU0460	3-oxoacyl-(acyl carrier protein) synthase II	4
GSU0461	3-oxoacyl-ACP reductase	2
GSU0470	sigma-54-dependent transcriptional response regulator	6
GSU0481	hypothetical protein	2
GSU0501	outer membrane protein assembly lipoprotein YfiO	2
GSU0504	hypothetical protein	2
GSU0511	leucyl aminopeptidase-like protein	6
GSU0513	dephospho-coenzyme A kinase	3
GSU0520	tRNA pseudouridine 13 synthase	4
GSU0523	pyridoxal-5\'-phosphate-dependent chorismate-binding enzyme	2
GSU0536	adenosine nucleotide alpha-hydrolase superfamily protein	7
GSU0538	ATP-independent chaperone	14

GSU0540	hypothetical protein	2
GSU0552	reverse transcriptase	2
GSU0569	nicotinamidase-like cysteine hydrolase	5
GSU0570	SAM-dependent methyltransferase	2
GSU0572	hydrolase, cyclic phosphodiesterase-like domain-containing	2
GSU0573	zinc-containing alcohol dehydrogenase	2
GSU0585	fumarylacetoacetate hydrolase family protein	4
GSU0596	response receiver	3
GSU0608	hypothetical protein	2
GSU0616	cytochrome c	3
GSU0645	16S rRNA processing protein RimM	3
GSU0659	polysaccharide deacetylase domain-containing protein	2
GSU0671	RNA pseudouridine synthase, RluA family	2
GSU0685	diploptene adenosyltransferase and reductase	2
GSU0710	hypothetical protein	2
GSU0714	hypothetical protein	4
GSU0715	hypothetical protein	3
GSU0716	C14 family peptidase	3
GSU0723	hypothetical protein	3
GSU0731	UDP-3-O	5
GSU0754	hypothetical protein	3
GSU0770	TetR family transcriptional regulator	2
GSU0772	flavodoxin	3
GSU0796	long-chain acyl-CoA thioesterase	2
GSU0802	short chain dehydrogenase	3
GSU0803	phosphoenolpyruvate synthase	4
GSU0860	5,10-methylenetetrahydrofolate reductase	2
GSU0861	5,10-methylenetetrahydrofolate reductase-associated protein	2
GSU0877	response regulator, PilZ domain-containing	3
GSU0880	molybdopterin-binding iron-sulfur cluster-binding oxidoreductase MopB-3	2
GSU0885	BioD and DRTGG domain-containing protein	7
GSU0887	hypothetical protein	4
GSU0915	hypothetical protein	5
GSU0943	PilZ domain-containing protein	7
GSU0944	cystathionine gamma-synthase/beta-lyase	9
GSU0972	AAA ATPase	5
GSU0973	hypothetical protein	5
GSU0974	hypothetical protein	6
GSU0982	phage protein D	2
GSU0983	phage tail spike protein	4
GSU0986	phage baseplate outer wedge protein (acidic lysozyme)	3
GSU0987	hypothetical protein	15
GSU0988	hypothetical protein	9
GSU0989	NHL repeat domain-containing protein	4
GSU0992	hypothetical protein	2
GSU0998	replicative DNA helicase	6
GSU1004	nitrogen fixation master sensor histidine kinase, PAS domain-containing	4
GSU1015	hypothetical protein	3
GSU1021	hypothetical protein	4
GSU1028	agmatine deiminase	9
GSU1044	NADH pyrophosphatase	2

GSU1059	succinyl-CoA synthetase subunit alpha	3
GSU1076	Holliday junction DNA helicase RuvA	4
GSU1077	Holliday junction DNA helicase RuvB	4
GSU1079	PEP motif-containing protein exosortase substrate	3
GSU1111	ribosomal RNA large subunit methyltransferase N	2
GSU1117	response regulator	2
GSU1126	uracil-DNA glycosylase	2
GSU1129	sigma-54-dependent transcriptional response regulator	5
GSU1130	chromosome segregation ATPase SMC	5
GSU1165	GAF domain phosphoenolpyruvate--protein phosphotransferase PtsP	7
GSU1173	methylated DNA--protein cysteine S-methyltransferase	2
GSU1185	adenosine kinase	2
GSU1190	tRNA 2-selenouridine synthase	4
GSU1232	hypothetical protein	2
GSU1265	sensor histidine kinase response regulator	3
GSU1278	hypothetical protein	2
GSU1290	sensor histidine kinase CheA associated with MCPs of class 34H	2
GSU1291	response regulator	2
GSU1293	LuxR family transcriptional regulator	2
GSU1312	radical SAM domain-containing iron-sulfur cluster-binding oxidoreductase	2
GSU1313	carboxymuconolactone decarboxylase family protein	2
GSU1324	RNA-binding protein	3
GSU1327	homocysteine S-methyltransferase domain-containing protein	2
GSU1350	thiamin biosynthesis thiocarboxylate synthase	5
GSU1351	sulfite reductase subunit	5
GSU1361	Piwi domain-containing protein	2
GSU1370	oxidoreductase, aldo/keto reductase family	3
GSU1380	ferrous iron transport protein B	2
GSU1382	iron/manganese-dependent transcriptional regulator	2
GSU1403	23S rRNA pseudouridine 2605 synthase	7
GSU1419	helix-turn-helix XRE domain-containing protein	2
GSU1452	TrmA family RNA methyltransferase	2
GSU1492	twitching motility pilus retraction protein	7
GSU1523	5\'(3\')-nucleotidase/polyphosphatase	2
GSU1533	exodeoxyribonuclease V subunit gamma	4
GSU1538	cytochrome c	2
GSU1539	exonuclease III	2
GSU1548	hypothetical protein	2
GSU1553	hypothetical protein	2
GSU1564	Glu/Leu/Phe/Val dehydrogenase	5
GSU1582	lysine--8-amino-7-oxononanoate aminotransferase	5
GSU1591	tRNA pseudouridine 55 synthase	3
GSU1596	tRNA (N6-threonylcarbamyl-A37) modification ATPase	3
GSU1600	phosphate acyltransferase	5
GSU1604	acyl carrier protein	4
GSU1612	phosphoglyceromutase	2
GSU1620	hypothetical protein	6
GSU1655	response receiver sensor histidine kinase response regulator, PAS and GAF domain-containing	3
GSU1656	response receiver sensor diguanylate cyclase, PAS domain-containing	4
GSU1686	deoxycytidylate deaminase	4

GSU1696	MoxR family ATPase	6
GSU1716	adenosine-5\'-phosphosulfate reductase, glutathione-dependent	14
GSU1717	sulfate adenylyltransferase subunit 2	28
GSU1718	sulfate adenylyltransferase, subunit 1	58
GSU1721	7-cyano-7-deazaguanine synthase	3
GSU1722	creatinine amidohydrolase superfamily protein	4
GSU1746	integration host factor subunit beta	4
GSU1754	translation elongation factor P-lysyl-lysine 2,3-aminomutase	2
GSU1778	type II secretion system secretin lipoprotein PulQ	2
GSU1783	type II secretion system ATPase PulE	8
GSU1790	ATP-dependent Lon protease (La)	8
GSU1800	nucleoid maintenance ATPase YjeE	3
GSU1820	nitrogen regulatory protein P-II uridylyltransferase, GlnD	4
GSU1821	N-acetylmuramyl-L-alanine amidase	4
GSU1830	MEMO-like protein	5
GSU1864	KsgA/Dim1 family 16S ribosomal RNA methyltransferase	4
GSU1865	UGMP family protein	2
GSU1870	sensor diguanylate cyclase, GAF domain-containing	2
GSU1877	oxidoreductase, 2-nitropropane dioxygenase family	3
GSU1881	phosphoenolpyruvate--protein phosphotransferase	2
GSU1889	lipopolysaccharide ABC transporter periplasmic protein LptA	3
GSU1892	3-deoxy-D-manno-octulosonate-8-phosphate phosphatase	4
GSU1897	nucleoside phosphorylase	2
GSU1917	undecaprenyl pyrophosphate synthase	2
GSU1930	GTP-binding domain-containing protein	2
GSU1932	SPOR domain-containing protein	2
GSU1935	biotin operon repressor and biotin--acetyl-CoA carboxylase ligase	3
GSU1939	sensor histidine kinase cyclic nucleotide phosphodiesterase	4
GSU1943	PEP motif-containing protein exosortase substrate	7
GSU1949	PEP motif-containing protein exosortase substrate	2
GSU1955	adenylyltransferase	2
GSU1961	glycosyltransferase	2
GSU1965	polysaccharide pyruvyl transferase-related domain-containing protein	2
GSU1971	hypothetical protein	2
GSU1982	ATPase	2
GSU1983	protein tyrosine kinase	2
GSU1994	PEP motif-containing protein exosortase substrate	2
GSU1997	iron-sulfur cluster-binding oxidoreductase, cyano_FeS_chp family	3
GSU2001	DNA mismatch repair protein	4
GSU2024	hypothetical protein	2
GSU2032	type IV pilus biogenesis ATPase PilM	2
GSU2052	indolepyruvate oxidoreductase subunit B	2
GSU2059	protein phosphoaspartate phosphatase CheX	5
GSU2062	response receiver-modulated nucleotide cyclase	3
GSU2065	inorganic polyphosphate/ATP-NAD kinase	3
GSU2067	recombination factor protein RarA	2
GSU2068	6-phosphofructokinase	6
GSU2069	HAD superfamily hydrolase	3
GSU2088	glycosyltransferase	2
GSU2092	hypothetical protein	2
GSU2098	carbon monoxide dehydrogenase, catalytic subunit	2

GSU2102	glycerol dehydratase-activating enzyme	3
GSU2183	Fic family protein	2
GSU2189	sensor histidine kinase	6
GSU2214	protein glutamate methylesterase CheB associated with MCPs of class 40H, response receiver domain-containing	2
GSU2220	scaffold protein CheW associated with MCPs of class 40H	2
GSU2223	response receiver CheY associated with MCPs of class 40H	2
GSU2231	PSP1 superfamily protein	3
GSU2238	guanylate kinase	4
GSU2242	ADP-heptose--lipopolysaccharide heptosyltransferase	2
GSU2245	UDP-2-acetamido-2,6-dideoxy-beta-L-mannose 2-epimerase	7
GSU2248	hypothetical protein	4
GSU2256	ADP-heptose--lipopolysaccharide heptosyltransferase	2
GSU2261	lipid-A-disaccharide synthase	4
GSU2278	peptide chain release factor 2	6
GSU2282	CBS and CorC_HlyC domain-containing protein	5
GSU2307	carbonic anhydrase	2
GSU2332	cytidylate kinase-like domain-containing protein	3
GSU2336	trehalose-6-phosphatase	2
GSU2358	maltooligosyltrehalose trehalohydrolase	2
GSU2361	trehalose/maltose transglucosylase and maltokinase	2
GSU2365	dTDP-4-dehydrorhamnose reductase	5
GSU2370	acetyl-CoA carboxylase, carboxyl transferase subunit beta	3
GSU2400	acetoacetate decarboxylase family protein	4
GSU2409	ATP-independent chaperone	2
GSU2410	ATP-independent chaperone	2
GSU2450	hydrolase	2
GSU2455	hypothetical protein	2
GSU2458	transpeptidase	2
GSU2475	sensor sigma-54-dependent transcriptional regulator	8
GSU2477	radical SAM domain-containing iron-sulfur cluster-binding oxidoreductase	2
GSU2487	amino acid kinase	3
GSU2489	magnesium-dependent deoxyribonuclease	6
GSU2527	nitrite/sulfite reductase domain-containing protein	27
GSU2544	pyridoxal-5\'-phosphate-dependent enzyme, class III	2
GSU2552	lipoprotein	2
GSU2556	U32 family peptidase	2
GSU2559	pppGpp 5\'-phosphohydrolase and exopolyphosphatase, HD domain-containing	2
GSU2561	hypothetical protein	3
GSU2569	tRNA-specific 2-thiouridylase MnmA	4
GSU2570	nitrogen fixation iron-sulfur cluster assembly cysteine desulfurase NifS	3
GSU2571	helix-turn-helix iron-sulfur cluster-binding transcriptional regulator IscR	2
GSU2609	PilB/PulE/GspE family ATPase	2
GSU2619	queuine tRNA-ribosyltransferase	4
GSU2620	S-adenosylmethionine--tRNA ribosyltransferase-isomerase	2
GSU2645	cytochrome c	2
GSU2655	branched-chain 2-oxoacid dehydrogenase complex, E1 protein subunit beta	2
GSU2656	branched-chain alpha-keto acid dehydrogenase E2 subunit	7
GSU2682	hypothetical protein	2
GSU2699	molybdopterin synthase, large subunit	2
GSU2704	pyranopterin monophosphate cyclase	3
GSU2705	molybdopterin adenylyltransferase MoaB	6

GSU2719	bidirectional NAD-reducing hydrogenase, small subunit	2
GSU2720	bidirectional hydrogenase complex protein HoxU	2
GSU2721	bidirectional NAD-reducing hydrogenase, diaphorase subunit	2
GSU2722	bidirectional hydrogenase complex protein HoxE	2
GSU2749	NOL1/NOP2/Sun (tRNA and rRNA cytosine-C5-methyltransferase) family protein	2
GSU2797	electron transfer flavoprotein subunit beta	5
GSU2887	lipoprotein cytochrome c	2
GSU2967	ferritin-like domain-containing protein	8
GSU2989	L-threonine-0-3-phosphate decarboxylase	4
GSU2994	cobalt-precorrin-4 C11-methyltransferase	3
GSU2995	cobalt-sirohydrochlorin C20-methyltransferase	2
GSU2997	cobalt-precorrin-5B C1-methyltransferase	2
GSU2998	hypothetical protein	4
GSU3001	cobalt ABC transporter ATP-binding protein	2
GSU3010	adenosylcobinamide kinase and adenosylcobinamide phosphate guanylyltransferase	3
GSU3013	GTP-binding protein YsxC	6
GSU3056	flagellar biosynthesis protein FlhA	2
GSU3057	dihydropyrimidine dehydrogenase subunit A	13
GSU3058	ferredoxin-NADP(+) reductase subunit alpha	8
GSU3062	radical SAM domain-containing iron-sulfur cluster-binding oxidoreductase	2
GSU3067	UDP-N-acetylenolpyruvoylglucosamine reductase	2
GSU3086	23S rRNA (2-N-methyl-G2445)-methyltransferase	4
GSU3090	DNA primase	3
GSU3092	hypothetical protein	4
GSU3094	phosphoribosyl-ATP pyrophosphatase	4
GSU3097	imidazole glycerol phosphate synthase subunit HisH	3
GSU3103	N5-glutamine S-adenosyl-L-methionine-dependent methyltransferase	2
GSU3109	IclR family transcriptional regulator	5
GSU3113	metal-dependent hydrolase	7
GSU3127	AraC family transcriptional regulator	4
GSU3146	pyranopterin triphosphate synthase	4
GSU3161	methionine sulfoxide reductase A	3
GSU3172	type VI secretion system needle sheath protein TssB	2
GSU3173	type VI secretion system needle sheath protein TssC	7
GSU3185	hypothetical protein	2
GSU3210	nicotinate/nicotinamide mononucleotide adenylyltransferase	2
GSU3212	gamma-glutamyl kinase	2
GSU3238	ferredoxin, Rieske superfamily	2
GSU3250	nucleic acid-independent polyadenylating polymerase	2
GSU3255	glycoside hydrolase	2
GSU3262	excinuclease ABC subunit B	4
GSU3286	uroporphyrinogen III C2,C7-methyltransferase and uroporphyrinogen III synthase	5
GSU3297	D-lactate/glycolate dehydrogenase, iron-sulfur cluster-binding protein	6
GSU3309	ATPase	2
GSU3314	lipoprotein	2
GSU3320	SAM-dependent methyltransferase	2
GSU3323	polyphosphate kinase	5
GSU3335	hypothetical protein	2
GSU3343	SpoVR-like family protein	3

GSU3347	U32 family peptidase	7
GSU3348	Hsp33-like chaperonin	3
GSU3349	cyclase/hydrolase	2
GSU3351	hypothetical protein	5
GSU3354	ADP-ribose pyrophosphatase	2
GSU3358	hypothetical protein	3
GSU3359	hypothetical protein	3
GSU3360	zinc-dependent peptidase	5
GSU3368	2-C-methyl-D-erythritol 4-phosphate cytidylyltransferase	5
GSU3369	selenocysteine synthase	4
GSU3373	16S rRNA (5-methyl-C967)-methyltransferase	4
GSU3376	response receiver-modulated diguanylate cyclase	5
GSU3387	AraC/XylS family transcriptional regulator	2
GSU3396	GntR family transcriptional regulator	3
GSU3414	hypothetical protein	5
GSU3437	sensor histidine kinase, PAS and GAF domain-containing	2
GSU3442	hypothetical protein	2
GSU3448	acetate kinase-like protein	2
GSU3464	tRNA uridine 5-carboxymethylaminomethyl modification protein GidA	6
GSU3549	hypothetical protein	4
GSU3593	hypothetical protein	2

Supplementary Table 6.2a: *D. reducens* proteins significantly increased and decreased during co-culture growth (48-hour) relative to pure culture growth

Note: Proteins also significantly increased in 72-hour co-culture designated with bold text

Locus Tag	Description	CoC/Pure (log2)	p-value
Dred_0220	**50S ribosomal protein L22**	**4.82**	**<0.01**
Dred_0218	**50S ribosomal protein L2**	**4.00**	**<0.01**
Dred_2490	**30S ribosomal protein S21**	**3.62**	**<0.01**
Dred_2158	AsnC family transcriptional regulator	3.46	<0.01
Dred_2266	MOSC domain-containing protein	3.38	<0.01
Dred_0226	**50S ribosomal protein L24**	**3.36**	**<0.01**
Dred_0225	**50S ribosomal protein L14**	**3.36**	**<0.01**
Dred_0233	**50S ribosomal protein L30**	**3.26**	**<0.01**
Dred_2470	hypothetical protein	3.24	<0.01
Dred_0230	**50S ribosomal protein L6**	**3.20**	**<0.01**
Dred_1957	translation initiation factor IF-2	3.17	<0.01
Dred_1951	**30S ribosomal protein S15**	**3.11**	**<0.01**
Dred_2161	radical SAM domain-containing protein	3.03	<0.01
Dred_2505	**30S ribosomal protein S20**	**3.00**	**<0.01**
Dred_3141	hypothetical protein	3.00	<0.01
Dred_2351	1-(5-phosphoribosyl)-5-[(5-phosphoribosylamino)methylideneamino] imidazole-4-carboxamide isomerase; EC_number=5.3.1.16	2.99	<0.01
Dred_0222	**50S ribosomal protein L16**	**2.99**	**<0.01**
Dred_2369	phosphoribosylaminoimidazole-succinocarboxamide synthase; EC_number=6.3.2.6	2.92	<0.01
Dred_0204	**50S ribosomal protein L1**	**2.89**	**<0.01**
Dred_2366	**phosphoribosylformylglycinamidine synthase II; EC_number=6.3.5.3**	**2.87**	**<0.01**
Dred_2535	**50S ribosomal protein L21**	**2.86**	**<0.01**
Dred_0215	**50S ribosomal protein L3**	**2.85**	**<0.01**
Dred_0244	**50S ribosomal protein L17**	**2.82**	**<0.01**
Dred_0221	**30S ribosomal protein S3**	**2.71**	**<0.01**
Dred_2884	phenylacetate--CoA ligase; EC_number=6.2.1.30	2.68	<0.01
Dred_3189	**indolepyruvate ferredoxin oxidoreductase; EC_number=1.2.7.8**	**2.67**	**<0.01**
Dred_1055	copper amine oxidase domain-containing protein	2.61	<0.01
Dred_2860	S-layer domain-containing protein	2.61	<0.01
Dred_0242	**30S ribosomal protein S4**	**2.59**	**<0.01**
Dred_1906	**inosine-5prime-monophosphate dehydrogenase; EC_number=1.1.1.205**	**2.46**	**<0.01**
Dred_0161	**pantoate--beta-alanine ligase; EC_number=6.3.2.1**	**2.41**	**<0.01**
Dred_1149	3-deoxy-7-phosphoheptulonate synthase; EC_number=2.5.1.54	2.40	<0.01
Dred_1658	hypothetical protein	2.40	<0.01
Dred_0282	**acetolactate synthase 3 regulatory subunit; EC_number=2.2.1.6**	**2.38**	**<0.01**
Dred_2056	signal recognition particle protein	2.34	<0.01
Dred_1680	bifunctional pyrimidine regulatory protein PyrR uracil phosphoribosyltransferase; EC_number=2.4.2.9	2.28	<0.01

Dred_2364	**phosphoribosylaminoimidazole synthetase; EC_number=6.3.3.1**	**2.28**	**<0.01**
Dred_0014	**D-3-phosphoglycerate dehydrogenase**	**2.27**	**<0.01**
Dred_2082	**DRTGG domain-containing protein**	**2.26**	**<0.01**
Dred_0210	30S ribosomal protein S12	2.21	0.03
Dred_1978	30S ribosomal protein S2	2.14	<0.01
Dred_0224	30S ribosomal protein S17	2.14	0.04
Dred_0216	50S ribosomal protein L4	2.11	<0.01
Dred_1352	**fructose 1,6-bisphosphatase II; EC_number=3.1.3.11**	**2.10**	**<0.01**
Dred_2896	acetolactate synthase 3 regulatory subunit	2.10	<0.01
Dred_0232	**30S ribosomal protein S5**	**2.03**	**<0.01**
Dred_1615	**50S ribosomal protein L20**	**2.03**	**<0.01**
Dred_0241	30S ribosomal protein S11	2.02	<0.01
Dred_2379	**hypothetical protein**	**1.99**	**0.05**
Dred_1950	polynucleotide phosphorylase/polyadenylase; EC_number=2.7.7.8	1.96	<0.01
Dred_0219	**30S ribosomal protein S19**	**1.92**	**<0.01**
Dred_3318	degV family protein	1.91	0.01
Dred_3306	**30S ribosomal protein S18**	**1.90**	**<0.01**
Dred_2534	**50S ribosomal protein L27**	**1.89**	**<0.01**
Dred_2227	**hypothetical protein**	**1.87**	**<0.01**
Dred_1644	copper amine oxidase domain-containing protein	1.87	<0.01
Dred_0231	**50S ribosomal protein L18**	**1.85**	**<0.01**
Dred_3249	**Orn/DAP/Arg decarboxylase 2**	**1.85**	**<0.01**
Dred_0257	**30S ribosomal protein S9**	**1.85**	**<0.01**
Dred_0256	**50S ribosomal protein L13**	**1.84**	**<0.01**
Dred_2277	**iron-containing alcohol dehydrogenase**	**1.83**	**<0.01**
Dred_2192	**5,10-methylenetetrahydrofolate reductase**	**1.80**	**<0.01**
Dred_0227	50S ribosomal protein L5	1.79	<0.01
Dred_2368	phosphoribosylformylglycinamidine synthase PurS	1.77	<0.01
Dred_1377	**extracellular solute-binding protein**	**1.75**	**<0.01**
Dred_0006	DNA gyrase subunit B; EC_number=5.99.1.3	1.74	<0.01
Dred_2064	aIF-2BI family translation initiation factor; EC_number=5.3.1.23	1.74	<0.01
Dred_1280	GTP-binding protein YchF	1.70	<0.01
Dred_2159	radical SAM domain-containing protein	1.67	<0.01
Dred_0229	**30S ribosomal protein S8**	**1.66**	**<0.01**
Dred_1612	threonyl-tRNA synthetase; EC_number=6.1.1.3	1.62	<0.01
Dred_3164	protein tyrosine phosphatase	1.61	<0.01
Dred_0133	phosphoglycerate kinase; EC_number=2.7.2.3	1.60	<0.01
Dred_2055	**30S ribosomal protein S16**	**1.59**	**<0.01**
Dred_0223	50S ribosomal protein L29	1.57	<0.01
Dred_2657	hypothetical protein	1.57	<0.01
Dred_1741	peptidylprolyl isomerase; EC_number=5.2.1.8	1.54	<0.01
Dred_0479	**hypothetical protein**	**1.54**	**<0.01**
Dred_0217	50S ribosomal protein L23	1.54	<0.01
Dred_0214	**30S ribosomal protein S10**	**1.52**	**<0.01**
Dred_1979	transcriptional repressor CodY	1.50	<0.01
Dred_0690	hypothetical protein	1.49	<0.01
Dred_2836	glycine cleavage system H protein	1.49	<0.01
Dred_2091	GTP cyclohydrolase II; EC_number=3.5.4.25	1.47	<0.01
Dred_1309	hypothetical protein	1.46	0.01
Dred_3174	transcription termination factor Rho	1.45	0.01

Dred_0094	4-diphosphocytidyl-2C-methyl-D-erythritol kinase	1.44	<0.01
Dred_0132	**type I glyceraldehyde-3-phosphate dehydrogenase; EC_number=1.2.1.12**	**1.43**	**<0.01**
Dred_1237	hypothetical protein	1.43	0.02
Dred_0273	acetylglutamate kinase; EC_number=2.7.2.8	1.42	<0.01
Dred_0234	50S ribosomal protein L15	1.42	<0.01
Dred_2769	basic membrane lipoprotein	1.42	<0.01
Dred_0115	histone family protein DNA-binding protein	1.41	<0.01
Dred_1145	hypothetical protein	1.40	<0.01
Dred_1927	putative nucleotide-binding protein	1.40	0.04
Dred_0251	indole-3-glycerol-phosphate synthase; EC_number=4.1.1.48	1.40	<0.01
Dred_1169	gamma-glutamyl phosphate reductase; EC_number=1.2.1.41	1.39	<0.01
Dred_2497	GrpE protein	1.39	<0.01
Dred_1940	aspartate kinase I; EC_number=2.7.2.4	1.39	0.01
Dred_0203	50S ribosomal protein L11	1.36	<0.01
Dred_1519	GreA/GreB family elongation factor	1.35	0.01
Dred_0782	**phospho-2-dehydro-3-deoxyheptonate aldolase**	**1.34**	**<0.01**
Dred_0254	tryptophan synthase subunit alpha; EC_number=4.2.1.20	1.34	<0.01
Dred_3308	**30S ribosomal protein S6**	**1.33**	**<0.01**
Dred_0771	extracellular solute-binding protein	1.33	<0.01
Dred_0211	30S ribosomal protein S7	1.32	<0.01
Dred_1687	orotidine 5prime-phosphate decarboxylase; EC_number=4.1.1.23	1.31	<0.01
Dred_2352	imidazole glycerol phosphate synthase subunit HisH	1.28	<0.01
Dred_2913	2-nitropropane dioxygenase	1.28	<0.01
Dred_0367	electron transfer flavoprotein subunit beta	1.26	0.02
Dred_0189	glutaminyl-tRNA synthetase; EC_number=6.1.1.18	1.26	<0.01
Dred_2563	trigger factor	1.26	<0.01
Dred_1647	tyrosyl-tRNA synthetase; EC_number=6.1.1.1	1.25	<0.01
Dred_3185	putative dissimilatory sulfite reductase subunit D	1.23	<0.01
Dred_3307	single-strand binding protein	1.23	0.05
Dred_1702	phosphopantothenoylcysteine decarboxylase/phosphopantothenate--cysteine ligase; EC_number=6.3.2.5	1.21	<0.01
Dred_2764	molybdopterin binding domain-containing protein	1.20	<0.01
Dred_0236	type I methionine aminopeptidase	1.19	<0.01
Dred_2232	carbamoyl phosphate synthase large subunit; EC_number=6.3.5.5	1.19	0.01
Dred_0240	30S ribosomal protein S13	1.17	<0.01
Dred_1093	hypothetical protein	1.14	<0.01
Dred_0314	biotin/lipoyl attachment	1.14	0.01
Dred_0135	phosphoglyceromutase; EC_number=5.4.2.1	1.10	<0.01
Dred_3140	hypothetical protein	1.10	0.02
Dred_3324	tRNA modification GTPase TrmE	1.08	<0.01
Dred_2561	ATP-dependent protease ATP-binding subunit ClpX	1.08	0.02
Dred_2050	50S ribosomal protein L19	1.08	<0.01
Dred_3198	hypothetical protein	1.07	<0.01
Dred_0670	UDP-N-acetylmuramyl-tripeptide synthetase	1.06	0.02
Dred_1816	beta-lactamase domain-containing protein	1.05	0.03
Dred_0727	extracellular solute-binding protein	1.04	<0.01
Dred_1980	ATP-dependent protease ATP-binding subunit HslU	1.04	<0.01
Dred_1165	homoserine dehydrogenase; EC_number=1.1.1.3	1.01	<0.01
Dred_0689	hypothetical protein	1.01	<0.01

Dred_1636	hypothetical protein	-1.00	<0.01
Dred_2210	GTP-dependent nucleic acid-binding protein EngD	-1.03	0.02
Dred_0276	ornithine carbamoyltransferase; EC_number=2.1.3.3	-1.03	0.03
Dred_1422	ATPase	-1.03	0.03
Dred_0773	hypothetical protein	-1.03	0.03
Dred_2873	chaperonin GroEL	-1.04	0.03
Dred_3183	arginyl-tRNA synthetase; EC_number=6.1.1.19	-1.04	0.03
Dred_1179	Ppx/GppA phosphatase	-1.05	0.03
Dred_0163	quinolinate synthetase	-1.05	0.03
Dred_0280	dihydroxy-acid dehydratase; EC_number=4.2.1.9	-1.09	0.03
Dred_2361	phosphoribosylamine--glycine ligase; EC_number=6.3.4.13	-1.09	0.03
Dred_3159	UDP-N-acetylglucosamine 2-epimerase; EC_number=5.1.3.14	-1.10	0.03
Dred_0202	NusG antitermination factor	-1.12	0.05
Dred_0136	phosphopyruvate hydratase; EC_number=4.2.1.11	-1.14	0.05
Dred_2376	hypoxanthine phosphoribosyltransferase; EC_number=2.4.2.8	-1.15	0.05
Dred_0271	N-acetyl-gamma-glutamyl-phosphate reductase; EC_number=1.2.1.38	-1.15	0.05
Dred_1736	thioredoxin reductase	-1.17	0.05
Dred_2809	glutamate synthase-like protein	-1.18	0.05
Dred_0183	DNA integrity scanning protein DisA	-1.18	0.05
Dred_2028	hypothetical protein	-1.19	0.05
Dred_0459	hypothetical protein	-1.19	0.05
Dred_1967	prolyl-tRNA synthetase	-1.20	0.05
Dred_0448	hypothetical protein	-1.20	0.05
Dred_1281	asparaginyl-tRNA synthetase	-1.20	0.05
Dred_0272	arginine biosynthesis bifunctional protein ArgJ; EC_number=2.3.1.1	-1.23	0.05
Dred_3150	F0F1 ATP synthase subunit beta; EC_number=3.6.3.14	-1.26	0.05
Dred_2878	putative molybdopterin biosynthesis protein MoeA/LysR substrate binding-domain-containing protein	-1.26	0.05
Dred_0170	nitrite and sulfite reductase 4Fe-4S subunit	-1.26	0.01
Dred_1947	peptidase M16 domain-containing protein	-1.27	0.01
Dred_2371	phosphoribosylaminoimidazole carboxylase, catalytic subunit; EC_number=4.1.1.21	-1.29	0.01
Dred_1100	phosphopentomutase; EC_number=5.4.2.7	-1.30	0.01
Dred_1913	class I and II aminotransferase	-1.31	0.01
Dred_1976	uridylate kinase	-1.31	0.01
Dred_1696	class I and II aminotransferase	-1.32	0.01
Dred_2360	TrpR like protein, YerC/YecD	-1.32	0.01
Dred_0274	acetylornithine aminotransferase	-1.32	0.01
Dred_2689	methylaspartate ammonia-lyase; EC_number=4.3.1.2	-1.33	0.01
Dred_1092	peptidase T-like protein	-1.34	0.01
Dred_0145	heterodisulfide reductase subunit	-1.35	0.01
Dred_2988	phosphoglyceromutase; EC_number=5.4.2.1	-1.35	0.01

Dred_0639	methyl-viologen-reducing hydrogenase subunit delta	-1.36	0.01
Dred_2562	ATP-dependent Clp protease proteolytic subunit; EC_number=3.4.21.92	-1.36	<0.01
Dred_2027	methyl-accepting chemotaxis sensory transducer	-1.36	<0.01
Dred_0779	methyl-accepting chemotaxis sensory transducer	-1.37	0.01
Dred_0049	pyruvate ferredoxin/flavodoxin oxidoreductase	-1.37	0.01
Dred_2362	bifunctional phosphoribosylaminoimidazolecarboxamide formyltransferase/IMP cyclohydrolase; EC_number=2.1.2.3	-1.39	0.01
Dred_0911	hypothetical protein	-1.40	0.01
Dred_2337	3-isopropylmalate dehydratase, small subunit	-1.41	0.01
Dred_1257	FMN-dependent alpha-hydroxy acid dehydrogenase	-1.42	0.01
Dred_1888	hypothetical protein	-1.44	<0.01
Dred_3254	isocitrate dehydrogenase; EC_number=1.1.1.41	-1.45	<0.01
Dred_2697	hypothetical protein	-1.46	0.01
Dred_1941	aspartate-semialdehyde dehydrogenase; EC_number=1.2.1.11	-1.47	0.01
Dred_0338	stress protein	-1.47	0.01
Dred_1049	peptidase U62, modulator of DNA gyrase	-1.49	0.01
Dred_2121	nitrite and sulfite reductase 4Fe-4S subunit	-1.49	0.01
Dred_1064	pyruvate carboxylase subunit B; EC_number=4.1.1.3	-1.50	0.01
Dred_0470	hypothetical protein	-1.50	0.02
Dred_1148	aspartate aminotransferase; EC_number=2.6.1.1	-1.51	0.02
Dred_0013	class V aminotransferase	-1.52	0.02
Dred_2441	putative CheW protein	-1.55	0.01
Dred_1716	ribulose-phosphate 3-epimerase; EC_number=5.1.3.1	-1.55	0.03
Dred_0283	ketol-acid reductoisomerase; EC_number=1.1.1.86	-1.55	0.03
Dred_2987	phosphopyruvate hydratase; EC_number=4.2.1.11	-1.58	0.03
Dred_1238	hypothetical protein	-1.61	0.03
Dred_3176	fructose-1,6-bisphosphate aldolase; EC_number=4.1.2.13	-1.62	0.03
Dred_1904	hypothetical protein	-1.63	0.03
Dred_2989	Triose-phosphate isomerase; EC_number=5.3.1.1	-1.64	0.03
Dred_2383	MCP methylation inhibitor CheC	-1.64	0.01
Dred_3206	hypothetical protein	-1.67	0.01
Dred_1430	methyl-accepting chemotaxis sensory transducer	-1.67	0.01
Dred_3214	putative aminopeptidase	-1.68	0.01
Dred_2160	delta-aminolevulinic acid dehydratase; EC_number=4.2.1.24	-1.69	<0.01
Dred_0638	4Fe-4S ferredoxin iron-sulfur binding domain-containing protein	-1.73	<0.01
Dred_2690	methylaspartate mutase subunit E	-1.78	<0.01
Dred_3193	AsnC family transcriptional regulator	-1.79	<0.01
Dred_2774	FAD-binding molybdopterin dehydrogenase	-1.82	0.01
Dred_1672	hypothetical protein	-1.82	<0.01
Dred_2017	TatD-related deoxyribonuclease	-1.83	<0.01
Dred_0396	hypothetical protein	-1.83	<0.01
Dred_0631	hypothetical protein	-1.84	<0.01
Dred_0129	formate--tetrahydrofolate ligase; EC_number=6.3.4.3	-1.85	<0.01
Dred_0764	class V aminotransferase	-1.88	<0.01
Dred_2459	hypothetical protein	-1.89	<0.01

Dred_1939	dihydrodipicolinate synthase; EC_number=4.2.1.52	-1.89	<0.01
Dred_3152	ATP synthase F1 subunit alpha; EC_number=3.6.3.15	-1.90	<0.01
Dred_2806	glutamine synthetase, type I; EC_number=6.3.1.2	-1.91	<0.01
Dred_2890	thiamine biosynthesis protein ThiC	-1.93	<0.01
Dred_2139	heavy metal transport/detoxification protein	-1.93	<0.01
Dred_2338	homoaconitate hydratase family protein; EC_number=4.2.1.33	-1.94	<0.01
Dred_1051	peptidase M24	-2.03	<0.01
Dred_0735	beta-lactamase domain-containing protein	-2.07	<0.01
Dred_0101	hypothetical protein	-2.11	<0.01
Dred_0612	hypothetical protein	-2.22	<0.01
Dred_2090	riboflavin synthase; EC_number=2.5.1.9	-2.24	<0.01
Dred_1265	hypothetical protein	-2.25	<0.01
Dred_1076	polyprenyl synthetase	-2.28	<0.01
Dred_0041	phosphoribulokinase/uridine kinase	-2.36	<0.01
Dred_3175	putative transaldolase; EC_number=2.2.1.2	-2.39	<0.01
Dred_3151	F0F1 ATP synthase subunit gamma; EC_number=3.6.3.15	-2.57	<0.01
Dred_2273	aldehyde ferredoxin oxidoreductase; EC_number=1.2.7.5	-2.73	<0.01
Dred_2937	4Fe-4S ferredoxin iron-sulfur binding domain-containing protein	-2.78	<0.01
Dred_3231	OsmC family protein	-2.93	<0.01
Dred_2805	glutamate synthase; EC_number=1.4.7.1	-3.24	<0.01
Dred_0322	Fis family transcriptional regulator	-4.53	<0.01

Supplementary Table 6.2b: *D. reducens* proteins exclusively detected during co-culture (48-hour) growth compared with pure culture growth

Note: Proteins also identified in the 72-hour co-culture proteome are designated with bold text.

Number of distinct peptides refers to the highest number of distinct peptides detected per protein in a particular replicate

Locus Tag	Description	Number of distinct peptides
Dred_0007	**DNA gyrase subunit A**	**8**
Dred_0009	metal dependent phosphohydrolase	3
Dred_0042	DNA polymerase III subunits gamma and tau; EC_number=2.7.7.7	2
Dred_0043	hypothetical protein	2
Dred_0046	**hypothetical protein**	**13**
Dred_0064	**AbrB family transcriptional regulator**	**4**
Dred_0097	threonine dehydratase; EC_number=4.3.1.19	5
Dred_0114	**MazG family protein**	**4**
Dred_0131	DeoR family transcriptional regulator	2
Dred_0200	50S ribosomal protein L33	2
Dred_0228	30S ribosomal protein S14	2
Dred_0248	anthranilate synthase component I; EC_number=4.1.3.27	10
Dred_0250	anthranilate phosphoribosyltransferase	15
Dred_0285	2-isopropylmalate synthase	16
Dred_0295	**glucosamine--fructose-6-phosphate aminotransferase; EC_number=2.6.1.16**	**9**
Dred_0398	peptide chain release factor 3	8

Dred_0444	hypothetical protein	6
Dred_0485	xylose isomerase domain-containing protein	2
Dred_0610	lipoyl synthase	6
Dred_0632	hypothetical protein	2
Dred_0673	UDP-N-acetylmuramoyl-L-alanyl-D-glutamate synthetase	3
Dred_0676	UDP-N-acetylmuramate--L-alanine ligase	3
Dred_0693	anaerobic ribonucleoside triphosphate reductase; EC_number=1.17.4.2	10
Dred_0707	two component transcriptional regulator	2
Dred_0732	adenine phosphoribosyltransferase; EC_number=2.4.2.7	4
Dred_0756	histidyl-tRNA synthetase; EC_number=6.1.1.21	2
Dred_0781	shikimate kinase; EC_number=2.7.1.71	5
Dred_0783	prephenate dehydratase; EC_number=4.2.1.51	7
Dred_0892	cobyrinic acid a,c-diamide synthase	2
Dred_0903	**helix-turn-helix domain-containing protein**	**3**
Dred_1069	NusB antitermination factor	3
Dred_1073	methylenetetrahydrofolate dehydrogenase (NADP(+)); EC_number=1.5.1.5	5
Dred_1078	deoxyxylulose-5-phosphate synthase	3
Dred_1084	DNA repair protein RecN	2
Dred_1086	response regulator receiver protein	3
Dred_1142	pseudouridine synthase	2
Dred_1147	phospho-2-dehydro-3-deoxyheptonate aldolase	2
Dred_1159	hypothetical protein	4
Dred_1160	GTP-binding protein EngA	5
Dred_1168	pyrroline-5-carboxylate reductase; EC_number=1.5.1.2	2
Dred_1256	**signal-transduction protein**	**9**
Dred_1271	Dak phosphatase	3
Dred_1325	heterodisulfide reductase subunit C	2
Dred_1336	**L-asparaginase II**	**6**
Dred_1443	LysR family transcriptional regulator	3
Dred_1485	ABC transporter-like protein	3
Dred_1600	carboxyl-terminal protease; EC_number=3.4.21.102	6
Dred_1614	**50S ribosomal protein L35**	**2**
Dred_1666	queuine tRNA-ribosyltransferase; EC_number=2.4.2.29	5
Dred_1669	**preprotein translocase subunit SecD**	**2**
Dred_1683	carbamoyl-phosphate synthase, small subunit	6
Dred_1684	**carbamoyl phosphate synthase large subunit**	**16**
Dred_1700	guanylate kinase; EC_number=2.7.4.8	5
Dred_1705	methionyl-tRNA formyltransferase	3
Dred_1725	sigma-54 dependent trancsriptional regulator	3
Dred_1742	hypothetical protein	4
Dred_1798	**6-phosphofructokinase; EC_number=2.7.1.11**	**2**
Dred_1812	ABC transporter-like protein	6
Dred_1815	Orn/Lys/Arg decarboxylase, major region	4
Dred_1885	**histone deacetylase superfamily protein**	**2**
Dred_1887	DNA mismatch repair protein MutS	2
Dred_1889	(dimethylallyl)adenosine tRNA methylthiotransferase	6
Dred_1920	recA protein	7
Dred_1921	**DEAD/DEAH box helicase domain-containing protein**	**13**
Dred_1922	**competence damage-inducible protein A**	**3**

Dred_1926	MiaB-like tRNA modifying protein YliG	5
Dred_1953	riboflavin biosynthesis protein RibF	2
Dred_1968	1-hydroxy-2-methyl-2-(E)-butenyl 4-diphosphate synthase; EC_number=1.17.7.1	6
Dred_1983	gid protein	7
Dred_1984	DNA topoisomerase I; EC_number=5.99.1.2	2
Dred_2011	tRNA-binding domain-containing protein	4
Dred_2043	NADH dehydrogenase subunit D; EC_number=1.6.5.3	6
Dred_2044	NADH (or F420H2) dehydrogenase subunit C	3
Dred_2045	NADH-quinone oxidoreductase subunit B; EC_number=1.6.99.3	2
Dred_2054	hypothetical protein	4
Dred_2067	signal recognition particle-docking protein FtsY	4
Dred_2072	**3-oxoacyl-(acyl-carrier-protein) reductase**	**4**
Dred_2089	**50S ribosomal protein L28**	**3**
Dred_2122	hypothetical protein	3
Dred_2150	thiamine biosynthesis protein ThiH	6
Dred_2152	small GTP-binding protein	3
Dred_2157	AsnC family transcriptional regulator	2
Dred_2173	xanthine phosphoribosyltransferase	5
Dred_2194	**hypothetical protein**	**4**
Dred_2274	two component sigma-54 specific Fis family transcriptional regulator	4
Dred_2292	DEAD/DEAH box helicase domain-containing protein	2
Dred_2313	6-phosphofructokinase; EC_number=2.7.1.11	2
Dred_2333	phage tail protein I	2
Dred_2363	phosphoribosylglycinamide formyltransferase	3
Dred_2367	**phosphoribosylformylglycinamidine synthase I**	**6**
Dred_2382	response regulator receiver protein	4
Dred_2385	CheD, stimulates methylation of MCP proteins	6
Dred_2449	HAD family hydrolase; EC_number=3.1.3.18	5
Dred_2492	RNA modification protein	2
Dred_2501	**GTP-binding protein LepA**	**3**
Dred_2536	ribonuclease	2
Dred_2537	hypothetical protein	2
Dred_2543	septum site-determining protein MinD	10
Dred_2548	rod shape-determining protein MreB	10
Dred_2551	redox-sensing transcriptional repressor Rex	7
Dred_2559	ATP-dependent protease La; EC_number=3.4.21.53	18
Dred_2752	glycyl-radical activating family protein	2
Dred_2757	**TRAP dicarboxylate transporter subunit DctP**	**3**
Dred_2840	**hypothetical protein**	**6**
Dred_2911	potassium transporter peripheral membrane component	2
Dred_2917	S-layer domain-containing protein	2

Dred_2985	**membrane-bound proton-translocating pyrophosphatase; EC_number=3.6.1.1**	**4**
Dred_3002	UDP-glucose 4-epimerase	3
Dred_3056	Cof-like hydrolase	5
Dred_3065	**excinuclease ABC subunit A**	**3**
Dred_3101	UTP-glucose-1-phosphate uridylyltransferase GalU	5
Dred_3114	heat shock protein DnaJ domain-containing protein	2
Dred_3115	heat shock protein 70	10
Dred_3136	mannose-1-phosphate guanylyltransferase/mannose-6-phosphate isomerase; EC_number=2.7.7.22	4
Dred_3143	copper amine oxidase domain-containing protein	15
Dred_3144	rod shape-determining protein Mbl	4
Dred_3168	hypothetical protein	9
Dred_3172	**50S ribosomal protein L31**	**2**
Dred_3190	**phenylacetate--CoA ligase; EC_number=6.2.1.30**	**12**
Dred_3244	CarD family transcriptional regulator	2
Dred_3298	radical SAM domain-containing protein	10
Dred_3321	cobyrinic acid a,c-diamide synthase	2
Dred_3323	tRNA uridine 5-carboxymethylaminomethyl modification protein GidA	2
Dred_3325	**single-stranded nucleic acid binding R3H domain-containing protein**	**6**

Supplementary Table 6.2c: *D. reducens* proteins exclusively detected during pure culture growth compared with co-culture growth (48-hour)
Note: Proteins that were detected in the 72-hour co-culture proteome are designated with red text. Number of distinct peptides refers to the highest number of distinct peptides detected per protein in a particular replicate

Locus Tag	Description	Number of distinct peptides
Dred_0028	hypothetical protein	10
Dred_0061	PSP1 domain-containing protein	8
Dred_0066	TatD family hydrolase	6
Dred_0099	bifunctional N-acetylglucosamine-1-phosphate uridyltransferase/glucosamine-1-phosphate acetyltransferase; EC_number=2.7.7.23	10
Dred_0105	threonine aldolase; EC_number=4.1.2.5	16
Dred_0126	ATP-dependent metalloprotease FtsH; EC_number=3.6.4.6	2
Dred_0127	nucleoside diphosphate kinase; EC_number=2.7.4.6	3
Dred_0128	hypothetical protein	2
Dred_0152	thioesterase superfamily protein	5
Dred_0180	ATPase	19
Dred_0195	FAD-dependent thymidylate synthase; EC_number=2.1.1.148	3
Dred_0269	hypothetical protein	2
Dred_0289	putative alpha-isopropylmalate/homocitrate synthase family transferase	3
Dred_0319	RND family efflux transporter MFP subunit	9

Dred_0321	hypothetical protein	40
Dred_0336	stress protein	3
Dred_0340	putative ATP/GTP-binding protein	2
Dred_0381	pyruvate kinase	4
Dred_0423	hydroxylamine reductase	10
Dred_0443	alpha-glucan phosphorylase; EC_number=2.4.1.1	20
Dred_0474	isopentenyl pyrophosphate isomerase; EC_number=5.3.3.2	3
Dred_0489	putative agmatinase	6
Dred_0514	DNA methylase N-4/N-6 domain-containing protein	6
Dred_0537	CRISPR-associated Csh2 family protein	7
Dred_0555	hypothetical protein	4
Dred_0560	phosphodiesterase	6
Dred_0577	dehydratase	4
Dred_0583	SMC domain-containing protein	2
Dred_0607	hypothetical protein	2
Dred_0608	dihydrolipoamide dehydrogenase	3
Dred_0609	lipoate-protein ligase B	4
Dred_0659	dinitrogenase iron-molybdenum cofactor biosynthesis protein	5
Dred_0665	histidinol-phosphatase; EC_number=3.1.3.15	5
Dred_0678	UDP-N-acetylglucosamine 1-carboxyvinyltransferase	3
Dred_0712	alanine racemase domain-containing protein	6
Dred_0721	glycine cleavage system H protein	4
Dred_0723	glycine dehydrogenase subunit 2; EC_number=1.4.4.2	10
Dred_0734	D-tyrosyl-tRNA(Tyr) deacylase	2
Dred_0738	phosphodiesterase	6
Dred_0761	UBA/THIF-type NAD/FAD binding protein	8
Dred_0774	aldo/keto reductase	7
Dred_0817	filamentation induced by cAMP protein Fic	4
Dred_0852	hypothetical protein	6
Dred_0982	hypothetical protein	5
Dred_1015	hypothetical protein	2
Dred_1019	chorismate synthase; EC_number=4.2.3.5	3
Dred_1021	3-dehydroquinate synthase	5
Dred_1101	pyrimidine-nucleoside phosphorylase; EC_number=2.4.2.2	4
Dred_1112	twin arginine-targeting protein translocase	6
Dred_1114	formate dehydrogenase; EC_number=1.2.1.2	3
Dred_1120	hypothetical protein	2
Dred_1124	RNA-binding S1 domain-containing protein	4
Dred_1129	deoxyribose-phosphate aldolase; EC_number=4.1.2.4	2
Dred_1273	hypothetical protein	5
Dred_1326	hypothetical protein	4
Dred_1345	molybdopterin oxidoreductase	2
Dred_1362	pyridoxal-5prime-phosphate-dependent enzyme subunit beta	8
Dred_1420	hypothetical protein	13
Dred_1423	von Willebrand factor, type A	5
Dred_1460	NAD+ synthetase	6
Dred_1549	hypothetical protein	2
Dred_1583	glucose-inhibited division protein A	3
Dred_1629	CRISPR-associated RAMP Csm3 family protein	2
Dred_1652	NADH dehydrogenase (quinone); EC_number=1.6.99.5	2
Dred_1654	hydrogenase	18
Dred_1655	NADH dehydrogenase (quinone); EC_number=1.6.99.5	14
Dred_1681	aspartate carbamoyltransferase; EC_number=2.1.3.2	2

Dred_1682	dihydroorotase, multifunctional complex type; EC_number=3.5.2.3	7
Dred_1693	methyl-accepting chemotaxis sensory transducer	4
Dred_1717	hypothetical protein	4
Dred_1720	extracellular ligand-binding receptor	3
Dred_1751	5-methyltetrahydropteroyltriglutamate--homocysteine S-methyltransferase; EC_number=2.1.1.14	2
Dred_1762	translation elongation factor G	27
Dred_1778	electron transfer flavoprotein subunit beta	7
Dred_1779	electron transfer flavoprotein subunit alpha	9
Dred_1780	3-hydroxybutyryl-CoA dehydrogenase; EC_number=1.1.1.157	3
Dred_1782	butyryl-CoA dehydrogenase; EC_number=1.3.99.2	5
Dred_1784	acetyl-CoA acetyltransferase; EC_number=2.3.1.9	4
Dred_1802	hypothetical protein	2
Dred_1910	adenosylcobinamide-phosphate guanylyltransferase; EC_number=2.7.7.62	3
Dred_1915	membrane dipeptidase; EC_number=3.4.13.19	7
Dred_1955	phosphoesterase domain-containing protein	2
Dred_1970	1-deoxy-D-xylulose 5-phosphate reductoisomerase; EC_number=1.1.1.267	4
Dred_2092	riboflavin synthase subunit alpha; EC_number=2.5.1.9	3
Dred_2197	UbiD family decarboxylase	11
Dred_2220	dinitrogenase iron-molybdenum cofactor biosynthesis protein	2
Dred_2223	dinitrogenase iron-molybdenum cofactor biosynthesis protein	3
Dred_2230	hypothetical protein	2
Dred_2263	methyl-accepting chemotaxis sensory transducer	2
Dred_2267	molybdenum cofactor biosynthesis protein C	6
Dred_2287	hypothetical protein	2
Dred_2299	hypothetical protein	2
Dred_2306	hypothetical protein	2
Dred_2310	GDSL family lipase	4
Dred_2314	acetyl-CoA carboxylase, carboxyl transferase subunit alpha; EC_number=6.4.1.2	3
Dred_2322	antibiotic biosynthesis monooxygenase	2
Dred_2353	imidazoleglycerol-phosphate dehydratase; EC_number=4.2.1.19	5
Dred_2374	beta-lactamase domain-containing protein	10
Dred_2378	MazG nucleotide pyrophosphohydrolase	3
Dred_2465	NADPH-dependent FMN reductase	2
Dred_2480	cytidine deaminase	2
Dred_2482	putative metalloprotease	6
Dred_2507	hypothetical protein	3
Dred_2518	RNP-1-like RNA-binding protein	2
Dred_2520	histidine triad (HIT) protein	8
Dred_2550	maf protein	3
Dred_2553	hypothetical protein	2
Dred_2577	HisJ family histidinol phosphate phosphatase	11
Dred_2649	hypothetical protein	2
Dred_2691	glutamate mutase, MutL	6
Dred_2692	methylaspartate mutase subunit S; EC_number=5.4.99.1	3
Dred_2738	S-layer domain-containing protein	2
Dred_2739	NLP/P60 protein	2
Dred_2751	UbiC transcription regulator-associated domain-containing protein	2
Dred_2799	endonuclease/exonuclease/phosphatase	2
Dred_2804	glutamate synthase small subunit	23

Dred_2807	glutamine synthetase, type I; EC_number=6.3.1.2	24
Dred_2824	thiamine pyrophosphate binding domain-containing protein	2
Dred_2831	hypothetical protein	3
Dred_2845	glycerol kinase	2
Dred_2857	methyl-accepting chemotaxis sensory transducer	2
Dred_2866	alanine dehydrogenase	3
Dred_2879	molybdenum cofactor synthesis domain-containing protein	8
Dred_2885	metalloendopeptidase glycoprotease family; EC_number=3.4.24.57	5
Dred_2887	peptidase M22, glycoprotease	2
Dred_2892	amidohydrolase	3
Dred_2930	spermidine synthase	11
Dred_2948	TetR family transcriptional regulator	3
Dred_2967	FAD-dependent pyridine nucleotide-disulfide oxidoreductase	15
Dred_2977	hypothetical protein	7
Dred_2981	two component transcriptional regulator	7
Dred_3031	UDP-N-acetylglucosamine 2-epimerase; EC_number=5.1.3.14	5
Dred_3033	polysaccharide biosynthesis protein CapD	3
Dred_3100	phosphoglucomutase; EC_number=5.4.2.2	6
Dred_3149	F0F1 ATP synthase subunit epsilon	6
Dred_3160	MazG nucleotide pyrophosphohydrolase	3

Supplementary Table 6.3: Additional *G. sulfurreducens* c-type cytochromes identified by proteomic analysis
Note: Number of distinct peptides refers to the highest number of distinct peptides detected per protein in a particular replicate
NI= protein not identified, NA=not applicable

Locus Tag	Protein name	Co/Pure (log2)	p-value	Number of distinct peptides detected in Co	Number of distinct peptides detected in Pure
GSU0592	lipoprotein cytochrome c	0.56	0.12	13	9
GSU0594	cytochrome c	-2.94	0.00	3	3
GSU0612	cytochrome c (PpcA)	0.23	0.58	4	2
GSU0616	cytochrome c	0.25	0.37	1	3
GSU0618	cytochrome c	-0.37	0.18	6	7
GSU0670	lipoprotein cytochrome c	-1.30	0.08	2	2
GSU2076	cytochrome c (OmcZ_	0.21	0.61	4	5
GSU2504	cytochrome c (OmcS)	0.10	0.66	10	5
GSU2513	lipoprotein cytochrome c, 1 heme-binding site	-2.55	0.00	1	1
GSU2645	cytochrome c	0.57	0.53	1	2
GSU2737	lipoprotein cytochrome c (OmcB)	0.35	0.11	20	18
GSU2811	cytochrome c	0.28	0.03	36	34
GSU2813	cytochrome c peroxidase	0.25	0.14	27	15
GSU3334	lipoprotein cytochrome c, 1 heme-binding site	0.32	0.40	8	3
GSU0364	cytochrome c	NA	NA	NI	1
GSU1538	cytochrome c	NA	NA	NI	2

Supplementary Table 6.4: Additional information for *D. reducens* proteins exclusively identified during co-culture growth

Note: includes data from Otwell et al., 2016 where growth conditions included sulfate reduction, Fe(III)-citrate reduction, Fe(III)-oxide reduction, and pyruvate fermentation

Number of distinct peptides refers to the highest number of distinct peptides detected per protein in a particular replicate

Locus Tag	Description	Number of distinct peptides detected	Number of replicates with detected peptides (out of 6)	Other notes/other proteins of interest
Dred_0248	anthranilate synthase component I; EC_number=4.1.3.27	10	6	Predicted to synthesize anthranilate from chorismate. Dred_0250 (anthranilate phosphoribosyltransferase), also in KEGG pathway, was identified in 48-hour co-culture with 15 distinct peptides, not identified in pure culture in this study
Dred_0781	shikimate kinase; EC_number=2.7.1.71	5	5	Involved in synthesis of chorismate in shikimate pathway. Furthermore, Dred_0782 (phospho-2-dehydro-3-deoxyheptonate aldolase) is involved in a previous step in the pathway and is increased 2.5-fold (p <0.01) in co-culture.
Dred_1147	phospho-2-dehydro-3-deoxyheptonate aldolase	2	5	First enzyme in the shikimate pathway. Dred_1149 is a paralog of Dred_0782 (see above) and was increased 5.3-fold (p <0.01) in co-culture relative to pure culture. Dred_1151 (3-phosphoshikimate 1-carboxyvinyltransferase) is involved in chorismate biosynthesis and is increased 1.9-fold in co-culture (p <0.01)
Dred_2173	xanthine phosphoribosyltransferase	5	6	
Dred_2840	hypothetical protein	6	6	Putative ABC transporter, metallic cation, iron-siderophore and vitamin B12 transporters family

Supplementary Table 6.5: Peptide biomarkers created for proteins of interest from dissimilatory metal-reducing bacteria

Note: highlighting denotes biomarker peptides validated in *G. sulfurreducens-D. reducens* co-culture. Transition ions are included for these peptides.

References:

Dalla Vecchia, E., Suvorova, E. I., Maillard, J., and Bernier-Latmani, R. (2014b). Fe(III) reduction during pyruvate fermentation by Desulfotomaculum reducens strain MI-1. Geobiology 12, 48–61. doi:10.1111/gbi.12067.

Otwell, A. E., Sherwood, R. W., Zhang, S., Nelson, O. D., Li, Z., Lin, H., et al. (2015). Identification of proteins capable of metal reduction from the proteome of the Gram-positive bacterium Desulfotomaculum reducens MI-1 using an NADH-based activity assay. *Environ. Microbiol.* 17, 1977–1990. doi:10.1111/1462-2920.12673.

Otwell AE, Callister SJ, Zink EM, Smith RD and Richardson RE (2016). Comparative Proteomic Analysis of Desulfotomaculum reducens MI-1: Insights into the Metabolic Versatility of a Gram-positive Sulfate and Metal-reducing Bacterium. Front. Microbiol. 7:191. doi: 10.3389/fmicb.2016.00191.

Wilkins, M. J., Callister, S. J., Miletto, M., Williams, K. H., Nicora, C. D., Lovley, D. R., Long, P. E. and Lipton, M. S. (2011), Development of a biomarker for Geobacter activity and strain composition; Proteogenomic analysis of the citrate synthase protein during bioremediation of U(VI). Microbial Biotechnology, 4: 55–63. doi:10.1111/j.1751-7915.2010.00194.x

Peptide sequence	MW	Locus tag	Organism	Description	Rationale for selection	Wild-type transitions (Q1)	Wild-type transitions (Q3)	Other notes
Gram-negative bacteria								
TPGLKDDPLFK	**1230.42**	**GSU1106**	***Geobacter sulfurreducens***	**citrate synthase**	**Developed as biomarker for *Geobacter* in Wilkins et al. 2011**	**616.30**	**504.7, 618.80, 727.7**	
IPVIAAFIYNLK	**1361.68**	**GSU1106**	***Geobacter sulfurreducens***	**citrate synthase**	**Developed as biomarker for *Geobacter* in Wilkins et al. 2011**	**681.70**	**869, 939.9, 1053**	
TIPETFEALPK	1253.47	Gbem_1652 /3905	*Geobacter bemidjiensis*	citrate synthase	Developed as biomarker for *Geobacter* in Wilkins et al. 2011			
SLVTDISYLDPQEGIR	1816.76	Gbem_1652 /3905	*Geobacter bemidjiensis*	citrate synthase	Developed as biomarker for *Geobacter* in Wilkins et al. 2011			Synthesis failed, no product shipped
AEDLAAQAK	924.01	GSU0466	*Geobacter sulfurreducens*	MacA	Indirectly involved in iron reduction, putatively involved in U(VI) reduction			
AIEVFEATLVTPDAPFDK	1971.25	GSU0466	*Geobacter sulfurreducens*	MacA	Indirectly involved in iron reduction, putatively involved in U(VI) reduction			Low sensitivity due to low intensity fragment ions
VTSTAADK	799.87	GSU0466	*Geobacter sulfurreducens*	MacA	Indirectly involved in iron reduction, putatively involved in U(VI) reduction			No signal in MRM-IDA, likely does not retain on trapping column
VTNTAADK	826.9	Gura_1316	*Geobacter uraniireducens*	cytochrome c peroxidase	Ortholog of GSU MacA			No signal in MRM-IDA, likely does not retain on trapping column
FAVTNTAK	858.99	GSU2813	*Geobacter sulfurreducens*	cytochrome c peroxidase	Paralog of GSU MacA			
VTNTASDK	842.9	Gbem_0020	*Geobacter bemidjiensis*	cytochrome c peroxidase	Ortholog of GSU MacA			No signal in MRM-IDA, likely does not retain on trapping column
FVVTNTASDK	1089.21	Desaf_0713	*Desulfovibrio africanus*	cytochrome c peroxidase	Ortholog of GSU MacA			
VIASLALSVFCAGLAFAADDIVLK	2415.92	GSU0612	*Geobacter sulfurreducens*	PpcA	Putatively involved in Fe(III) and U(VI) reduction			Poor synthesis with insufficent yield for optimization or detection
NGDVTFNHK	1039.12	Gbem_4049	*Geobacter bemidjiensis*	cytochrome c	Ortholog of GSU PpcB			
ATNGAAGPVVNWDPNNNR	**1866.95**	**GSU2737**	***Geobacter sulfurreducens***	**OmcB**	**Involved in soluble and insoluble Fe(III) reduction**	**623.40**	**729.7, 915.80, 1029.90**	
AITDADGILGFVNSHYLAAGGQLFG K	**2635.94**	**GSU2737**	***Geobacter sulfurreducens***	**OmcB**	**Involved in soluble and insoluble Fe(III) reduction**	**879.50**	**883.8, 940.3, 1226.8**	
DTNANGIGDPGELVSSNAFTNWAGV YGLALWK	**3338.61**	**GSU2737**	***Geobacter sulfurreducens***	**OmcB**	**Involved in soluble and insoluble Fe(III) reduction**	**614.40**	**661.47, 704.17, 747.87**	
TGYEYATR	970.75	GSU2737	*Geobacter sulfurreducens*	OmcB	Involved in soluble and insoluble Fe(III) reduction			
SAHAGGLLTAK	1033.18	GSU2737	*Geobacter sulfurreducens*	OmcB	Involved in soluble and insoluble Fe(III) reduction			
GGALTAAEAEK	1025.12	Gbem_337 9	*Geobacter bemidjiensis*	lipoprotein cytochrome c	Orthlog of GSU OmcB			
VIASTHFDDPLTAK	1522.74	Gbem_337 9	*Geobacter bemidjiensis*	lipoprotein cytochrome c	Orthlog of GSU OmcB			
FVDGSIATTGLPIK	**1426.68**	**GSU2504**	***Geobacter sulfurreducens***	**OmcS**	**Involved in extracellular electron transfer, localized to pili**	**710.10**	**729.7, 800.9, 1173**	
FNLAYEFTTIADASGNSIYGTDPNTSS LQGR	**3311.49**	**GSU2504**	***Geobacter sulfurreducens***	**OmcS**	**Involved in extracellular electron transfer, localized to pili**	**1104.60**	**959.7, 1232.8, 1396.1**	
DPIASVSAVGVYR	1344.24	Gbem_267 9	*Geobacter bemidjiensis*	cytochrome c	Ortholog of GSU OmcS			
PASLFGPYAR	1088.97	Gbem_267 9	*Geobacter bemidjiensis*	cytochrome c	Ortholog of GSU OmcS			
EESSTDTR	934.64	Gbem_1131	*Geobacter bemidjiensis*	cytochrome c	Ortholog of GSU OmcS			Does not retain on trapping column
VSVPALVEGVYELR	**1541.51**	**GSU2076**	***Geobacter sulfurreducens***	**OmcZ**	**Extracellular MHC, predicted to be involved in U(VI) reduction, current production**	**766.30**	**865.6, 964.60, 1245.8**	
VVATSPDFATNGYVTVK	**1777.01**	**GSU2076**	***Geobacter sulfurreducens***	**OmcZ**	**Extracellular MHC, predicted to be involved in U(VI) reduction, current production**	**885.10**	**953.10, 1312.3, 1399.1**	
IIASATLATGK	**1045.24**	**GSU2706**	***Geobacter sulfurreducens***	**OmcZ**	**Extracellular MHC, predicted to be involved in U(VI) reduction, current production**	**523.80**	**590.70, 749.20, 820.3**	
TINGPLSGK	894.03	GSU2076	*Geobacter sulfurreducens*	OmcZ	Extracellular MHC, predicted to be involved in U(VI) reduction, current production			
IVATGTNFAAGK	1157.33	GM21_1194	*Geobacter* sp. M21	cytochrome c family protein	Orthlog of GSU OmcZ			
IVATSPAFAR	1042.94	GSU1334	*Geobacter sulfurreducens*	cytochrome c	Paralog of OmcZ, predicted to be involved in U(VI) reduction			
IVGSSTAVK	869.01	Gmet_0930	*Geobacter metallireducens*	cytochrome c	Ortholog of OmcZ			
IVVTGTNFAAGK	1185.38	Gbem_3056	*Geobacter bemidjiensis*	cytochrome c	Ortholog of OmcZ			
AYNAASNSDLK	1161.25	Gbem_2590	*Geobacter bemidjiensis*	PilA	ortholog of GSU PilA			
SAIVELLDLNDEIR	1610.56	Gbem_127 9	*Geobacter bemidjiensis*	type IV pilus assembly protein PilB	ortholog of PilB in GSU			
FAEGNYSPK	1020.11	SO_1777	*Shewanella oneidensis*	MtrA	Part of metal reduction pathway in *Shewanella* spp.			
QSTLSADK	856.92	SO_1777	*Shewanella oneidensis*	MtrA	Part of metal reduction pathway in *Shewanella* spp.			Multiple problems mainly N-terminal Q conversion to pyE, poor signal

GVHGAIDSSK	978.05	SO_1777	*Shewanella oneidensis*	MtrA	Part of metal reduction pathway in *Shewanella* spp.			Does not retain well enough on trapping column to be useful for MRM
FDAFDSNK	951	SO_1778	*Shewanella oneidensis*	MtrC	Part of metal reduction pathway in *Shewanella* spp.			
FNVVSAAGK	900.03	SO_1778	*Shewanella oneidensis*	MtrC	Part of metal reduction pathway in *Shewanella* spp.			
ADLAFATLSGK	1101.26	SO_1778	*Shewanella oneidensis*	MtrC	Part of metal reduction pathway in *Shewanella* spp.			
AWLYGDIK	973.13	SO_1779	*Shewanella oneidensis*	OmcA	Part of metal reduction pathway in *Shewanella* spp.			
EFISDPSAYTK	1265.39	SO_1779	*Shewanella oneidensis*	OmcA	Part of metal reduction pathway in *Shewanella* spp.			
DYPAYTAGSR	1110.89	SO_1779	*Shewanella oneidensis*	OmcA	Part of metal reduction pathway in *Shewanella* spp.			
VECVTCHHLVDGK	1447.69	Ddes_2013	*Desulfovibrio desulfuricans*	cytochrome c3	Periplasmic, tetraheme cytochrome predicted to be involved in Fe(III), Cr(VI), U(VI) reduction			MW + 144Da after Cys alkylation
SLYYVVHAK	1087.27	Ddes_2013	*Desulfovibrio desulfuricans*	cytochrome c3	Periplasmic, tetraheme cytochrome predicted to be involved in Fe(III), Cr(VI), U(VI) reduction			
DLTGCAK	714.83	Ddes_2013	*Desulfovibrio desulfuricans*	cytochrome c3	Periplasmic, tetraheme cytochrome predicted to be involved in Fe(III), Cr(VI), U(VI) reduction			Low yield/poor signal and Cys-alkylation (+57Da) very labile
Gram-positive bacteria								
EALYIPNFGVEQR	**1535.71**	**Dred_0049**	***Desulfotomaculum reducens***	**pyruvate ferredoxin/flavodoxin oxidoreductase**	**Key enzyme in pyruvate oxidation**	**513.00**	**530.80, 588.7, 590.70**	
VLAIPALEISK	**1153.42**	**Dred_0049**	***Desulfotomaculum reducens***	**pyruvate ferredoxin/flavodoxin oxidoreductase**	**Key enzyme in pyruvate oxidation**	**577.50**	**757.8, 871.00, 942.00**	
GELPPLEFGRK	**1242.43**	**Dred_0635**	***Desulfotomaculum reducens***	**sulfate adenyltransferase**	**Highly abundant protein in *D. reducens*, found to be similarly abundant across growth conditions (Otwell et al., 2016)**	**557.80**	**465.10, 718.70, 815.8**	
VADKYEYDKVK	**1357.51**	**Dred_0635**	***Desulfotomaculum reducens***	**sulfate adenyltransferase**	**Highly abundant protein in *D. reducens*, found to be similarly abundant across growth conditions (Otwell et al., 2016)**	**467.10**	**573.7, 583.40, 619**	
ATFFTDDADHPGVQK	**1648.73**	**Dred_0635**	***Desulfotomaculum reducens***	**sulfate adenyltransferase**	**Highly abundant protein in *D. reducens*, found to be similarly abundant across growth conditions (Otwell et al., 2016)**	**550.50**	**592.2, 665.80, 739.50**	
LAVPGQFVHVR	1233.17	Dred_1685	*Desulfotomaculum reducens*	oxidoreductase FAD/NAD(P)-binding subunit	Identified in Otwell et al., 2015 as part of in vitro metal reductase complex			
GFTLPLPGSK	1024.22	Dred_1685	*Desulfotomaculum reducens*	oxidoreductase FAD/NAD(P)-binding subunit	Identified in Otwell et al., 2015 as part of in vitro metal reductase complex			
GTEILSQQKPGDR	1439.3	Dred_1685	*Desulfotomaculum reducens*	oxidoreductase FAD/NAD(P)-binding subunit	Identified in Otwell et al., 2015 as part of in vitro metal reductase complex			
VGFIPTVTK	961.16	Dred_1685	*Desulfotomaculum reducens*	oxidoreductase FAD/NAD(P)-binding subunit	Identified in Otwell et al., 2015 as part of in vitro metal reductase complex			
EQLDKLPNEY	1248.34	Dred_1685	*Desulfotomaculum reducens*	oxidoreductase FAD/NAD(P)-binding subunit	Identified in Otwell et al., 2015 as part of in vitro metal reductase complex			
GPLGNSYPLEQLK	1415.6	Dred_1685	*Desulfotomaculum reducens*	oxidoreductase FAD/NAD(P)-binding subunit	Identified in Otwell et al., 2015 as part of in vitro metal reductase complex			
GFTLPLPGSR	1054.95	DESHY_110150	*Desulfotomaculum hydrothermale*	oxidoreductase FAD/NAD(P)-binding subunit	Ortholog of Dred_1685			
GFTLPEPGQR	1111.96	Desku_1288	*Desulfotomaculum kuznetsovii*	oxidoreductase FAD/NAD(P)-binding subunit	Ortholog of Dred_1685			
AVEGAGADGLSVINTLLGMAIDVR	**2342.68**	**Dred_1686**	***Desulfotomaculum reducens***	**dihydroorotate dehydrogenase 1B**	**Identified in Otwell et al., 2015 as part of in vitro metal reductase complex**	**781.60**	**761.9, 875, 987.80**	
AVWQVYK	901.06	Dred_1686	*Desulfotomaculum reducens*	dihydroorotate dehydrogenase 1B	Identified in Otwell et al., 2015 as part of in vitro metal reductase complex			
NSTALPVIVK	1049.27	Dred_1686	*Desulfotomaculum reducens*	dihydroorotate dehydrogenase 1B	Identified in Otwell et al., 2015 as part of in vitro metal reductase complex			
LSPNVTDIAEIAR	1409.32	Dred_1686	*Desulfotomaculum reducens*	dihydroorotate dehydrogenase 1B	Identified in Otwell et al., 2015 as part of in vitro metal reductase complex			
ILPADTVILAVGSR	1435.43	Dred_2421	*Desulfotomaculum reducens*	NADH: flavin oxidoreductase	Identified in Otwell et al., 2015 as in vitro metal reductase			
IAEIVASFAK	1056.26	Dred_2421	*Desulfotomaculum reducens*	NADH: flavin oxidoreductase	Identified in Otwell et al., 2015 as in vitro metal reductase			
LTGETPVELTEEK	1453.62	Dred_2421	*Desulfotomaculum reducens*	NADH: flavin oxidoreductase	Identified in Otwell et al., 2015 as in vitro metal reductase			
FFYTPDLAR	1140.02	Desde_0941	*Desulfitobacterium dehalogenans*	NADH: flavin oxidoreductase	Ortholog of Dred_2421			
IVPQLYQAGR	1155.06	Desmer_1729	*Desulfosporosinus meridiei*	NADH: flavin oxidoreductase	Ortholog of Dred_2421			
VFEGHLLGQELK	**1369.57**	**Dred_2090**	***Desulfotomaculum reducens***	**riboflavin synthase**	**Riboflavin predicted to serve as soluble electron shuttle during Fe(III) with pyruvate in *D. reducens* (Dalla Vecchia et al., 2014)**	**457.50**	**562.60, 636.3, 687.80**	
ISLDSNLPVIFGVLTVDTIEQAIER	**2743.13**	**Dred_2090**	***Desulfotomaculum reducens***	**riboflavin synthase**	**Riboflavin predicted to serve as soluble electron shuttle during Fe(III) with pyruvate in *D. reducens* (Dalla Vecchia et al., 2014)**	**915.30**	**959.9, 1053.50, 1075.1**	
DLRPGSQVNLER	**1383.52**	**Dred_2092**	***Desulfotomaculum reducens***	**riboflavin synthase subunit alpha**	**Riboflavin predicted to serve as soluble electron shuttle during Fe(III) with pyruvate in *D. reducens* (Dalla Vecchia et al., 2014)**	**462.40**	**531.6, 630.7, 754.80**	
LGGHMVSGHVDGVGTIAGK	**1792.03**	**Dred_2092**	***Desulfotomaculum reducens***	**riboflavin synthase subunit alpha**	**Riboflavin predicted to serve as soluble electron shuttle during Fe(III) with pyruvate in *D. reducens* (Dalla Vecchia et al., 2014)**	**449.00**	**546.70, 560.90, 574.7**	

Supplementary Table 6.6: Comparison of average ion intensity of peptides of OmcS (GSU2504) shared between co-culture (48-hour) and pure cultures conditions

Note: ND= no peptides detected

NA=not applicable

Peptide sequence	Co48 1-1	Co48 1-2	Co48 1-3	Co48 2-1	Co48 2-2	Co48 2-3	Average	GS 1-1	GS 1-2	GS 1-3	GS 2-1	GS 2-2	GS 2-3	Average	Log2 Co48/GS	Fold change Co48/GS
AVAPSTYNRTEATTQTR	ND	ND	18.04	ND	ND	ND	18.04	ND	ND	ND	ND	ND	ND	NA	NA	NA
FNLAYEFTTIADASGNSIYGTDPNTSSLQGR	22.51	22.17	21.80	ND	21.14	21.28	21.78	ND	ND	ND	ND	ND	ND	NA	NA	NA
FVDGSIATTGLPIK	25.61	25.56	25.92	25.45	25.26	25.44	25.54	24.91	24.76	24.87	24.21	23.85	24.00	24.43	1.11	2.15
ILGGTGYQPK	25.99	25.78	26.12	25.25	25.23	25.43	25.63	23.96	24.11	24.34	22.99	23.24	23.26	23.65	1.98	3.94
NSGSYQNSNDPTAWGAVGAYR	21.45	20.82	21.86	ND	ND	ND	21.38	ND	ND	ND	ND	ND	ND	NA	NA	NA
QVPAAVAPSTYNR	ND	ND	ND	20.43	21.21	21.21	20.95	ND	ND	ND	ND	ND	ND	NA	NA	NA
SGDLTGTQASAYLSLAPFEEGTADYTVLK	23.88	23.95	24.45	23.54	23.58	23.90	23.88	21.54	21.33	22.80	20.55	ND	ND	21.55	2.33	5.02
SGDLTGTQASAYLSLAPFEEGTADYTVLKGHAK	ND	21.46	22.09	ND	ND	ND	21.78	ND	ND	ND	ND	ND	ND	NA	NA	NA
SLSGSYAFANQVPAAVAPSTYNR	22.95	23.69	23.64	22.54	22.54	22.61	22.99	21.26	ND	22.14	ND	ND	ND	21.70	1.29	2.45
SVNEMTAAYYGR	24.21	24.19	24.21	23.02	22.59	23.01	23.54	21.52	21.71	ND	ND	ND	ND	21.61	1.93	3.80
TADKFAPYQR	21.61	21.68	21.84	ND	ND	ND	21.71	ND	ND	ND	ND	ND	ND	NA	NA	NA

Chapter 7

Concluding Remarks

Advancing the understanding of metal reduction by Gram-positive bacteria

There is a clear underrepresentation of Gram-positive dissimilatory metal reducing microorganisms (DMRM) in the literature. A major reason for this is that *Geobacter* and *Shewanella* have been productive model organisms for decades, leading to countless studies revolutionizing understanding of microbial metal reduction. The researchers who isolated these DMRM back in 1988—Professors Derek Lovley and Kenneth Nealson—have driven progress in the field, focusing on *Geobacter* and *Shewanella* respectively. At a talk for the American Society for Microbiology General Meeting in 2014, Professor Nealson emphasized the importance of advancing understanding of microbial metal reduction in phylogenetically diverse organisms, including Gram-positive bacteria. Environmental genomic studies continue to report the presence of Gram-positive bacteria associated with metal reduction, and the number of described Gram-positive metal-reducing organisms is expanding. *Desulfotomaculum reducens* MI-1 is one of the first Gram-positive DMRM for which studies on metal reduction are starting to accumulate.

Most of these studies have been published in the last 5 years. Researchers from Dr. Bernier-Latmani's group at École Polytechnique Fédérale de Lausanne (EPFL) originally focused on U(VI) reduction in *D. reducens*. They studied U(VI) reduction by endospores, they analyzed the effect of competing electron acceptors on U(VI) reduction, and they performed a transcriptomic study analyzing differential expression in the presence and absence of U(VI). The genome of *D. reducens* was sequenced by Dr. Bernier-Latmani's group in 2010, which made the proteomic-based studies described in this dissertation possible. Furthermore, two studies on *D. reducens* were published by Dr. Bernier-Latmani's group in 2014, one analyzing Fe(III) reduction during pyruvate fermentation and the other analyzing Fe(III) reduction with the non-fermentable substrate lactate.

The research described in this dissertation adds to the growing literature on *D. reducens*. In Chapter 2, we searched for Fe(III) reductases in fractionated protein pools extracted from *D. reducens*. Dred_2421 (an NADH:flavin oxidoreductase) was identified from soluble protein fractions while a 2-subunit complex (Dred_1685-6) was identified from both soluble and insoluble protein fractions. Dred_2421 and the Dred_1685-6 complex were heterologously expressed, purified, and validated as not only Fe(III) reductases, but also Cr(VI) and U(VI) reductases. These were the first metal reductases identified and validated from a Gram-positive DMRM. We also performed a global comparative proteomic analysis of *D. reducens* during sulfate, Fe(III)-citrate, and Fe(III)-oxide reduction (all with lactate as electron donor) and pyruvate fermentation (Chapter 5). Based on differential protein abundance, we were able to make predictions of proteins involved in both sulfate and Fe(III) reduction. For instance, certain clusters of proteins were highly abundant on sulfate relative to Fe(III), including three loci containing heterodisulfide reductases (hdrs) (Dred_0633-4, Dred_0689-90, and Dred_1325-30). We predict that these proteins are involved in the sulfate reduction pathway in *D. reducens.* When instead *D. reducens* is reducing Fe(III) (an extracellular electron acceptor), it downregulates these hdr-containing loci. Another hypothesis generated from the comparative proteomic analysis was that Dred_0367-9 (a cluster with previously unknown function) is involved in lactate oxidation. These proteins are homologous to a recently described cluster that oxidizes lactate in *Acetobacterium woodii* through flavin-based electron bifurcation. Notable findings from the comparative proteomic analysis specific to Fe(III) reduction included that Dred_2421 (identified in Chapter 2) was ~2-fold increased during Fe(III)-citrate reduction relative to all other conditions. Furthermore, peptides for the sole multiheme c-type cytochrome annotated in the genome (Dred_0700-1) were identified only in the Fe(III)-oxide reduction

proteome, suggesting that the MHC may play a role in insoluble Fe(III) reduction. This comparative proteomic analysis was the first full-proteome analysis of a Gram-positive bacterium focused either on sulfate or Fe(III)-reducing conditions. In Chapter 6, we established Fe(III)-reducing co-cultures between *D. reducens* and the model DMRM *Geobacter sulfurreducens*. Co-cultures were fed pyruvate, and *G. sulfurreducens* depended on *D. reducens* for production of electron donor. Phenotypes observed during co-culture growth included increased rates of soluble and insoluble Fe(III) reduction, increased rates of pyruvate oxidation, and increased rates of cell growth relative to pure culture growth. These findings suggest that *D. reducens* and *G. sulfurreducens* form a mutually beneficial association while reducing Fe(III). Comparative analyses comparing protein abundance in co-culture versus pure cultures revealed that key *G. sulfurreducens* proteins involved in Fe(III) reduction were increased in the co-culture. For instance, type IV pili-related proteins (including the structural subunit PilA) were significantly increased during co-culture growth, as well as multiple MHCs. Targeted quantification of biomarker peptides through multiple reaction monitoring (MRM) assays was also performed in this co-culture. These peptides represented proteins of interest from *D. reducens* and *G. sulfurreducens* (for instance multiple MHCs). While *Geobacter* species have been previously analyzed during co-culture growth, studies are lacking on Fe(III)-reducing co-cultures. Studies with two metal-reducing organisms growing together on Fe(III) have not previously been reported.

Altogether, the literature documenting metal reduction in *D. reducens* has grown substantially in the last five years—more than for any other Gram-positive organism. Metal reduction by *Geobacter* and *Shewanella* species has been a focus of study for nearly three decades, and the literature continues to expand. With these initial studies in *D. reducens* as a

starting point, understanding of metal reduction in Gram-positive bacteria will hopefully continue to develop over the coming years.

Limitations

Throughout the course of this dissertation work, obstacles were encountered that are worth mentioning both to display the limitations of the current work as well as to provide insight for future research. First, while valuable results were obtained from protein purification-based screens for Fe(III) reduction activity (highlighted in Chapters 2-3), we also faced issues with the experimental workflow. Limitations in our studies include a loss of activity in membrane-associated proteins, inability to prevent oxygen exposure during the protein separation steps, and limited knowledge of the physiological electron donor used for Fe(III) reduction in poorly characterized organisms like *D. reducens*. Due to the extracellular nature of Fe(III) reduction, we expected to mainly identify membrane proteins with our Fe(III) reduction activity assay. However, the only membrane-associated protein with Fe(III) reduction activity recovered in the course of our studies was a complex identified in both the soluble and insoluble protein fraction from *D. reducens* (Chapter 2). Modifications of insoluble protein extraction protocols (e.g. varied concentrations of the detergent n-Dodecyl β-D-maltoside) failed to identify any additional membrane proteins. One DMRM not mentioned in this dissertation from which we attempted to identify Fe(III) reductases is the versatile deltaproteobacteria *Anaeromyxobacter dehalogenans* 2CPC. Across multiple experiments and varied workflows, we lost activity in the insoluble protein fraction from *A. dehalogenans*. We tested other electron donors (including NADPH, horse heart cytochrome c, riboflavin, flavin mononucleotide, and hydroquinone) but still failed to confidently identify any Fe(III) reductases. The Fe(III) reduction activity screen we developed, including three efficient and high-resolution non-denaturing protein separation steps, provided

useful results when applied to the poorly characterized organism *D. reducens*. However, for other DMRM of interest, we were unable to recover expected Fe(III) reduction activity, particularly in membrane-associated proteins. Utilizing the separations workflow described in this dissertation to screen for proteins that are not membrane-bound could prove especially powerful.

Another obstacle encountered throughout our studies was downstream processing of cells cultivated on Fe(III), which prevented use of this growth condition for certain experiments. For instance, we were unable to cultivate *D. reducens* on Fe(III) for the function-based proteomic screen. The organism produces a dark, cloudy precipitate during Fe(III) reduction, which was identified as vivianite during Fe(III)-citrate reduction with pyruvate in Chapter 6. This precipitate interfered with our non-denaturing proteomic workflow. During centrifugation of the cell lysate (which is necessary to remove precipitates that cannot be injected into the mass spectrometry instrument), the proteins appear to bind to the Fe-precipitates and are therefore pulled out of solution. Protein concentrations following centrifugation were practically zero, whereas prior to centrifugation were at expected concentrations (~5-10 mg/mL). These Fe-precipitates led to other experimental difficulties, including causing interference with fluorescent microscopy stains like acridine orange. Dr. Bernier-Latmani's group reported experimental difficulties with *D. reducens* when cultivated on Fe(III)-oxide. This prevented them from performing RNA or protein-based analyses on insoluble Fe(III). We were fortunately able to perform comparative proteomic analyses of *D. reducens* on insoluble and soluble Fe(III) (Chapter 5). However, we were unable to perform comparative proteomic analyses on cultures of *Geobacter sulfurreducens* and *A. dehalogens* cultivated on Fe(III)-oxide due to issues during peptide sample preparation. This appears to be a widespread issue in the study of microbial metal

reduction, as cells for most experiments in the literature are not actually prepared on Fe(III). Improving experimental methods for cells cultivated on Fe(III) would help advance this field, allowing for more environmentally relevant conditions to be studied.

Another limitation of the work described in this dissertation is that all of our studies were performed in batch culture. Careful attempts were made to harvest cultures at the same growth phase (generally mid-late exponential phase). However, it is possible that growth phase effects lead to artifacts in our data. A series of chemostats would have been ideal for many of the experiments conducted by our group. An undergraduate researcher spent several months attempting to construct this type of system in our laboratory but unfortunately was unsuccessful. Anaerobic chemostats, equipped with sampling ports and feed/waste/gas lines, may be a worthwhile investment in the future for any researchers continuing the work described here.

A final limitation relevant to this dissertation is inherent to the utilization of proteomic-based analyses. While mass spectrometry-based methods have improved rapidly over the past decade, there are still weaknesses with advanced proteomic techniques. Put simply, different techniques and downstream data processing workflows tend to have both advantages and disadvantages. In the Accurate Mass and Time (AMT) tag data presented in this dissertation, ion intensities of all peptides detected for a particular protein were averaged. These average peptide ion intensity values were then compared between conditions, meaning that the exact same peptide is not always compared 1:1 across conditions. As different peptides have different ionization efficiencies, using averaged values (especially if a small number of unique peptides was identified) can skew abundance comparisons. However, in a similar study using isobaric tag for relative and absolute quantitation (iTRAQ), we lost a substantial fraction of proteins when only including peptides common to conditions. Therefore, in an attempt to present a more global

proteomic analysis of *D. reducens* across various growth conditions, certain abundance ratios were likely not representative of protein abundances in the cell. While proteomic data presented in this dissertation is mainly based on proteins where high numbers of peptides were identified, where artifacts resulting from differences in ionization efficiency are lessened, this limitation is important to note.

Future Directions

With the research described in Chapters 5 and 6, comparative proteomic datasets were generated that will be publically available. As more studies are conducted on metal reduction by Gram-positive bacteria, it is my hope that these datasets will serve as a reference point. It is possible that phylogenetically-related Gram-positive organisms utilize similar pathways for metal reduction (and/or sulfate reduction), and comparing differential abundance patterns between related organisms can provide insight into conserved pathways. For instance, in Chapter 5, multiple hypotheses are made regarding proteins involved in sulfate and Fe(III) reduction in *D. reducens* based on differential protein abundance. Species of *Desulfosporosinus* and *Desulfitobacterium* contain highly similar proteins to many of the *D. reducens* proteins highlighted in Chapter 5 (for instance proteins within the hdr-containing loci). Similar patterns of differential expression of *D. reducens* orthologs in *Desulfosporosinus* and *Desulfitobacterium* would help form stronger hypotheses about protein function and could lead to a knew understanding of conserved pathways of electron transfer. During the course of this project, collaborators from Pacific Northwest National Laboratory developed a publically available ortholog prediction tool to which gene and protein expression data can be overlaid (SPOCS, Species Paralogy and Orthology Clique Solver). As global datasets for other Gram-positive

DMRM are generated, tools like SPOCS could be especially useful for highlighting similar patterns of differential abundance.

The final research chapter (Chapter 6) opens up many possible avenues for future investigations. Our studies suggest that co-culture growth of *D. reducens* and *G. sulfurreducens* confers a mutual benefit to the organisms during Fe(III)-reducing conditions. Studies of this kind, where two DMRM are grown together on Fe(III)-reducing conditions, have not previously been reported. It is important to expand understanding of Fe(III) reduction in pure culture to the microbial community level, as a consortia of organisms are undoubtedly driving the process in the environment. A range of future studies can be conducted utilizing the established *D. reducens*-*G. sulfurreducens* co-culture. Cultivation in a chemostat would be far superior to batch culture in order to minimize growth phase effects as well as to better characterize rates of substrate utilization and product accumulation. Furthermore, analyzing growth of the co-culture cultivated on an electrode would be particularly compelling. Electrode-based studies have been conducted in both *Geobacter* and *Shewanella* in order to study extracellular electron transfer, but for the most part have not been expanded to other organisms. During co-culture growth on an electrode, it would be interesting to compare conductivity relative to pure culture *G. sulfurreducens* growth. Given the increased Fe(III) reduction rates of the co-culture observed on both soluble and insoluble Fe(III), it is possible that current production during cultivation on an electrode would also be increased. *D. reducens* has not been tested for growth on an electrode, so this could also be explored. In addition, many interesting studies could be performed in order to provide further insight into proteomic observations made in Chapter 6. The *G. sulfurreducens* type IV pili as well as certain multiheme c-type cytochromes were increased in abundance during co-culture growth. Gene knockouts could be constructed in order to test for involvement of these

proteins in co-culture growth. Knockout mutants could also help to elucidate the mechanism of interspecies electron transfer (IET) occurring in the co-culture. In several studies where a *Geobacter* species is the electron-donating organism, direct interspecies electron transfer (DIET) was found to occur. In our scheme, *D. reducens* is donating electrons to *G. sulfurreducens,* potentially through acetate and hydrogen. If *G. sulfurreducens* is also receiving electrons through DIET, then even with a deletion of the key hydrogenase (*hyb*) and acetate utilization gene (citrate synthase), *G. sulfurreducens* cells should still be able to grow. Studies of this kind provided initial evidence for the existence of DIET. Furthermore, metabolomics-based studies are warranted. An excreted secondary metabolite could be involved in the enhanced growth phenotypes observed during co-culture cultivation. Supernatants could be analyzed and compared between pure culture and co-culture growth, which could provide insight into exchange of a soluble secondary metabolite.

Our work has also set the stage for utilization of peptide biomarkers to monitor metal reduction in the environment through multiple reaction monitoring (MRM). An initial aim of this project was to quantify peptide biomarkers in environmental samples from a U(VI)-contaminated site in Rifle, CO where biostimulation studies have taken place. A number of obstacles prevented us from reaching this goal. However, we designed 73 peptides representing known metal reductases (or other proteins of interest) from 12 different species of bacteria. All known U(VI)-reductases at the time of literature searching were included. Isotopically-labeled synthetic peptides were purchased, and optimization for each of these peptide biomarkers was performed at the Cornell Proteomics & Mass Spectrometry Facility. In Chapter 6, we were able to validate some of these peptide biomarkers in *D. reducens* and *G. sulfurreducens*. However, most still remain to be validated in experimental culture and/or environmental samples. A complete list of

the 73 peptide biomarkers, including optimization conditions for those validated with MRM analysis, is provided in Chapter 6. In the coming years, as both environmental proteomic techniques and understanding of microbial metal reduction advance, utilization of peptide biomarkers to monitor remediation of contaminant metals will potentially become an attainable goal.

Appendix: Proteomic analysis of *D. reducens* endospores

Along with the cultivation conditions described in Chapter 5, we performed AMT tag-based proteomic analysis on *D. reducens* endospores. The endospore-forming ability of *Desulfotomaculum* species is another trait that differentiates this genus from Gram-negative organisms with simliar metabolic capabilities. Understanding of endospores is based heavily on analyses of representative *Clostridium* and *Bacillus* species, and proteomic investigations of spores of Peptococcaceae have not taken place. Spores of *D. reducens* are of particular interest because there is evidence that they have metal reduction capability (Junier et al., 2009). For these reasons, comparative proteomic analysis was performed on endospores of *D. reducens* relative to pyurvate fermentation conditions. Previously published protocols were followed in order to induce sporulation of cultures cultivated on pyruvate, and cultures were harvested when >50% of cells were sporulated, as determined by microscopy (Junier et al., 2009).

729 proteins were confidently detected in the *D. reducens* endospore proteome, meaning that peptides were identified in at least 50% of the replicates and at least 2 unique peptides were identified. 39 proteins were significantly increased relative to pyruvate fermentation conditions (>2-fold increase, p-value <0.05), and these are displayed in **Appendix Table 1**. Comparing proteins confidently identified in the endospore proteome to proteins identified on all growth conditions analyzed (sulfate reduction, Fe(III)-citrate reduction, Fe(III)-oxide reduction, and pyruvate fermentation) reveals that 40 proteins are completely unique. These proteins exclusively identified in the *D. reducens* endospore proteome are displayed in **Appendix Table 2.**

Appendix Table 1: Proteins significantly increased in abundance in the endospore proteome relative to pyruvate fermentation conditions

Locus Tag	Description	Log_2 Spore/Pyr	p-value
Dred_2518	RNP-1-like RNA-binding protein	3.90	<0.01
Dred_0042	DNA polymerase III subunits gamma and tau; EC_number=2.7.7.7	3.61	<0.01
Dred_2163	porphobilinogen deaminase; EC_number=2.5.1.61	3.32	<0.01
Dred_0398	peptide chain release factor 3	3.19	<0.01
Dred_0763	BadM/Rrf2 family transcriptional regulator	3.19	<0.01
Dred_0751	ribosome small subunit-dependent GTPase A	2.99	<0.01
Dred_1887	DNA mismatch repair protein MutS	2.84	<0.01
Dred_2346	NAD-dependent DNA ligase; EC_number=6.5.1.2	2.76	<0.01
Dred_1160	GTP-binding protein EngA	2.71	<0.01
Dred_2466	phosphoenolpyruvate synthase; EC_number=2.7.9.2	2.55	<0.01
Dred_3066	excinuclease ABC subunit B	2.49	<0.01
Dred_2537	hypothetical protein	2.37	0.01
Dred_2950	acriflavin resistance protein	2.26	0.01
Dred_3130	group 1 glycosyl transferase	2.16	0.01
Dred_2307	magnesium and cobalt transport protein CorA	2.16	<0.01
Dred_2081	CoA-binding domain-containing protein	2.11	<0.01
Dred_1426	hypothetical protein	1.91	<0.01
Dred_0450	hypothetical protein	1.91	0.02
Dred_0298	hypothetical protein	1.87	0.02
Dred_2831	hypothetical protein	1.86	<0.01
Dred_0731	single-stranded-DNA-specific exonuclease RecJ	1.75	<0.01
Dred_2522	periplasmic binding protein/LacI transcriptional regulator	1.74	0.01
Dred_2451	oligopeptide/dipeptide ABC transporter ATPase	1.67	0.05
Dred_2048	HSR1-like GTP-binding protein	1.66	<0.01
Dred_2371	phosphoribosylaminoimidazole	1.64	0.04

	carboxylase, catalytic subunit; EC_number=4.1.1.21		
Dred_1983	gid protein	1.53	0.01
Dred_1955	phosphoesterase domain-containing protein	1.52	<0.01
Dred_2884	phenylacetate--CoA ligase; EC_number=6.2.1.30	1.49	0.04
Dred_2996	hypothetical protein	1.46	0.04
Dred_1112	twin arginine-targeting protein translocase	1.45	0.01
Dred_1637	peptidase U32	1.44	0.01
Dred_2093	riboflavin biosynthesis protein RibD; EC_number=1.1.1.193	1.41	0.05
Dred_0443	alpha-glucan phosphorylase; EC_number=2.4.1.1	1.32	<0.01
Dred_2292	DEAD/DEAH box helicase domain-containing protein	1.31	0.01
Dred_2805	glutamate synthase; EC_number=1.4.7.1	1.29	0.01
Dred_1471	citrate transporter	1.25	0.04
Dred_1817	hypothetical protein	1.16	0.04
Dred_1432	ABC transporter-like protein	1.10	0.03
Dred_0281	acetolactate synthase, large subunit, biosynthetic type; EC_number=2.2.1.6	1.04	<0.01

Note: Protein identification is based on peptide detection in at least 50% of replicates and by at least 2 unique peptides

Appendix Table 2: Proteins exclusively detected in the endospore proteome

Locus Tag	Description	Distinct peps
Dred_0058	Orn/Lys/Arg decarboxylase, major region	2
Dred_0573	electron transfer flavoprotein subunit alpha	2
Dred_0652	carbon-monoxide dehydrogenase, catalytic subunit	2
Dred_0998	YD repeat-containing protein	2
Dred_1120	hypothetical protein	2
Dred_1163	stage IV sporulation protein A	2
Dred_1206	hypothetical protein	2
Dred_1251	MarR family transcriptional regulator	2

Dred_1302	respiratory-chain NADH dehydrogenase domain-containing protein	2
Dred_1429	recombination factor protein RarA	3
Dred_1479	adenosylmethionine decarboxylase	2
Dred_1490	butyryl-CoA dehydrogenase	2
Dred_1495	bifunctional acetaldehyde-CoA/alcohol dehydrogenase	2
Dred_1556	multi-sensor hybrid histidine kinase	2
Dred_1557	methyl-accepting chemotaxis sensory transducer	2
Dred_1562	extracellular solute-binding protein	4
Dred_1653	NADH dehydrogenase (ubiquinone), 24 kDa subunit	6
Dred_1766	hypothetical protein	2
Dred_2177	basic membrane lipoprotein	2
Dred_2232	carbamoyl phosphate synthase large subunit	2
Dred_2235	extracellular solute-binding protein	15
Dred_2381	flagellar motor switch protein FliM	3
Dred_2583	cell divisionFtsK/SpoIIIE	2
Dred_2593	phage minor structural protein	2
Dred_2652	ABC transporter-like protein	5
Dred_2654	NLPA lipoprotein	4
Dred_2722	hypothetical protein	2
Dred_2727	metal dependent phosphohydrolase	3
Dred_2778	TetR family transcriptional regulator	2
Dred_2851	signal transduction histidine kinase regulating citrate/malate metabolism	2
Dred_2856	putative PAS/PAC sensor protein	2
Dred_2932	ABC transporter-like protein	2

Dred_3046	glycosyl transferase family protein	2
Dred_3064	hypothetical protein	2
Dred_3089	metal dependent phosphohydrolase	2
Dred_3091	Ig family protein	2
Dred_3180	signal peptide peptidase SppA, 36K type	2
Dred_3204	membrane lipoprotein lipid attachment site	3
Dred_3207	glycine betaine ABC transporter substrate-binding protein	6
Dred_3278	formate C-acetyltransferase	9

Note: Protein identification is based on peptide detection in at least 50% of replicates and by at least 2 unique peptides. Distinct peps refers to the highest number of unique peptides detected in a single replicate.

References:

Junier, P., Frutschi, M.,Wigginton, N. S., Schofield, E. J., Bargar, J. R., and Bernier-Latmani, R. (2009). Metal reduction by spores of *Desulfotomaculum reducens*. *Environ. Microbiol*. 11, 3007–3017. doi: 10.1111/j.1462-2920.2009.02003.x.